ABSTRACT

BEHAVIOR OF STRUCTURAL CONCRETE MEMBERS STRENGTHENED BY COMPOSITE FABRICS

by
Jian Chen

The new technique of using Fiber Reinforced Polymer (FRP) materials to repair and strengthen various concrete members is becoming more and more popular in structural retrofitting field. Among all the confining materials, Carbon Fiber Reinforced Polymer (CFRP) fabric jackets are identified as an effective way to enhance the strength and ductility of concrete members due to its superior mechanical properties. This study investigates the detailed structural behavior of confined concrete members using CFRP fabric jackets by both analytical and experimental approaches.

A series of CFRP wrapped concrete cylinder tests were conducted to study the compressive stress-strain behavior for CFRP confined concrete members, Based on the test results, the CFRP system can significantly increase the ductility and ultimate compressive strength of normal concrete specimens. Also, a complete stress-strain equation was derived to model the fabric-confined concrete and verified by various experimental tests results.

In order to fully apply this new technique to structural engineering, more experiments were conducted by wrapping CFRP fabric to the large structure members such as beams and columns in this study. The flexural behavior of the large concrete beams wrapped by CFRP fabrics was investigated based on the experiments at the NJIT Structures Laboratory. Different wrapping methods were applied. Test results show that the CFRP confinement can significantly increase the ultimate flexural strength of

Reinforced Concrete (RC) beams. However, the contribution of fabrics may vary due to the different wrapping methods applied. Experimental results are compared with the finite element modeling using the ANSYS computer program. A practical design method similar to ACI strength method is also proposed to predict the ultimate strength of the beam specimens. Good agreements are achieved for both methods.

Structural behavior of the RC slender columns wrapped with CFRP fabrics under combined axial load and biaxial bending were also investigated in this research. Seven slender columns with different wrapping methods were tested and analyzed. It can be concluded that both longitudinal and transverse fabric do help increase the load capacity of the column specimens, although the longitudinal fabric tends to decrease the deformability of the columns. The columns with both wrapping methods applied achieve a better strength and ductility performance. A modified computer program accounting for the proposed stress-strain equation for fabric-confined concrete has been used to verify the present experimental results. A satisfactory agreement is attained for both ascending and descending branches of the load-deformation curves.

BEHAVIOR OF STRUCTURAL CONCRETE MEMBERS STRENGTHENED BY COMPOSITE FABRICS

by

Jian Chen

A Dissertation
Submitted to the Faculty of
New Jersey Institute of Technology
in Partial Fulfillment of the Requirements for the Degree of
Doctor of Philosophy in Civil Engineering

Department of Civil and Environmental Engineering

January 2005

APPROVAL PAGE

BEHAVIOR OF STRUCTURAL CONCRETE MEMBERS STRENGTHENED BY COMPOSITE FABRICS

Jian Chen

Dr. C. T. Thomas Hsu, Dissertation Advisor — Date
Professor of Civil and Environmental Engineering, NJIT

Dr. William R. Spillers, Committee Member — Date
Distinguished Professor of Civil and Environmental Engineering, NJIT

Dr. Dorairaja Raghu, Committee Member — Date
Professor of Civil and Environmental Engineering, NJIT

Professor Walter Konon, Committee Member — Date
Professor of Civil and Environmental Engineering, NJIT

Dr. Pedro Munoz, Committee Member — Date
President, PRM Engineering, MA

BIOGRAPHICAL SKETCH

Author: Jian Chen

Degree: Doctor of Philosophy

Date: January 2005

Undergraduate and Graduate Education:

- Doctor of Philosophy in Civil Engineering
  New Jersey Institute of Technology, New Jersey, 2005

- Master of Science in Civil Engineering
  Xi'an University of Architecture and Technology, Xi'an, Shaanxi, China, 2000

- Bachelor of Science in Civil Engineering
  Xi'an University of Architecture and Technology, Xi'an, Shaanxi, China, 1997

Major: Civil Engineering

This dissertation is dedicated to

" my beloved family "

ACKNOWLEDGMENTS

The work presented in this thesis has been carried out under the direction of my advisor, Professor C. T. Thomas Hsu, to whom I am much indebted for his guidance, constant encouragement and invaluable suggestions throughout the years.

I would like to thank my committee members: Professor William R. Spillers, Professor Dorairaja Raghu, Professor Walter Konon and Dr. Pedro Munoz for their constructive evaluations and suggestions.

The author acknowledges Sika Corporation for the donation of all CFRP composite materials. Special thanks go to Mr. David White at Sika for his help and expertise on CFRP application. The author also acknowledges the NSF grant # CMS 9413725 which was used for developing the Material Testing System (1000 kip MTS 815) for Research and Development of High Performance Cementitious Composites here at New Jersey Institute of Technology.

The graduate assistantship received from the Department of Civil and Environmental Engineering and some research assistantship during the summers from Professor C. T. Thomas Hsu are greatly appreciated.

Special thanks go to Mr. Allyn Luke, Assistant to the Chairman for Laboratories, for his knowledge and assistance on the experiment setup in the Structures Laboratory. Special thanks also go to Dr. Insang Lee, Dr. Zhichao Zhang, Mr. Sun Punurai, Mr. Xiaobin Lu and Mr. Libin Yin for their help in mixing and testing of the specimens.

Finally, I would like to thank my parents and my wife for their love, support and understanding throughout my study at NJIT.

TABLE OF CONTENTS

TABLE OF CONTENTS
(Continued)

Chapter **Page**

TABLE OF CONTENTS
(Continued)

Chapter **Page**

TABLE OF CONTENTS
(Continued)

Chapter **Page**

LIST OF TABLES

LIST OF FIGURES

LIST OF FIGURES
(Continued)

LIST OF FIGURES
(Continued)

LIST OF FIGURES
(Continued)

LIST OF FIGURES
(Continued)

Chapter **Page**

LIST OF FIGURES
(Continued)

Chapter **Page**

LIST OF FIGURES
(Continued)

Chapter **Page**

LIST OF FIGURES
(Continued)

Chapter **Page**

LIST OF FIGURES
(Continued)

Chapter **Page**

LIST OF FIGURES
(Continued)

Chapter **Page**

LIST OF FIGURES
(Continued)

Chapter **Page**

CHAPTER 1

INTRODUCTION

1.1 General

In recent years, a significant part of the infrastructure in North America is in urgent need of strengthening and rehabilitation. According to a study reported by CERF, Civil Engineering Research Foundation, ASCE (1994), over 50% percent of all bridges in North America were built before 1940, and approximately 42% of these bridges are considered to be structurally deficient and functionally obsolete. Even among the bridges built after the Second World War, a large percentage of them were originally designed for smaller vehicles, lighter loads, and a lower traffic volume than commonly experienced today. The cost of replacing and strengthening all deficient structures is prohibitive. All the alarming statistic underscores the importance of developing reliable and cost effective repair and strengthening techniques for existing structures. A particularly challenging problem in this area is the rehabilitation of reinforced concrete structures. Limited financial resources and current technology together will not be enough to solve the problem. High-tech solutions must be investigated so innovative use of new technologies and materials can be employed to rebuild the infrastructure.

Historically, concrete members have been repaired by post tensioning or jacketing with new concrete in conjunction with a surface adhesive. This method is very time-consuming and cannot effectively enhance the properties of concrete structures. Since the mid 1960's, steel jacketing has proved to be an effective measure for retrofitting and has been widely used in practice. However, steel plates have a durability problem unique to this application, because corrosion may occur along the adhesive interface. This type

of corrosion adversely affects the bond at the steel plate/concrete interface and is difficult to monitor during routine inspections. The problem was extremely worse in the United States, where deicing salts were heavily used to enhance winter road safety. Additionally, special equipment is necessary to install the heavy plates. Engineers have to search for alternative materials.

Recently, the repair of understrengthened or damaged reinforced concrete members by the external bonding of fiber Reinforced polymer materials has received considerable attention. Fiber reinforced polymers (FRP), or simply composites, wrapped or epoxy-bonded to the web or tension side of concrete, in the form of thin laminates or fabric, have been used successfully in the aerospace and automotive industry for two decades. They are generally constructed of high performance fibers such as carbon, aramid, or, glass which are placed in a resin matrix. By selecting among the many available fibers, geometry and polymers, the mechanical and durability properties can be tailored for particular application. This synthetic quality makes FRP a good choice for civil engineering application as well. The FRP offers the engineer an outstanding combination of properties, such as low weight (making them much easier to handle on site), immunity to corrosion, excellent mechanical strength and stiffness, and the ability of formation in very long length, thus eliminating the need for lapping at joints. Although FRP is a relatively expensive material compare to steel, the total rehabilitation project costs is about 20% (Mufti, et al., 1991) lower by using FRP than steel due to the savings in construction expenses. The FRP-strengthening technique has found wide attractiveness and acceptance among researchers and engineers today in many parts of the world.

1.2 Literature Review

The repair of reinforced concrete (RC) members by the external bonding of fiber reinforced polymers (FRP) is becoming increasingly popular in the construction industry. One of the FRP materials called FRP fabric or composite jacket receives more and more attention in recent years. Although not strong enough as compared with FRP laminates and plates, FRP fabrics are extremely easy to handle and can be applied to almost every kind of structure members. The new technique of strengthening reinforced concrete structures by externally bonded FRP fabrics was started in 1980s and has attracted researchers around the world since then.

1.2.1 Stress-Strain Behavior of Concrete Confined with FRP Fabrics.

Fiber reinforced polymer (FRP) composite materials have recently been applied to retrofit of structural members. Several composite Jacketing systems have been developed and validated in laboratory or field conditions. Matsuda et al. (1990) tested a system for retrofit of a bridge pier using unidirectional carbon fiber sheets wrapped longitudinally and transversely in the potential plastic hinge region or in the region of the main bar cutoff. The carbon fiber sheets were bonded to the concrete surface using epoxy resin. Priestley and Seible (1991,1993) have experimentally studied another composite wrapping system using E-glass fiber, which is more economical than carbon fiber. Their test results on 40% scale bridge piers wrapped with the glass fiber composite jacketing demonstrated significant improvement of seismic performance with increased strength and ductility. Saadatmanesh et al. (1994) has proposed a wrapping system using glass fiber composite straps for column retrofits. Seible et al. (1995) used an automatic machine to wrap carbon tows around a column to achieve continues jacketing. All these

successful retrofit systems can be categorized as in situ fabricated jacketing, which involved hand or automated machine placement of epoxy saturated glass or carbon fabrics on the surface of existing concrete structures. On the other hand, Xiao et al. (1996), Xiao and Ma (1997) researched a prefabricated jacketing system on retrofitting reinforced concrete columns. The prefabricated jacketing system has been found to have superior constructability in terms of the quality control and speed of the construction.

Despite the successful application of various composite jacketing systems in laboratory models as well as in situ structure members, research on the fundamental interaction mechanisms between the composite jackets and confined concrete is still very limited. To effectively predict the structural behavior of reinforced concrete members, such as beams, columns and slabs, confined with FRP fabrics, a detailed analytical stress-strain model should be set up and compared with the experimental results of structural members. Current design procedures are simple extensions of the confinement models developed for normal reinforced concrete. However, recent studies have demonstrated that such models may not be conservative for fabric jacketing members.

As one of the early attempts to model the FRP confined concrete, Fardis and Khalili (1982) proposed a hyperbolic function based on their limited test data on concrete cylinders wrapped with bidirectional FRP fabrics under uniaxial compression loading. Although the hyperbolic function was mainly derived from Ahmad's (1982) stress-strain model for comfined concrete, they did present a predictive equation for maximum stress and strain:

$$f'_{cc} = f'_{co}\left[1 + 4.1\left(\frac{f_{com} \cdot t}{d \cdot f'_c}\right)\right] \tag{1.1}$$

$$\varepsilon'_{cc} \approx 0.002 + 0.001\frac{E_{com} \cdot t}{d \cdot f'_c} \tag{1.2}$$

where f'_{cc} and ε'_{cc} = maximum strengths and failure strains of confined concrete; f'_{co} and ε'_{co} =unconfined concrete strengths and failure strains; f_{com} and E_{com} =strengths and modulus of the composite in the hoop direction; t is the thickness of fabrics; and d represents diameter of concrete core.

Cusson and Paultre (1995) modified Khalili's (1982) equation, wherein

$$f'_{cc} = f'_{co} + 2.1 f'_{co}\left[\frac{2 f_{com} \cdot t}{f'_{co}(d - 2t)}\right]^{0.7} \tag{1.3}$$

$$\varepsilon'_{cc} = \varepsilon'_{co} + 0.21\left[\frac{2 f_{com} \cdot t}{f'_{co}(d - 2t)}\right]^{1.7} \tag{1.4}$$

Nanni and Bradford (1995) investigated into the behavior of FRP-encased concrete with three different types of fiber wraps; namely, braide aramid FRP tape, filament-wound E-glass, and preformed hybrid glass-aramid FRP shells. They found out that the stress-strain model of Fardis and Khalili (1982) grossly underestimated the ultimate strains. They further suggested that the response of FRP-confined concrete could be modeled by a simple bilinear curve with a bend point at a strain of about 0.003. However, they did not develop an equation.

Rochette and Siere (1996) used an incremental finite-element approach to evaluate the response of fiber–wrapped square columns. They modeled concrete as an elastic-perfectly plastic material. Their analytical model compared favorably with their own test results, however did not provide a simple tool for the practitioners.

Karbhari and Gao (1997) developed an experimental test based on a variety of reinforcing fiber types, orientations, and jacket thickness. Their results showed a bilinear

stress-strain curve for concrete confined with fabrics rather than the two- part ascending and descending curves as seen in steel spiral reinforcement confined concrete. They summarized previous models from Khalili (1982), Mander (1988), and Cusson (1995) and presented a new empirical equation:

$$f'_{cc} = f'_{co} + 2.1 f'_{co} \left(\frac{2 f_{com} \cdot t}{d \cdot f'_{co}} \right)^{0..87} \tag{1.5}$$

$$\varepsilon'_{cc} = \varepsilon'_{co} + 0.01 \left(\frac{2 f_{com} \cdot t}{d \cdot f'_{co}} \right) \tag{1.6}$$

Although the above proposed equations attempt to address the prediction of ultimate behavior of FRP confined concrete, they fall short of modeling the true response of the composite that changes as the stress level increases further. Also, the detailed axial stress-lateral strain behavior and the effect of Poisson's ratio were not discussed in their work.

Based on thirty 6 in. (152.4mm) by 12 in. (304.8mm) cylindrical tests, Samamn, Mirmiran, and Shahawy (1998) pointed out that performance of a concrete column under axial loading is significantly enhanced by lateral confinement. It has been suggested that the concrete be referred as a restraint-sensitive material while the FRP fabric as a restraint-passive material. Before a certain stress level, the load is mainly carried by concrete alone. After that stress level, the ultimate behavior of the system is solely dependent on the confining properties of FRP fabric. Therefore the stress-strain behavior shows a complete bilinear behavior. In their research, a simple model was presented to predict the complete stress-strain behavior in both axial and lateral directions. This model is based on correction between the dilation rate of concrete and hoop stiffness of the restraining member. The parameters of the model are directly related to the material properties of the FRP jackets and concrete core. Their stress-strain curves favorably agree

with the results of the present studies, as well as tests by other FRP materials. The proposed equation is derived from the four-parameter relationship of Richard and Abbott (1975):

$$f_c = \frac{(E_1 - E_2)\varepsilon_c}{\left[1 + \left(\frac{(E_1 - E_2)\varepsilon_c}{f_o}\right)^n\right]^{1/n}} + E_2\varepsilon_c \tag{1.7}$$

where ε_c and f_c = axial strain and stress of concrete; E_1 and E_2 = first and second slopes in the stress-strain curve; f_o = reference plastic stress at the intercept of the second slope with the stress axis; and n = a curve-shaped parameter that controls the curvature of transition zone. This equation also applies to stress-lateral strain relationship.

Spoelstra and Monti (1999) represented a uniaxial model for concrete confined with FRP as well as steel jackets. The model, which is suitable to be inserted into fiber-type beam-column models, explicitly accounts for the continuous interaction with the confining device due to the lateral strain of concrete, through an incremental-iterative approach. The relation between the axial and lateral strains is implicitly derived through equilibrium between the confined concrete and the confining device. The model is compared with a set of experimental tests of stress-strain behavior and shows a good agreement. The stress-strain relationship is shown as follow:

$$f_c = \frac{f'_{cc} \cdot \left(\frac{\varepsilon_c}{\varepsilon_{cc}}\right) \cdot r}{r - 1 + \left(\frac{\varepsilon_c}{\varepsilon'_{cc}}\right)^r} \tag{1.8}$$

Where

$$r = \frac{E_c}{E_c - E_{sec}} \tag{1.9}$$

$$E_{sec} = \frac{f'_{cc}}{\varepsilon'_{cc}} \tag{1.10}$$

f'_{cc} and ε'_{cc} = maximum strengths and failure strains of confined concrete, E_c = concrete modulus of elasticity.

In Japan, Miyauchi, Inoue, and Kuroda (1999) carried out two sets of cylinder tests confined by the CFRP jackets under uniaxial loading. The unconfined concrete strength and the size of specimens were investigated as these two main factors influenced the behavior of the confined concrete. According to their test results, the stress-strain relationship of the confined concrete can be classified into two types: one is an increasing type which shows a bilinear behavior; the other one is a decreasing type which is more similar to the behavior of normal concrete. A simple stress-strain equation of both types was thus formulated.

Saafi, Toutanji and Li (1999) presented a detailed experimental study of concrete columns confined with FRP tubes. 36 FRP confined concrete cylinders were tested under compression. Test variables include type of the fiber, thickness of the tube, and concrete compressive strength. Results show that external confinement can significantly enhance the strength, ductility, and energy absorption capacity of the concrete. Equations to predict the compressive stress and ultimate strain of the confined concrete were developed based on Khalili (1982), Mander (1988). Also, the following expression was proposed to estimate the stress-strain response of the FRP confined concrete.

$$f = \frac{A\varepsilon}{1 + B\varepsilon + C\varepsilon^2} \tag{1.11}$$

$$A = E_1 \tag{1.12}$$

$$B = \frac{E_1}{f_a} - \frac{2}{\varepsilon_1} + \frac{E_2 E_1 \varepsilon_1}{f_a^2} \tag{1.13}$$

$$C = \frac{1}{\varepsilon_1^2} - \frac{E_1 E_2}{f_a^2} \tag{1.14}$$

where f and ε are the stress and strain, respectively, E_1 is the slope of the first zone, E_2 is the slope of intersection point between the two zones of the stress-strain response. f_1 and ε_1 are the axial stress and strain of the intersection point. Although this equation has a satisfactory agreement with the test results, it underestimates the ultimate load results of FRP confined concrete columns.

Xiao and Wu (2000) tested 36 concrete cylinders confined by CFRP fabric jackets with different unconfined concrete strengths and thickness of CFRP jackets. It is found that the concrete strength and confinement modulus, defined as the ratio of transverse confinement stress to transverse strain, are the most influential factors affecting the stress-strain behavior of confined concrete. The test results indicated that the failure of the confined concrete was mainly due to the rupture of the FRP jackets. In order to describe the main mechanical features of the confined concrete, they suggested a new bilinear stress-strain equation based on the theory of elasticity.

For the initial performance:

$$f_c = E_c \varepsilon_c + 14\left(\frac{f'_c \cdot d}{2t \cdot E_j}\right)^{0.8} f_r \tag{1.15}$$

For the stabilized performance after achieving the unconfined strength of concrete.

$$f_c = \alpha \cdot f'_c + k \cdot f_r \tag{1.16}$$

Where E_c and E_j = Modulus of Concrete and FRP jackets. f_r = Confinement stress of FRP jackets. α and k = Experimental parameter based on the tests.

Most recently, Fam and Rizkalla (2001) compared the behavior of the concrete confined by GFRP jackets to that of the concrete confined by steel plates and CFRP sheets. They evaluated the behavior of the GFRP confined concrete using a smooth and roughened GFRP/concrete interface. Test results indicated that loading of GFRP jackets reduced the confinement effectiveness. A simple analytical model was also presented to study the effects of fabric structure, interface condition between the shell and the concrete core, stiffness of the jackets, and failure models.

1.2.2 Flexural Strengthening of RC Beams by Externally Bonded FRP Fabrics

Strengthening with externally bonded FRP fabrics has been used to repair and retrofit many kinds of structures. Currently, this new technique has been applied to strengthen such structures as columns, beams, walls, slabs, etc. The use of external FRP fabrics may be classified as flexural strengthening, improving the ductility, and shear strengthening.

A lot of research work has been conducted to study the repair of RC beams using steel plates and FRP stripes. However, researches on flexural strengthening using FRP fabric sheets or jackets only started recently. In the late 1990's, several experiments were conducted to strengthen both virgin and precracked RC beams using FRP composite sheets. Due to its super light weight and superior mechanical properties, FRP fabric sheets and jackets quickly received much attention among various FRP materials.

Arduini and Nanni (1997) did the first research on bending behavior of RC beams strengthened with carbon FRP (CFRP) sheets. 18 RC beams, half virgin and half precracked, using CFRP composite sheets were carried out in situ. In the research, several variables were investigated, including two CFRP materials, two concrete surface preparations, two different cross sections, and different numbers and location of CFRP

plies. The test results showed that the effect of CFRP strengthening was considerable, but the effect of some of the tested variables was modest. Also, a modified analytical model based on Arduini's early work (1991) has been extended to simulate the load-deflection behavior as well as the failure mode of precracked RC specimens. Most important features of Arduini's model are nonlinear constitutive relationship for concrete in compression and tension, concrete-adhesive interface properties, and the effects of precracking and unloading. The agreement between the experimental and analytical results is quite satisfactory.

Spadea, Bencardino, and Swamy (1998) tested four beams with and without CFRP sheets. The CFRP sheets were bonded on the tension face under four-point bending over a span of 15.74ft. (4.8m). Two of the beams were also provided with CFRP plates on the side with carefully designed external anchorage at the ends. The tests showed that bonding the CFRP sheet on the tension surface of a RC beam, without consideration of the end-anchorage stresses could lead to a significant degradation in the structural response of the confined beam. Carefully design external anchorage, on the other hand, could lead to an increase in load capacity of up to 70% and also substantial regain of its structural ductility.

CangaRao and Vijay (1998) studied the pure bending behavior of concrete beams continuously wrapped with CFRP fabric based on their various test data. In their research, 24 RC beams strengthened with CFRP wraps were tested under four-point bending. The improvements in flexural as well as ductility are considerable according to the test results. In addition, bending test results from the wrapped beams were also compared with those of other identical concrete beams strengthened with bonded steel

plates. Some factors governing the percentage increase in the ultimate strength were discussed by using four different CFRP configurations. All the wrapped beams were analyzed by considering traditional force equilibrium equations and the analytical results were compared with the experimental results.

Pareek, Kurata, and Sotoyama (1999) also conducted several experiments to obtain fundamental data on flexural strengthening of RC beams bonded by CFRP fabric. In their study, 5 types of CFRP and 1 type of aramid-fiber jackets were applied to 7 RC beams. Also, different bonding methods of continuous CFRP fabric to RC beams were examined. The flexural strength, load-deflection behavior, strain distribution over CFRP jackets, stiffness and failure modes of RC beams have been taken into consideration. According to their test results, the U-shaped bonding method was the most effective method in improving the flexural strength of RC beams.

Maeda, Komaki, and Tsubouchi (2001) pointed out that when CFRP was adhered to the lower part of RC beams for the purpose of bending strengthening, delamination of CFRP might cause insufficient tensile strength and brittle failure. In order to solve this problem, they installed a new flexible layer with excellent deformability between the CFRP and Concrete surface. After the bending test, it showed that the flexible layer alleviated stress concentration of CFRP fabric and improved the bond behavior. Therefore, they identified that the delamination resistance could be improved by these effects.

El-Mihilmy and Tedesco (2000) developed a simple and direct analytical procedure for evaluating the ultimate flexural capacity of FRP strengthened RC beams. The procedure was derived from the equilibrium equations and compatibility of strains

and was applicable to both singly and doubly reinforced concrete sections. The procedure was also validated by comparisons with results of experimental data from the literature. They further established upper and lower limits of FRP that may be bonded to a RC beam to ensure the ductile behavior of RC beams.

Bonacci and Maaje (2001) compiled and analyzed the current experimental database to study the behavior trends of RC beams strengthened with externally bonded FRP. A total of 127 specimens from 23 separate studies were included in the database. An analysis of trends in failure modes, strength gain, and deformability was conducted. They found out that failure by debonding of FRP was prevalent among specimens. Also, most specimens with external reinforcement added showed strength increase of 50% or more in combination with considerable deflection capacity. They further suggested that future research on FRP boding should focus on conditions that were similar to what was observed in the field, including the effects of sustained load during repair as well as corrosion damage.

White, Soudki, and Erki (2001) studied the response of RC beams strengthened with CFRP wraps subjected to a high rate of loading. 9 RC beams were tested under four different loading schedules. Some beams were subjected to 1 to 12 cycles of loading. They further presented a finite-element layered analysis to predict the moment-curvature response of CFRP strengthened RC beams. The model included the effects of strain rate and correlated well with the experimental data.

Shahawy, Chaallal, and Beitelman (2001) tested eight 20-ft (6.1m) long precracked RC T-girders reinforced with CFRP wraps. The test results demonstrated that the level of preload prior to the installation of CFRP wraps did not affect the overall

behavior of the specimens. It was also clear that partially wrapped members exhibited less ductility and strength than the corresponding fully wrapped members. Therefore, the use of partial wrapping should only be used when full wrapping was not feasible.

In order to provide adequate safety from brittle failure, Yost and Gross (2002) developed a flexural design methodology for RC beams reinforced with FRP. In their research, safety for FRP reinforced flexural members were evaluated based on total material strain energy density (SED) at the critical cracked section. A proposed minimum energy factor of safety (EFS) of 25 was derived from a companion analysis of under-reinforced steel beams. They concluded that the minimum EFS for FRP reinforced members was only achievable provided the service stress in the concrete was restricted to $0.35 f'_c$. Therefore, high strength concrete was recommended to make more efficient of the FRP tensile strength.

More recent experiment was done by Sheikh and Derose (2002). Nearly full-scale wall-slab specimens and two RC beams were tested using CFRP and GFRP fabric wraps. Test results showed that FRPs were effective in strengthening for flexural as well as shear. Over-reinforcing in flexural resulted in shifting the failure to shear mode. Available analytical procedures and building code provisions were founded to simulate the behavior of specimens retrofitted with FRP reasonably well.

Alagusundaramoorthy, Haril and Choo (2003) studied the effectiveness of both CFRP sheets and fabrics in the flexural strength of concrete beams. Four-point bending flexural tests were conducted up to failure on nine concrete beams strengthened with different layouts of CFRP sheets and fabrics. An analytical procedure, based on compatibility of deformations and equilibrium of forces, was presented to predict the

flexural behavior of beams strengthened with CFRP sheets and fabrics. Comparison was made between the test results and the analytical calculations.

1.2.3 Behavior of RC Columns Confined with FRP Fabric

Reinforced concrete columns, particularly those built prior to the 1970's, often have little confinement to the concrete core or lateral support to the longitudinal reinforcing bars. Poorly confined columns are recognized to behave in a brittle manner, exhibiting little deformation capacity. Increased loads, column deterioration, or seismic retrofit may require that additional confinement be provided to ensure adequate force and deformation capacity.

In recent years, FRP composite jackets have been used to provide additional confinement to RC compression members. A number of studies, including Demers (1996), Harmon and Slattery (1992), Howie and Kharbari (1994), Eckel (1993), Labossiere (1992), Nanni (1992), and Rochette and Labossiere (1996), have been conducted investigating the axial behavior of concrete columns with FRP jackets. These studies have all indicated that FRP jackets enhance the compressive strength of the confined concrete. However, most of the studies were carried out on plain concrete cylinders. The use of such small-scale specimens results in much stiffer jacket that needs retrofit application. Large-scale or even full-scale column specimens as well as detailed analytical model need to be investigated.

One of the earliest studies on large-scale RC columns confined by FRP jackets was conducted by Seible and Priestley (1997). They developed a detail design method to select FRP jacket thickness. Their method was based on three typical column failure modes, including shear failure, Flexural hinge confinement failure, and lap-splice

clamping. Furthermore, the FRP jackets designs were validated through large-scale bridge column model tests at the Powell Structural Research Laboratories. The test results showed this design guideline was an effective method which could be applied to other confining materials.

Xiao and Ma (1997, 1999) conducted a series of tests to study the seismic retrofit of RC circular columns using prefabricated composite jacketing. The first three 1:2 scale model columns were tested under constant axial loads and cyclic horizontal forces in a single curvature condition. The retrofitted columns showed a significant improvement in seismic performance. They also presented an analytical model, which was based on the moment curvature analysis by considering the bond slips of the lap-spliced longitudinal bars. After 2 years, another three 1:2 RC columns were tested at the same condition but using cyclic shear forces in a double curvature. The test results showed the similar effect as the fist three columns. The presented design analysis was also validated by both test results.

Toutanji and Balaguru (1998) presented the results of an experimental study on the performance of large concrete specimens confined with both CFRP and GFRP composite sheets. The experiments were carried out in the three different environments, including room temperature, wet-dry exposure, and freeze-thaw condition. Test results showed that in the wet-dry condition, specimens wrapped with CFRP experienced no reduction in strength and ductility, whereas samples wrapped with GFRP experienced reduction. In the case of freeze-thaw exposure, both CFRP and GFRP samples experienced significant reduction in strength and ductility.

The previous studies are mainly concentrated on circular columns under concentric loading. However, in field application, there is no column that is under perfect concentric loading. Therefore, Parvin and Wang (2001) conducted an experimental study on the behavior of FRP jacketed square concrete columns subjected to eccentric loading. In this research, nine large square columns wrapped with different layers of CFRP fabric were test subjected to eccentric loading. The effects of various eccentricities were also examined. They further developed a nonlinear finite-element analysis to compare with the test results. They suggested that although FRP jackets can greatly enhance the strength and ductility of RC columns under eccentric loading, a smaller enhancement factor should be used in this case.

Corrosion of RC columns is also a challenging problem in column retrofitting. Pantazopoulou, Bonacci, and Sheikh (2001) presented an experimental parametric study on repairing corrosion damaged RC columns with FRP jackets. In their study, several small-size RC columns were subjected to accelerated corrosion conditions and repaired by both CFRP and GFRP fabrics. The efficacy of each repair system was evaluated by (1) assessing the post-repair corrosion resistance of the specimens; and (2) the mechanical strength and ductility enhancement under concentric loading.

Wang and Restrepo (2001) proposed an analytical method for evaluating the short-term axial load-deformation behavior of RC columns confined with GFRP jackets and steel hoops. Six columns with different cross sections were tested under concentric loading and showed satisfactory agreement with the analytical model. They also presented a closed-form equation that can be used in hand calculation.

Pessiki, Harries, and Kestner (2001) presented a very detailed experimental study of the axial behavior of concrete columns confined with FRP jackets. A total of sixteen small-scale plain concrete specimens and eight full-scale RC columns using CFRP jackets were tested under concentric loading. Improvement in the axial load-carrying and deformation capacities of FRP jacketed concrete members were reported. Several important factors, including shape of the section, transverse dilation, and effective confined regions, were identified and discussed.

In order to effectively upgrade current obsolete codes on FRP jacketing design of bridge piers. Monti and Santini (2001) proposed a design equation to determine the optimal thickness of FRP jackets. A parametric study based on a fiber-section model equipped with a newly developed FRP-confined concrete model was performed. The study showed that the equation, despite its simplicity, yields excellent prediction of the ductility increase obtained through FRP wrapping. The design equation was also used in available experimental test and has been demonstrated to be very effective.

The Federal Highway Administration (FHWA) design procedure for columns confined with steel and FRP materials is based on six critical assumptions. In the purpose of validating the six assumptions, most recently, Harmon, Gould, and Ramakrishnan (2002) presented a series of structural models for predicting the behavior of circular confined concrete columns subjected to concentric loading. The detailed models, including crack path model, moment curvature model, force displacement model, and shear model, were discussed using principles of mechanics. Also, experimental results using FRP jacketed concrete columns were compared with analytical models. The results

from this process suggest that the six assumptions are not always consistent with the behavior. The simplified model is proposed as the basis of future design procedures.

Pantelides and Gergely (2002) presented analysis and design procedures for a CFRP composite seismic retrofit of a reinforced concrete three-column bridge bent. The CFRP jackets was designed using performance-based criteria to provide a target displacement ductility based on seismic retrofit measures for the columns, bent cap, and bent cap-column joints. In situ test results showed that the seismic retrofit was successful, and the bridge bent strengthened with CFRP composite reached a displacement ductility level and doubled the hysteretic energy dissipation of the as-built bent. A description of the CFRP composites layout and validation of the design assumption from the experimental results was also presented in this research.

1.3 Objectives of Proposed Research

The new technique of using FRP materials to repair and strengthen various concrete members is becoming more and more popular in structural retrofitting field. Among all the confining materials, FRP fabric jackets are identified as an effective way to enhance the strength and ductility of concrete members due to its superior mechanical properties. In order to take full advantage of this application, detailed structural behavior of confined concrete using FRP jackets need to be investigated. Therefore, both analytical and experimental studies become an urgent task in this field.

However, most of current researches are mainly focused on the experimental study of confined concrete members. The detailed analytical model, such as complete stress-strain relationship is limited, and to a certain degree, contradictory. Also, both

experimental and analytical studies of FRP confined large-scale structure member, such as beams and columns, are very limited. Especially no one has studied the behavior of biaxially loaded concrete columns confined with FRP jackets. Besides some of previous theoretical analysis for confined RC beams and columns are solely based on traditional force equilibrium and they are only suitable to an empirical design prediction. The design approach for concrete structures with CFRP fabrics is far from complete and straightforward.

To further understand the structural behavior of various structural members confined with CFRP fabric jackets, the following objectives of this research have been established:

1. To investigate the compressive behavior of normal concrete cylinders confined with CFRP fabric and steel hoops under axial loading.
2. To derive complete compressive stress-strain relationship for CFRP confined concrete cylinders under axial loading.
3. To investigate the flexural behavior of RC beams confined with CFRP fabric jackets on the tension face.
4. To propose an analytical method to estimate the flexural strength of the RC beams confined with CFRP jackets.
5. To investigate the compressive behavior of biaxially loaded RC columns confined with CFRP fabric jackets.
6. To modify existing finite-segment computer program for biaxilly loaded RC columns using proposed stress-strain relationship and also compare with the experimental test results.

1.4 Originality of Proposed Research

Considering that the rehabilitation of the infrastructure is an important matter for the US, the proposed research is expected to generate both the scientific knowledge and

engineering method for the application of CFRP fabric in the infrastructure field. With the developed stress-strain model for CFRP-confined concrete, an analytical model based on compatibility of deformation and equilibrium of forces is used to study the flexural behavior of FRP-confined RC beams. Also, the proposed research presents a modified finite-segment analysis for 1/4-scale RC columns under biaxial loading.

The proposed experimental test will help understand the behavior of strengthened concrete beams and columns; it will also be used to verify the validity of previous proposed analytical model. The proposed research will greatly increase the applicability of the strengthening methods with externally epoxy-bonded CFRP fabric. It will also broaden the knowledge related to the reinforced concrete structures as well.

The originality of the proposed research can be found in the following aspects:

1. The behavior of normal concrete specimens with different strength confined by different layers of CFRP fabric jackets was investigated. Steel hoop effect, aggregate size effect, and the direction effect of the fabrics were also studied in this research.

2. In the proposed research, a complete stress-strain relationship was presented for normal concrete confined with CFRP fabrics based on the experimental tests.

3. Large-scale RC beams were tested during the research. In this research, not only beams with different layers of fabric were studied, but also beams with different fabric-wrapping direction were investigated as well.

4. An effective analytical model based on compatibility of deformation and equilibrium of forces is used to predict the flexural behavior of CFRP-confined RC beams.

5. The proposed research modifies the existing computer analysis for biaxially loaded RC columns using the proposed stress-strain model developed in this research. Also, biaxially loaded RC columns confined by CFRP jackets are tested to verify the proposed analytical model.

CHAPTER 2

COMPRESSIVE STRESS-STRAIN BEHAVIOR OF NORMAL CONCRETE CONFINED WITH CFRP FABRICS

2.1 Introduction

In recent years, normal concrete strengthened or repaired with Carbon Fiber Reinforced Polymer (CFRP) fabrics has gained acceptance from engineers and researchers. Many old or damaged building and bridge members have been using CFRP wrapping as a new and efficient retrofit measure. With the increasing application of CFRP fabrics on concrete structures, more information on the properties of the fabric-strengthened concrete is needed.

For a rational design of concrete structure, the complete stress-strain curve of its material becomes a necessity. Since concrete is strengthened with CFRP fabrics, a new stress-strain relationship for the confined concrete is needed. Nowadays, most researches consider the CFRP, adhesive and the concrete as a whole system (confined concrete). And a number of empirical expressions for the stress-strain relationship of this confined concrete have been proposed and can be found in the literature (see Chapter I). However, Most of these expressions only use several linear equations to describe a complete stress-strain behavior, which are not accurate and sometimes overestimate the compressive strength. An effective stress-strain expression for fabric-confined concrete is still needed studying.

In this research, an extensive experimental study about CFRP fabric-wrapped normal concrete was carried out at the NJIT Concrete Laboratory. To fully study the stress-strain behavior of normal concrete confined with CFRP fabrics, more than one

hundred concrete cylinders were cast and tested. Several test factors such as thickness of the fabric, concrete strength, hoop effect and aggregate size were studied during the tests. Based on the test results, a uniform stress-strain expression was proposed and verified with the test results of present and other experimental work.

2.2 Experimental Scheme

2.2.1 Material

2.2.1.1 Carbon Fiber Reinforced Plastic. Sika Corporation, USA, provided the CFRP used in this research. SikaWrap Hex 230C, which is a kind of woven composite fabric, was employed in this study. CFRP fabric is unidirectional and has a longitudinal tensile strength of 140 ksi (960 MPa). The lateral strength of the fabric is negligible. The fabric strips are elastic until break. The represented properties are given in Table 2.1.

The advantages of the CFRP are: very high strength, outstanding fatigue resistance, non-corrosion, excellent alkali-resistance, low weight, low thickness, available in any length, economic to apply. The disadvantage is its relatively high material cost.

2.2.1.2 Epoxy Resin. The epoxy resin (Sikadur-330) used in this research is also provided by Sika, USA. The epoxy consists of two components; part A is in white, part B is in dark gray. The mix ratio of part A and part B is four to one by weight. The properties are also given in Table 2.1.

The advantages of this epoxy can be listed in the following: high mechanical strength, high creep resistance under permanent load, high temperature resistance, long open life, easy to mix and apply, solvent free. This Epoxy can be applied to slightly damp

concrete surfaces. Also the Epoxy exhibits non-sag in vertical and overhead applications, sets without tackiness, rapid curing even at low temperatures, and shrinkage-free curing.

Table 2.1 Properties of Sika's CFRP System

	SikaWrap Hex 230C	Sikadur -330
Tensile strength	>140 ksi (965 MPa)	4.35 ksi (30 MPa)
Elongation at break	1.33%	1.5%
E-modulus	10600 ksi (73034 MPa)	-------
Flexural Modulus	-------	551 ksi (3800 MPa)
Thickness	0.013 inch (0.33 mm)	-------
Strength per inch width	1,870 lbs./layer 8,322 N/layer	-------
HDT	-------	118F (47C)
Adhesive strength on concrete	-------	>0.3 ksi(concrete failure) (2.1 MPa)

2.2.1.3 Concrete Cylinders. The materials consisted of Type I cement satisfying with ASTM 150, sand from local source, crushed stone with maximum aggregate size of 3/8 in. (9.53mm) and 3/4 in. (19mm). The mixture designs of the concrete specimens including two different strengths are listed in Table 2.2.

2.2.1.4 Steel Hoops. The tie confinement with circular hoops was constructed by 12-gage steel wires (f_y =66.1 ksi or 455 MPa). The circular hoops at different spacing of 2 inches (50.8mm) and 4 inches (101.6mm) were put into 4 in. (102mm) by 8 in. (203mm) plastic mold. In order to fix the tie confinement in the position, the circular hoops were connected with one another by 22-gage soft wire as shown in Appendix B.3.

Table 2.2 Mix Designs of Concrete Specimens

Concrete Compressive Strength	Water /Cement ratio	Cement (lbs/ yd^3)	Stones (lbs/ yd^3)	Sand (lbs/ yd^3)	Water (lbs/ yd^3)
3000 psi (20.67 MPa)	0.70	480 (2791 N/m^3)	1763 (10252 N/m^3)	1433 (8332 N/m^3)	300 (1744 N/m^3)
5000 psi (34.45 MPa)	0.48	708 (4117 N/m^3)	1728 (10048 N/m^3)	1184 (6884 N/m^3)	340 (1977 N/m^3)

2.2.2 Mixing, Casting and Curing

To minimize scattering, all specimens followed the same procedures for material mixing, casting, and curing.

All concrete materials described in the previous section were mixed by a rotary mixer. The 4 in. (102mm) by 8 in. (203mm) cylinder molds were prepared and lubricated with oil before the concrete was poured. When mixed with steel hoops, the hoops were put into the mold and attached to the surface of the mold by scotch tapes. The mixing sequence used was as follows: Firstly, the coarse and fine aggregates were loaded into the mixer and dry mixed for 2 to 3 minutes. Next, the cement was added and mixed for another 1 to 2 minutes. Then, 80% of the water was added to cementitious material. The remainder of 20% of the water was last added after 2 to 3 minutes. After all the materials were added, the small rotary mixer had to continue mixing for few minutes, until a homogeneous mixture was achieved. The resulting mixture was then molded into 4 in. (102mm) by 8 in. (203mm) cylindrical specimens.

During casting, both table vibrator and steel bar were used to compact the specimens. All specimens were demolded after 24 hours and cured in a standard curing room for 28 days to achieve expected strength.

2.2.3 Installation of CFRP Strengthening System

Proper procedure and quality control of installation of carbon fiber strips is critical to the successfulness of CFRP strengthening system. The bond strength of the CFRP strengthening system in this research was significantly affected by the surface conditions of the specimens.

2.2.3.1 Surface Treatment. The concrete substrate to be strengthened has to be sound and clean. Sandpaper and sand blasting was utilized to treat the concrete surfaces in this research. The uneven concrete on all specimen surfaces was sanded using sandpapers. Some hard part was removed by the sand blasting. All the specimens were washed and treated carefully before the epoxy was applied.

2.2.3.2 Bonding of Composite Materials to Cylinders. The epoxy was mixed by hand according to the ratio of 4:1 by weight. The epoxy was applied uniformly to both carbon fiber and concrete substrate. The fabric wraps were compressed to the concrete substrate with an ordinary paint roller. The extra epoxy was squeezed out and removed. The thickness of the epoxy was controlled to be about one twentieth of an inch (1.2 mm) in this research. The specimens were cured at room temperatures for at least 24 hours before testing. The whole procedure can be seen from Figure 2.1.

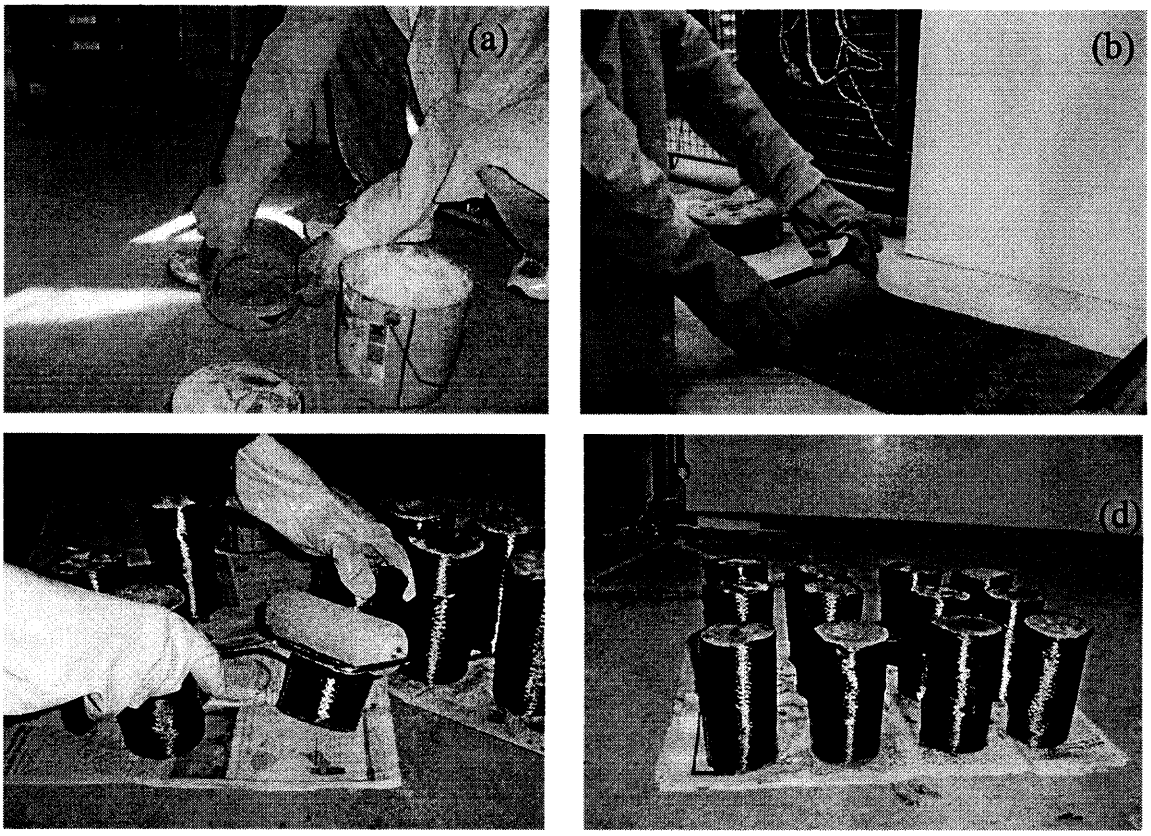

Figure2.1 Installation of CFRP fabrics to the cylinders.
(a) Mixing epoxy; (b) Wrap the specimen with fabrics;
(c) Consolidate the fabrics jacket; (d) let the specimens dry for 24 hours.

2.2.4 Experimental Setup

The stress-strain curve of concrete is measured in the NJIT Concrete Laboratory by a uniaxial compression test.

A total of 129 4 x 8-in (102× 203-mm) cylinders were tested in NJIT Concrete Lab. The details of specimens are shown in Table 2.3. Before testing, specimens were wrapped with different CFRP fabric layers and sawed at both ends to get flat and strong surface and then capped with a sulfur compound at both ends. The final height was 8 inches (203 mm). Most concrete cylinders were tested in a closed-loop servo hydraulic

MTS 815 concrete testing machine, which has 1 million lbs (4450 kN) loading capacity. Two extensometers at the middle half of the cylinder height were used to get strain and two strain values obtained were averaged. Another extensometer was wrapped around the cylinder to obtain the circumstantial strain. An electronic data acquisition system was used to record loads and corresponding strains. The split tension tests were carried out using MTS 810 material testing machine. The experiment setup for both split tension test and compression test can be seen from Appendix B.1 and B.2.

Table 2.3 List of Concrete Specimens

Concrete cylinders	Layers of fabric	Expected Strength (f'_c) (psi)	Numbers of specimens	Stress-strain curve	Steel hoop
compression test A	No	3000 (20.67 MPa)	6	Yes	No
	1 layer	3000 (20.67 MPa)	6	Yes	No
	2 layers	3000 (20.67 MPa)	6	Yes	No
	3 layers	3000 (20.67 MPa)	6	Yes	No
compression test A	No	5000 (34.45 MPa)	6	Yes	No
	1 layer	5000 (34.45 MPa)	6	Yes	No
	2 layers	5000 (34.45 MPa)	6	Yes	No
	3 layers	5000 (34.45 MPa)	6	Yes	No
compression test A	No	5000 (34.45 MPa)	8	Yes	Yes
	1 layer	5000 (34.45 MPa)	8	Yes	Yes
	2 layers	5000 (34.45 MPa)	8	Yes	Yes
	3 layers	5000 (34.45 MPa)	8	Yes	Yes
compression test A	No	5000 (34.45 MPa)	3	No	No
	2 layers *	5000 (34.45 MPa)	5	Yes	No
compression test B	No	5000 (34.45 MPa)	3	No	No
	1 layer	5000 (34.45 MPa)	3	Yes	No
	2 layer	5000 (34.45 MPa)	3	Yes	No
split tension test	No	3000(20.67 MPa)	4	No	No
	1 layer	3000 (20.67 MPa)	4	No	No
	2 layers	3000 (20.67 MPa)	4	No	No
	3 layers	3000 (20.67 MPa)	4	No	No
split tension test	No	5000 (34.45 MPa)	4	No	No
	1 layer	5000 (34.45 MPa)	4	No	No
	2 layers	5000 (34.45 MPa)	4	No	No
	3 layers	5000 (34.45 MPa)	4	No	No

* fabric wrapped at two different directions.

2.3 Experimental Results

Both compression test and split tension test were carried out to investigate into the stress-strain behavior of the fabric-confined concrete. Two different coarse aggregate sizes were used in this research. 3/4 inch (19mm) aggregates were used for compression test A and split tension test. Since all the column specimens tested in this research uses smaller aggregates. 3/8 inch (9.5mm) aggregates were thus used in the compression test B to study the effect of coarse aggregate size on the stress-strain behavior of the confined concrete.

2.3.1 Split Tension Test Results

The true tensile strength of the concrete is too difficult to determine. One common approach has been to use the splitting tensile strength f_{ct} to determine the tension strength of normal concrete. The split tension test uses a standard concrete cylinder placed on its side in the testing machine. A compressive line-load is applied uniformly along the length of the cylinder, with two wooden plates supported along the full length of the bottom and the top of the cylinder. The line-load produces a transverse tensile stress, and the cylinder will split in half along a diameter when its tensile strength is reached. This tensile strength is referred as the splitting tensile strength f_{ct} and can be calculated as by the following expression:

$$f_{ct} = \frac{2P}{\pi l d} \tag{2.1}$$

Where f_{ct} = Splitting tensile strength

P = Applied load at splitting

l = Length of the cylinder

d = Diameter of the cylinder

According to the ACI Code Commentary, for normal-weight concrete, the split tensile strength is approximately equal to 6-8$\sqrt{f_c'}$.

Table 2.4 Split Tension Test Results

Specimens Strength	Fabric layers	Load1 (kips)	Load2 (kips)	Load3 (kips)	Load4 (kips)	Average (kips)	f_{ct} (psi)	$\frac{f_{ct}}{\sqrt{f_c'}}$
3000psi (21 MPa)	No	22.3 (99kN)	20.8 (93kN)	21.0 (93kN)	21.6 (96kN)	21.4 (95kN)	426.3 (2.9MPa)	7.8
	1layer	37.0 (165kN)	34.6 (154kN)	35.8 (159kN)	34.0 (151kN	35.3 (157kN)	703.5 (4.8MPa)	12.8
	2layers	45.7 (203kN)	44.0 (196kN)	45.1 (201kN)	43.9 (195kN	44.7 (199kN)	889.0 (6.1MPa)	16.2
	3layers	47.2 (210kN)	46.0 (205kN)	47.0 (209kN)	45.9 (204kN	46.5 (207kN)	926.1 (6.4MPa)	16.9
5000psi (34 MPa)	No	28.6 (127kN)	28.7 (128kN)	27.6 (123kN)	27.5 (122kN	28.1 (125kN)	559.0 (3.9MPa)	7.9
	1layers	51.1 (227kN)	45.7 (203kN)	49.9 (222kN)	45.2 (201kN	48.0 (214kN)	954.7 (6.6MPa)	13.5
	2layers	57.0 (254kN)	55.2 (246kN)	61.9 (275kN)	59.2 (263kN	58.3 (259kN)	1160.88 (8.0MPa)	16.4
	3layers	63.9 (284kN)	59.4 (264kN)	59.8 (266kN)	60.0 (267kN	60.8 (271kN)	1210.04 (8.3MPa)	17.1

Note: d=4 inch (102mm); l=8 inch (203mm)

To obtain the tensile strength of the fabric-confined concrete, twenty-four 4 in (102mm) by 8 in. (203mm) cylinders with different compressive strength were wrapped with different layers of fabric and tested using MTS 810 machine. The test setup can be seen from Appendix B. Split tension test results for CFRP strengthened concrete cylinders are listed in Table 2.4. It shows that CFRP fabric has significantly increased the tensile strength of both 3000 psi (20.67 MPa) and 5000 psi (34.45 MPa) concrete cylinders. As the layers of fabric wrapping increase, the tensile strength also increases.

The tensile strength of concrete cylinders wrapped with three layers fabric is almost twice as much as that of the unconfined one. From the table, the concrete cylinders with higher unconfined compressive strength also show higher tensile strength although the ratio between the tensile strength and corresponding unconfined compressive strength seems to be constant. Therefore, thickness of fabric jackets and unconfined compressive strength can be considered as two critical factors that determine the ultimate tensile strength for CFRP strengthened concrete.

2.3.2 Compression Test Results

The compressive behavior of the normal concrete confined with CFRP fabric was investigated in this study. The concrete without CFRP wrapping is called herein as normal concrete and the concrete with CFRP fabric wrapped is termed as confined concrete. The main objective of this study is to obtain stress-strain curves of the confined concrete and compare with those of the normal concrete. The experimental results are discussed in the following aspects.

2.3.2.1 Axial Stress-Strain Relationship. Average axial stress versus axial and lateral strains of confined concrete are shown in Figure 2.2 and 2.3, respectively, for specimens with different unconfined concrete strengths. The average axial stress-strain relationship for unconfined concrete cylinders is also shown in Figure 2.2-2.3. As shown in the figure, the initial portions of stress-strain responses of the confined concrete essentially follow the curves of unconfined concrete. After achieving the approximate unconfined concrete strength, the axial stress-axial strain as well as axial stress-lateral strain relationships of most specimens start to get softened and eventually exhibit an almost linear behavior until sudden failure due to the rupture of CFRP jackets. Such

"bilinear" behavior can be seen from the test results of both 3000 psi (20.67 MPa) and 5000 psi (34.45 MPa) concrete cylinders. The ultimate behavior of confined concrete is solely dependent on the material properties of the CFRP jackets. Although some specimens exhibit a brittle descending part of stress-strain curve, the postpeak behavior is not very obvious as compared with that of unconfined normal concrete. The detailed stress-strain curves for all the cylinders are listed in Appendix C. Other axial stress-strain behavior is discussed below.

Compressive Strength:

Figure 2.2-2.3 and Table 2.5 show that the CFRP fabric jackets have significantly increased the compressive strength of confined concrete. Some specimens confined with three layers Fabric almost achieve 13,000 psi (89.57 MPa), which is three times as much as that of the unconfined concrete. Also, the compressive strength increases a lot as the layers of fabric increase, which means the thickness of the CFRP jackets is a critical factor to the strength of confined concrete. Comparing the stress-strain relationships of 3000 psi (20.6 MPa) and 5000 psi (34.4 MPa) concretes, one finds the specimens with higher unconfined compressive strength exhibit a higher confined strength. However, the difference is not very much, which further shows that the ultimate strength of the confined concrete is mainly dependent on the properties of fabric jackets.

Ductility:

Observing the stress-strain curves of Figure 2.2-2.3, one can find out that the overall ductility of confined concrete is considerably improved by using the CFRP jackets. From

Table 2.5, the ultimate strain of the concrete confined with three layers of fabrics almost achieves 0.02, which is very impressive as compared with the normal concrete without fabric confinement. Also from Figure 2.2 and 2.3, the area under the stress-strain curves of both 3000 psi (20.6MPa) concrete and 5000 psi (34.4MPa) concretes are significantly increased with the help of the CFRP fabrics, which further shows the energy absorption and ductility of the confined concrete are well enhanced by the CFRP fabrics as well. Also, the CFRP confinement increases the ultimate axial strain and at the same time reduces the lateral strain, which means the dilation rate of the cylinders has been limited by the CFRP jackets. Therefore the thickness of the CFRP jackets and unconfined compressive strength can be considered as the important factors to determine the ductility of confined concrete. Note that the ultimate strain and the overall ductility of the confined concrete seem to decrease, as the unconfined compressive strength increases.

Table 2.5 Average Compression Test Results for CFRP Strengthened Specimens

Specimen		Max stress (psi)	Ultimate axial strain	Ultimate lateral strain	Chord modulus E_c (psi)	Initial modulus E_0 (psi)
3000psi (21MPa) normal concrete	control	2944.6 (20.3MPa)	0.0052	0.0135	3053124 (21036MPa)	3277137 (22579MPa)
	1 layer	7480.5 (51.5MPa)	0.0132	0.0100	1690107 (11645MPa)	3907987 (26926MPa)
	2 layers	9470.1 (65.2MPa)	0.0165	0.0077	1415310 (9751MPa)	3712382 (25578MPa)
	3 layers	11936.8 (82.2MPa)	0.0197	0.0055	1310048 (9026MPa)	3363131 (23172MPa)
5000psi (34MPa) normal concrete	control	5014.4 (34.5MPa)	0.0088	0.0135	2751460 (18958MPa)	2953907 (20352MPa)
	1 layer	8197.0 (56.5MPa)	0.0099	0.0087	3200174 (22048MPa)	3729933 (25699MPa)
	2 layers	9947.8 (68.5MPa)	0.0125	0.0061	4888012 (33678MPa)	5713462 (39366MPa)
	3 layers	12334.8 (85.0MPa)	0.0174	0.0059	4955946 (34146MPa)	7201387 (49618MPa)

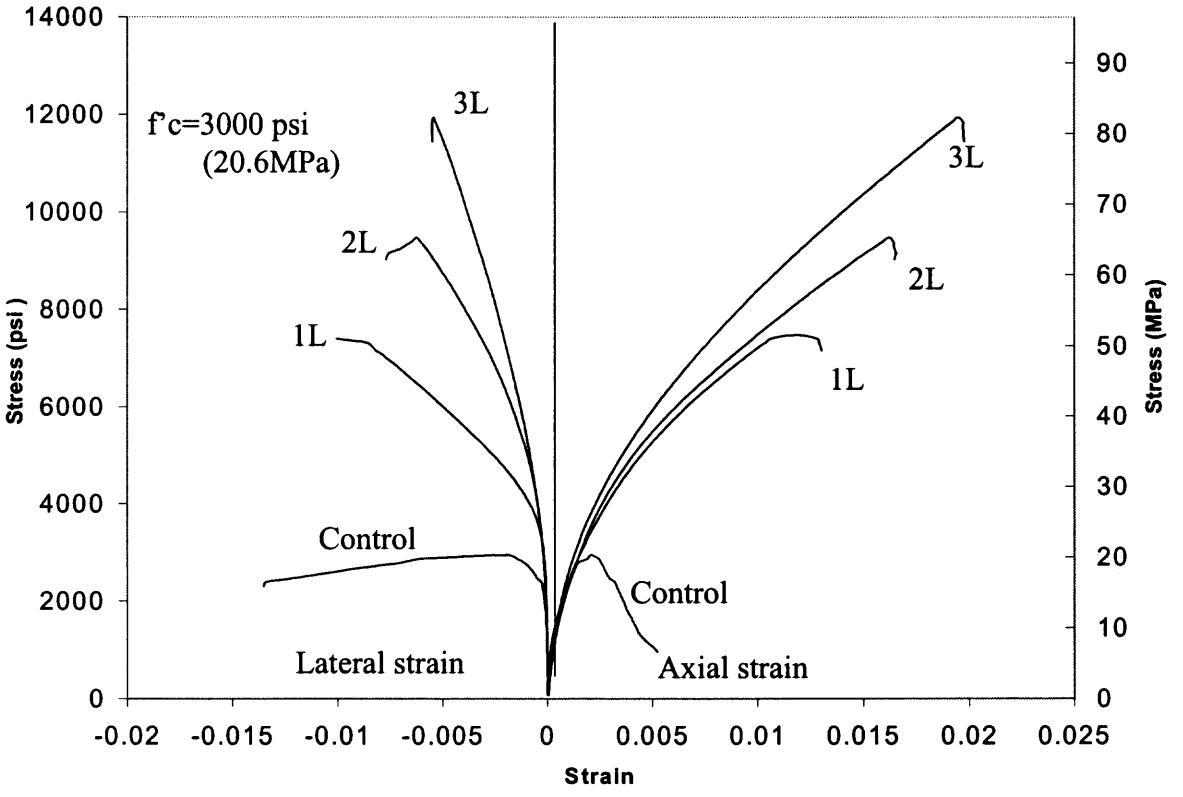

Figure 2.2 Axial stress-strain curves of 3000psi concrete with CFRP fabrics.

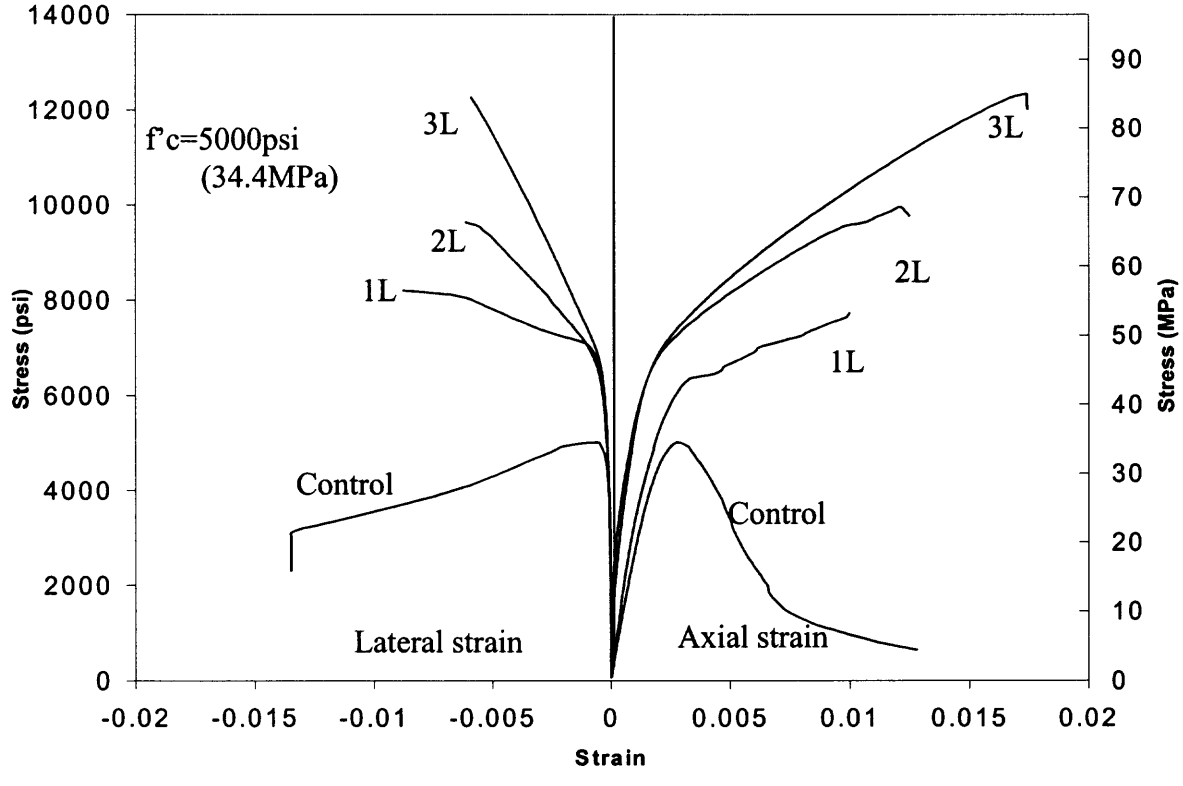

Figure 2.3 Axial stress-strain curves of 5000psi concrete with CFRP fabrics.

Figure 2.4 Failure conditions of CFRP strengthened specimens.
(From left to right: 1 layer, 2 layers and 3 layers)

Failure Mechanism:

The failure of fabric-confined concrete cylinders in the compression test has been found to be very explosive. The test specimens failed are mostly due to the rupture of the carbon fiber jackets. Most failures occurred at or near the middle part of the specimens. For some specimens, the rupture of the jackets was accompanied by slight delamination between the layers. Figure 2.4 and Appendix B.4-6 give the physical conditions of the specimens after testing. It shows that 1-layer specimen has the most severe failure condition, while the 3-layer specimen shows very little rupture condition. The whole failure process can be explained by two phases: Before the concrete achieves its approximate unconfined strength, the loading is mainly carried by the concrete itself. As the compression load increases, the concrete starts to dilate. After the concrete core

expands to some degree, the load is then transferred to the CFRP jackets until the jackets are broken. As a result, the ultimate behavior of confined concrete totally depends on the properties of the jackets rather than the concrete. The specimens are considered as a failure when the fabrics are being ruptured and the load suddenly drops to zero.

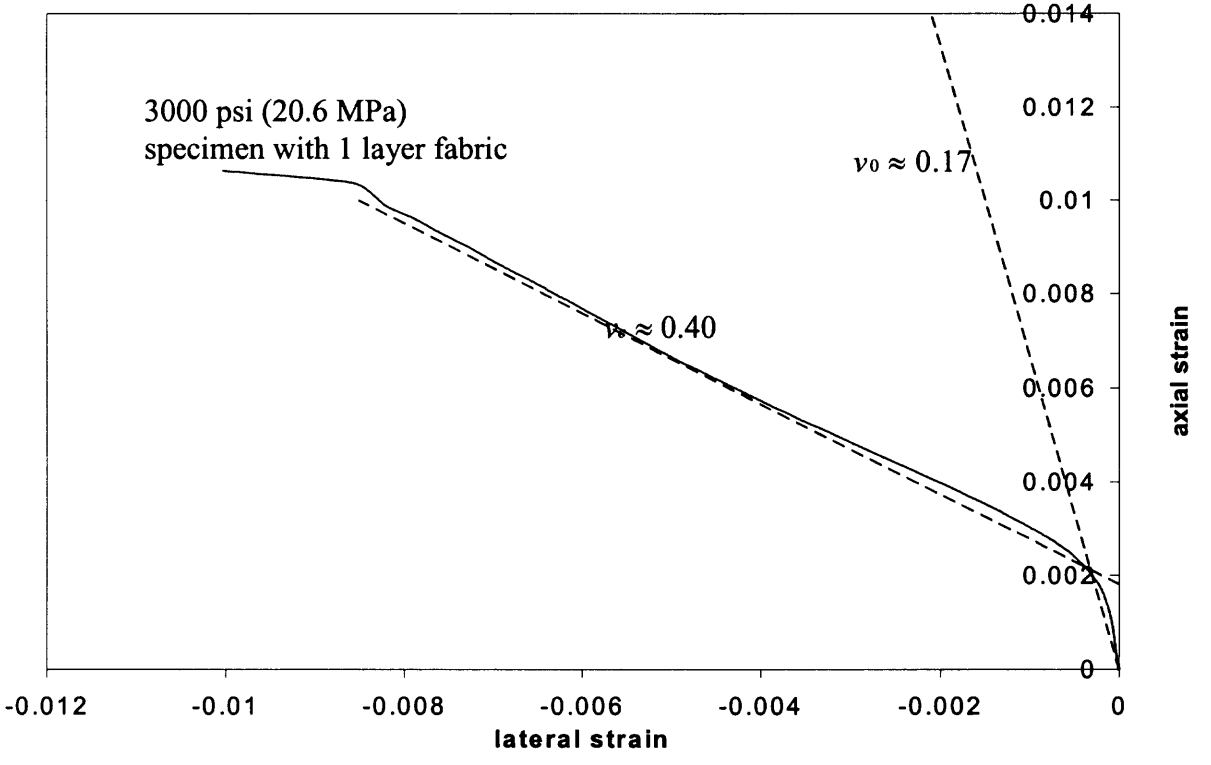

Figure 2.5 Typical axial-lateral strain relationship of CFRP strengthened concrete.

2.3.2.2 Axial -Lateral Strain Relationship. Typical relationship for axial and lateral strains is shown in Figure 2.5 for the specimen with 3000 psi (20.6MPa) strength and 1 layer of CFRP jacket. The complete axial-lateral strain curves are listed in Appendix C.13-20. As shown in Figure 2.5, the overall axial-lateral strain relationship also demonstrates an approximate bilinear behavior. The initial slope of the axial strain and lateral strain relationship is very close to the dashed line corresponding to a slope value of 0.17, which represents the typical initial Poisson Ratio for normal concrete and is

almost the same as for all the specimens with different layers. As the axial strain increases, the ratio between the lateral strain and axial strain also increases, that indicates the acceleration of lateral dilation of the concrete. The curves appear to eventually converge to a certain line, which gives the Poisson Ratio approximately equal to 0.40. For other specimens, this value does not change much because of the fabric thickness.

Table 2.6 Compression Test Results for CFRP Strengthened Specimens with Steel Hoops

Specimen 5000psi (34.4MPa)		Max stress (psi)	Ultimate axial strain	E_c (psi)	E_0 (psi)
2 in. (51mm) spacing hoops	Control	5013.9 (34.5MPa)	0.0150	3407879 (23480MPa)	3608529 (24863MPa)
	1 layer	8436.1 (58.1MPa)	0.0120	4292567 (29576MPa)	6235136 (42960MPa)
	2 layers	10071.1 (69.4MPa)	0.0162	3603247 (24826MPa)	5655136 (38964MPa)
	3 layers	11804.3 (81.3MPa)	0.0220	2520039 (17362MPa)	4152372 (28610MPa)
4 in. (102mm) spacing hoops	Control	4536.3 (31.3MPa)	0.0160	3853873 (26553MPa)	4616303 (31806MPa)
	1 layer	8037.9 (55.4MPa)	0.0090	3750314 (25840MPa)	4655222 (32074MPa)
	2 layers	10743.6 (74.0MPa)	0.0150	2855726 (19676MPa)	4652601 (32056MPa)
	3 layers	12414.8 (85.5MPa)	0.0130	2630140 (18122MPa)	5256366 (36216MPa)

2.3.2.3 Hoop Effect. Steel hoops were put into some 5000psi (34.4MPa) concrete specimens to study the hoop effect. Table 2.6 gives the compression test results of the concrete specimens confined by both CFRP jackets and steel hoops. Two different spacings for the steel hoops are studied in this research. Complete stress-strain curves of the specimens with hoops are listed in Appendix C.21-34. The figures show that the stress-strain relationships of the specimens confined by both CFRP and hoops are very similar to those of the specimens that are only confined with CFRP. The average stress-

strain curves for specimens confined with only CFRP, CFRP and 2 in (51mm) spacing hoops, and CFRP and 4 in (102mm) spacing hoops are shown in Figure 2.6. It can be seen from the Figure that all three types of confinements result in a similar stress-strain behavior. Therefore, it is concluded that the steel hoops do not contribute more strength and ductility improvements when the concrete cylinders are reinforced with the CFRP jackets. In another word, if the specimen is confined by both CFRP and steel hoops, the stress-strain relationship, especially the ultimate behavior of the confined concrete, is still determined by the confinement effect of CFRP alone.

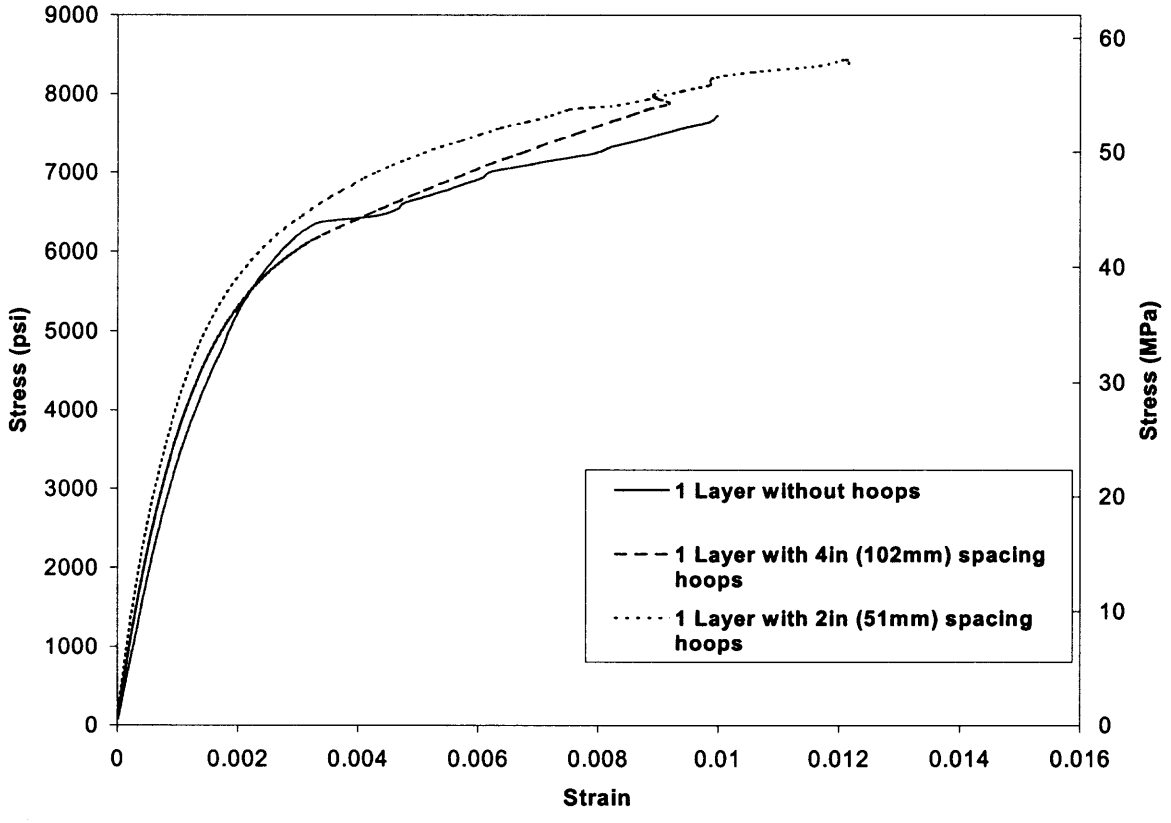

Figure 2.6 Comparison of average stress-strain curves of 5000 psi concrete specimens confined by both fabrics and steel hoops.

2.3.2.4 Fabric Orientation Effect. All the fabric composites used in this research are made of strips of high strength fibers. The fibers are unidirectional, which means it can only carry forces at one direction. The force applied at the other direction can be ignored. Therefore, the majority of the cylinder specimens in the research were only wrapped in the way that the fiber direction was perpendicular to the height of the cylinder. To study whether the orientation of the fabric has an effect on the confined concrete strength, some 5000 psi (34.4MPa) concrete cylinders were wrapped with an additional layer of fabric, which was perpendicular to its original normal wrapping direction. The detailed configuration of these two different wrappings can be seen from Figure 2.7

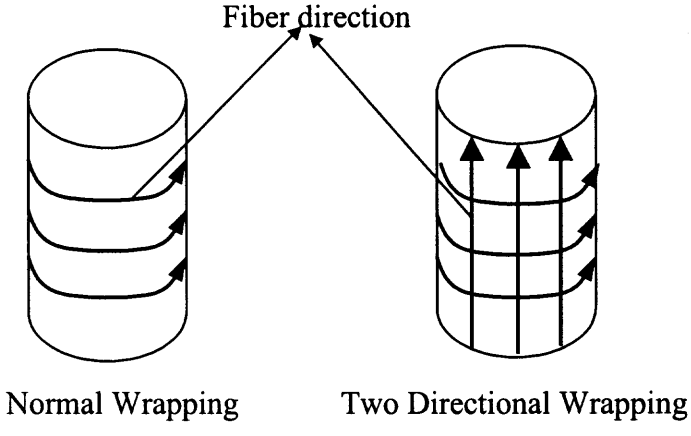

Figure 2.7 Two different wrapping methods.

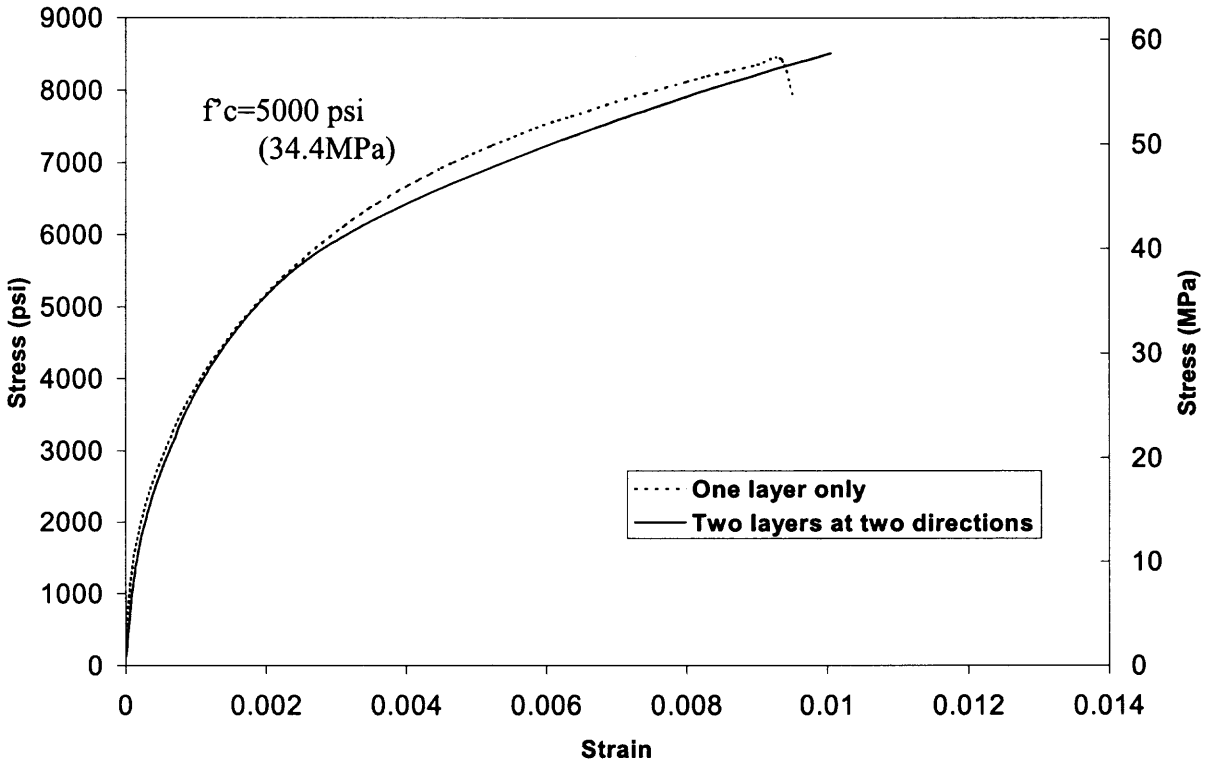

Figure 2.8 Average stress-strain curves of concrete cylinders wrapped with two different layers of fabrics.

A new batch of 5000 psi (34.4MPa) cylinders was tested to study this effect. Five of them were wrapped with two layers of fabric at two different directions. The others were wrapped with one layer of fabric using normal wrapping method. The test results are listed in Appendix C.35 and Table 2.7. The average stress-strain curves of these two types of cylinders are also illustrated in Figure 2.8. The failure conditions of these cylinders can also be seen from Appendix B.6. Figure 2.8 depicts that the average stress-strain curve of the cylinders with two layers of fabrics at two directions are very identical to that of the one-layer cylinders, which means with the additional layer of the fabrics at 90-degree direction, the stress-strain behavior of the confine-concrete does not change much. This is because at the pure axial loading condition, the additional layer of fabric is unable to carry any axial loading. The stress-strain behavior of the cylinder is still

determined by the concrete core and the original layer of fabrics. Therefore it can be concluded that the fabric orientation at 90-degree direction has little effect on the confined concrete at axial loading.

Table 2.7 Test Results for Concrete Cylinder Wrapped at Two Different Directions

Specimen 5000psi (34.4MPa)	Max stress (psi)	Ultimate axial strain	E_c (psi)	E_0 (psi)
Specimen 1	7321 (50.4MPa)	0.0085	3407176 (23474MPa)	3826931 (26367MPa)
Specimen 2	8037 (55.4MPa)	0.0089	3853813 (26553MPa)	4216703 (29049MPa)
Specimen 3	7798 (53.7MPa)	0.0081	3603548 (24828MPa)	4215236 (29041MPa)
Specimen 4	8436 (58.1MPa)	0.0095	4220139 (29077MPa)	4152242 (28608MPa)
Specimen 5	8037 (55.4MPa)	0.0120	3812833 (26270MPa)	4412203 (30399MPa)

Table 2.8 Test Results for Fabric-confined Cylinders Using Different Coarse Aggregates

Specimen 5000psi (34.4MPa)		Max stress (psi)	Ultimate axial strain	E_c (psi)	E_0 (psi)
3/4 in. (19mm) Stones	1 layer	7081 (48.8MPa)	0.0078	4292567 (29572MPa)	38235136 (26340MPa)
	2 layers	9390 (64.7MPa)	0.0125	3603247 (24826MPa)	5255136 (36208MPa)
3/8 in. (9.5mm) Stones	1 layers	7640 (52.6MPa)	0.0083	4185796 (28840MPa)	3752603 (25855MPa)
	2 layers	9267 (63.8MPa)	0.0115	3690140 (25424MPa)	51596666 (35550MPa)

2.3.2.5 Size Effect of Coarse Aggregate. In this research, 3/4 in. (19mm) coarse aggregate was used in the cylinder specimens and RC beam specimens. However, due to the limitation of the form size, the column specimens have to use 3/8 in. (9.5mm) coarse aggregate. In order to examine whether the size difference of the coarse aggregate will have an effect on the stress-strain behavior of the confined concrete, a new batch of

5000psi (34.4MPa) concrete cylinders using 3/8 in. (9.5mm) stones were cast and wrapped with different layers fabric.

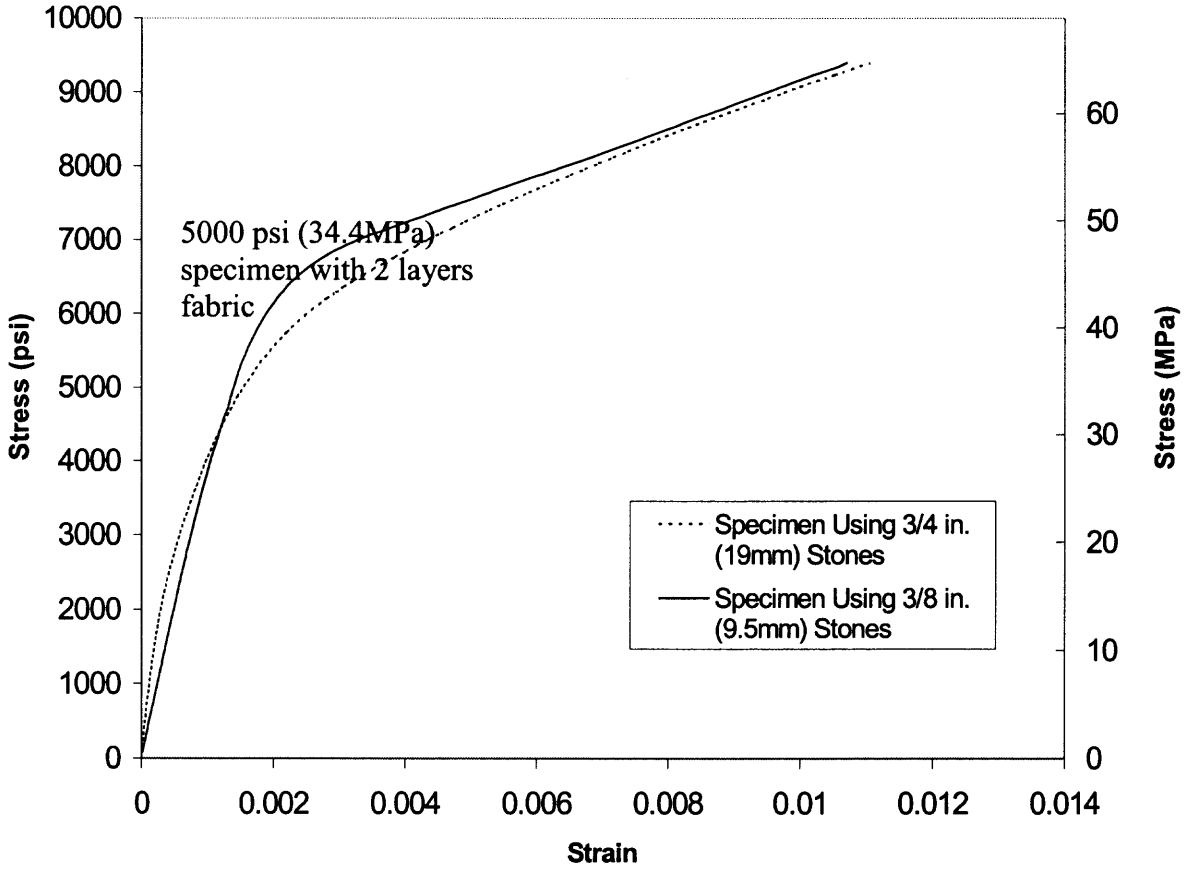

Figure 2.9 Comparison of the fabric-confined concrete cylinders using different coarse aggregates.

Test results are shown in Appendix C.36-37. The average stress-strain curves of these specimens were compared with those of specimens using 3/4 in. (19mm) stones. The results of comparison are given in Figure 2.9, Appendix C.38 and Table 2.8. Figure 2.9 shows that the stress-strain curve of cylinder using 3/4 in. (19mm) stones is almost identical to that of cylinder using 3/8 in. (9.5mm) stones. This is because the stress-strain behavior of fabric-confined concrete is mainly determined by the properties of the CFRP fabrics. The concrete core only affects the behavior of the elastic part. Thus it is

concluded that the size of coarse aggregate does not have an effect on the stress-strain behavior of fabric-confined concrete.

2.4 Stress-strain Equation for Fabric Confined Concrete

In order to fully understand the structural behavior of various structural members confined by CFRP fabrics, a complete stress-strain equation of the confined concrete is needed. However, not many previous studies have given a suitable stress-strain equation for fabric strengthened concrete. In this research a simple analytical equation is proposed to describe the whole stress-strain curve of confined concrete based on experimental results. The following assumptions are used to develop such the proposed empirical equation.

1. Fabric wraps are considered as the confinement of the concrete core. Concrete and fabric are working together as a whole system. The proposed equation is good for the confined concrete only.

2. The Epoxy between concrete and fabric will not fail.

3. The stress-strain behavior of confined concrete can be approximated as a bilinear behavior. The second part is totally dependent on the Fabric properties.

4. The proposed equation will not describe any descending part of the stress-strain behavior due to its very brittle failure characteristic of the confined-concrete.

5. The steel hoop, fiber orientation and the coarse aggregate size have no effects on the proposed equation.

2.4.1 Proposed Stress-strain Equation.

Figure 2.10 shows a typical stress-strain curve for fabric confined concrete. The curve has an approximate bilinear shape and has no obvious descendent part. According to experimental results for cylinder specimens, the behavior of the concrete-fabric system can be defined by two phases. In the first phase, the axial loading is mainly carried by the concrete core. So the stress-strain curve almost follows the shape of unconfined concrete. After the concrete reaches its ultimate value of unconfined compressive strength, the dilation rate of the concrete starts to increase due to the microcracks developed within the concrete core that results in a significant confinement pressure force from the fabric jackets. Since the concrete core has already cracked, the behavior of the confined system is mainly dependent on the fabric jackets in the second phase. Therefore, the stress-strain curve follows a different slope that is mainly determined by material properties of the fabric. Also, because the final failure of the fabric is explosive and brittle, discussion of the descendent part of the stress-strain curve become meaningless.

To represent the bilinear response of fabric confined concrete, the four-parameter relationship of Samaan and Mirmiran (1998), which is used to define concrete confined by fiber tubes, is used and calibrated as follows:

$$f_c = \frac{(E_1 - E_2)\varepsilon_c}{\left[1 + \left(\frac{(E_1 - E_2)\varepsilon_c}{f_o}\right)^n\right]} + E_2\varepsilon_c \qquad (2.2)$$

f_c and ε_c are axial stress and axial strain of the fabric confined concrete. All the other parameters are described in Figure 2.10. They can be described as follows:

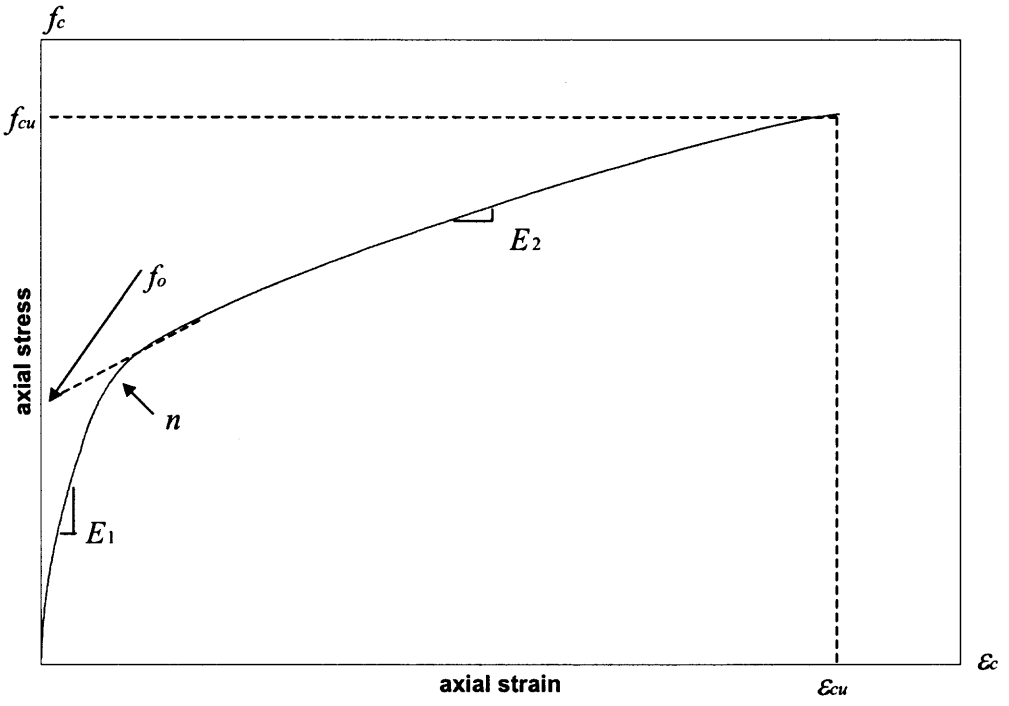

Figure 2.10 Parameter of bilinear stress-strain curve of fabric-confined concrete.

E_1 is the first slope in the stress-strain curve, since the initial performance of the confined concrete is very similar to the unconfined concrete. The ACI equation for secant modulus of normal concrete can be used here.

$$E_1 = 57\sqrt{f'_c} \text{ (ksi)} = 57{,}000\sqrt{f'_c} \text{ (psi)} \tag{2.3}$$

$$E_1 = 4{,}730\sqrt{f'_c} \text{ (MPa)} \tag{2.4}$$

Where f'_c is the compressive strength of unconfined concrete.

E_2 is the second slope in the stress-strain curve of the confined concrete. According to the test results, as the concrete core approaches its unconfined strength, microcracks grow to the extent that the Poisson's ratio can no longer describe the relationship between the lateral and axial strains. And the fabric jacket becomes the sole

remaining device against catastrophic failure. Therefore, E_2 is a function of the stiffness of the fabric, and to a less extent, the unconfined strength of the concrete, as follows:

$$E_2 = 40.4 f_c'^{0.2} + 1.345 \frac{E_f . t_f}{D} \text{ (ksi)} \tag{2.5}$$

$$E_2 = 189.2 f_c'^{0.2} + 1.345 \frac{E_f . t_f}{D} \text{ (MPa)} \tag{2.6}$$

The parameters for E_2 are directly from the experimental results of over 40 cylinders by curve fitting. Appendix C.39-44 show the equation has a good agreement with the experimental results. E_f is the effective modulus of elasticity of fabric jacket. And t_f is the thickness of the fabric jacket, which can be obtained from the material properties of the fabric jackets. D is the diameter of the concrete core.

f_o is the referent stress at the interception of the second slope with the stress axis. Samaan and Mirmiran (1998) suggested that the intercept stress is a function of the confining pressure and the unconfined concrete strength. According to the curve fitting of the experimental results, the equation can be estimated as follows:

$$f_o = 0.85 f_c' + 1.9 f_r + 1 \text{ (ksi)} \tag{2.7}$$

$$f_o = 0.85 f_c' + 1.9 f_r + 6.89 \text{ (MPa)} \tag{2.8}$$

f_r is the confining pressure of the fabric jacket. According to Figure 2.11, a simple equation for f_r can be derived from the equilibrium condition and deformation compatibility condition. f_f is the tensile strength of the fabric jackets. Obviously, f_r will increase as the layers of the fabric increases.

$$f_r = \frac{2 f_f . t_f}{D} \tag{2.9}$$

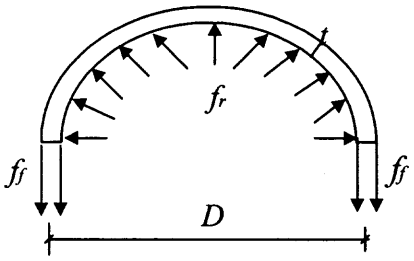

Figure 2.11 Definition of the confining pressure.

n is a shape parameter that mainly controls the curvature of the transition zone of the stress-strain curve. It is can be shown that the shape curve is not very sensitive to this parameter. A constant value of 0.95 is used based on curve fitting of the test results.

Appendix C.38-44 list the comparison of the average stress-axial strain curves with the proposed model. They show that the analytical equation can satisfy all the experimental results pretty well. Although the equation is the true reflection of the experimental results, its effectiveness still need to be validated by other various test results.

Since the axial stress-lateral strain curve is also bilinear, and the transition zone occurs at the same stress level. The proposed equation can also be used to describe stress-lateral strain relationship. However, some parameter values need to be changed based on the experimental curves.

2.4.2 Prediction of Ultimate Stress and Strain

Although the proposed stress-strain equation can fully describe the stress-strain behavior of the fabric-confined concrete, a simple empirical equation is needed to predict the ultimate stress and ultimate strain of the confined concrete. From various literatures, it is generally assumed that the ultimate confined concrete strength (f_{cu}) is related to the

confining pressure f_r. Therefore, a simple equation can be used to predict the ultimate stress of the confined concrete.

$$f_{cu} = f'_c + k_1 f_r \tag{2.10}$$

$$\frac{f_{cu}}{f'_c} = 1 + k_1 \frac{f_r}{f'_c} \tag{2.11}$$

In Equation 2.10 and 2.11, k_1 is coefficient of effectiveness that represents how much the confined strength (f_{cu}) of concrete is increased over its unconfined value (f'_c). Most stress-strain models assume k_1 as a constant factor (for example, k_1 = 4.1 by Richart et al. 1928). This assumption is not valid because the confinement becomes less effective when the lateral pressure reaches a certain level. Therefore, Saatcioglu and Razvi (1992) suggest that k_1 is inversely proportional to the Poisson's ratio. Both Samaan (1998) and Xiao (2000) suggest k_1 should be an equation related to the confining pressure f_r. Based on their assumption, the following equation for k_1 was proposed by regression analysis.

$$k_1 = 3.65\, f_r^{-0.25} \text{ (ksi)} \tag{2.12}$$

$$k_1 = 6.14\, f_r^{-0.25} \text{ (MPa)} \tag{2.13}$$

Figure 2.12 shows the detailed regression analysis for these equations. Once this relation is substituted in Equation 2.10, the ultimate confined strength f_{cu} can be related to the confining pressure by:

$$f_{cu} = f'_c + 3.65 f_r^{0.75} \text{ (ksi)} \tag{2.14}$$

$$f_{cu} = f'_c + 6.14 f_r^{0.75} \text{ (MPa)} \tag{2.15}$$

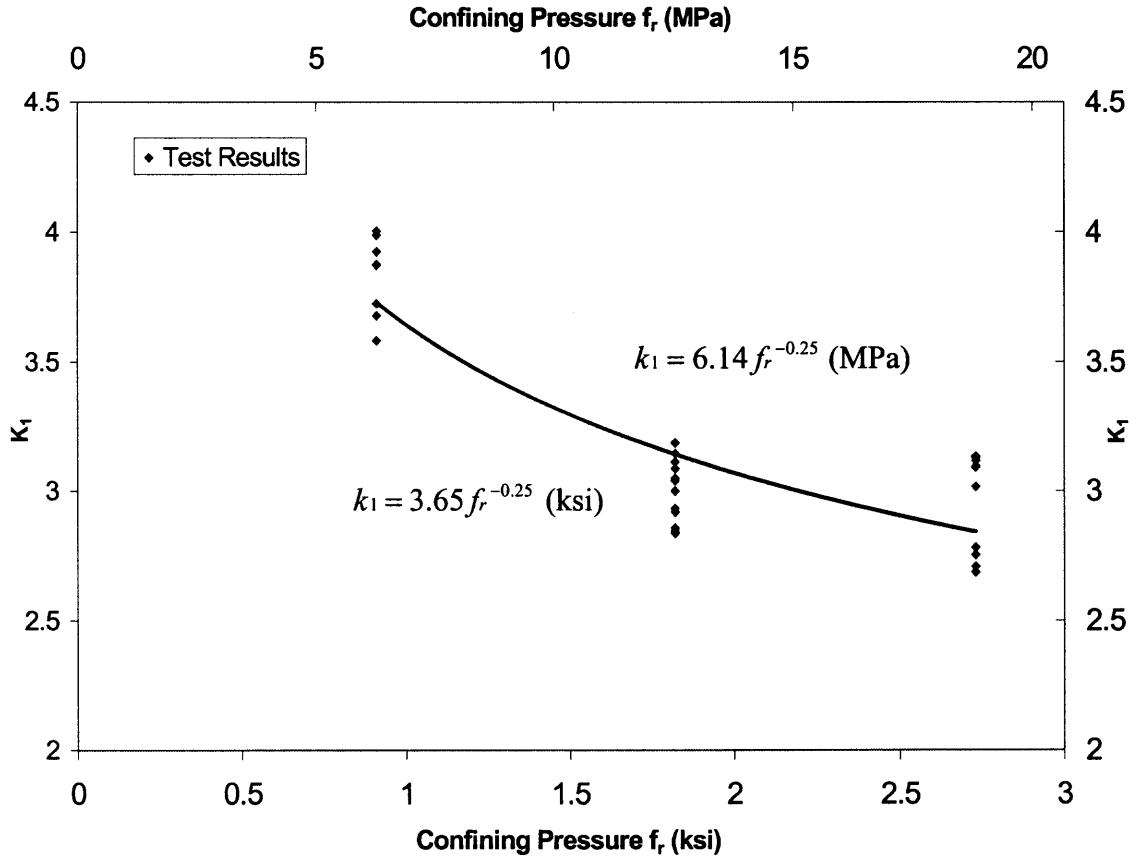

Figure 2.12 Test data and regression equation for confinment coefficient k_1.

Figure 2.13 shows the predicted strength of confined concrete versus test results of the present study, as well as those by Samaan (1998) and Xiao (2000). Good correlation is noted, with most test results being within a $\pm 10\%$ margin of error. Therefore, the proposed empirical equation for the ultimate stress prediction has been found to be valid and effective.

Based on the ultimate stress of the confined concrete, the ultimate strain (ε_{cu}), i.e., the point at which the stress-strain response is terminated, is determined from the geometry of the bilinear curve shown in Figure 2.10.

$$\varepsilon_{cu} = \frac{f_{cu} - f_0}{E_2} \tag{2.16}$$

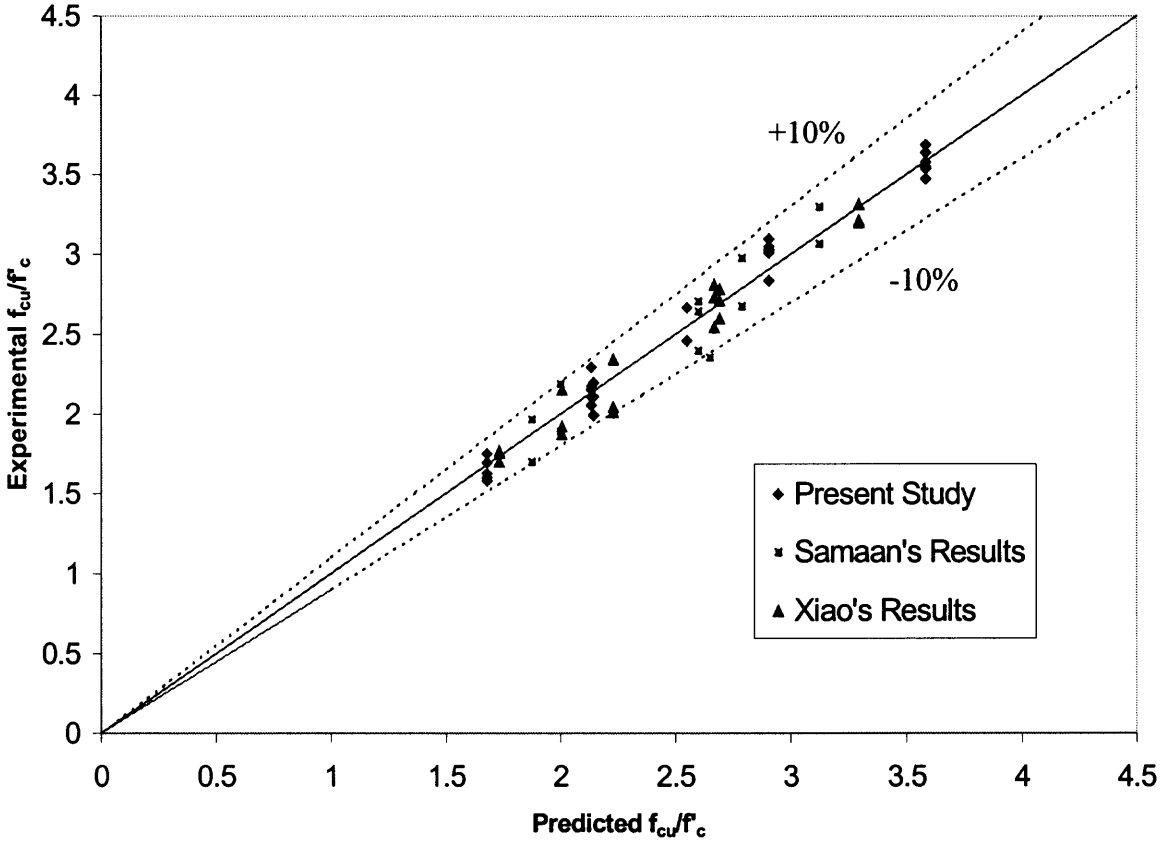

Figure 2.13 Predicted versus experimental ultimate strength f_{cu}.

2.4.3 Verification of Proposed Stress-strain Equation

Since the proposed equation is derived from the curve fitting of present experimental results, it has to be verified by the test results by others to truly validate its effectiveness. The comparisons of present result with three different studies are presented in the following sections.

Xiao's Test Results for Carbon Fiber-wrapped Concrete Cylinders

Xiao and Wu (2000) tested a total of thirty-six 6 in.× 12 in. (152mm×305mm) concrete cylinders wrapped in one, two and three layers of carbon fiber fabrics with three different unconfined concrete strength. The reported tensile strength and modulus of elasticity for fabric jackets are 229 ksi (1577MPa) and 15239 ksi (105000MPa), respectively. The

jacket thickness is 0.015 in. (0.381mm). Figure 2.14 shows the experimental versus predicted stress-strain curves for 4000 psi (27.6 MPa) specimens with different layers of fabric jackets. A very good agreement with the proposed equation is evident.

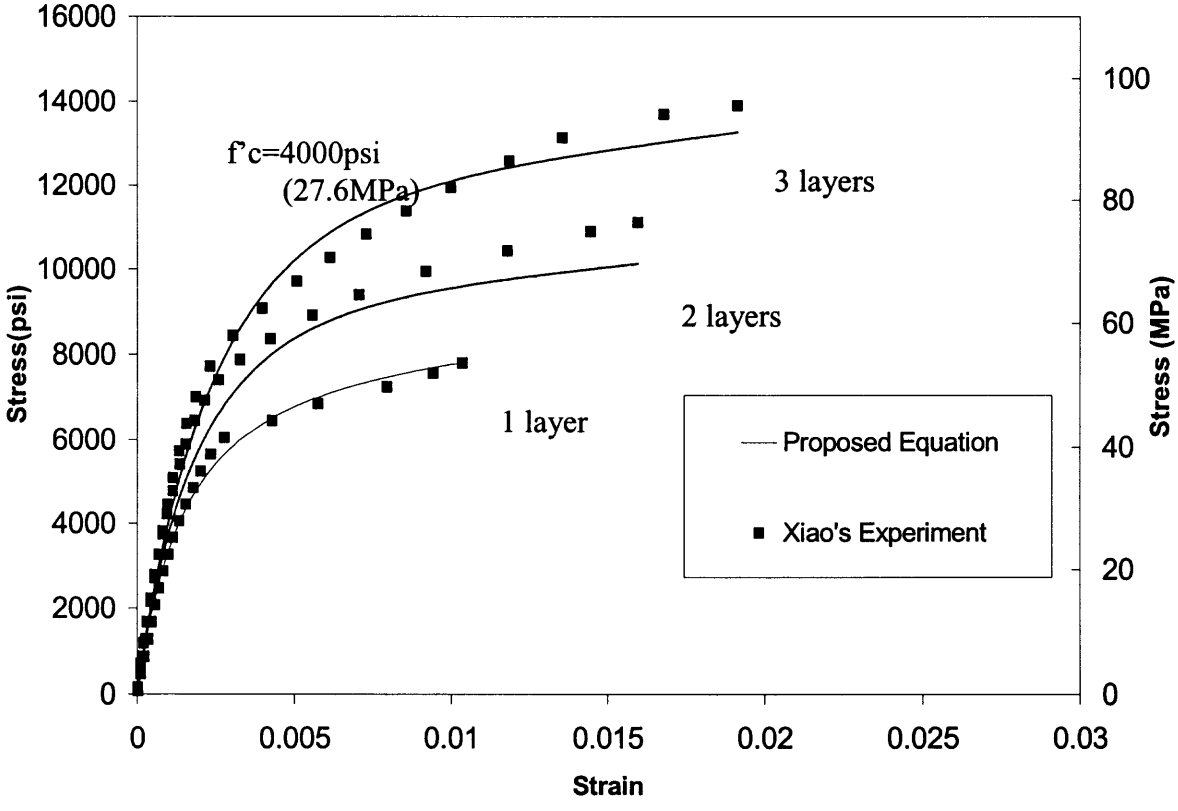

Figure 2.14 Comparison of the proposed equation with test results of Xiao (2000).

Samaan's Test Results for E-glass Fiber Wrapped Concrete Cylinders

Samaan and Mirmiran (1998) tested a total of thirty 6 in. × 12 in. (153mm × 305mm) concrete cylinders wrapped with six, ten and fourteen plies of E-glass fiber. The tensile strength and tensile modulus of the fabric jackets are 317 ksi (2186MPa) and 10100 ksi (69640 MPa), respectively. The thickness for each ply of the fabric is 0.0095 in. (0.24 mm). The concrete core strength is approximately 4.5 ksi (31 MPa). The experimental

versus the predicted stress-strain curves for the specimens with different plies of fabric are shown in Figure 2.15. Good agreement is noted for the shape of the curves. However, the experimental stresses are a little bit lower than the predict values from the proposed model. This is probably attributed to the fact that the reported manufacturer's data may overestimate the jacket's tensile strength.

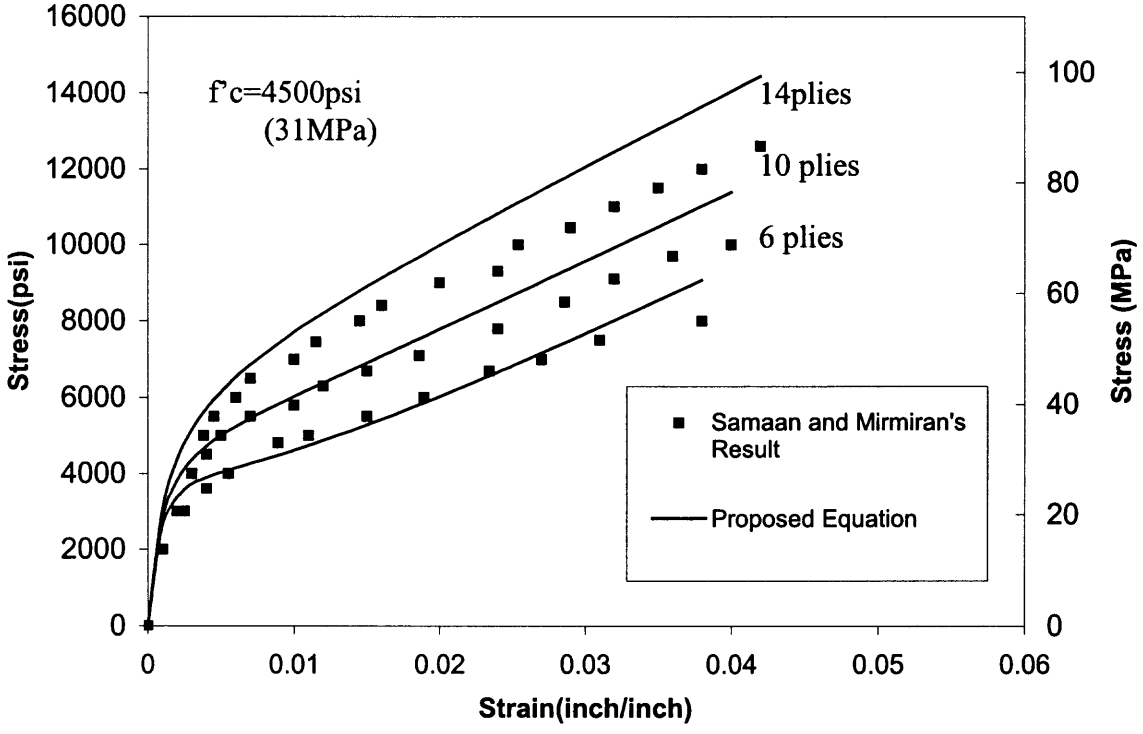

Figure 2.15 Comparison of the proposed equation with test results of Samaan and Mirmiran (1998).

Saafi's Test Results for Carbon Fiber Wrapped Concrete Cylinders

Saafi and Toutanji (1996) tested a total of thirty 6 in. × 12 in. (153mm × 305mm) concrete cylinders wrapped by CFRP or GFRP fabric jackets with different jacket thickness. The reported tensile strength is 508 ksi (3500 MPa) for the CFRP jacket and 80 ksi (550 MPa) for GFRP jacket. Three different thicknesses were used for both CFRP and GFRP

wrapped specimens. The experimental versus predicted stress-strain curves for CFRP wrapped specimens are shown in Figure 2.16. A very good correlation is achieved.

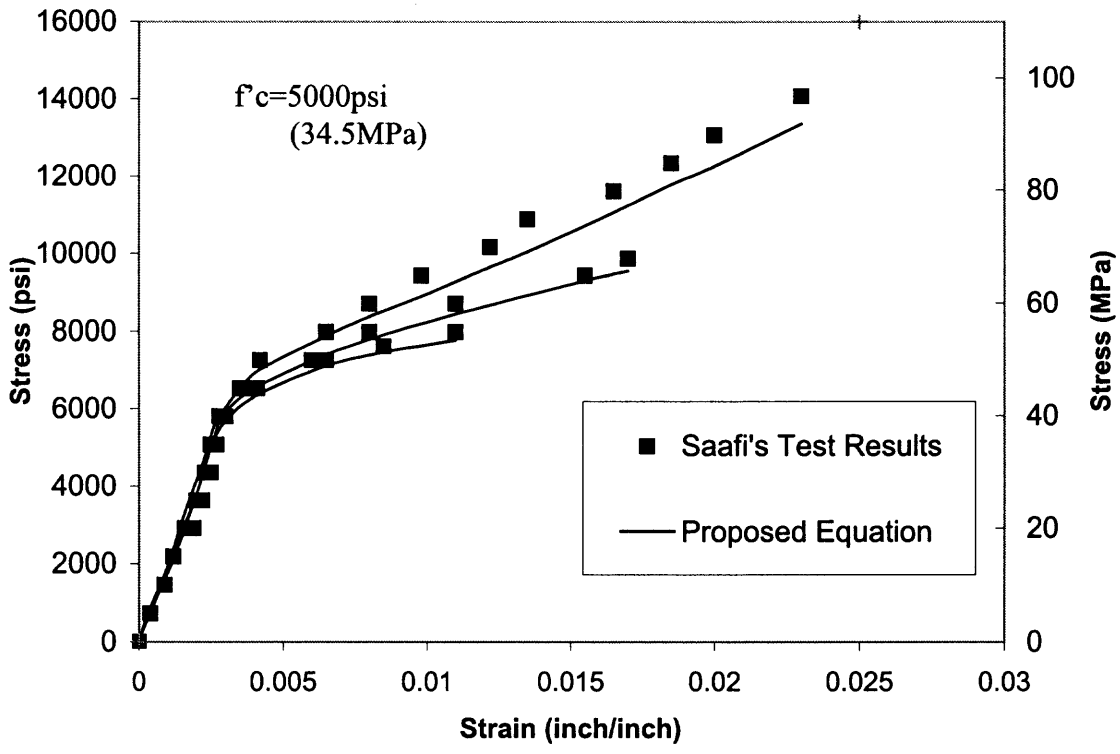

Figure 2.16 Comparison of the proposed equation with test results of Saafi and Toutanji (1996).

2.5 Summary of Proposed Stress-Strain Equation

A uniform stress-strain equation (2.1) is proposed and verified in this research. Empirical equations (2.14, 2.15 and 2.16) used to predict the ultimate stress and strain of the fabric-confined concrete are also presented. The related parameters in these equations are derived from direct curve fitting of the present experimental results. The proposed equations can be used to describe the axial stress-strain behavior for any normal concrete confined with FRP fabric jackets. Various factors, such as unconfined concrete strength, jacket thickness, steel hoop effect, fiber orientation and coarse aggregate size effect, are

considered and reflected in these equations. In order to truly validate the effectiveness of these equations, some test results by others were quoted and compared with current proposed model, and very good agreements were achieved. Thus the proposed equation is valid and ready to apply to the analysis of structural concrete members.

However, due to the brittle failure characteristic of the confined concrete, the proposed equations cannot predict the descending behavior of the stress-strain curve. Also, based on the experimental results, the proposed equations are very sensitive to the material properties of confining materials such as the tensile strength of the fabric jacket. Because of the complicate interaction behavior among fabric, Epoxy and concrete, the manufacturer's data for material properties may not truly reflect the performance of the confining jackets in the specimens. In most cases, it will either overestimate or underestimate the strength of the jackets, which will cause the inevitable errors from the proposed model. A more advanced experimental method to determine the real properties of the confining materials in the specimens is needed to enhance the accuracy of the proposed equation.

CHAPTER 3

FLEXURAL BEHAVIOR OF REGULAR RC BEAMS STRENGTHENED BY CFRP FABRICS

3.1 Introduction

Reinforced concrete beams deteriorate over time due to environmental aging, fatigue, and other reasons. Wrapping concrete beams with carbon fiber fabrics is a simple, convenient and corrosion-resistant strengthening system. This system easily matches the contours of the member surface being wrapped. Superior mechanical and chemical properties, in addition to simplicity and effectiveness, are the attractive features of carbon wrapping. Before implementation of the proposed strengthening technique for field application, various structural performance evaluations of the fabric-wrapped RC beams under certain conditions are necessary. As it performs as a main structural function, the flexural behavior of the fabric-wrapped RC beam needs more detailed investigation and analysis.

Based on the stress-strain behavior of fabric-confined concrete from the cylinder tests, an extensive experimental study was carried out in this research. Five large-scale RC beams with different fabric layers and different wrapping methods were cast and tested in the NJIT laboratory. Many experimental factors such as flexural strength, structural ductility, post-crack behavior and the failure mechanism were investigated during the tests. Also, an analytical study using both ACI method and finite element method were conducted to predict the flexural behavior of the fabric-confined concrete beams. The experimental results and analytical predictions were compared and analyzed during the course of this study.

3.2 Experimental Scheme

3.2.1 Design of Concrete Beams

All the beams to be tested are designed to fail in bending. That means if the beams fail in shear first, one will be unable to determine whether the externally wrapped CFRP fabrics do help or not to carry the bending force, let alone to decide how much contribution it would make to the whole flexural resistance of the beam. Thus, the shear reinforcement in the concrete should be designed more than enough to withstand its maximum shear force. At the same time, the flexural reinforcement ratio ρ should be lower enough to make sure the beam will fail in bending. Although the lower the flexural reinforcement ratio is, the more likely the failure will be in bending. However, ACI still suggests a minimum reinforcement ratio for a regular beam design. Therefore, the flexural reinforcement ratio ρ should also be not less than the minimum reinforcement ratio ρ_{min}.

Based on the above reasons, Two No.3 bars were used as the main flexural reinforcement. A total of twenty-two No.2 stirrups were used for each beam with a spacing of 6 inch (152mm) at the middle and 3 inch (76mm) at the ends. Two No. 2 bars were also used in the compression area for stirrup support only. The detailed configuration of the each beam can be seen from Figure 3.2-3.5.

3.2.2 Materials

3.2.2.1 Carbon Fiber Reinforced Plastic and Epoxy. Sika Corporation, USA, provided the CFRP wrap used in this research. SikaWrap Hex 230C, which is a kind of woven composite fabric, was employed in this study. CFRP fabric is unidirectional and has a longitudinal tensile strength of 140 ksi (960 MPa). The lateral strength of the

fabrics is negligible. The fabric strips are elastic until break. The represented properties are given in Table 2.1.

The epoxy resin (Sikadur-330) used in this research was also provided by Sika, USA. The epoxy consists of two components; part A is in white, part B is in dark gray. The mix ratio of part A and part B is four to one by weight. The properties are also given in Table 2.1.

3.2.2.2 Concrete. The concrete used in the beam consists of Type I cement satisfying with ASTM 150, sand from local source, crushed stone with maximum aggregate size of 3/4 in. (19mm). All beams in this research use the same mix design. They are listed in Table 3.1.

Table 3.1 Mix Design of Concrete Beams

Concrete Compressive Strength	Water /Cement ratio	Cement (lbs/yd^3)	Stones (lbs/yd^3)	Sand (lbs/yd^3)	Water (lbs/yd^3)
4500 psi (30.96 MPa)	0.68	500 (2907 N/m^3)	1763 (10252 N/m^3)	1433 (8332 N/m^3)	264 (1535 N/m^3)

3.2.2.3 Reinforcement. Two No.3 bars were used at the bottom of the beams to carry the tensile force due to bending. The yield stress of the No.3 bars is 58 ksi (400MPa). The complete stress-strain behavior of the No.3 bar can be obtained from the uniform tension test. The average test result is shown in Appendix A. Shear stirrups are made of No.2 bars. Two No.2 bars were used at the top of the beam for purpose of tieing the bars together.

3.2.3 Cast and Cure of Concrete Beams

Five 10ft. (3m) long RC beams having cross-sectional dimension of 6 in.× 12 in. (152mm× 305mm) were cast at the concrete laboratory of NJIT. All concrete materials described in the previous section were mixed by a rotary mixer. The 10-ft. (3m) wooden mold were prepared and lubricated with oil before the concrete was poured. Then the steel rebars were tied and put into the oiled form. The mixing sequence used was the same as the cylinders which have been described in chapter Two. During casting, an electrical vibrator was used to compact the specimens. All specimens were demolded after 48 hours and cured in a standard curing room for 28 days.

Five batches of concrete were used to fabricate the beams. For each batch, Three 4 in.× 8 in. (102mm× 203mm) cylinders were made at the same time. The cylinders were cast and cured at the same conditions as the beams and they were tested at the same time when the beams were tested. Compressive strength of the cylinders from all batches are given in Table 3.2

Table 3.2 Maximum Compressive Strength of Concrete Cylinders

Concrete Batch	Compressive Strength f'_c (psi)			
	Cylinder 1	Cylinder 2	Cylinder 3	Average
1	4572 (31.5MPa)	4156 (28.6MPa)	4023 (27.7MPa)	4250 (29.3MPa)
2	4614 (31.8MPa)	3967 (27.3MPa)	4370 (30.1MPa)	4317 (29.8MPa)
3	4012 (27.6MPa)	4288 (29.5MPa)	3956 (27.3MPa)	4085 (28.1MPa)
4	4567 (31.5MPa)	4674 (32.2MPa)	4873 (33.6MPa)	4705 (32.4MPa)
5	4672 (32.2MPa)	4700 (32.4MPa)	4325 (29.8MPa)	4566 (31.5MPa)

3.2.4 Installation of CFRP Strengthening System

3.2.4.1 Beam Surface Treatment. The concrete surface of the beams to be strengthened has to be sound and clean. Sandpaper and sand blasting was utilized to treat the concrete surfaces in this research. All the dust particles were cleaned using an airbrush. Some hard part was removed by the sand blasting. All the specimens were washed and treated carefully before the epoxy was applied.

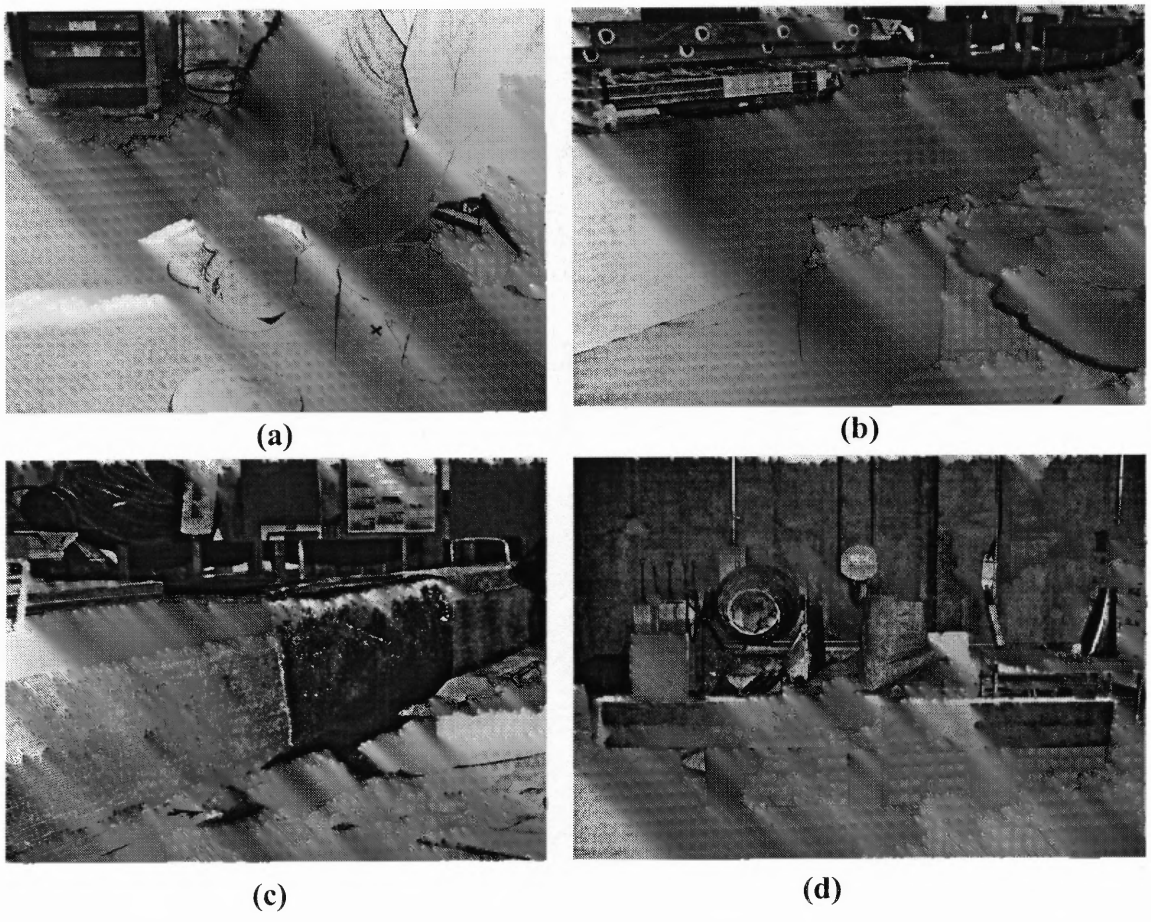

Figure 3.1 Installation of CFRP fabrics on beam surfaces.
(a) Mixing epoxy; (b) Apply the epoxy on the surface of the concrete;
(c) Wrap the fabric jacket on the beam; (d) let the specimens dry for 24 hours.

3.2.4.2 Bonding of Composite Materials to Beams. The bonding procedures of RC beams are very similar to those of the cylinders. The details can be seen from Figure 3.1. However, in order to investigate into the effect of the wrapping configuration on the final load-deflection behavior of RC beams, three different wrapping methods were used in this research. In addition to the control beam that has no wrapping at all, two beams were wrapped longitudinally at the bottom and two sides of the beam surface. One beam was wrapped vertically along its four sides. And the other one combined both of the longitudinal and vertical wrappings. The details of the wrapping configuration are shown in Figure 3.2-3.5.

3.2.5 Beam Configuration

All beam configurations are listed below. As mentioned earlier, there are three different wrapping configurations. All beams have the same length, concrete compressive strength, steel reinforcement, cross sectional areas and stirrup spacing. For control beam CJ1 (Figure 3.2), there is no fabric around the beam. For beam CJ2 (Figure 3.3), one layer of fabric was wrapped longitudinally at the bottom and two sides of concrete surface, which means that the fiber direction of fabric composites is along the beam span. For beam CJ3 (Figure 3.3), same configuration as CJ2 was used but two layers of fabric was installed. For beam CJ4 (Figure 3.4), one layer of the fabric was wrapped vertically along the perimeter of the cross sectional area, which means the fiber direction of fabric composites is perpendicular to the beam span. For beam CJ5 (Figure 3.5), one layer of fabric was wrapped longitudinally at first and then another layer of the fabric was wrapped vertically afterwards.

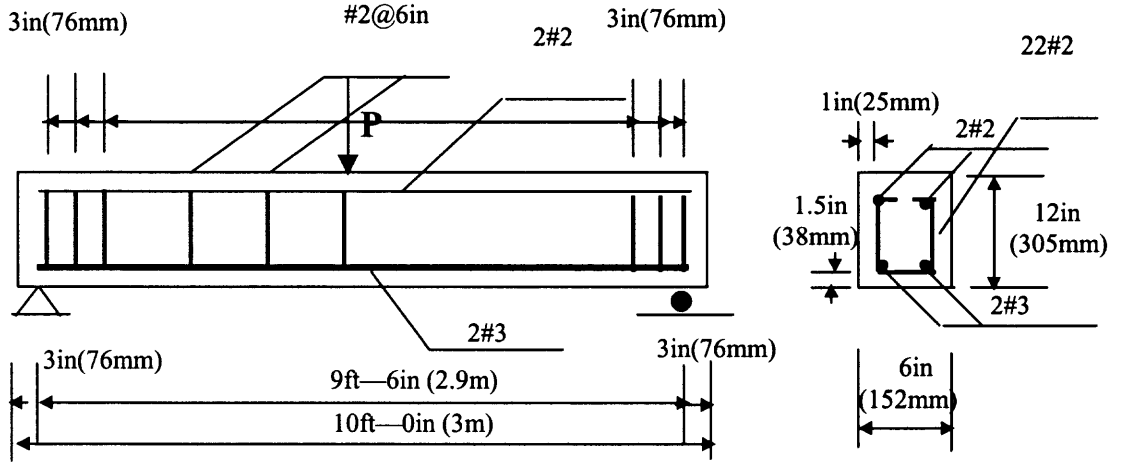

Figure 3.2 Specimen details of beams CJ1.

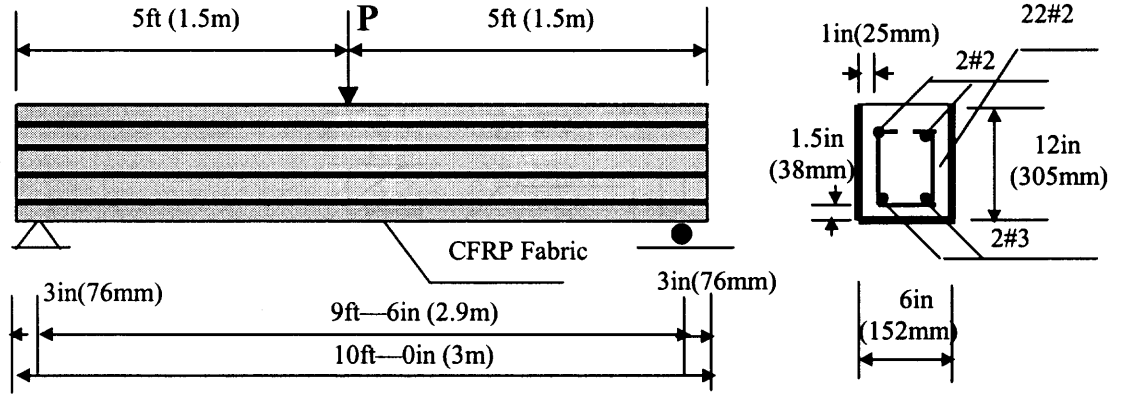

Figure 3.3 Specimen details of beams CJ2 and CJ3.

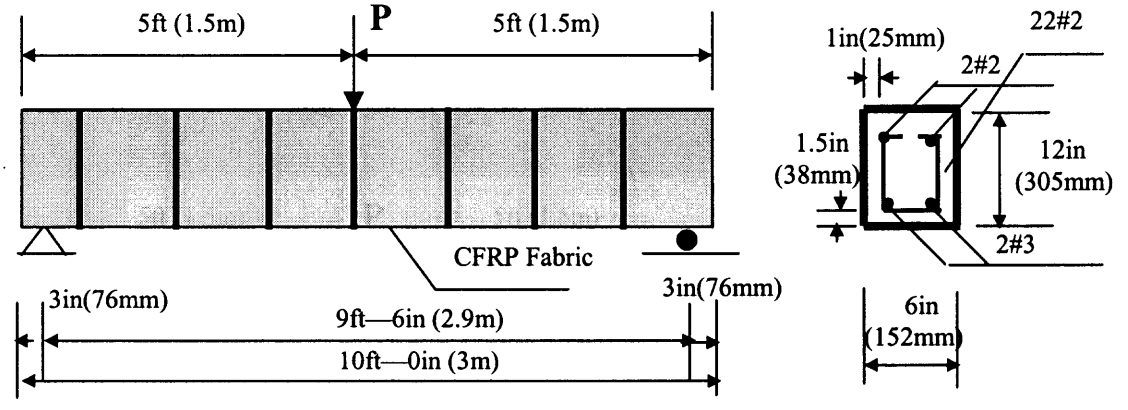

Figure 3.4 Specimen details of beams CJ4.

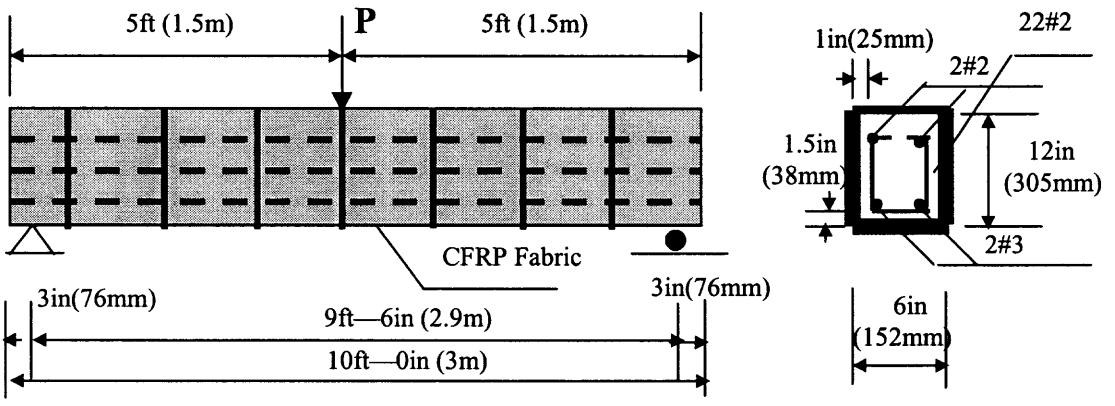

Figure 3.5 Specimen details of beams CJ5.

3.2.6 Experimental Setup and Test Procedures

All beams were tested on the 220-kip (979kN) MTS testing system at the NJIT Structures Laboratory. Two steel rollers served as the supports were placed under both ends of the beam, respectively. One point load was applied right at the middle span of the beam specimen. The detailed experimental setup for each beam is listed in Appendix B.7-11. Four pairs of mechanical strain gages (or called demec gages) were installed at mid-span of one side of the beam before the test got started. They were located 5 inch each side from the mid-span of the beam. The strains were measured at different loading steps during the entire test. (Appendix B.12) The data were used to calculate the strains and plot the Moment-Curvature curve. An automatic data acquisition system was used to monitor the loadings as well as the mid-span deflection. The load was applied by a hydraulic jack and measured by a load cell. Deflection control was used in all the tests. A constant loading rate of 0.001 in/sec (0.025mm/sec) was used during the whole experiment process. Deflection measurements were taken at the mid-span of the beam using a LVDT. All beams were statically tested to failure in a single load cycle. The test procedures for each beam can be described as follows:

(a) Beam CJ1

The first beam tested was the control beam CJ1 (Appendix B.7). It was a typical flexural failure. As the load went up to 5 kips (22 kN), the first tension crack started from the middle span of the beam and extended from the bottom to the top. As the load continued increasing, more flexural cracks developed while there was no obvious increase in load. After the load reached around 5.5 kips (24.5 kN), the load started to maintain at a constant level while the mid-span deflection kept increasing. During this process, more flexural cracks developed and the initial crack became larger and larger. Finally the load suddenly dropped down at the same time the concrete at the top of the beam got crushed (Figure 3.6).

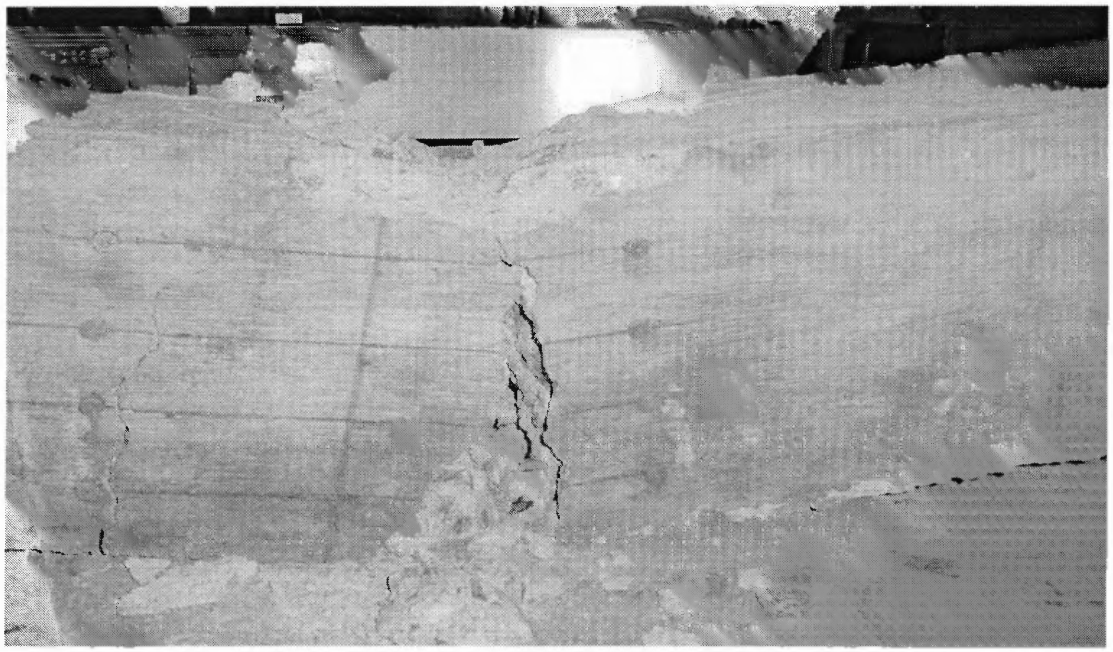

Figure 3.6 Failure of beam CJ1.

(b) Beam CJ2

The next beam was CJ2 (Appendix B.8), which was longitudinally wrapped with one lay of fabric at the bottom and two sides of the beam. At first, the load-deflection curve

followed the similar shape as that of the control beam. After the load reached around 12 kips (53 kN), sound of the delamination between the concrete and CFRP fabric was noticed. However, no visible crack and delamination were found on the specimen. The sound continued until the load reached 15.4 kips (68.5 kN), when one of the first fabric strips was ruptured at the bottom of the beam. As the load increased, more and more strips under the beam either were broken or delaminated. Afterwards, the rupture and delamination extended to the sides of the concrete. When the load went up to 17.2 kips (76.5 kN), a sudden drop of the load occurred as a result of concrete crush in the compression zone. More and more fabric strips were broken and delaminated as the load kept dropping. Finally the test stopped at 8.4 kips (37.4 kN) and all the bottom strips were gone (Figure 3.7).

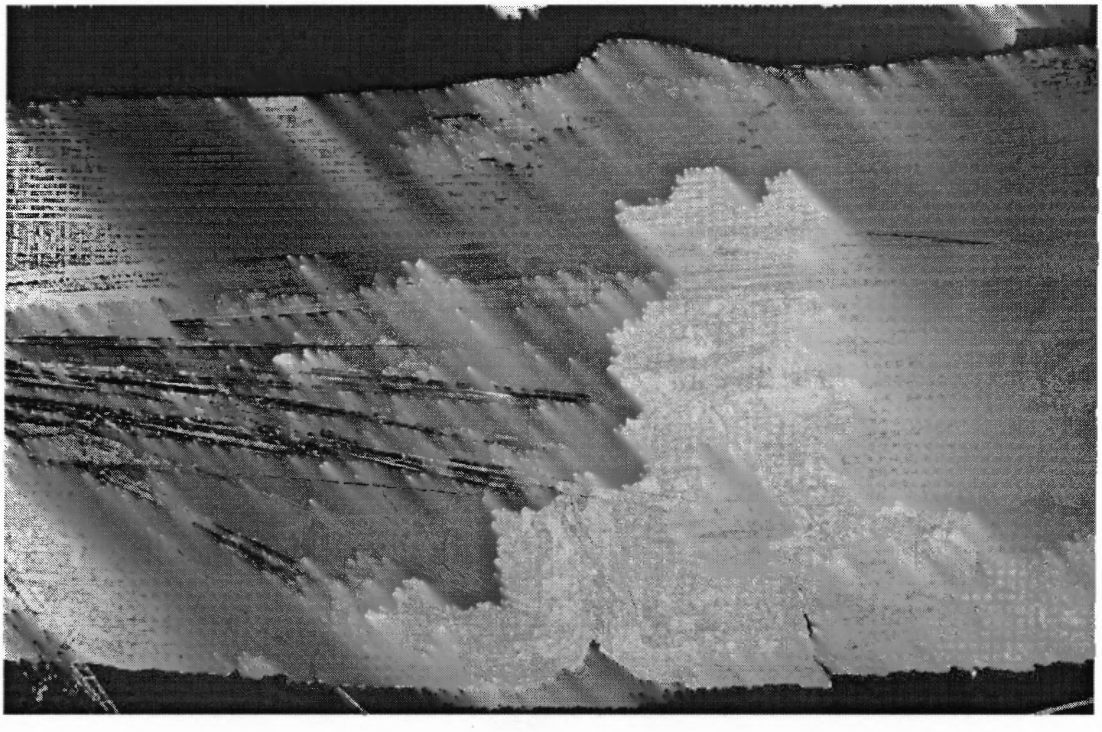

Figure 3.7 Failure of beam CJ2.

(c) Beam CJ3

The third beam tested was CJ3 (Appendix B.9). CJ3 and CJ2 had the same wrapping method but with two layers of fabric. Therefore the test procedures were very similar to those of the CJ2. The sound of delamination firstly started at about 11.5 kips (51.2 kN), but the first visible rupture of the fabric strip occurred much later at 17.5 kips (77.9 kN). It was because the rupture and the delamination of the fabric strips started from the inner layer where was not visible. As the load continued increasing, more and more fabric strips stared to rupture and delaminate. When the load went up to 20.2 kips (90 kN). The concrete at the top got crushed, and then the load started to drop quickly. The test finally stopped at 15.3 kips (67.6 kN) (Figure 3.8).

Figure 3.8 Failure of beam CJ3.

(d) Beam CJ4

The fourth beam tested was CJ4 (Appendix B.10). This beam was vertically wrapped with one layer of fabrics. Therefore, only the compression zone of the concrete was

confined and strengthened by the fabrics. The first flexural crack started at the mid-span of the beam when the load climbed to 5.3 kips (23.6 kN). There was no clear sound of delamination between the fabric and the concrete during the whole process. The crack started to extend when the load continued to grow. Meanwhile, the mid-span deflection started to increase at a higher rate while there was no significant increase in load. The load maintained almost at the same level until it reached about 6.2 kips (27.6 kN), when there was a sudden small load drop because another major flexural crack occurred near the initial crack. Then the load maintained at around 6 kips (26.7 kN) for a long time until the tension steel was broken. At this time the mid-span deflection reached about 4in (102mm). During the whole process, the concrete in the compression zone was intact because the added fabric confinement effect improved its compression capacity and ultimate strain of the confined concrete (Figure 3.9). The final failure of the beam was characterized as yielding and breaking of tension steels.

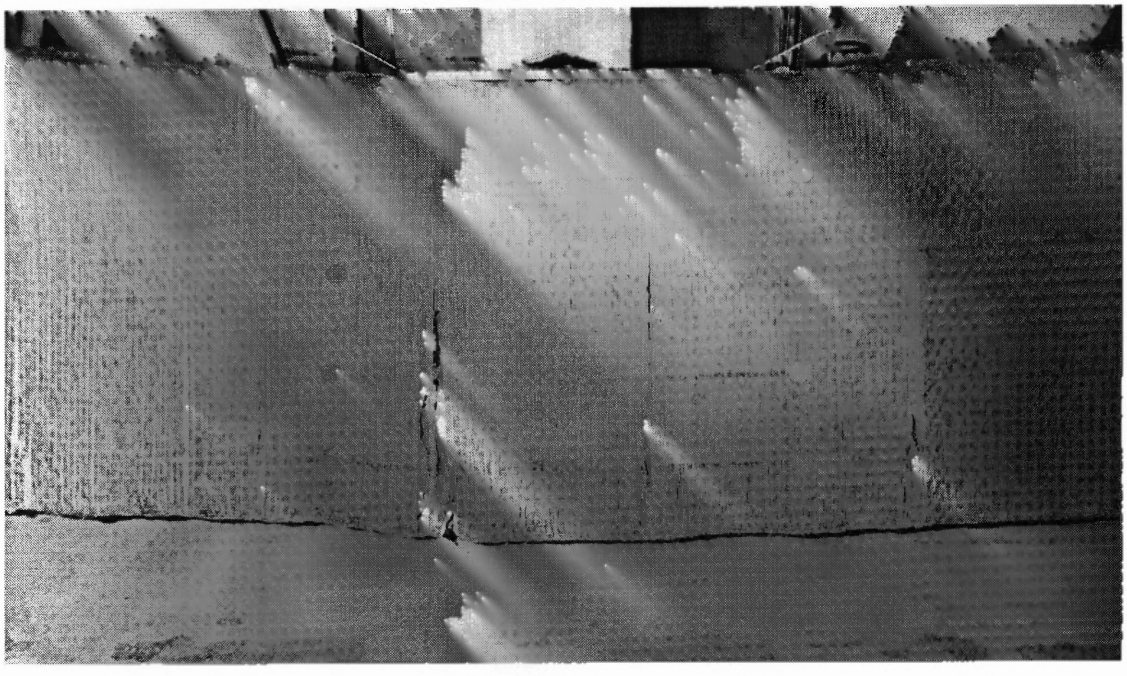

Figure 3.9 Failure of beam CJ4.

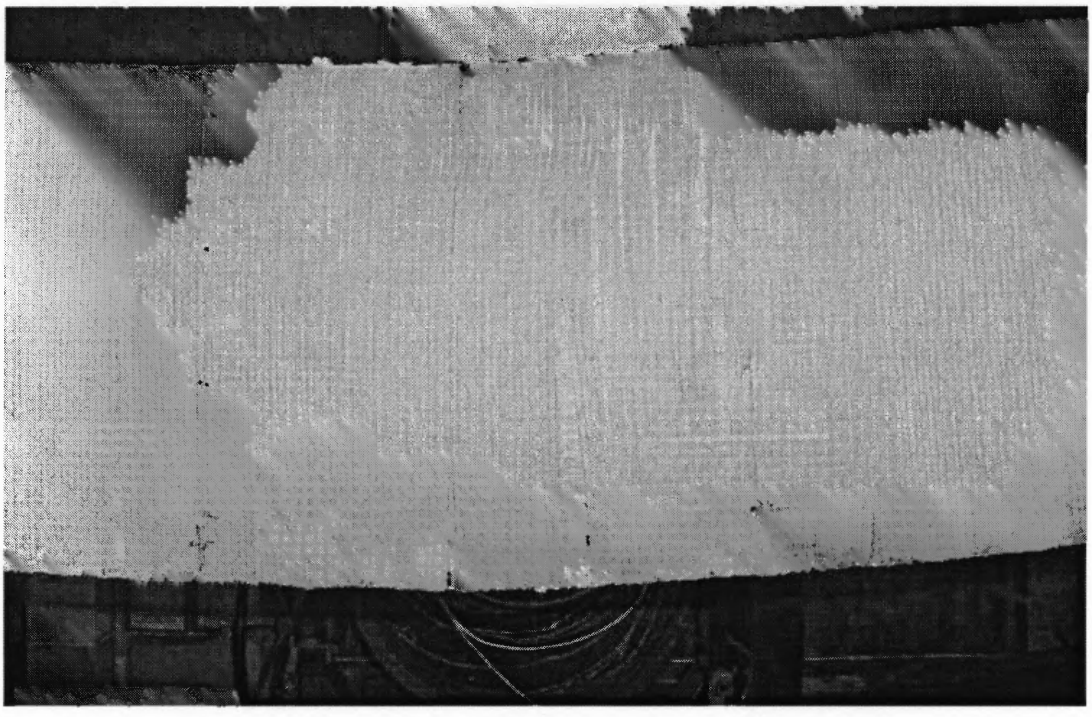

Figure 3.10 Failure of beam CJ5.

(e) Beam CJ5

The final beam tested was CJ5 (Appendix B.11). This beam was firstly wrapped with longitudinal fabrics, and then a layer of transverse fabrics was installed on the surface of longitudinal fabrics. No clear sound of delamination was heard before the load reached about 13 kips (57.9 kN). After this moment, continuous sound of rupture and delamination between the fabric and concrete were noticed. However, due to added transverse confinement, not any visible rupture or delamination was found. When the load went up to 15.7 kips (69.9 kN), the first flexural crack occurred near the mid-span. At this time some of the longitudinal fabric strips had already broken inside. The load maintained at a relatively stable level after it reached 17.9 kips (79.7 kN). This stable level continued for a long time as the mid–span deflection kept increasing. During this phase, more flexural cracks had developed near the initial crack. The specimen finally

failed when the mid-span deflection reached about 3 in (76 mm). A huge rupture of fabric strips inside the confinement made the load drop to zero suddenly. Similar to beam CJ4, the concrete in the compression zone remained intact and the final failure was due to the rupture of the longitudinal fabrics.

3.3 Test Results and Discussions

3.3.1 Flexural Strength

From Table 3.3 and Figure 3.11, it can be concluded that CFRP fabrics do help in flexural strengthening of RC beams. However, due to different wrapping methods, the contribution of fabrics varies. The longitudinal CFRP fabric strengthening greatly increases the load capacity of the confined beams as compared with the control beam CJ1. Beam CJ3, which is strengthened by 2 layers of longitudinal fabrics, has the highest load capacity up to 20 kips (89 kN). This is almost four times of the capacity of the control beam. Also, Figure 3.11 shows that the strength of beam CJ3 is a little higher than that of CJ2. Therefore, the thickness of the CFRP can be considered as an important factor for studying the effect of longitudinal strengthening. However, for beam CJ4, it can be seen from the figure that with the transverse confinement only, the load capacity of the beam is only a little bit higher that that of the control beam. This is because that the transverse confinement only strengthens the concrete in the compression zone of the beam. Due to its unidirectional characteristics, the fabrics cannot help carry any tension forces and flexural moments in the beam. Therefore, the final load and moment capacity of the beam is still mainly determined by the tension reinforcement. Beam CJ5 further consolidates this reason. With two different wrapping applied, CJ5 only shows a slight

increase in loading than beam CJ2. Therefore, It can be concluded that only the longitudinal wrapping can significantly increase the loading capacity of the RC beams. Based on the experimental results, added transverse confinement can help prevent fabric debonding and improves overall shear capacity and bond behavior. However, this help will not significantly affect the flexural strength of the RC beams, but it does increase the ductility of the beam behavior as discussed below.

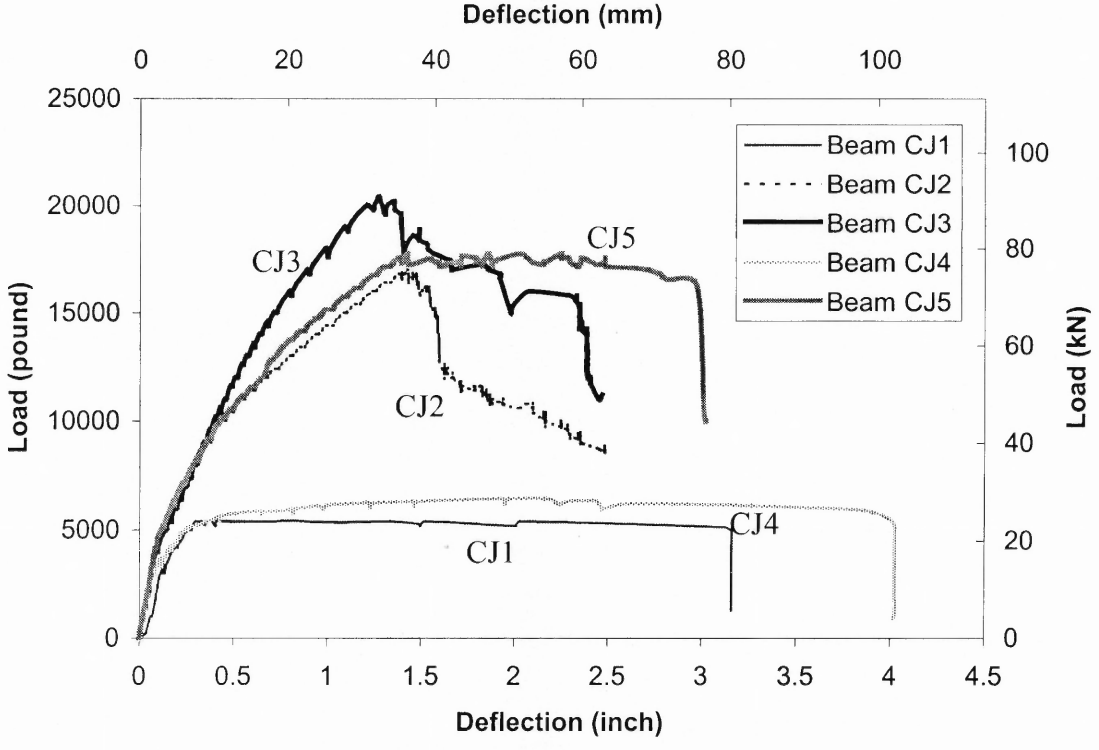

Figure 3.11 Comparison of load-deflection curves of test beams.

3.3.2 Ductility

Energy-absorbing characteristics of concrete beams are denoted by ductility or deformability indices. Ductility of the reinforced concrete beams is defined as the ratio of curvature, deflection, or rotation at ultimate to yielding of steel. However, for concrete beams with composite wrapping or steel rebars or the combination of both, a better

measure of the energy absorption should be considered. Conventionally the area under the moment-curvature or the load-deflection curve should be used as a measurement of the ductility for RC beams and CFRP-wrapped RC beams. Based on this concept, both the load-deflection and moment-curvature curves are investigated for the test beams. Figure 3.12 shows the comparison of moment-curvature curves for five test beams. The mid-span curvatures of the beams are derived from Mid-span longitudinal strains (Appendix B.12) over the height of the beams based on the basic strength material principles. However, some of the experimental curves are not complete because the strain gages are broken due to the rupture of the fabrics.

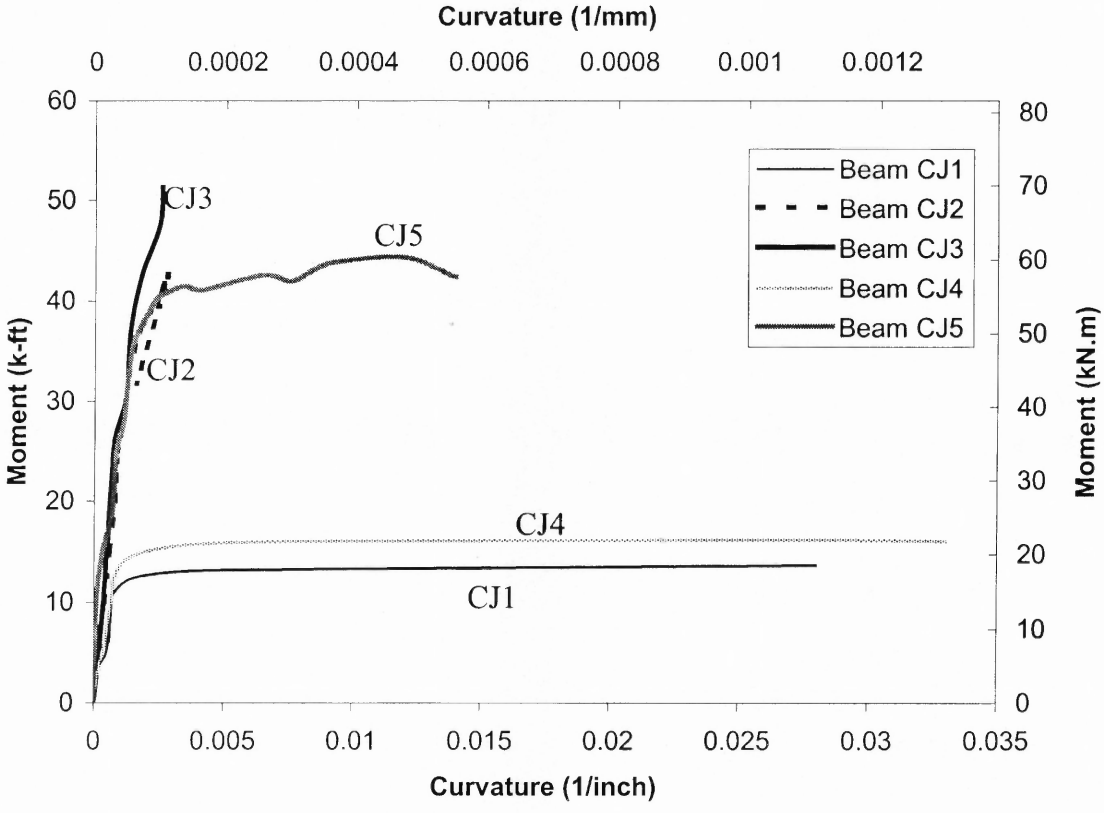

Figure 3.12 Comparison of moment-curvature curves of test beams.

From Figure 3.11 and 3.12, one can see that beam CJ1 has a very good ductility performance because of the yielding of the steel rebars. Comparing the results of CJ1 to those of beam CJ2 and CJ3, the deflection and curvature of beam CJ2 and CJ3 have been greatly decreased. The maximum deflections are decreased from 3.16 in (80.3mm) of CJ1 to 2.4 in (61mm) of CJ3. Also, the mid-span curvatures are decreased from 0.028 1/in (0.001 1/mm) of CJ1 to 0.0026 1/in (0.0001 1/mm) of CJ3. It can be concluded that as the longitudinal layers of fabrics increase, the decrease of curvature will become greater. This is mainly due to the facts that the longitudinal fabric wrappings limit the deformation behavior of the beam. However, considering that the huge load increases for beam CJ2 and beam CJ3, the overall areas under the load-deflection and moment curvature curves still increase slightly. Therefore, the ductility of beam CJ2 and CJ3 remains intact. A better ductility performance can be seen from the test results of Beam CJ4. The transverse confinement of the fabric wrapping strengthens the concrete in the compression zone, and thus increases the ultimate strain of the confined concrete. Although the load does not increase much, the ultimate mid-span deflection and curvature do increase as compared with CJ1, which shows an overall better strength and ductility than those of CJ1. Finally, the best strength and ductility can be seen from beam CJ5. Both longitudinal and transverse wrappings are used for CJ5. As a result, the beam CJ5 has the same load capacity as beam CJ2, and also it has the same deformation capacity as beam CJ1. The overall area of energy absorption is also highly increased as compared with that of beam CJ4. This is because that the longitudinal fabrics help increase the load capacity of beam, meanwhile the confinement in the compression zone due to the transverse wrapping help prevent earlier crush of the concrete.

Table 3.3 Experimental Results of Test Beams

Test Beam	Concrete Strength (psi)	Ultimate Load (kips)	Ultimate Deflection (inch)	Load Increase Compared to CJ1	Failure mode
CJ1	4250 (29.3MPa)	5.4 (24.5kN)	3.16 (80.3mm)		Concrete crush & steel yielding
CJ2	4317 (29.8MPa)	17.0 (75.7kN)	2.49 (63.2mm)	214%	Fabric rupture & concrete crush
CJ3	4085 (28.1MPa)	20.2 (89.9kN)	2.47 (62.7mm)	274%	Fabric rupture & concrete crush
CJ4	4705 (32.4MPa)	6.45 (28.7kN)	4.02 (102mm)	19%	Steel yielding and breaking
CJ5	4566 (31.5MPa)	17.8 (79.2kN)	3.02 (76.7mm)	229%	Fabric rupture& delamination

3.3.3 Failure Mechanism

Figure 3.6-3.10 list the failure conditions for each beam. Control beam CJ1, which has no fabric applied, has demonstrated a typical flexural failure. Since only ρ_{min} has been used for tension reinforcement, the steel rebars have yielded very early in the test. The beam sustains a very large deformation and has exhibited a tension and ductile failure. Figure 3.6 and 3.11 show that the beam finally fails due to the crushing of the concrete near the loading area after an extensive tension crack. Beam CJ2 and CJ3 have a very similar failure mechanism because both of them are wrapped by longitudinal fabrics only. The failure for both of them is mainly due to the concrete crush in the compression zone after extensive rupture and some delaminations of the fabrics and tension cracks. At the end of the test, the CFRP fabrics get delaminated and broken at the bottom and sides of the beam. It is because more layers of fabrics are used, beam CJ3 does show a much less severe rupture and delamination condition in the fabrics as compared with beam CJ2. If one examines inside the fabric jackets, one can find out very clear flexural cracks in the

tension zone. Furthermore, if one looks through the cracks, one can see that the steel rebars in the tension zone of the beam have not deformed much as that of CJ1 because the added fabrics greatly decrease the deflection of the beam. Since the rupture of fabrics has been sudden and explosive, both beams show somehow a more brittle failure condition than the control beam CJ1. Beam CJ4, which has been wrapped by transverse fabric confinement only, has shown a much better ductile failure. Due to the added confinement effect from the fabrics, the concrete in the compression zone of the beam has been greatly strengthened and maintained a very good condition during the whole test. If a beam does not fail in compression, then a higher strain in tension steel at failure can be expected. This beam finally fails when the tension steel has been broken with a very high tensile strain. Large flexural cracks can also been seen from Figure 3.9 because no longitudinal fabrics are used. At last, beam CJ5, which has been wrapped by both longitudinal and transverse fabrics, combines the failure conditions of both CJ2/3 and CJ4. Because of the transverse confinement, the concrete in the compression zone has been strengthened and thus maintained a good condition during the test. On the other hand, the larger strain in the tension zone due to the strong concrete at compression can be taken by both steel rebars and longitudinal fabrics. Since the steel is much more ductile than the fabrics, the beam finally fails due to the rupture of the longitudinal CFRP fabrics. Figure 3.10 shows that inside the transverse confinement, most of the fabric strips inside are either broken or delaminated. Although the final failure of CJ5 still exhibits some brittle and explosive rupture of the fabrics, it behaves a much more ductile performance than those of CJ2/3 due to the added transverse confinement. From the

investigations of all five beams, all the rupture and delamination of fabrics occur beneath the surface of the concrete, which means the epoxy used in this research is effective.

3.4 Theoretical Analysis of RC beams Wrapped with CFRP Fabrics

3.4.1 Basic Assumptions

Before the analytical model is presented, the following assumptions should be considered:

1. Plane sections remain plane during bending.
2. A linear strain distribution is used for ultimate load calculation.
3. Shrinkage and creep effects are neglected and perfect bond between steel and concrete elements are assumed.
4. If the concrete is wrapped with transverse fabrics, it is considered as confined concrete; otherwise, it is treated as normal concrete. For fabric-confined concrete, the stress-strain curve presented in Chapter Two is used. For normal concrete, the classical stress-strain curve by Hsu (1990) is used.
5. The stress-strain curves from the direct tension tests are used for reinforcement steel. Most of the beams use yield strength f_y as the design strength. Some of the beam will use ultimate strength f_u due to the large strain in the steel.
6. The epoxy between the concrete and fabrics will not fail.

3.4.2 Modified ACI Equations for Ultimate Load

Based on the concept of strain compatibility and force equilibrium, ACI presents an empirical approach to analyze and design reinforced concrete beam. According to ACI 318-95, for a simply reinforced RC beam, compressive force (C) and force in the tension steel (T_s) are:

$$C = 0.85 f'_c ab \tag{3.1}$$

By neglecting concrete tensile stresses for simplicity,

$$T = T_s = A_s f_y \tag{3.2}$$

Where f'_c is the compressive strength of the concrete, a is the height of the equalvent stress block. b is the width of the cross section, A_s is the cross-sectional area of the steel rebars. f_y is the steel yield strength (if steel yields).

The height of the equivalent rectangular compressive stress block can be obtained by the force equilibrium:

$$C = T \tag{3.3}$$

$$a = \frac{A_s f_y}{0.85 f'_c b} \tag{3.4}$$

Whether the steel yields or not should be checked by the strain compatibility conditions (Figure 3.13). From the figure, the tensile strain in the steel can be obtained by:

$$\varepsilon_s = \frac{d-c}{c}(\varepsilon_c) \geq \frac{f_y}{E_s} \tag{3.5}$$

$$c = \frac{a}{\beta_1} \tag{3.6}$$

Where c is the depth from the neutral axis to the top of the concrete, d id the effective depth of the beam, ε_s is the strain of the steel, ε_c is strain of the extreme compressive strain of the concrete, for balance condition, ε_c=0.003. E_s is the elastic modulus of the steel, β_1 is a constant.

When this condition is satisfied, steel yields and a value based on equation (3.4) can be accepted. Then the design moment of the beam can be obtained by taking the moment about the center of the concrete compression block.

$$M = T_s(d - \frac{a}{2}) \tag{3.7}$$

Beam CJ1 can be analyzed using this approach. The detailed calculation is listed in Appendix G.

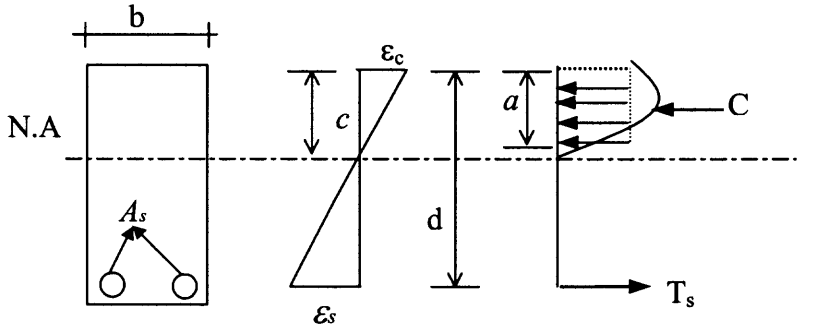

Figure 3.13 Strain distribution and force equilibrium conditions for beam CJ1.

Theoritically, ACI approach can be used to analyze and design any RC beams. However, for RC beams wrapped with CFRP fabrics, both compression force (C) and tension force (T) may change due to added materials. Therefore, some modifications should be made to the ACI equations in order to analyze fabric-confined RC beams.

(a) RC beams with longitudinal wrapping only (CJ2/CJ3)

Figure 3.14 shows the stress distribution and force equilibrium for beam CJ2/CJ3. Because of its unidirectional characteristics, longitudinal CFRP fabric can only help carry tension force in the beam. Therefore, the fabrics in the compression zone can be neglected. According to stress distribution, force in CFRP fabrics that are in the tension zone are considered at two segment levels: the tension force in the side fabrics (T_{fab1}) and the tension force in the bottom fabrics (T_{fab2}). The total tension force due to CFRP fabric can be summed as :

$$T_{fab} = T_{fab1} + T_{fab2} = \sum_{1}^{2} (A_{fab})_i (\text{Avg}.f_{fab})_i \tag{3.8}$$

$$(f_{fab})_i = (\text{Avg}.\varepsilon_{fab})_i E_{fab} \tag{3.9}$$

Where f_{fab}, A_{fab}, ε_{fab}, E_{fab} are the stress, area, strain and modulus of elasticity of the CFRP fabrics. The average strain is considered in the fabric using a strain profile that has zero strain at the neutral axis and reaches its maximum strain at the bottom layer of the beam in a linear manner. This approach accounts for the tension force in the longitudinal CFRP fabric on the sides of the beam.

Since the exact strain in the fabric is unknown until the depth of neutral axis are determined, thus approximate values will be assumed based on the linear stress variations. For example, a balance condition occurs when the concrete strain reaches 0.003 and the maximum ε_{fab} arrives at beam bottom. Then the depth of neutral axis can be obtained by

$$c = \frac{d\varepsilon_c}{\varepsilon_c + \varepsilon_s} \tag{3.10}$$

Then, if it is found that the tensile force is not matched by the compression force, ε_{fab} should be reduced by suitable margins and a new equilibrium equation has to be solved and refined. This calculation may take two or three iterations and could be easily solved by a simple spreadsheet programming.

Once the strain in the fabric has been obtained, the total tensile force in the beam can be expressed as:

$$T = A_s f_y + \sum_{1}^{2} (A_{fab})_i (\text{Avg}.f_{fab})_i \tag{3.11}$$

According to the force equilibrium, substitute Equation 3.11 into Equation 3.3. One can obtain

$$0.85f'_c ab = A_s f_y + \sum_1^2 (A_{fab})_i (\text{Avg.}\varepsilon_{fab})_i E_{fab} \tag{3.12}$$

This equation can be used to solve for a.

After the depth of the neutral axis is determined, checks are made to verify the stress in tension steel and its validity of linear strain variation. After verifying all the assumptions, moment can be taken about the centroid of compression or the bottom of the beam. Moments about the bottom of the beam give:

$$M = 0.85f'_c ba(h - \frac{a}{2}) - A_s f_y (h - d) - T_{fab1} d'_1 \tag{3.13}$$

where h is the height of the beam and d'_1 represents the moment arm for CFRP fabrics.

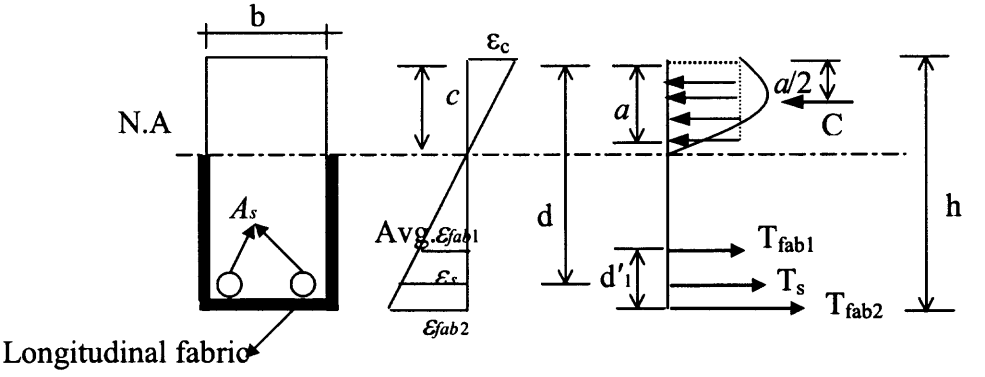

Figure 3.14 Strain distribution and force equilibrium conditions for beam CJ2/CJ3.

Beam CJ2 and CJ3 are analyzed using this approach, the detailed calculations for each beam are listed in Appendix G. Theoretical comparisons of ultimate loads are also shown in Table 3.4. Slight lower values of ultimate load are obtained for analytical predictions as compared with the experimental results.

(b) RC beam with transverse wrapping only (CJ4)

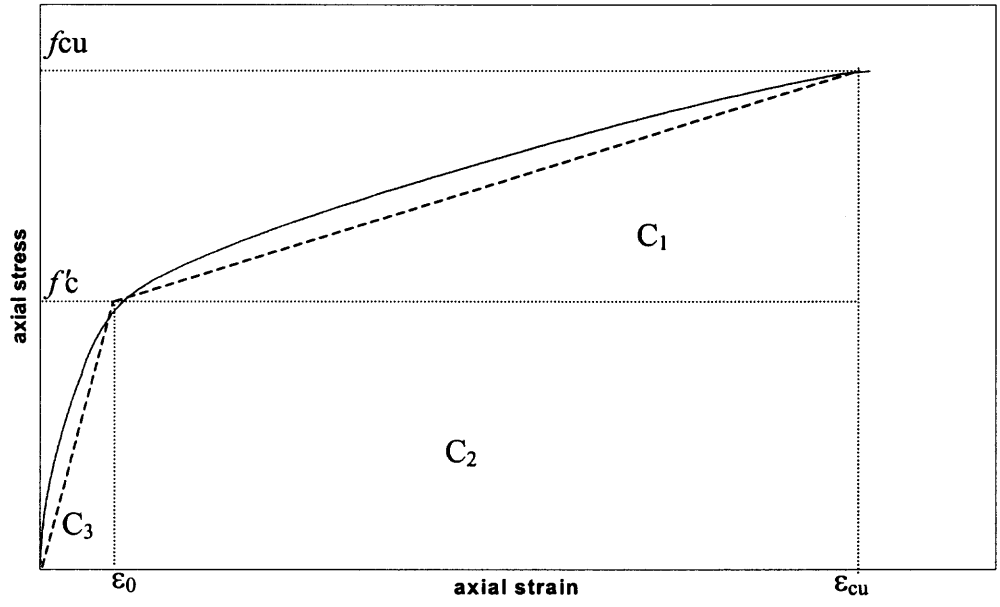

Figure 3.15 Approximate stress-strain curve for fabric-confined concrete.

For RC beam wrapped with transverse fabrics only, the concrete in the compression zone is greatly strengthened. This part of concrete can be considered as a confined concrete. Since the confined concrete has a very different stress-strain properties than the normal concrete. The equivalent compressive stress block used in equation 3.1 cannot be used here any more. A new equation needs to be derived to describe the compression force due to the fabric-confined concrete. It is well known that the compression force in the concrete can be obtained by calculating the area under the stress-strain curve. Based on the investigation from the cylinder test, the stress-strain curve of the fabric-confined concrete shows an approximate bilinear behavior. Therefore, two straight lines were used to replace the original stress-strain curve in Figure 3.15. It is assumed that when the strain reaches the unconfined concrete ultimate strain ε_0 and the stress reaches unconfined concrete strength f'_c, the stress-strain curve changes to the

second slope and finally ends when the stress and strain of the confined concrete reach their maximum values. The maximum value f_{cu} and ε_{cu} can be easily obtained by solving Equations 2.14 and 2.16, respectively. The area under this modified bilinear curve can be divided by three simple areas. Therefore the total compression force due to the confined concrete can be summed as:

$$C = C_1 + C_2 + C_3 \tag{3.14}$$

where C_1, C_2, C_3 represents the compression forces due to the three simple areas under the stress-strain curve shown in Figure 3.15, respectively.

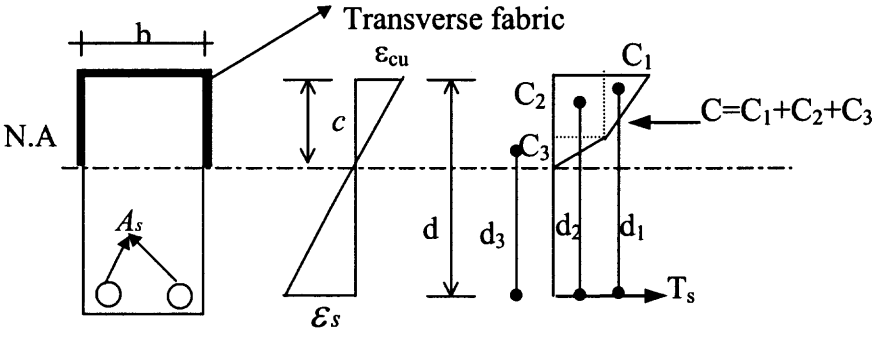

Figure 3.16 Strain distribution and force equilibrium conditions for beam CJ4.

Figure 3.16 shows the strain distribution and force equilibrium conditions for beam CJ4. Since the transverse wrapping can not take any tensile force, the tensile force in fabrics below the neutral axis is nelgected. The compression force in the confined concrete can be further written as:

$$C = \frac{1}{2}b(f_{cu} - f'_c)(c - \frac{\varepsilon_0}{\varepsilon_{cu}}c) + f'_c b(c - \frac{\varepsilon_0}{\varepsilon_{cu}}c) + \frac{1}{2}bf'_c\frac{\varepsilon_0}{\varepsilon_{cu}}c \tag{3.15}$$

After finding the compression force, Equation 3.3 can be used to solve the depth of the neutral axis c, i.e.

$$A_s f_y = \frac{1}{2}b(f_{cu} - f'_c)(c - \frac{\varepsilon_0}{\varepsilon_{cu}}c) + f'_c b(c - \frac{\varepsilon_0}{\varepsilon_{cu}}c) + \frac{1}{2}bf'_c\frac{\varepsilon_0}{\varepsilon_{cu}}c \tag{3.16}$$

once c is attained from Equation 3.16, Equation 3.5 can be used to check the strain in the tension steel. If the tension steel area is very small, the strain in the steel ε_s may reach a very a big value. When ε_s is very close to the ultimate steel strain ε_{su}, the ultimate steel stress f_{su} in stead of f_y may be used. For beam CJ4 analysis, since ρ_{min} is used in the beam, both f_y and f_{su} are used in the calculation. When the f_{su} is used, it shows a much better agreement with the experimental results. If the calculated ε_s value from Equation 3.5 is greater than ε_{su}, which means the steel has alrady broken before the confined concrete reached its ultimate strain, then the ε_{cu} value used in Equation 3.16 should be recalculated from the strain distribution in Figure 3.16. (Assume $\varepsilon_s = \varepsilon_{su}$). The c value should be calculated again also. Final moment capacity can be obtained by taking the moment about the centroid of the tension steel.

$$M = \sum_{1}^{3} C_i d_i \tag{3.17}$$

Where d_i is the moment arm for each compression force.

Appendix G lists the calculation of beam CJ4 using the above approach. The comparison between the analytical and experimenatl results is shown in Table 3.4.

(b) RC beam with both longitudinal and transverse wrappings (CJ5)

Both longitudinal and transverse fabric wrapping are used for CJ5. Due to the unidirectional characteristics, the transverse fabric below the neutral axis and the longitudinal fabricc above the neutral axis are neglected for their effectness. Since the concrete above the neutral axis is still conisdered as confined concrete, Equation 3.15 can be used here to describe the compression force. For th same reason, Equation 3.11 can be

used to define tension force. Thus the foce equrilibrium equation 3.3 can be rewritten as follows:

$$A_s f_y + \sum_{1}^{2} (A_{fab})_i (\text{Avg}.f_{fab})_i = \frac{1}{2} b(f_{cu} - f'_c)(c - \frac{\varepsilon_0}{\varepsilon_{cu}} c) + f'_c b(c - \frac{\varepsilon_0}{\varepsilon_{cu}} c) + \frac{1}{2} b f'_c \frac{\varepsilon_0}{\varepsilon_{cu}} c \qquad (3.18)$$

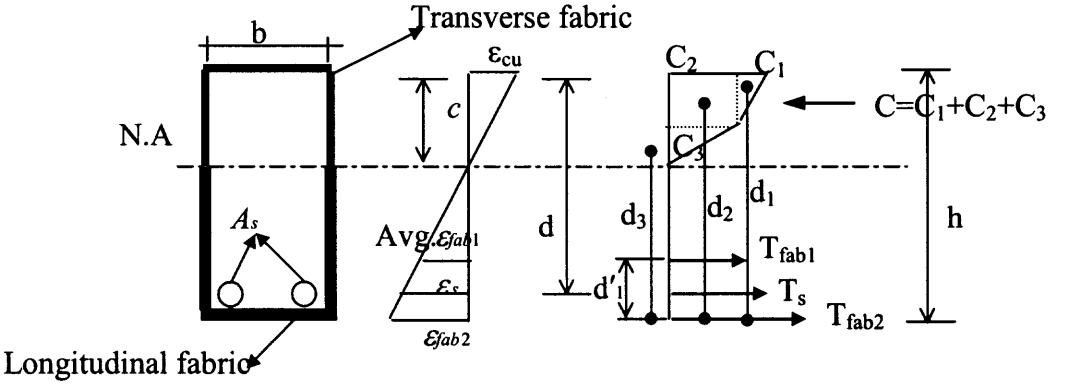

Figure 3.17 Strain distribution and force equilibrium conditions for beam CJ5.

Figure 3.17 shows the strain distribution and force equilbrium conditions for beams with two different wrappings. The same procedures used for beam CJ2/CJ3 can be used here to obtain the tensile strain in the longitudinal fabrics and the depth of neutral axis. The balance condition assumes that when confined concrete reaches its ultimate strain ε_{cu}, and the fabric also reaches its ultimate strain ε_{fab}. Then c value is thus obtained by the strain distribution and force equilibrium Equation 3.18. If the compression force does not equal to tension force, a new value of ε_{fab} should be assumed. More iterations are needed to carry out until the correct c value has been found. The strain in the tension steel should also be checked by the strain distribution. Finally, the moment capacity can be obtained by taking moment about the bottom of the beam.

$$M = \sum_{1}^{3} C_i d_i - A_s f_y (h - d) - T_{fab1} d'_1 \qquad (3.19)$$

Table 3.4 Experimental Results versus Analytical Results

Test Beam	Concrete Strength (psi)	Ultimate Load P_{Exp} (kips)	Ultimate Load P_{ACI} (kips)	Ultimate Load P_{ANSYS} (kips)	P_{Exp}/P_{ACI}	P_{Exp}/P_{ANSYS}
CJ1	4250 (29.3MPa)	5.4 (24.5kN)	4.73 (21.0kN)	4.8 (21.4kN)	1.14	1.13
			6.24* (27.7kN)		0.87*	
CJ2	4317 (29.8MPa)	17.0 (75.7kN)	13.4 (59.6kN)	16.2 (72.1kN)	1.27	1.05
			14.5* (64.5Mpa)		1.17*	
CJ3	4085 (28.1MPa)	20.2 (89.9kN)	17.3 (76.9kN)	19.6 (87.2kN)	1.16	1.03
			18.0* (80.1kN)		1.12*	
CJ4	4705 (32.4MPa)	6.45 (28.7kN)	4.77 (21.2kN)	5.5 (24.5kN)	1.35	1.17
			6.33* (28.2kN)		1.02*	
CJ5	4566 (31.5MPa)	17.8 (79.2kN)	13.9 (61.9kN)	18.5 (82.3kN)	1.28	0.96
			15.3* (68.1kN)		1.16*	

* Steel ultimate strength f_{su} =80 ksi is used

However, since the confined concrete has a very high ultimate strain, in some case the CFRP fabrics may reach its ultimate strain ε_{fab} before the concrete reaches ε_{cu}. Therefore if the calculated tensile strain in the fabrics is far more than its ultimate strain ε_{fab}, the average strain in the bottom fabrics should remain at ε_{fab} and start the iterations by reducing the strain in the confined concrete until the new c value can be found. The compression force Equation 3.15-19 will also be changed using the actual strain value instead of ultimate value ε_{cu}. It can be expected that the final moment capacity of the beam will become smaller due to the early rupture of the fabrics. Beam CJ5 in this

research is exactly in this case because the very low tensile steel ratio is used in the beam. The detailed calculation of beam CJ5 is listed in Appendix G.

Table 3.4 compares the analytical values from the modified ACI equations to the experimental values, which shows that the ultimate loads computed by the modified ACI equations give more conservative values than the experimental ultimate loads and the ultimate loads derived from the finite element method. If f_{su} value was used instead of f_y, design yield strength, a better agreement between all ultimate loads can be achieved.

3.4.3 Finite Element Method

As mentioned in the literature review, much work including some computer programs has been done to analyze the load-deflection behavior of RC beams wrapped with CFRP fabrics since 1980s. But all these efforts are based on beam theory and usually employed two-dimensional models. With the rapid development of digital computing, there are many comprehensive engineering software packages available (such as ANSYS, ADINA, and ABAQUS) to solve these problems. All of these packages have sophisticated nonlinear equation solvers, and convergence control techniques. There are also having 3-D solid elements that are suitable for modeling reinforced concrete structures. Finite element analysis can give more insight into the problem in question and usually gives more accurate results as compared with the traditional methods.

ANSYS was used in this research to analyze the load-deflection behavior of the test specimens. The concrete in the test beams is modeled with 3-D block elements (Solid65 in ANSYS) with cracking and crushing capabilities. For beams with longitudinal fabrics (CJ2/CJ3), the normal concrete material properties are used. For beams with transverse fabrics (CJ4/CJ5), the confined concrete material properties

described in Chapter Two are used. Reinforcement is modeled with 3-D spar elements (Link8 in ANSYS) with bilinear material properties. Longitudinal CFRP fabric is modeled with spar elements (Link8) with elastic linear properties. Transverse fabrics and steel stirrups are neglected in the modeling.

All the beams are modeled as simply supported beams. Boundary conditions are applied accordingly. At a cross section, the beam is modeled with sixteen Solid65 elements with equal sizes. Meshing in the longitudinal direction is set to twenty elements along the length of the beam. Figure 3.18 shows the finite element model. A total of 520 elements are used to model each specimen, among which 320 are Solid65 8-node block elements, 40 are Link8 2-node bar elements and 160 are Link8 fabric elements. The solution time for each run is approximately 1-2 hours.

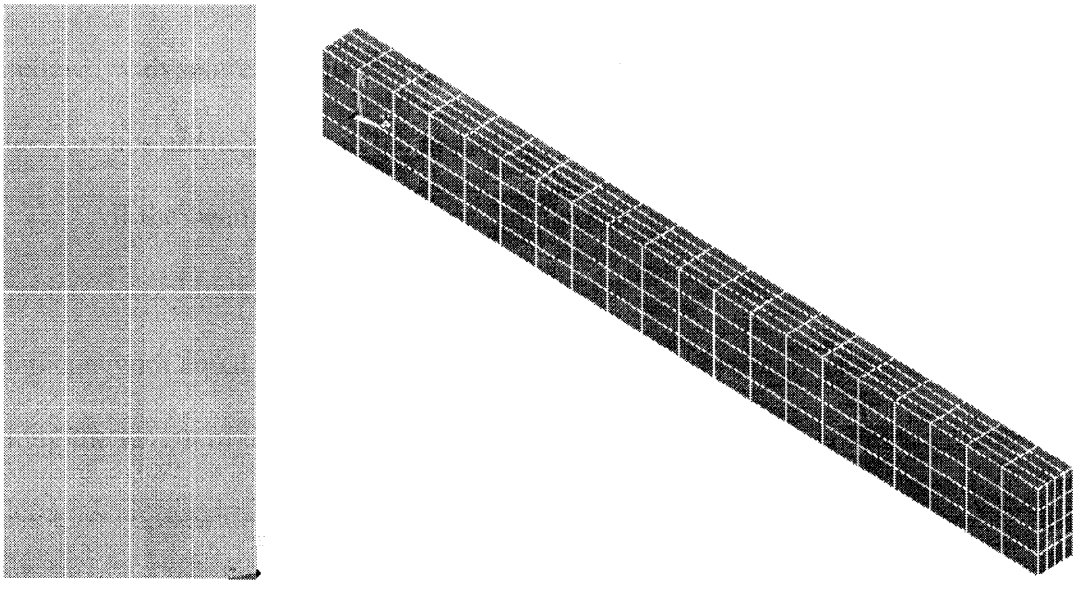

Cross Section Isotropic view

Figure 3.18 Finite element model for test beams.

Concentrated load is applied at the center of the beam. Small increases are applied to the load levels. For each load level, the middle span deflections are calculated. The program stops when the solution cannot converge at certain level. Finally the overall load-deflection curve can be obtained. To verify the finite element model, the analytical load-deflection curves using this model are compared to test results. The ultimate load capacity from ANSYS is also compared with the modified ACI method. Since the moment-curvature curves from the test results are not quite complete, as mentioned earlier, no moment-curvature curves are calculated from the ANSYS program.

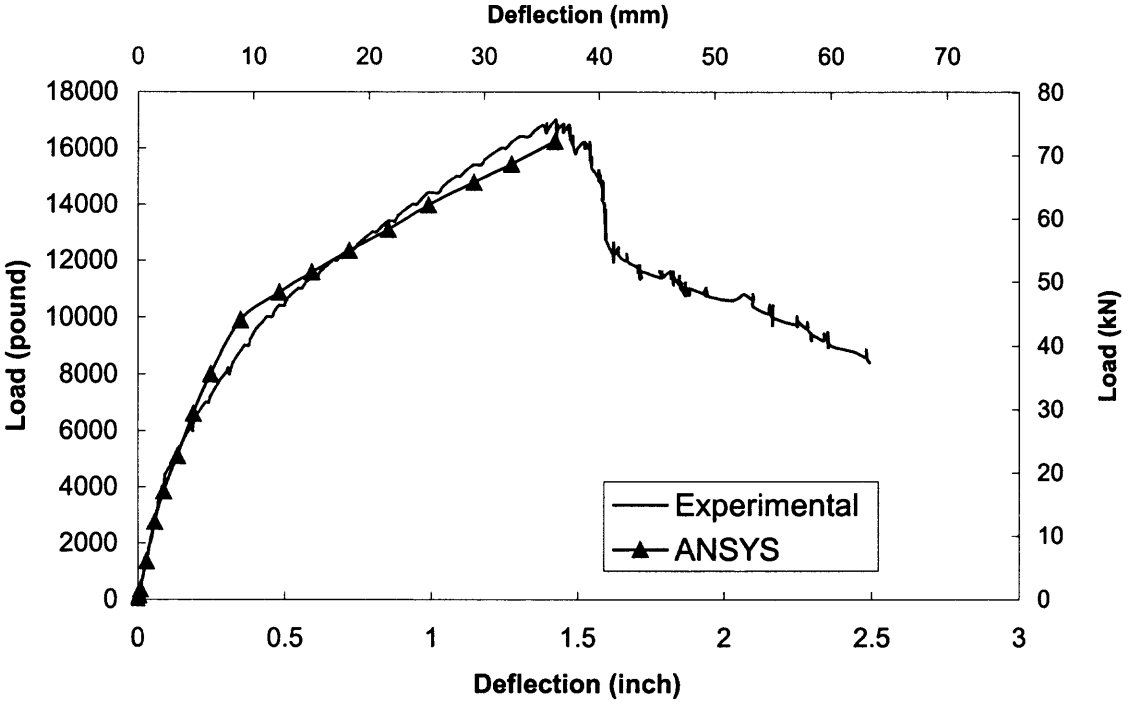

Figure 3.19 Analytical versus experimental results for beam CJ2.

Appendix D.11-15 lists the experimental versus ANSYS results for all the test beams. Figure 3.19 gives a typical comparison of the load –deflection curves between experimental and analytical results for beam CJ2. From the figures and Table 3.4, one can clearly see that good agreements are obtained for all the beams. It is noticed that the

ultimate loads from the ANSYS are usually a little lower than the experimental results. Although the differences are very small, it is probably because the design yielding strength of steel has been used for the ANSYS model. Figure 3.19 also shows that the deflections from ANSYS are in good agreement with the experimental curves. It is noted that ANSYS cannot model the descending part of concrete stress-strain behavior. But in experiments, the post-peak deformation is usually very large due to the yielding of the steel rebars. Overall, the load-deflection curves calculated from ANSYS are quite satisfactory as compared with the experimental results, from zero to the ultimate capacity.

3.5 Summary and Recommendations

Different wrapping methods are applied and investigated in this research. Based on present experimental results, pure longitudinal fabric wrapping has significantly increased the flexural strength of the test beams, but it has also decreased the deformation of the beam. As a result, the beams fail in a less ductile mode. On the other hand, pure transverse fabric confinement has greatly increased the deformability and ductility of the test beams, but it almost has no effect on the flexural strength capacity of the beam. The beam wrapped with both longitudinal and transverse fabrics has the best overall flexural performance due to its high strength, high deformability and a good ductile failure. Considering that the two-directional fabrics are already in the market, the applications of the two-directional fabrics are recommended. However, due to the construction difficulties, the transverse wrapping is usually very hard to apply to the top of the beams in an actual construction, the use of the two-directional wrapping method is still limited.

Ultimate load capacities of wrapped beams can be predicted using the conventional beam-bending theory (in accordance with ACI 318-95) by properly accounting for tensile forces in carbon layers and compressive forces in the confined concrete. Related design equations and design examples for the test beams are presented in this research. When compared with the experimental results, a somehow conservative value has been obtained for all test beams. Due to its simlicity and effectiveness, this modified ACI method can be recommended to every designer or engineer for analyzing and designing RC beams with CFRP fabric wrapping. Finite element approach using the ANSYS program is also presented in this research. A comparison of the load-deflection curves between experimental and analytical results shows an excellent agreement for all the test specimens.

CHAPTER 4

BEHAVIOR OF BIAXIALLY LOADED RC SLENDER COLUMNS STRENGTHENED BY CFRP FABRICS

4.1 Introduction

The use of CFRP fabrics in the concrete columns of bridge and high-rise buildings has become increasingly popular since 1980's. The CFRP fabrics can greatly increase the strength, ductility and overall structural performance of the strengthened columns. However, as far as the fabric-confined concrete columns are concerned, most of the previous research work has concentrated on members subjected to axial compression only. In practice, some columns are subjected to bending about both principal axes simultaneously, especially the corner columns of the building and the columns in the bridges. Therefore basic experimental and analytical studies for the behavior of biaxially loaded fabric-wrapped RC columns have become a necessity.

In this research, seven quarter-scale slender columns were wrapped with CFRP layers and tested under biaxial compression loads. Three different wrapping methods were utilized during the experiments. Several experimental factors such as strength, structural ductility, post-crack behavior and the failure mechanism were studied during the tests. Also, an analytical study based on the finite segment method and confined concrete stress-strain model was proposed to analyze both load-deflection and moment-curvature behavior of the fabric-confined columns.

4.2 Experimental Scheme

4.2.1 Design of Concrete Columns

All the columns to be tested are designed to be slender columns. That means the cross-sectional dimensions of the columns have to be small compared with its length. Generally, the degree of slenderness is expressed in terms of the slenderness ratio l/r, where l is the unsupported length of the column and r is the radius of gyration of its cross section. Based on this concept, same column dimensions from the experimental works of Tsao (1991) and Bahn (1994) are adopted in this research. Due to the size limitations of the testing machine, the total length of the column is set to be 4 ft. (1.22m) and the nominal square cross section is 3.0×3.0 in. (76×76 mm), which results in a slenderness ration of 55. Two 7.0×7.0×8.0 in. (178×178×203 mm) concrete loading brackets are provided at the column ends to assist with the application of biaxially eccentric load. All the columns are designed to be tested in the combination of both axial compression and biaxial bending. Based on the investigations from Tsao (1991) and Bahn (1994), the column which has the same eccentricities at both coordinate axes will has the most critical secondary moment. Therefore, eccentricities used in this research are 2 inch (50.8mm) in both directions. The details of the test specimens can be seen in Table 4.2 and Figure 4.4-4.7.

Four No. 3 steel rebars are designed as main compression bars. The cover with 0.5 in. (12.7 mm) thickness to the longitudinal bars is to protect the steel bars. 12-gage plain steel wire is also used at a 3 in (76 mm) spacing for the lateral ties. The two brackets in each column are heavily reinforced with No.3 steel rebars to prevent any premature failure. The details of steel rebars can be found in Figure 4.1.

4.2.2 Materials

4.2.2.1 Carbon Fiber Reinforced Plastic and Epoxy. The same fabric materials used in cylinder testes and beam tests are used here; namely SikaWrap Hex 230C for longitudinal and transverse fabrics and Sikadur-330 for the Epoxy adhesive. The properties for both of them are given in Table 2.1.

4.2.2.2 Concrete. The concrete used in the column consists of Type I cement satisfying with ASTM 150, sand from local source, crushed stone with maximum aggregate size of 3/8 in. (9.5mm). The concrete is expected to have a average 5000 psi (34.5 Mpa) compressive strength after 28 days. All columns in this research use the same mix design, and they are listed in Table 4.1.

Table 4.1 Mix Design of Concrete Columns

Concrete Compressive Strength	Water /Cement ratio	Cement (lbs/ yd^3)	Stones (lbs/ yd^3)	Sand (lbs/ yd^3)	Water (lbs/ yd^3)
5000 psi (34.45 MPa)	0.57	676 (3930 N/m^3)	1309 (7612 N/m^3)	1500 (8722 N/m^3)	370 (2151 N/m^3)

4.2.2.3 Reinforcement

Four No.3 bars are used in the columns to resist the combined force due to the axial compression and biaxial bending. The yield stress of the No.3 bars is 58 ksi (400MPa). The complete stress-strain behavior of the No.3 bar is shown in Appendix A. 12-gage steel wires are used as stirrups. Five U-shape No.3 steel bars are used to reinforce the loading brackets. The detailed steel arrangement can be seen from Figure 4.1.

Figure 4.1 Steel reinforcement for test columns.

4.2.3 Cast and Cure of the Concrete Columns

To minimize scattering, all specimens followed the same procedures for material mixing, casting, and curing.

A total of seven slender columns were cast at the concrete laboratory of NJIT. They were divided by five batches with two columns cast each batch. Wooden form (Figure 4.2) and steel rebars (Figure 4.1) were prepared before the concrete was mixed. The same mixing procedures used in cylinder and beam tests were used here. For each batch of concrete, three 4 in. × 8 in. (102mm × 203mm) cylinders were made at the same time to predict the compressive strength of the concrete columns. The average stresses for the cylinders are listed in Table 4.2. All specimens were demolded after 48 hours and cured in a standard curing room for 28 days to achieve an expected strength.

Table 4.2 Test Outline of Column Specimens

Specimen	f'_c (psi)	Main Bars	e_x (inch)	e_y (inch)	L (inch)	Fabric Applied
CJC1 (Trial)	5500 (37.9MPa)	4#3	0.765 (19.4mm)	1.848 (46.9mm)	48 (1219mm)	None
CJC2	5235 (36.1MPa)	4#3	2 (50.8mm)	2 (50.8mm)	48 (1219mm)	None
CJC3	5785 (39.9MPa)	4#3	2 (50.8mm)	2 (50.8mm)	48 (1219mm)	One layer Transverse
CJC4	5065 (34.9MPa)	4#3	2 (50.8mm)	2 (50.8mm)	48 (1219mm)	Two layers Transverse
CJC5	6146 (42.3MPa)	4#3	2 (50.8mm)	2 (50.8mm)	48 (1219mm)	One layer Longitudinal
CJC6	5538 (38.2MPa)	4#3	2 (50.8mm)	2 (50.8mm)	48 (1219mm)	Two layers Transverse
CJC7	6138 (42.3MPa)	4#3	2 (50.8mm)	2 (50.8mm)	48 (1219mm)	Longitudinal + Transverse

Where f'_c = Compressive strength of concrete

e_x, e_y =Eccentricities along X-Axis and Y-axis, respectively.

L = Total length of Column specimens

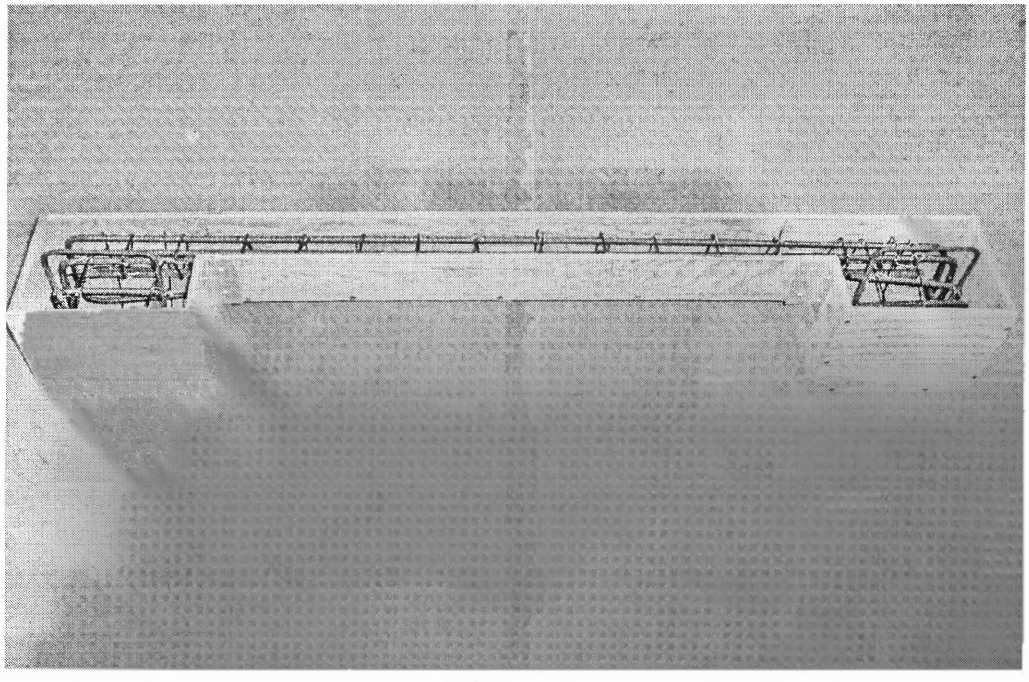

Figure 4.2 Wooden form for the test columns.

4.2.4 Installation of CFRP Strengthening System

As we mentioned before, the concrete surface of the column to be strengthened has to be well treated before the CFRP fabric is applied. Similar procedures used to bond RC beam specimens can be used here. The trial column and the control column have no fabric applied. Three of the columns were wrapped by transverse fabric only with different layers. One column was wrapped by one layer of longitudinal fabric only. The last one was wrapped by both longitudinal and transverse fabric. Since column CJC4 failed at the brackets, half of the specimens were wrapped with transverse fabric at the brackets too. The detailed installation procedures are shown in Figure 4.3

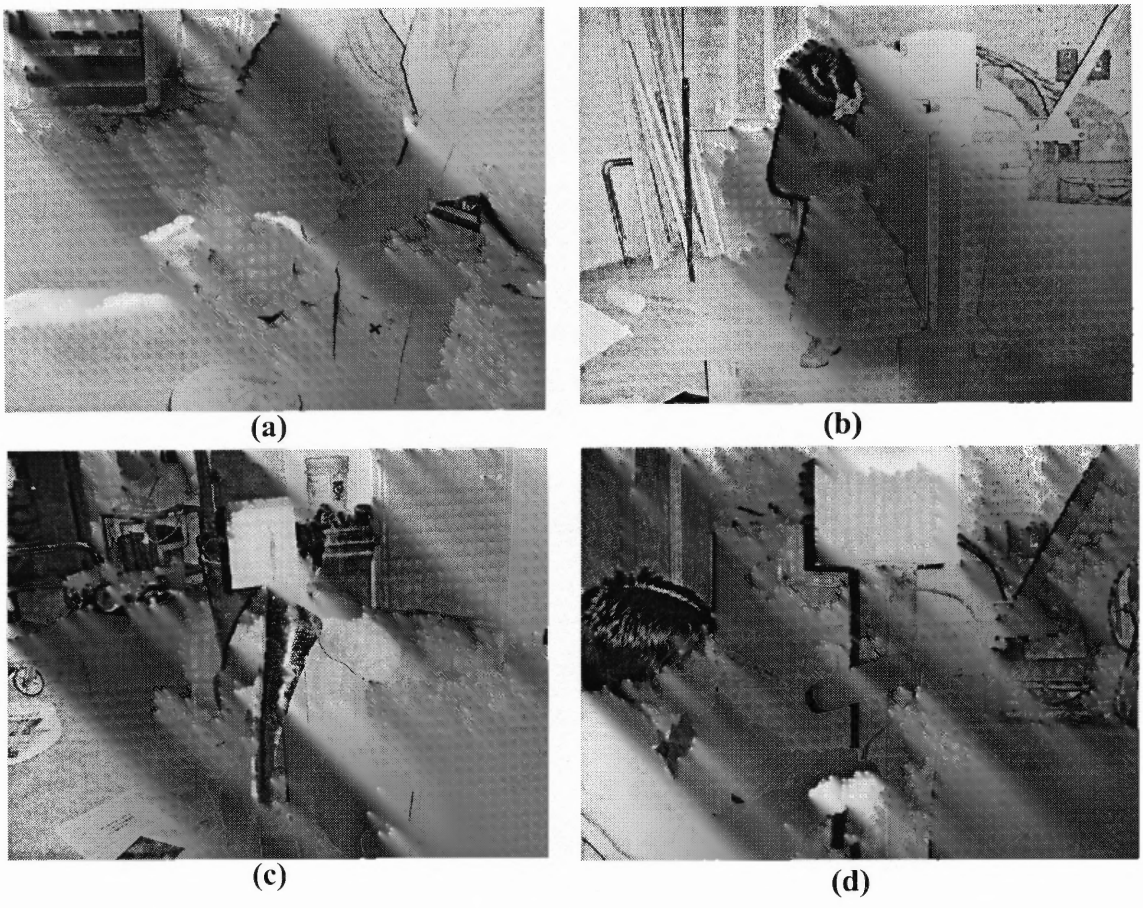

Figure 4.3 Installation of CFRP fabrics to the columns.
(a) Mixing epoxy; (b) Apply the epoxy on the surface of the concrete;
(c) Wrap the fabric jacket around the column; (d) Consolidate the specimen.

4.2.5 Column Specimens Configuration

All Column configurations are listed below. As mentioned earlier, there are three different wrapping configurations. All column specimens have the same length, concrete compressive strength, steel reinforcement, cross sectional areas and stirrup spacing. For trial column CJC1 and control column CJC2 (Figure 4.4), there is no fabric attached. For beam CJC3 (Figure 4.5), one layer of fabrics is wrapped transversely on four sides of the column surface. For beam CJC4 and CJC6 (Figure 4.5), the same configuration as CJC3 is used but two layers of fabrics are used. It is noted that from column CJC5, the transverse fabrics are also provided at two brackets for extra strengthening. For beam CJC5 (Figure 4.6), one layer of the fabrics is wrapped longitudinally along the length of the column. For column CJC7 (Figure 4.7), one layer of fabrics is wrapped longitudinally at first, and then another layer of the fabrics is wrapped transversely afterwards.

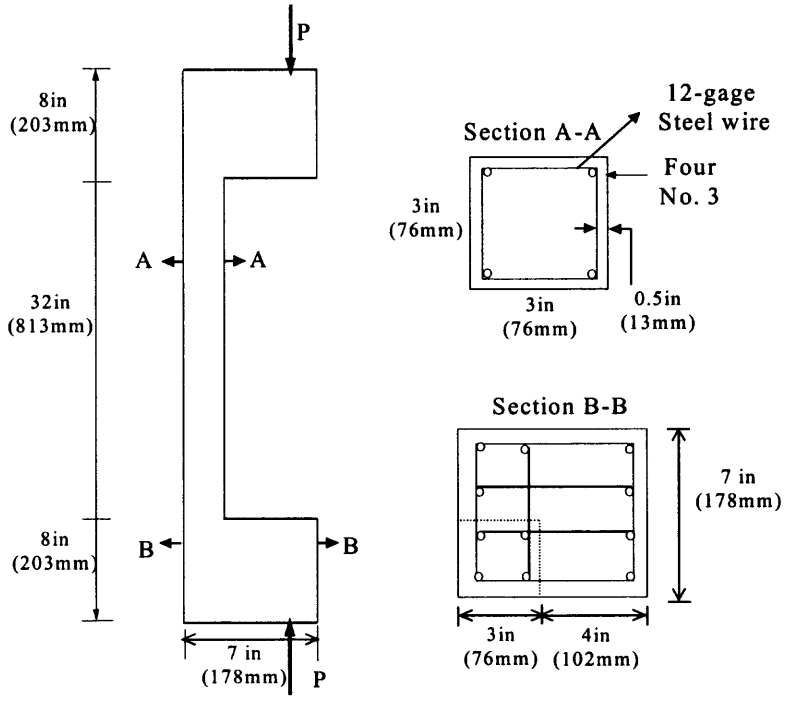

Figure 4.4 Column configuration of CJC1/CJC2.

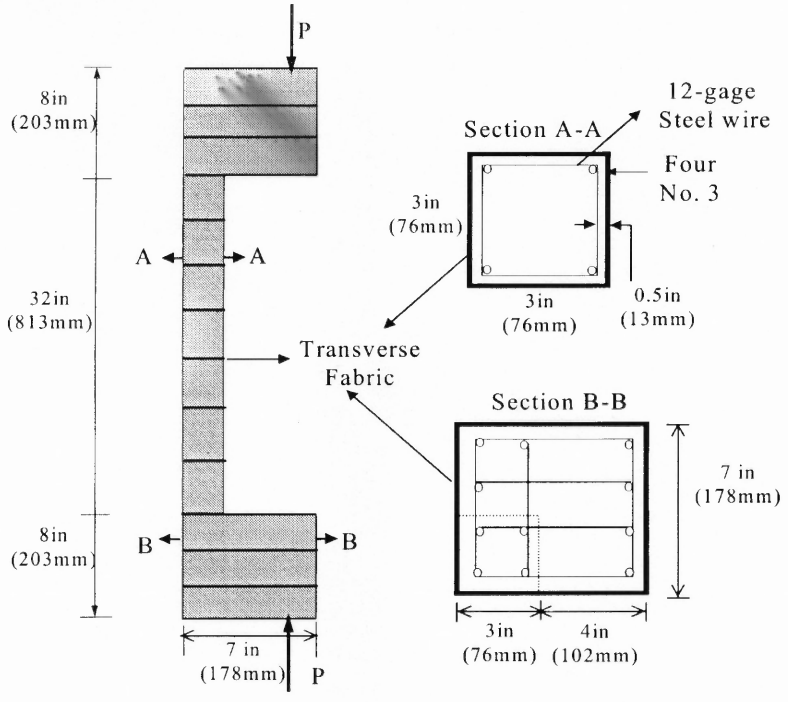

Figure 4.5 Column configuration of CJC3/CJC4/CJC6.

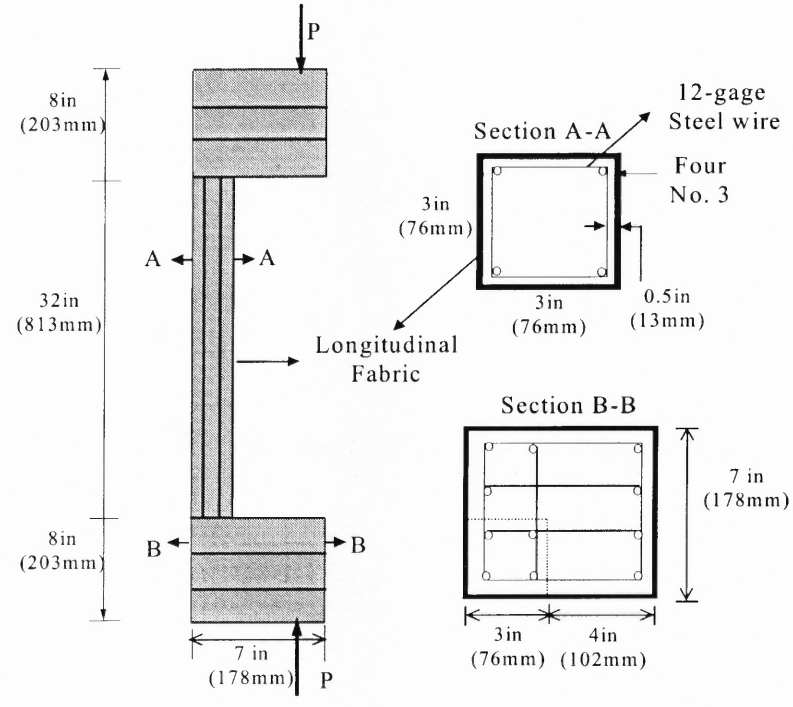

Figure 4.6 Column configuration of CJC5.

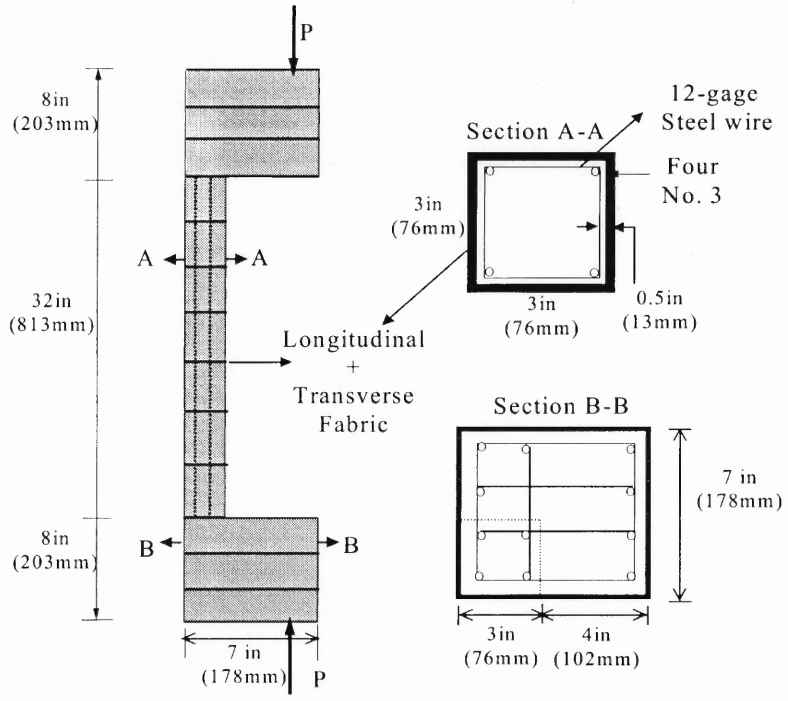

Figure 4.7 Column configuration of CJC7.

4.2.6 Experimental Setup

The column tests were conducted by an electro-hydraulic closed loop servo controlled materials testing system (MTS) under stroke control. To obtain the complete ascending and descending branches of biaxial load-deflection curve, loads were applied at a very small increment, which is 0.05 in. (1.3mm) per minute for stroke control.

To avoid local failure at the column ends, steel plates were attached to each end of the specimens. The axial load was transmitted to column at each end by the steel plates. Hinged end conditions were achieved by putting steel ball bearings on the steel plates. The desired eccentricities were obtained by moving the ball bearings to the proper positions relative to the center of the cross section. The column specimens were adjusted so that the centerline of the end bearing facing the load cell coincide with its center line.

Subsequently, a small load was applied to keep the specimens in place. A typical test setup is shown in Figure 4.8.

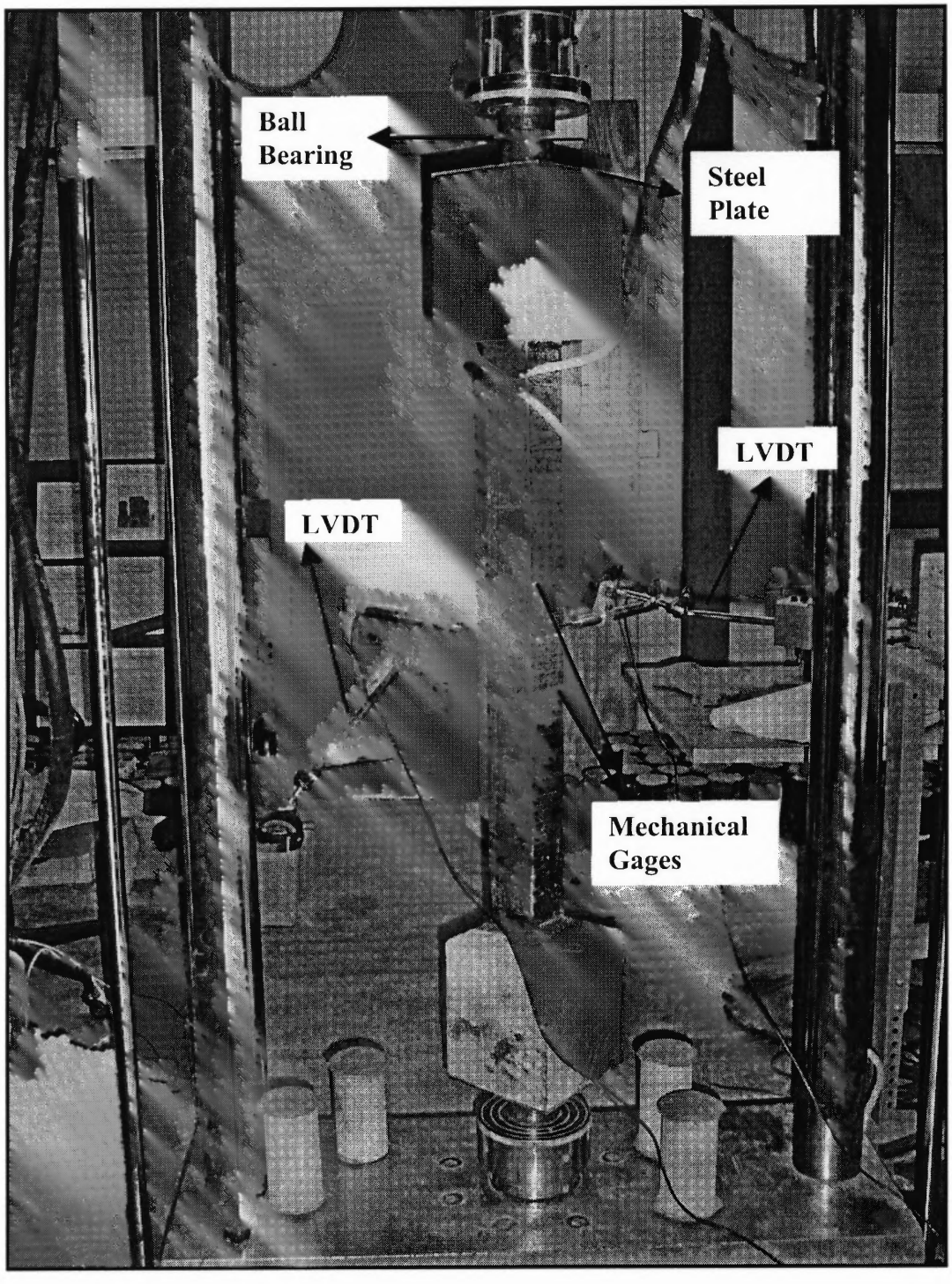

Figure 4.8 Typical column specimen setup.

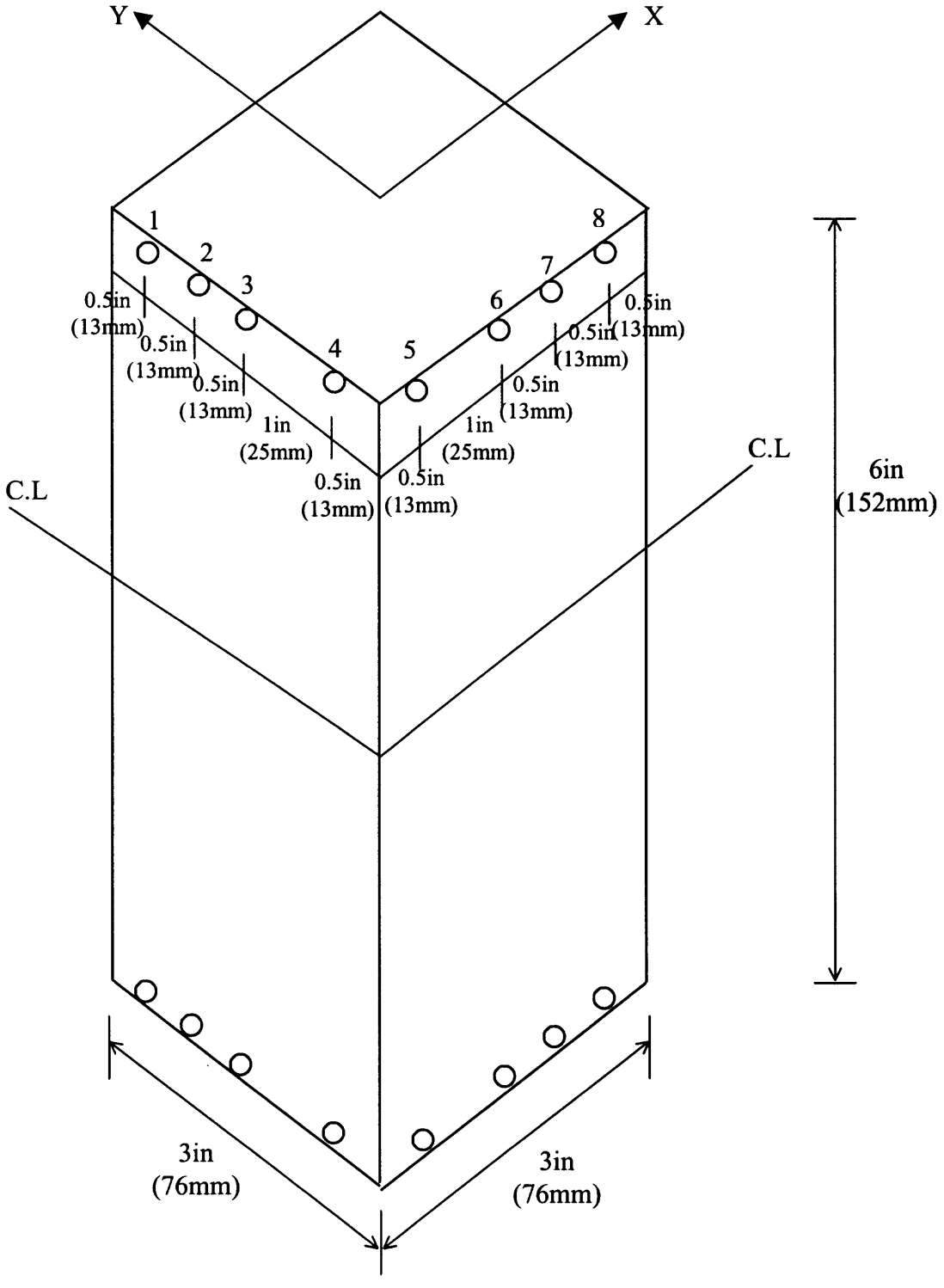

Figure 4.9 Arrangement of mechanical strain gages over column segment.

Two 2 inch (51mm) range linear voltage differential transducers (LVDT) were used to measure the deflections at mid-height of the column specimens in both X and Y directions. The LVDTs were connected to a computerized data acquiring system that was connected to the MTS machine itself. Then the deflections from LVDT as well as axial load from the load cell were recorded to the computer as a rate of 10 times per second until the specimen failed. The LVDTs needed to be adjusted during the test process because the deflection at each direction might exceed the limit of the reading range. Eight mechanical strain gages were provided to measure the vertical strain at the central portion of the column so that the average curvature in both X and Y directions at mid-height could be attained. Figure 4.9 shows the arrangement of mechanical gages for the present slender column specimens. At every 1 kips (4.5 kN) loading level, the strain values for each pair of mechanical gages were recorded (Appendix B.20). If the concrete or fabric failed outside the 6 in. (152 mm) measured range, further measurements were not recorded. The reason was that at this time, the plastic hinge rotated outside of the measured areas at mid-height.

4.2.7 Test Procedures

The test procedures for each beam can be described as follows:

(a) Column CJC1

The first column tested was a trial column CJC1 (Appendix B.13). The eccentricities at X and Y directions are 0.765 in (19.4mm) and 1.848 in (46.9mm), respectively. No fabric was applied. When the load reached 7.8 kips (34.7 kN), the first flexural crack occurred at the foot of the column. As the load increased, more cracks developed around the initial crack. Therefore, the plastic hinge occurred at the end of the column. When load reached

9.7 kips (43.2 kN), the load started to drop as the deflection started to increase quickly. When the load dropped to around 5 kips (22.3 kN), the specimen failed due to the crush of the concrete in the compression zone (Figure 4.10). No obvious buckling was found. Since the eccentricity was different at two axes, the deflection at y direction was much higher than that at x direction.

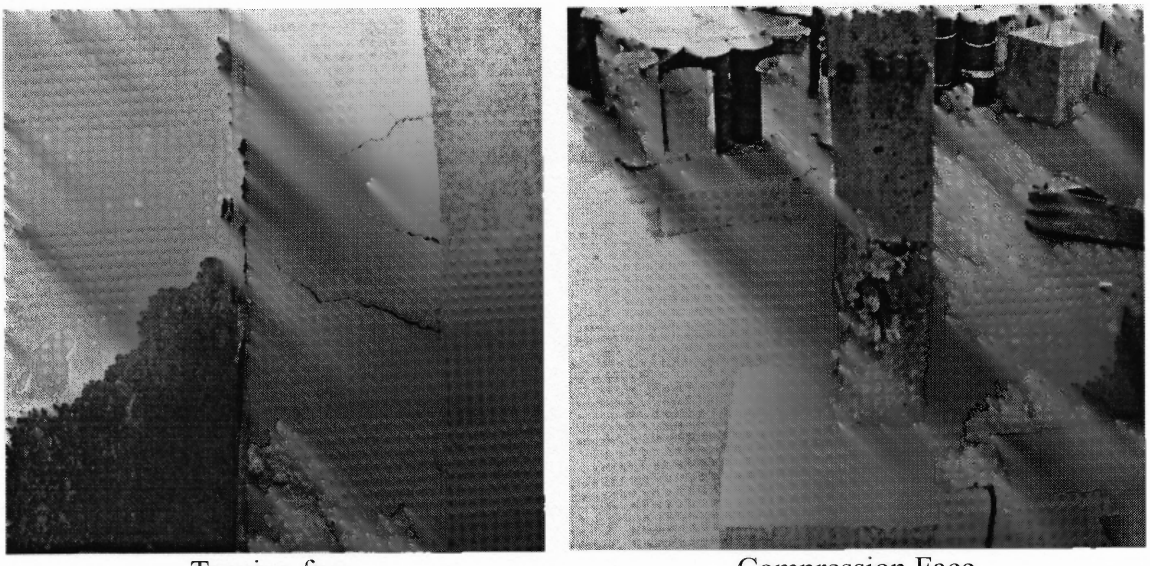

Tension face Compression Face

Figure 4.10 Failure of column CJC1.

(b) Column CJC2

The second column tested was control column CJC2 (Appendix B.14). Starting from this one, all the column specimens used the same eccentricities at both directions. No fabric was applied on this column. When load reached around 7 kips (31.2 kN), the initial crack occurred at the tension face around the center of the column. Another two flexural cracks developed near the initial crack as the load went up. Obviously the plastic hinge occurred exactly at the center of the column. The load started to drop after it reached 8 kips (35.6kN). Due to the rotation of the plastic hinge, the deflection at both directions started

to increase rapidly. The specimen finally failed when the concrete at the compression sides totally got crushed (Figure 4.11). There was no obvious buckling of the steel bars.

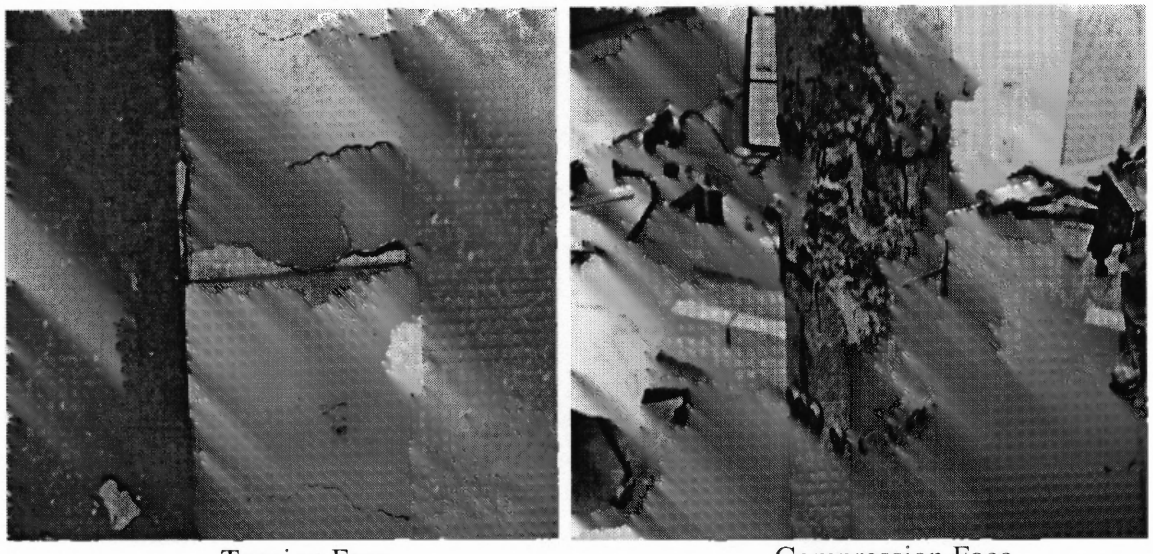

Tension Face Compression Face

Figure 4.11 Failure of column CJC2.

(c) Column CJC3

The next column was CJC3 (Appendix B.15), which was transversely wrapped with one layer of fabric around the four sides of the column. Since the column was completely wrapped, the initial crack could not be seen from the outside. However, the continuous sound of the delamination between the concrete and CFRP fabric was heard after the load reached around 8.5 kips (37.8 kN). One of the first fabric strip was delaminated at the tension face near the center of the column when the load reached 8.9 kips (39.6 kN). As the load went up, more and more strips started to get ruptured and delaminated. It was clear that the plastic hinge occurred exactly at the center of the column. The load started to drop after it reached 9.8 kips (43.6 kN). When the specimen finally failed around 6 kips (26.7 kN), the fabrics at the center of the column were totally ruptured. At this time,

the column exhibited several flexural cracks at the tension faces and crush of the concrete at the compression faces. No steel buckling could be seen from the specimen.

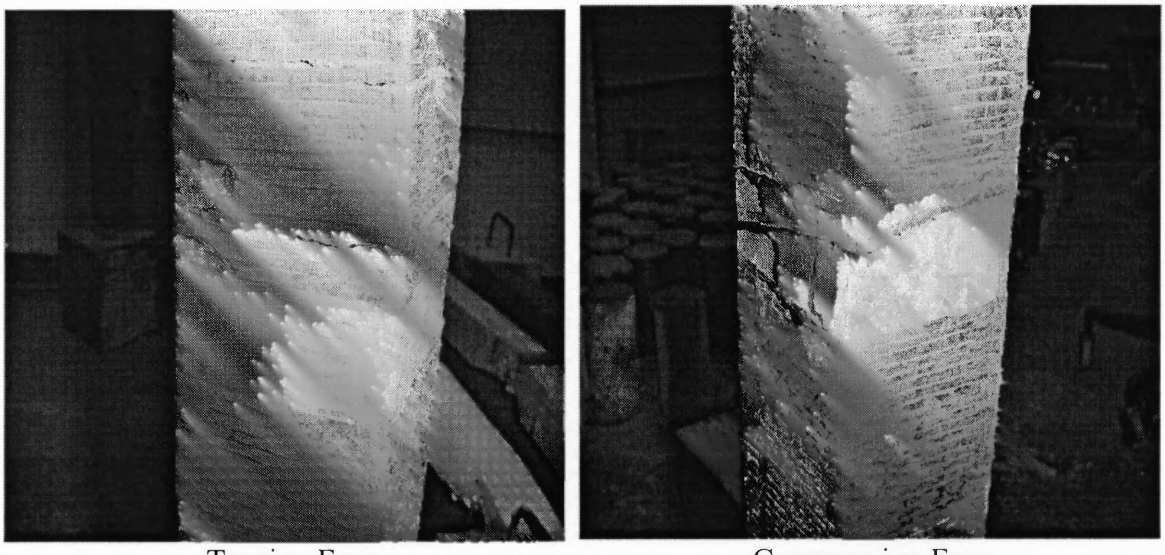

Tension Face Compression Face

Figure 4.12 Failure of column CJC3.

(d) Column CJC4

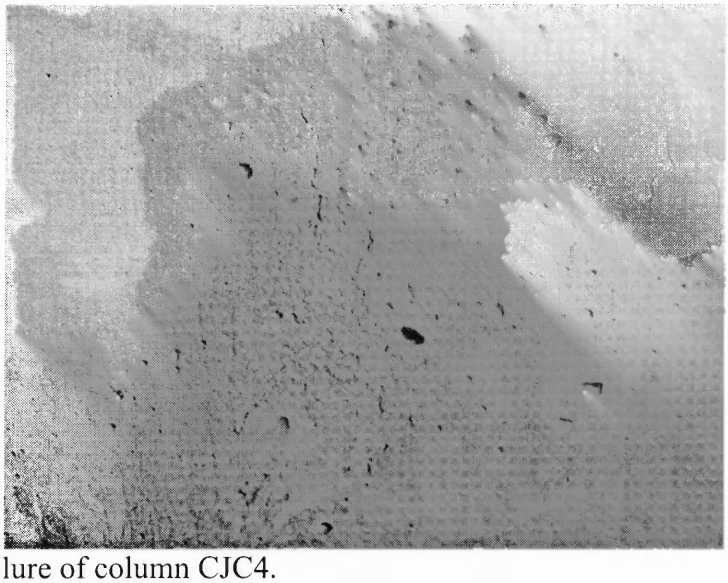

Figure 4.13 Failure of column CJC4.

The fourth column tested was CJC4 (Appendix B.16), which was transversely wrapped with two layers of fabric. This test was unsuccessful because the specimen failed very

early at the top bracket of concrete column (Figure 4.13). To avoid future bracket failure, the brackets were wrapped transversely starting from column CJC5. A new specimen with two layers of transverse fabric was cast and tested as column CJC6 to replace CJC4.

(e) Column CJC5

The next test column was CJC5 (Appendix B.17), which was longitudinally wrapped with one layer of the fabrics. As mentioned before, the brackets were wrapped to avoid early failure. One of the first longitudinal fabric strips started to delaminate at the center of the column when the load went up to 7.8 kips (34.7 kN), More delaminations and rupture were found near the center of the column as the load increased. When load started to drop at 9.8 kips (44 kN), nearly half of the fabric strips at the tension faces had been delaminated or ruptured. The specimen finally failed suddenly when one of the steel bars buckled (Figure 4.14). Flexural cracks could be clearly found when the longitudinal fabric strips were ruptured.

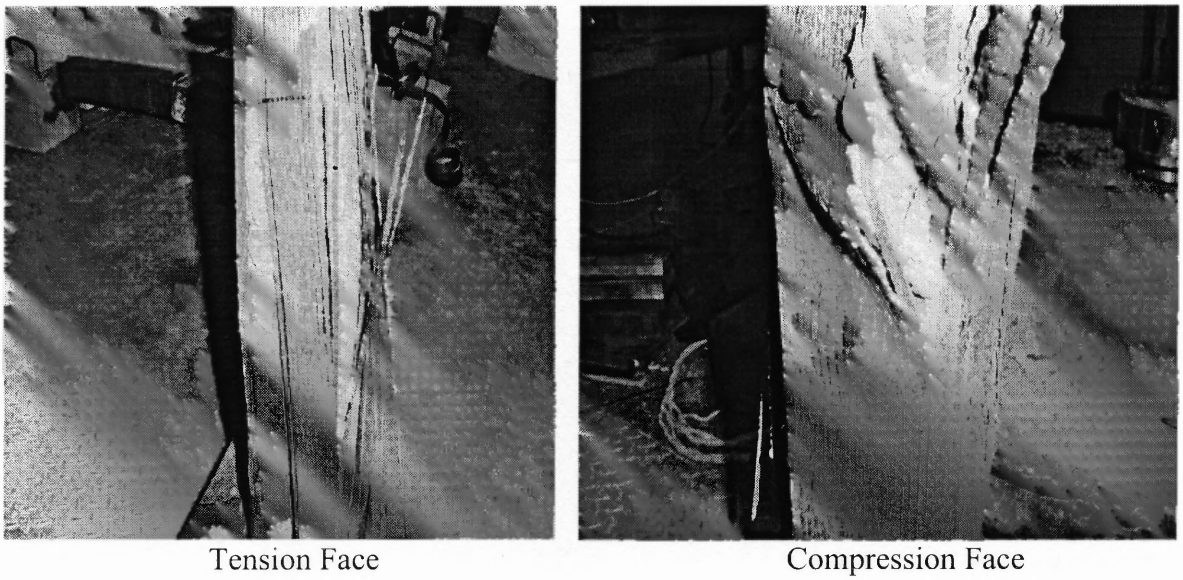

Tension Face Compression Face

Figure 4.14 Failure of column CJC5.

(f) Column CJC6

Column CJC6 (Appendix B.18) was to replace column CJC4, which failed pre-maturedly. Column CJC6 was transversely wrapped with two layers of fabrics. It has the same wrapping configuration as column CJC3 but with two layers of fabrics. Therefore the test procedures of this specimen were very similar to those of column CJC3. The noise of delamination was heard at about 6 kips (26.7 kN), and the first visible rupture of the fabric strip was noticed later around 8.5 kips (37.8 kN) at the center of the column. This was because the rupture and the delamination of the fabric strips started from the inner layer of the fabrics that could not be seen from the specimen. As the load continued growing, more fabric strips stared to get ruptured and delaminated at the center. When the load went up to 10.2 kips (45.4 kN). There was a large crack occurred near the initial delaminated strip, and then the load started to drop quickly. The test finally stopped at 6.1 kips (27.1 kN) (Figure 4.15) with no obvious steel buckling found. Compared to column CJC3, the delamination and rupture of the fabrics were much slighter, especially in the compression zone.

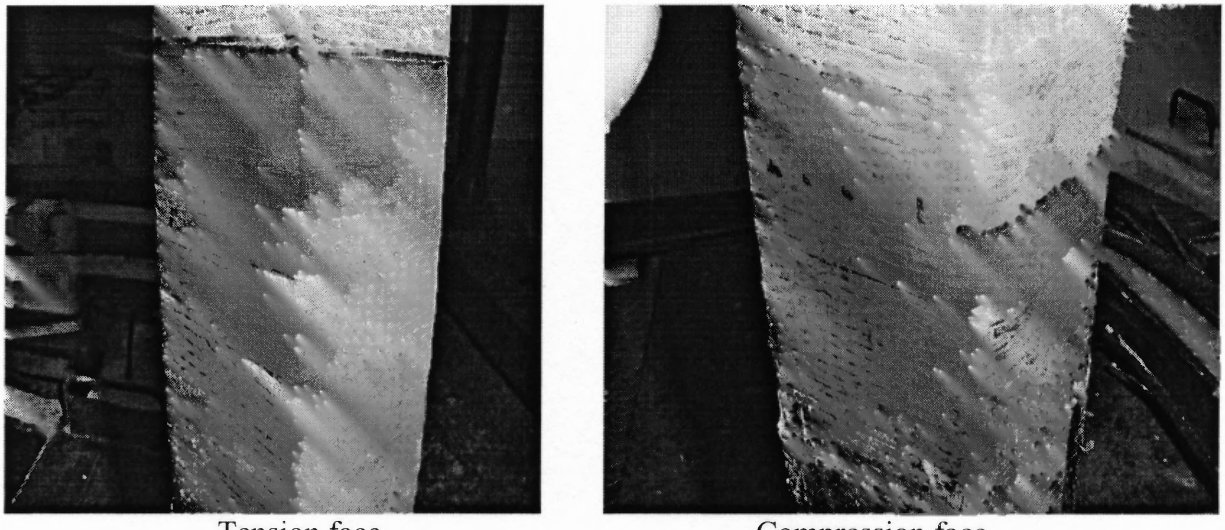

Tension face Compression face

Figure 4.15 Failure of column CJC6.

(g) Column CJC7

The final beam tested was CJC7 (Appendix B.19). This beam was wrapped with one layer of longitudinal fabric inside first, then with another layer of transverse confinement outside. No clear noise of delamination was heard before the load reached about 10 kips (44.5 kN). After this moment, continuous noise of rupture and delamination between the fabric and concrete was noticed. However, due to added transverse confinement, no visible rupture or delamination was found from outside of the column. When the load went up to 12.5 kips (55.6 kN), the first flexural crack occurred near the end of the column. Through the crack one could see some broken longitudinal fabric strips inside. The load started to drop after it reached 13.3 kips (59.2 kN). As the load continued to drop, the initial crack became larger and larger, which showed the plastic hinge occurred near the foot of the column. The specimen finally failed at 7.6 kips (33.8 kN) with no steel buckling and only a slight fabric rupture exhibited on the tension sides.

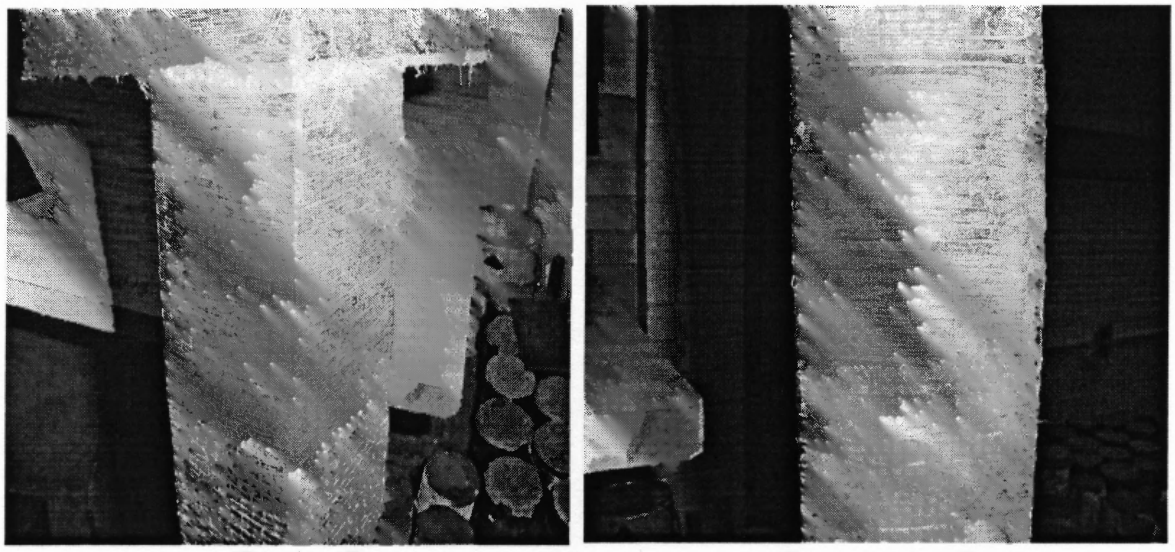

Tension Face Compression Face

Figure 4.16 Failure of column CJC7.

Table 4.3 Conditions of Column Specimens at Failure

Specimen	Location of Plastic Hinge	Exposed Steel Bars	No. of buckled Bars	Remarks
CJC1 (Trial)	Near lower bracket	Yes	None	Trial only
CJC2	At middle-height	Yes	None	Successful test
CJC3	At middle-height	No	None	Successful test
CJC4	At top bracket	No	None	Pre-mature failure at bracket
CJC5	At middle-height	Yes	One	Successful test
CJC6	At middle-height	No	None	Successful test
CJC7	Near top bracket	No	None	Successful test

4.3 Results and Discussions

4.3.1 Analysis of Test Results

Experimental test results of trial column CJC1 and column CJC4 are not analyzed, since they are either a trial specimen for set-up or a pre-mature failure specimen. Five test columns, CJC2, CJC3, CJC5, CJC6, and CJC7 are discussed in this research study. The applied load, P, can be determined directly from both MTS system and the data acquisition system. The deflections (d_x and d_y) are also recorded directly from the data acquisition system that is connected with two LVDTS.

The experimental values of bending moments in X and Y direction, M_x and M_y, are computed using the experimental axial load values and the load eccentricities (e_x and e_y) which are corrected for the mid-height deflections of the column (i.e.

$M_x = P(e_y + d_y)$ and $M_y = P(e_x + d_x)$). The experimental ultimate load and moment capacities for all five columns are summarized in Table 4.4.

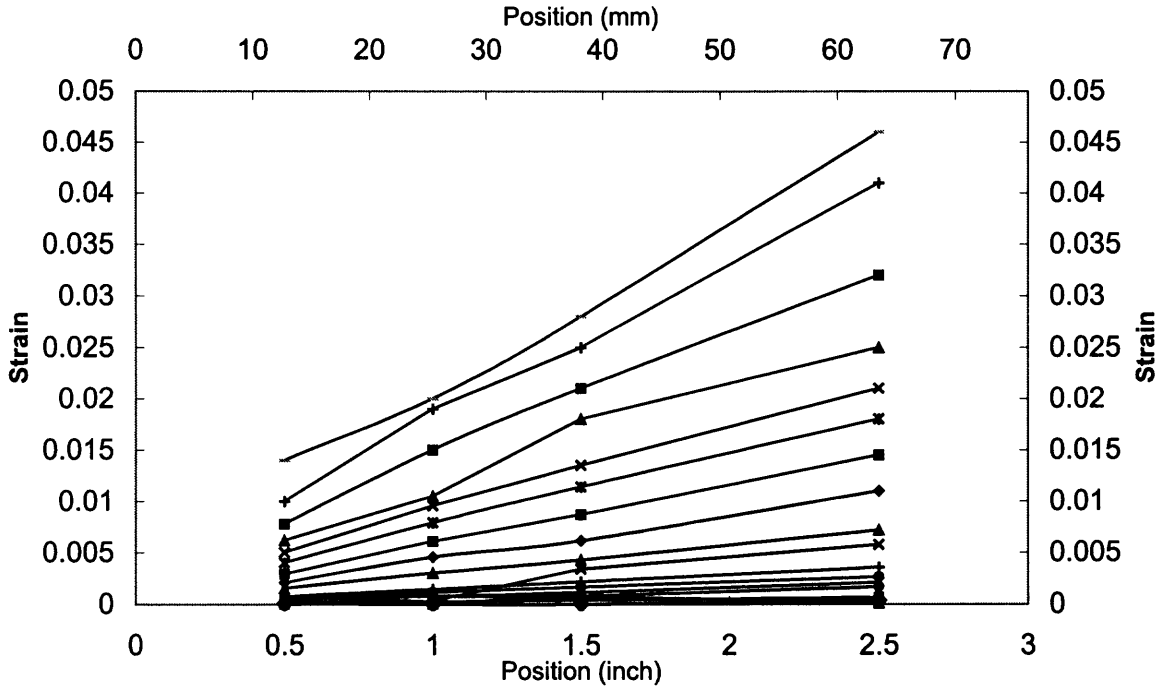

Figure 4.17 Typical strain-position curve for column CJC3 in X direction.

The longitudinal strain, ε, can be calculated by $\varepsilon = (l_i - l_0)/l_0$, when l_0 represents the initial length of mechanical strain gages at zero loading and l_i represents the length of the mechanical strain gages at each loading. At present study, l_0=6 in (152mm) as shown in Figure 4.9. After determining the strain from the mechanical strain gage points which locate at 1,2,3 and 4 for X direction and at 5,6,7 and 8 for Y direction (Figure 4.9), the strain-position curves can be drawn. They are shown in Appendix E. Figure 4.17 also gives a typical strain-position curve for column CJC3 in X-direction. The slope of the strain-position curve can be used to calculate its corresponding curvature which is shown in Figure 4.19 for CJC3 and Appendix F. Usually, a strain distribution

curve is linear. If the strain distribution curve is not linear, a straight line by a linear regression method is used to compute its curvature value.

When the deflection values and curvature values for each column has been computed, the complete load-deflection curve and moment-curvature curve for each column can thus be constructed as listed in Appendix F, Figure 4.18, and Figure 4.19, respectively.

4.3.2 Axial Loading Capacity

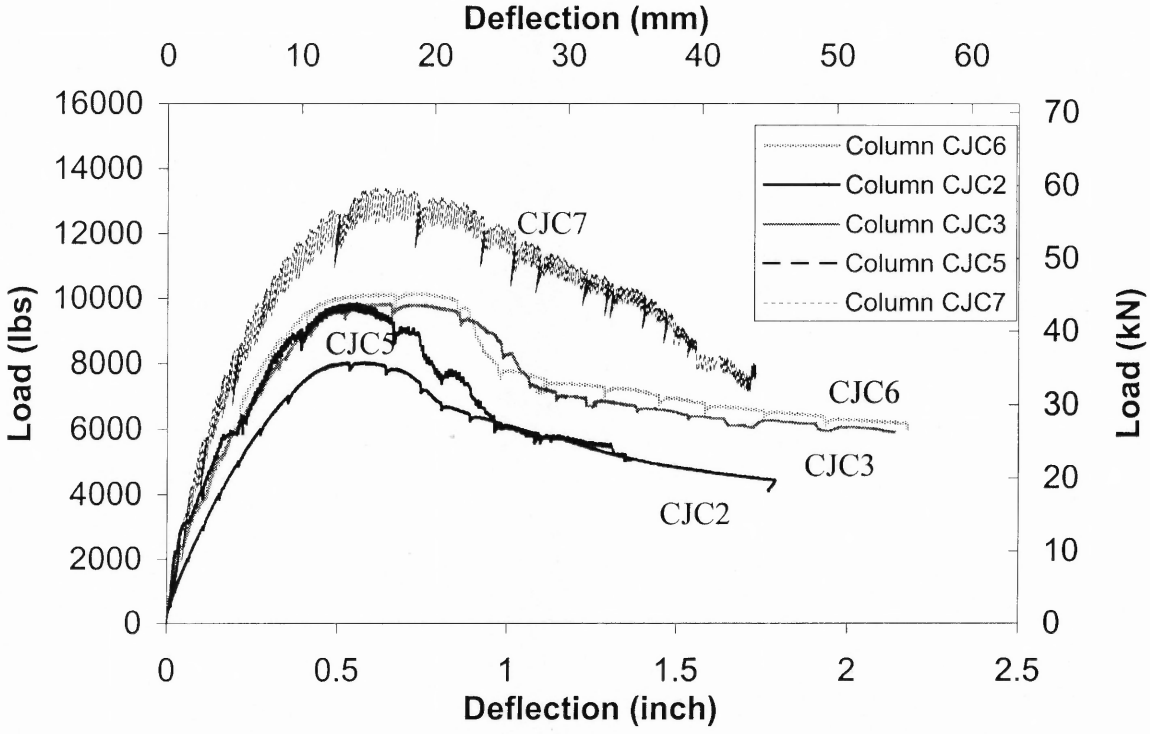

Figure 4.18 Comparison of load-deflection curves at X direction for test columns.

Since the eccentricities are exactly the same for both X and Y directions, the experimental results for both directions are expected to be the same too. The minor differences in the results are due to the measurement errors. Therefore only the results at one direction are discussed in this chapter. Figure 4.18 shows the load-deflection curves

at X direction for all the specimens. Table 4.4 lists the experimental values of maximum loads and moments. From the figure and table, it can be concluded that CFRP fabrics do help increase the load capacity for slender RC columns under biaxial loading. However, the contribution of fabrics may vary due to the different wrapping methods applied. Compared to the control column CJC2, the transverse CFRP fabrics in column CJC3 and CJC6 have increased the load capacity of the confined column by over 25%. This is because that the compressive stress and strain of concrete in the column has been greatly increased by the transverse fabric confinement. However, compare the experimental results between column CJC3 and CJC6, one notices that the column with two layers of transverse fabrics, CJC6, has only a slight increase in load capacity over the column with one layer of fabrics, CJC3. This shows that the thickness of the fabrics is not a crucial factor to the strengthening effect of the biaxially loaded columns. For column CJC5, the longitudinal fabrics only help increase the load capacity by 23% over the control column, which is much less as compared with those of the beam specimens in Chapter Three. This can be explained by the fact that a RC column is generally a compression member. The strengthening effect gained from the longitudinal fabrics is for the tension only. Therefore, the overall load increase is not that impressive as compared with the tension members like RC beams. Finally, column CJC7 with two directional wrappings has the highest load capacity up to 13 kips (58 kN), which is 60% over the control column. Therefore, one can conclude that both transverse and longitudinal fabrics increase the axial load capacity. However, the increase due to the fabric in the biaxially loaded column specimens is not that significant as compared with those in the beam specimens. This is mainly because there exists a huge secondary moment and axial compression

force in the column specimens that fail the CFRP fabrics rather quickly once the concrete gets crushed.

4.3.3 Deformability and Ductility

Similar Energy-absorbing concept from Chapter Three is used here to measure the ductility for all the test columns. Figure 4.19 shows the comparison of moment-curvature curves at X direction for all five test columns. The mid-height curvatures of the columns have been derived from the strain-position curves (Appendix E). However, some of the experimental curves are not complete because the measurement of the strain gages is disrupted due to the rupture of the fabrics. Also, if the final failure of the column does not occur at or near the mid-height, the measured values may not reflect the true curvature values, since all columns are supposed to bend in a single curvature.

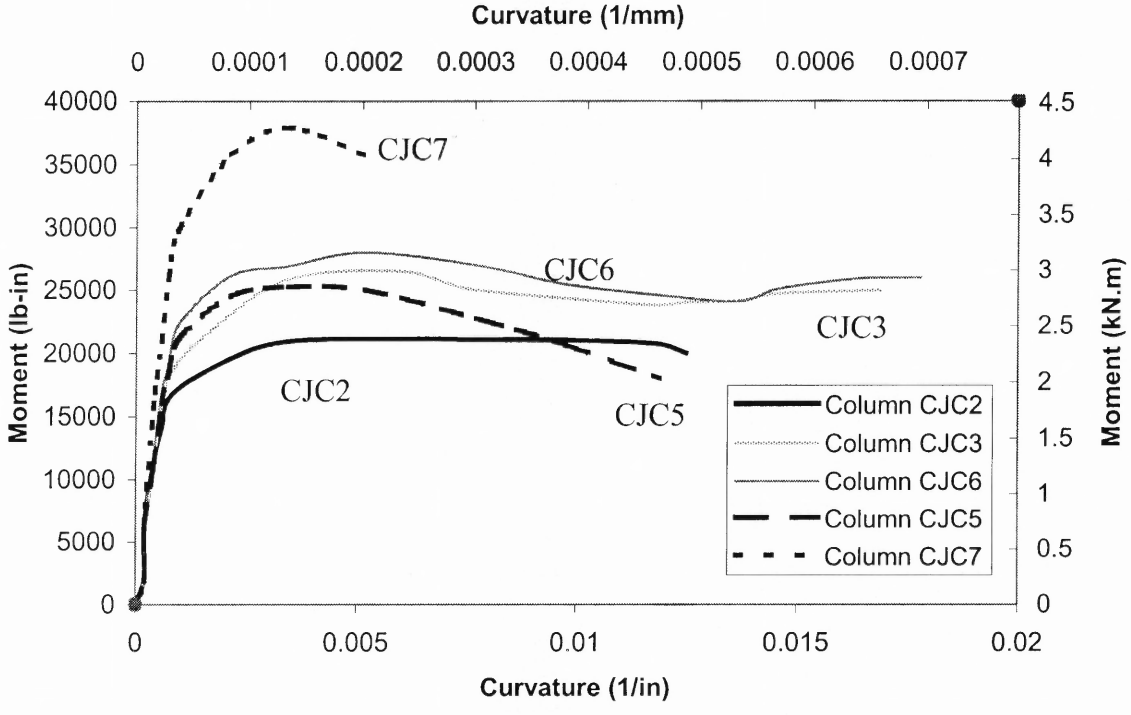

Figure 4.19 Comparison of moment-curvature curves at X direction of test columns.

From Figures 4.18 and 4.19, column CJC3 and column CJC6 have a better ductility performance than the control column because the transverse fabrics help increase the ultimate deflection. The nearly identical deflection behavior between these two further shows that the thickness of the fabric has not much effect on the behavior of the column specimens. Column CJC5, which is wrapped with longitudinal fabrics only, has a much less deflection than all the other columns. This is because the longitudinal fabrics cannot strengthen the concrete in the compression zone, it thus cannot prevent the early crush of the concrete. Consequently the column reduces its ultimate deflection and results in somehow a brittle failure. The best ductility is achieved from Column CJC7, because both longitudinal and transverse wrappings were used. Column CJC7 has high load capacity as well as high deflection values. The overall area of energy absorption is also highly increased as compared with that of other columns. The longitudinal fabrics help increase the load capacity of the column, meanwhile the confinement in the compression zone due to the transverse wrapping also helps prevent earlier crush of the concrete so that much more deformations are gained during the loading process.

Table 4.4 Experimental Results of Test Columns

Tested Column	Ultimate Load P (kips)	Ultimate Moment $M_x(M_y)$ (lb-in)	Ultimate Deflection $d_x(d_y)$ (inch)	Load Increase Compared to CJC2	Failure mode
CJC2	8 (35.6kN)	21120 (2.4kN.m)	1.78 (45.2mm)		Concrete crush & steel yielding
CJC3	9.8 (43.6kN)	26000 (2.9kN.m)	2.14 (54.4mm)	22.5%	Fabric rupture & concrete crush
CJC5	9.83 (43.7kN)	25260 (2.9kN.m)	1.3 (33mm)	23%	Fabric rupture & Steel Buckling
CJC6	10.1 (45kN)	28000 (3.2kN.m)	2.17 (55.1mm)	26.3%	Fabric rupture
CJC7	13.4 (59.6kN)	37868 (4.3kN.m)	1.74 (44.2mm)	67.5%	Fabric rupture

4.3.4 Failure Conditions

Figures 4.10-4.16 depict the failure conditions for each column. Control column CJC2, which has no fabric applied, has demonstrated a typical biaxial compression failure. Although the steel bars do yield to a certain degree, there is no buckling occurred. Figure 4.11 shows that the column finally fails due to the crushing of concrete at mid-height. Columns CJC3 and CJC6 show a very similar failure mechanism because both of them are wrapped by transverse fabrics only. The failure of both columns is mainly due to the rupture and some delaminations of the fabrics as well as concrete crushing in the compression zone. Figure 4.12 and Figure 4.15 show that all the fabrics around the mid-height of the columns have been ruptured and delaminated from the concrete surface. However, because more layers of fabrics have been used, column CJC6 shows a much less severe condition in the fabrics as compared with column CJC3. Column CJC5, which is wrapped by the longitudinal fabrics only, has a very quick load drop and shows a rather brittle failure. The final failure condition of the fabrics is very explosive as illustrated in Figure 4.14. The steel bars in column CJC5 have also buckled due to the increased load capacity. At last, column CJC7, which is wrapped by both longitudinal and transverse fabrics, has achieved an overall better ductile failure. Because of the transverse confinement, the concrete in the compression zone has been strengthened and thus has maintained a good condition during the test. Figure 4.16 shows that the final failure comes with a very slight rupture of transverse fabric on the tension side. Although the final condition of the longitudinal fabric cannot be seen from the outside, they have been already ruptured before the concrete gets crushed in the compression zone. All column specimens expect CJC7 have developed the plastic hinge right near the mid-height of the

column. Column CJC7 fails near the top bracket of the column. Figure 4.20 shows the final failure conditions for all five specimens. From the investigation of all five beams, both longitudinal and transverse fabrics seem to have effect to prevent the buckling of the columns due to their added confinement, which in turn help hold the concrete together even after concrete crushing.

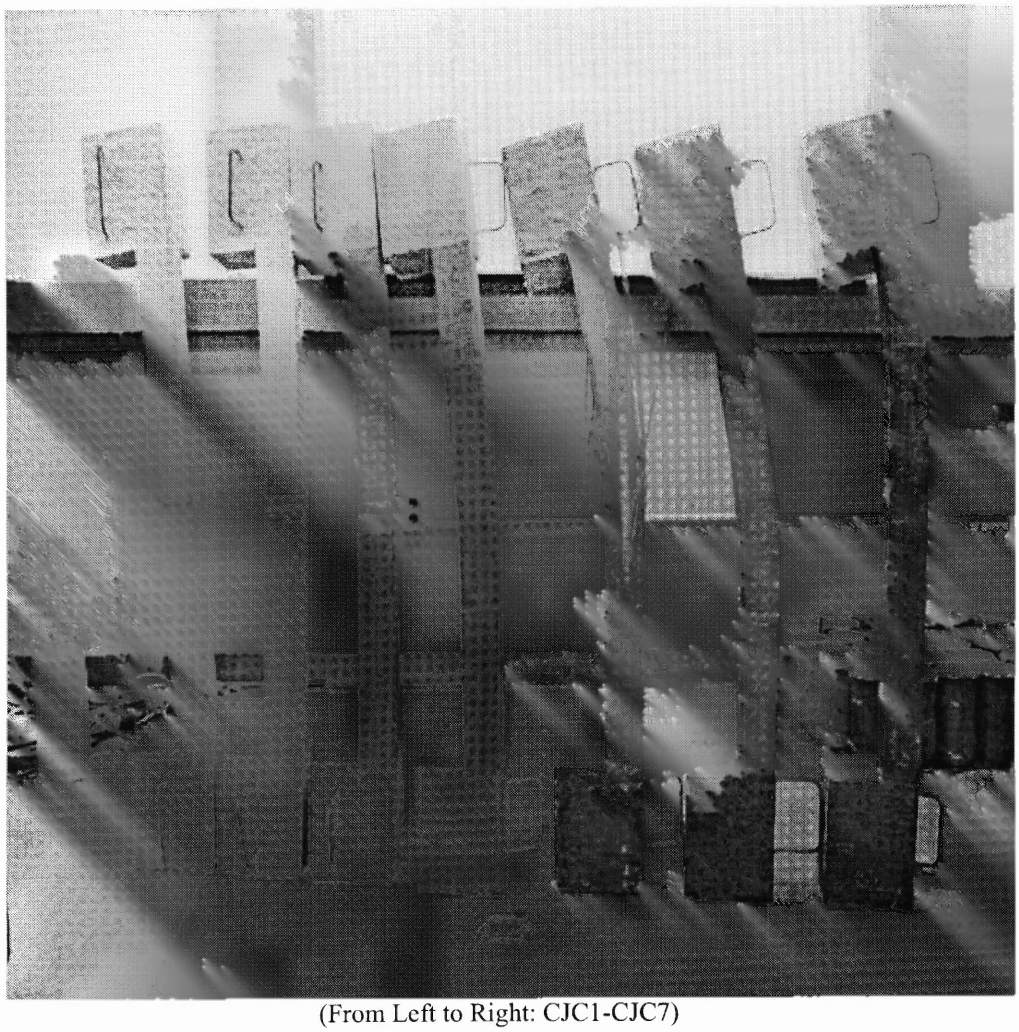

(From Left to Right: CJC1-CJC7)

Figure 4.20 Final conditions of column specimens.

4.4 Modified Finite-segment Analysis for Fabric-confined Slender Column under Combined Biaxial Flexure and Axial Load

This section discusses an analytical method to study the behavior of slender RC column under combined biaxial bending and axial loading. A brief discussion of conventional finite segment model is presented. Analysis of RC column subjected to combined biaxial bending and axial loading should be approached from the standpoint of a three dimensional structural analysis.

Unlike the finite segment model, finite element model idealizes each structural member as an assemblage of a large number of finite elements. These elements can be one-dimensional or two-dimensional, or even three-dimensional for concrete elements. The cost and time involved become prohibitive if three-dimensional elements are used. In addition, there are some difficulties involved in implementing an idealized empirical concrete model in the finite element model. Thus, the conventional finite segment method is extended here to study the slender fabric-wrapped RC column under biaxial bending and axial loading.

4.4.1 Basic Assumptions

The original numerical procedures proposed by Wang and Hsu (1990) is modified in this chapter. The load-deflection curve, moment-curvature curve and ultimate load are predicted through the developed computer program. The special computer analysis is based on the following assumptions:

1. Plane sections remain plane during bending.
2. If the concrete is wrapped with transverse fabric, it is considered as confined concrete; otherwise, it is treated as normal concrete. For fabric-confined concrete, the stress-strain curve presented in Chapter Two is used. For normal concrete, the classical stress-strain curve by Hsu (1990) is used.

3. No twisting occurs and the effects of axial and shear deformation are ignored.

4. Shrinkage and creep effects are neglected and perfect bond between steel and concrete elements is assumed.

5. The epoxy between the concrete and fabric will not fail.

6. Under zero loading, the segment lengths are straight; and under loading, the curvature varies linearly along segments.

4.4.2 Idealized Stress-strain Relations for Column Analysis

Once the strain in any discrete element is proposed, the corresponding stress can be obtained from the idealized stress-strain relationships. Therefore, a complete stress-strain curve for each material is necessary for analysis. In this research, different wrapping methods are applied to the columns, thus the stress-strain relationships of each wrapping method must be used in the computer analysis.

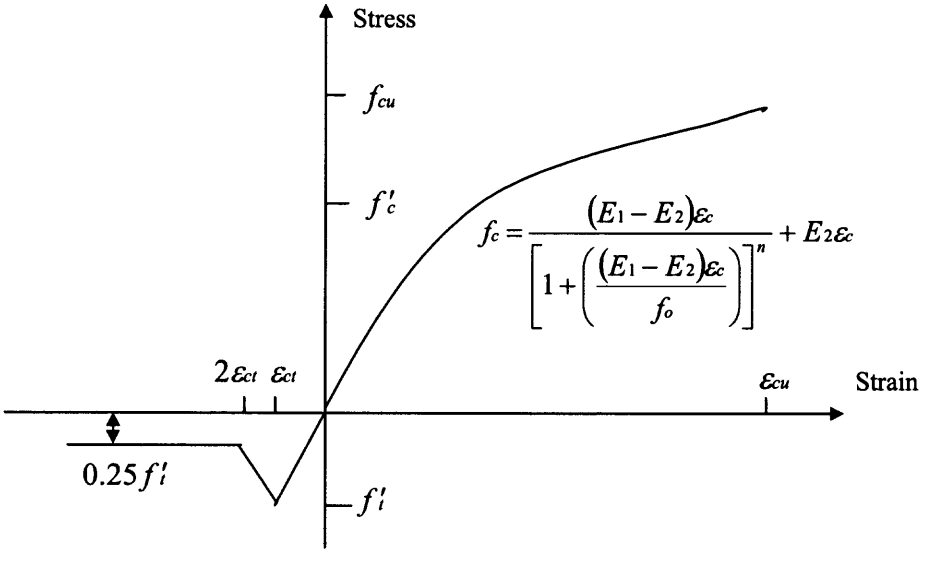

Figure 4.21 Stress-strain curve for fabric-confined concrete.

4.4.2.1 Stress-strain Relationship for Concrete. For concrete confined with transverse fabric, the concrete and fabric are considered as confined concrete, thus the proposed bilinear stress-strain curve from Chapter Two can be used here to model the compression part of the stress-strain curve. Although the fabrics do help increase the tensile strength for confined concrete, this increase can be neglected as compared with the huge increase in the compression part. Therefore the tension part of the curve is still treated as a normal concrete, which can be found from Hsu (1974). The complete stress-strain curve is shown in Figure 4.21. In this figure, f_{cu} and ε_{cu} represent the ultimate compressive stress and strain for the confined concrete, and f_t' and ε_{ct} represent the ultimate tensile stress and strain for the confined concrete, respectively.

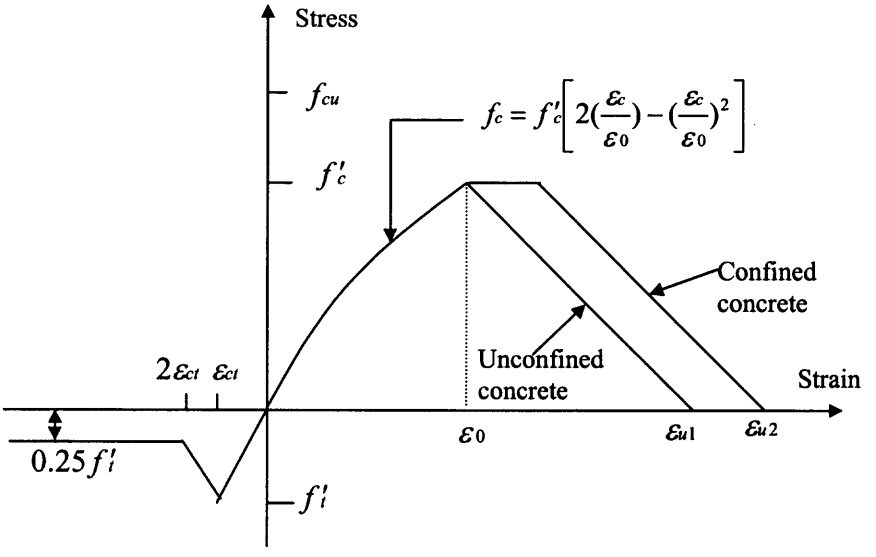

Figure 4.22 Stress-strain curve for normal concrete.

For concrete wrapped with longitudinal fabrics only, the fabrics and concrete are treated separately. Therefore, the traditional stress-strain curve for normal concrete is used here. A modified Cranston-Chatterji stress-strain curve is shown in Figure 4.22. In the figure, ε_{u1} and ε_{u2} represent the ultimate strain for unconfined normal concrete and

confined normal concrete, respectively. ε_0 is the strain corresponding to the maximum compressive stress of the concrete.

4.4.2.2 Stress-strain Relationship for Steel. An idealized piecewise linear curve is used to model the stress-strain relationship for the steel bars in the column. Figure 4.23 shows the idealized stress-strain curve including the strain hardening. The whole curve is linearly connected by five different strain-strain points which is selected from original complete stress-strain curve for the steel. In the figure, f_y and f'_y are the yielding stresses of the steel. f_{yi} and ε_{yi} represent the compressive stress and strain for different loading level. f'_{yi} and ε'_{yi} represent the tensile stress and strain, respectively.

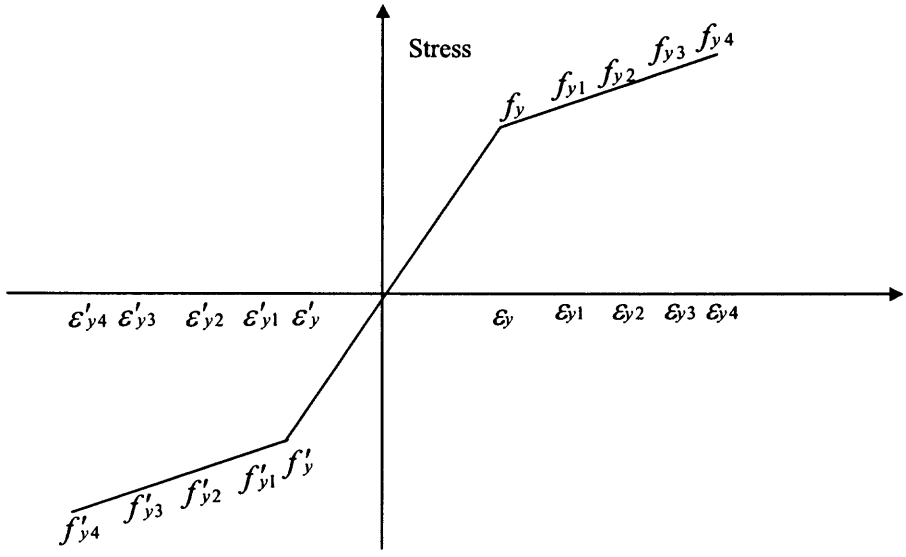

Figure 4.23 Idealized stress-strain curve for steel bars.

4.4.2.3 Stress-strain Relationship for CFRP Fabric. As mentioned before, the longitudinal fabrics should be modeled separately from the concrete. Since the CFRP fabrics are perfectly elastic in tension before they reach their ultimate strain, a simple linear relationship is used to model the longitudinal fabrics. In Figure 4.24, f_{fab} and ε_{fab} represent the ultimate tensile stress and strain of the fabric, respectively. The compression part of the stress- strain curve is neglected since the fabrics can not take any compression forces.

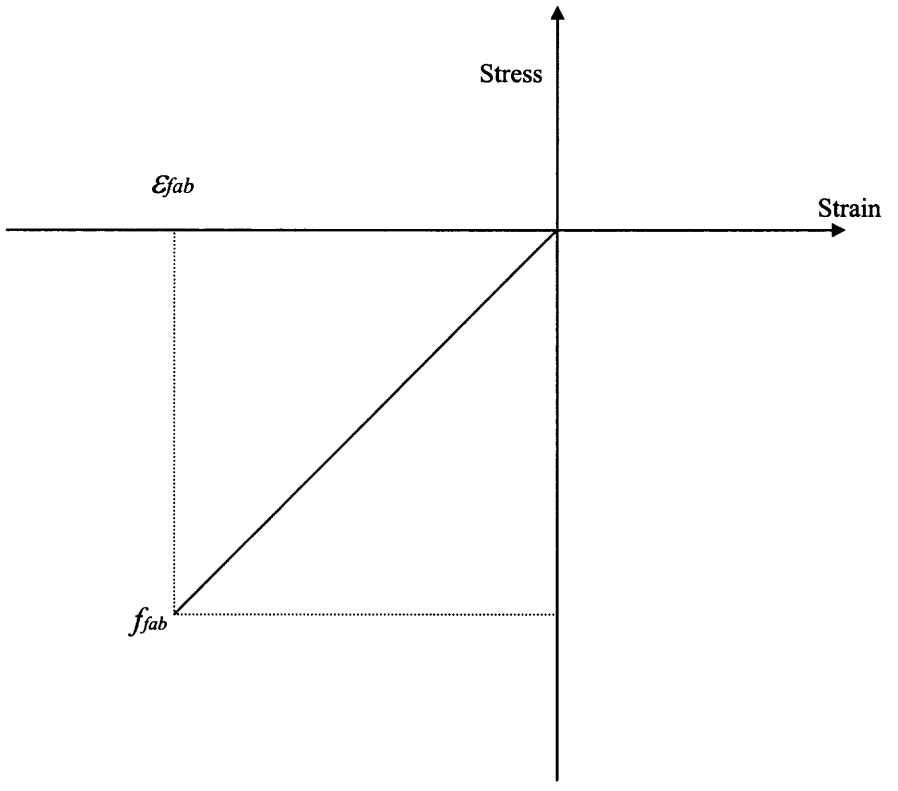

Figure 4.24 Stress-strain curve for longitudinal fabric wrapping.

4.4.3 Introduction of the Computer Program

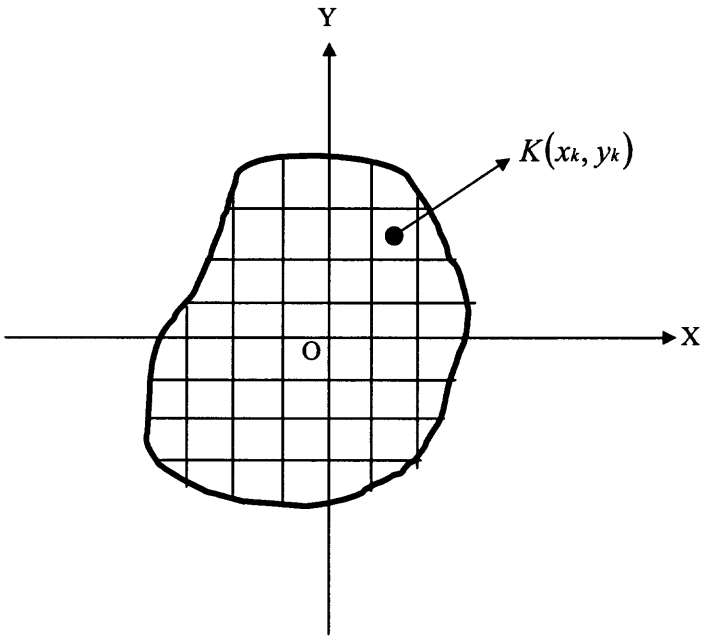

Figure 4.25 Cross section and coordinate system.

The finite segment concept is used in this computer analysis. The cross section of the structural member is divided into m small elements as depicted in Figure 4.25. The strain, ε_k, at the centroid (x_k, y_k) of an element k is assumed to be uniform across the element and for a given section the stress resultants P, M_x and M_y may be expressed as follows according to the sectional equilibrium conditions:

$$\left.\begin{aligned} P &= \sum_{k=1}^{m} E_k \varepsilon_k \alpha_k \\ M_x &= \sum_{k=1}^{m} E_k \varepsilon_k \alpha_k y_k \\ M_y &= \sum_{k=1}^{m} E_k \varepsilon_k \alpha_k x_k \end{aligned}\right\} \tag{4.1}$$

Where α_k is the area of element k with its centroid at point (x_k, y_k) and the secant modulus of elasticity $E_k = f_k/\varepsilon_k$ is used here.

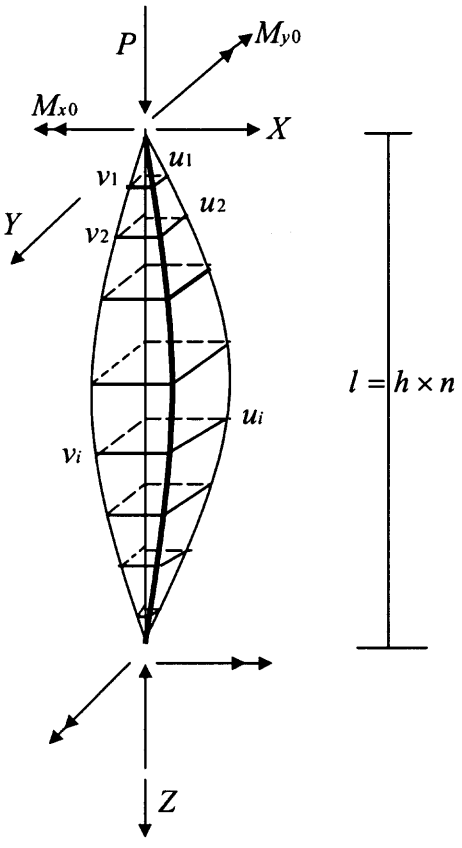

Figure 4.26 Slender column.

Figure 4.26 shows a slender column under combined biaxial flexure and axial compression. The column is divided into n segments having equal length of $h = l/n$. And the deflection in x and y directions at the division points between these segments are denoted by $u_0, u_1, ..., u_i, ..., u_n$ and $v_0, v_1, ..., v_i, ..., v_n$ respectively. The equilibrium equation at i cross section can be given as follows:

$$\left.\begin{aligned} P &= \sum_{k=1}^{m} E_{ki}\varepsilon_{ki}\alpha_k \\ M_{x0} + Pu_i &= \sum_{k=1}^{m} E_{ki}\varepsilon_{ki}\alpha_k y_k \\ M_{y0} + Pv_i &= \sum_{k=1}^{m} E_{ki}\varepsilon_{ki}\alpha_k x_k \end{aligned}\right\} \qquad (4.2)$$

$$i = 0,1,2,...,n$$

where M_{x0} and M_{y0} are the end moments. According to the plane section assumption, the strain ε_k is given by

$$\varepsilon_k = \varepsilon_0 + \phi_x y_k + \phi_y x_k \tag{4.3}$$

where ε_0 is the strain at coordinate origin and ϕ_x and ϕ_y are the curvatures with respect to x and y axes respectively.

To obtain the equations for load-moment-curvature relationships, substitute Equation (4.3) to Equation (4.1), one has

$$\left.\begin{aligned} P &= \sum_{k=1}^{m} E_k \alpha_k \varepsilon_0 + \sum_{k=1}^{m} E_k \alpha_k y_k \phi_x + \sum_{k=1}^{m} E_k \alpha_k x_k \phi_y \\ M_x &= \sum_{k=1}^{m} E_k \alpha_k y_k \varepsilon_0 + \sum_{k=1}^{m} E_k \alpha_k y_k^2 \phi_x + \sum_{k=1}^{m} E_k \alpha_k x_k y_k \phi_y \\ M_y &= \sum_{k=1}^{m} E_k \alpha_k x_k \varepsilon_0 + \sum_{k=1}^{m} E_k \alpha_k x_k y_k \phi_x + \sum_{k=1}^{m} E_k \alpha_k x_k^2 \phi_y \end{aligned}\right\} \tag{4.4}$$

Equation (4.4) can also be expressed in the following matrix form:

$$[K]\{c\} = \{F\} \tag{4.5}$$

where

$$\{c\} = [\varepsilon_0 \quad \phi_x \quad \phi_y]^T$$
$$\{F\} = [P \quad M_x \quad M_y]^T$$
$$[K] = \begin{bmatrix} K_{11} & K_{12} & K_{13} \\ K_{21} & K_{22} & K_{23} \\ K_{31} & K_{32} & K_{33} \end{bmatrix}$$

in which

$$K_{11} = \{E\}^T \{\alpha\}$$
$$K_{12} = \{E\}^T [Y] \{\alpha\} = K_{21}$$
$$K_{13} = \{E\}^T [X] \{\alpha\} = K_{31}$$
$$K_{22} = \{E\}^T [Y][Y] \{\alpha\}$$
$$K_{23} = \{E\}^T [X][Y] \{\alpha\} = K_{32}$$
$$K_{33} = \{E\}^T [X][X] \{\alpha\}$$

$$\{E\} = [E_1 \quad E_2 \quad \ldots \quad E_m]^T$$

where

$$\{\alpha\} = [\alpha_1 \quad \alpha_2 \quad \ldots \quad \alpha_m]^T$$

$$[X] = \begin{bmatrix} x_1 & & & \\ & x_2 & 0 & \\ & 0 & \ddots & \\ & & & x_m \end{bmatrix}$$

$$[Y] = \begin{bmatrix} y_1 & & & \\ & y_2 & 0 & \\ & 0 & \ddots & \\ & & & y_m \end{bmatrix}$$

For a short column, we can directly use Equation (4.4) or (4.5) due to the ignorance of the deflection. For a slender column, however, the deflection must be taken into account and at an arbitrary division point i, Equation (4.4) becomes:

$$\left.\begin{aligned} P &= (K_{11})_i \varepsilon_{0i} + (K_{12})_i \phi_{xi} + (K_{13})_i \phi_{yi} \\ M_{x0} + Pu_i &= (K_{21})_i \varepsilon_{0i} + (K_{22})_i \phi_{xi} + (K_{23})_i \phi_{yi} \\ M_{y0} + Pv_i &= (K_{31})_i \varepsilon_{0i} + (K_{32})_i \phi_{xi} + (K_{33})_i \phi_{yi} \\ & i = 0,1,2,\ldots,n. \end{aligned}\right\} \tag{4.6}$$

Also, the following equations between the curvature and deflection can be derived according to difference equation:

$$\left.\begin{aligned} \phi_{xi} &= (2u_i - u_{i-1} - u_{i+1})/h^2 \\ \phi_{yi} &= (2v_i - v_{i-1} - v_{i+1})/h^2 \end{aligned}\right\} \tag{4.7}$$

Substituting Equation (4.7) into Equation (4.6), and summation of all equations at different division points, including end conditions, the following load-moment-curvature-deflection relationships can be achieved:

$$[G]\{\omega\} = \{R\} \tag{4.8}$$

And for pined-ended conditions:

$$u_0 = v_0 = u_n = v_n = 0 \tag{4.9}$$

where

$$\{R\} = [(1 \quad e_y \quad e_x)_1 \cdots (1 \quad e_y \quad e_x)_{n-1}]^T Ph^2$$

$$\{\omega\} = [(\varepsilon_0 \quad u \quad v)_1 \cdots (\varepsilon_0 \quad u \quad v)_{n-1}]^T$$

$$[G] = \begin{bmatrix} g_{11} & g_{12} & & & & \\ g_{21} & g_{22} & g_{23} & & 0 & \\ & g_{32} & g_{33} & g_{34} & & \\ & & \ddots & \ddots & \ddots & \\ & 0 & & g_{n-2,n-3} & g_{n-2,n-2} & g_{n-2,n-1} \\ & & & & g_{n-1,n-2} & g_{n-1,n-1} \end{bmatrix}$$

$$(e_x)_i = M_{y0}/P \qquad (e_y)_i = M_{x0}/P \tag{4.10}$$

in which

$$g_{ii} = \begin{bmatrix} h^2K_{11} & 2K_{12} & 2K_{13} \\ h^2K_{21} & 2K_{22} - Ph^2 & 2K_{23} \\ h^2K_{31} & 2K_{32} & 2K_{33} - Ph^2 \end{bmatrix}_i$$

$$g_{ij} = \begin{bmatrix} 0 & -K_{12} & -K_{13} \\ 0 & -K_{22} & -K_{23} \\ 0 & -K_{32} & -K_{33} \end{bmatrix}_i$$

$$i, j = 1,2,\ldots, n-1.$$

For other end conditions, the load-deformation relation can be obtained by modifying Equation (4.8) and one can also take lateral loadings into account in the present analysis by expressing Equation (4.10) as

$$(e_y)_i = (M_{x0} + M_{xi})/P \qquad (e_y)_i = (M_{y0} + M_{yi})/P \tag{4.11}$$

where M_{xi} and M_{yi} are the moments at cross-section i due to lateral loadings in x and y directions respectively.

Because Equation (4.8) is highly nonlinear, the moment-curvature and load-deflection curves can only be achieved by step-by-step computations using Equations (4.7) and (4.8). Moreover, Equation (4.8) can be used for both proportional and

nonproportional loading problems. The numerical computations can therefore predict not only the ascending branch but also the descending branch of the load-deformation relationship. Since the secant modulus of elasticity is used, the iterative process of the present numerical analysis does not accumulate many errors, which make the present numerical analysis converge very quickly. If more complicate stress-strain relationships, such as the proposed equation from Chapter two, are used in the program, it is necessary to choose the allowable incompatibilities to ensure suitable increment for iteration. However, the procedure will still occasionally not converge if the stiffness of the section becomes very small.

4.4.4 Comparison of Experimental and Analytical Results

Load-deflection and moment-curvature curves are computed using the proposed computer program. Based on the analysis results from Bahn (1994) and Tsao (1991), the number of segments selected only has a slight influence on the stress- strain curve of the slender column. They suggested that the column with eight segments would have the most satisfactory results. Therefore, a total of 8 segments and 64 members in the cross section are used in this program. Figure 4.27 shows a general cross section of the slender column for computer analysis. Depending on the properties of the specimen, the number of the total elements may vary. The fabric elements are only added for the column with longitudinal fabrics. In this case, the fabric element can be considered as four thin elements around the surface of the cross section. Depending on the accuracy of the final results, they can be divided into more small elements to fit with concrete elements. In modeling, they can be treated as elastic steel elements that can only take tension forces.

Their corresponding stress-strain curve has been listed in a subroutine of the proposed computer program.

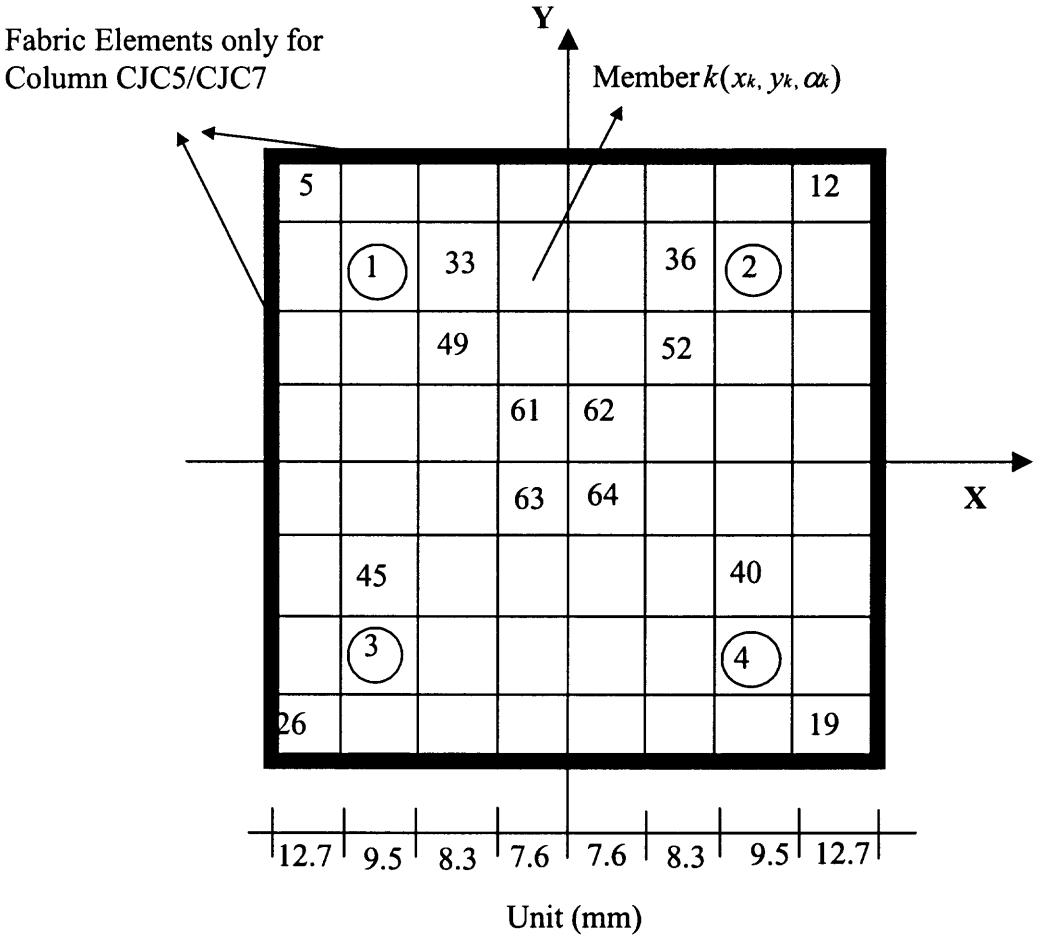

1-4 : Steel Member
5-64: Confined concrete member for CJC3/CJC6/CJC7
Normal concrete member for CJC2/CJC5

Figure 4.27 Cross section of slender column for computer analysis.

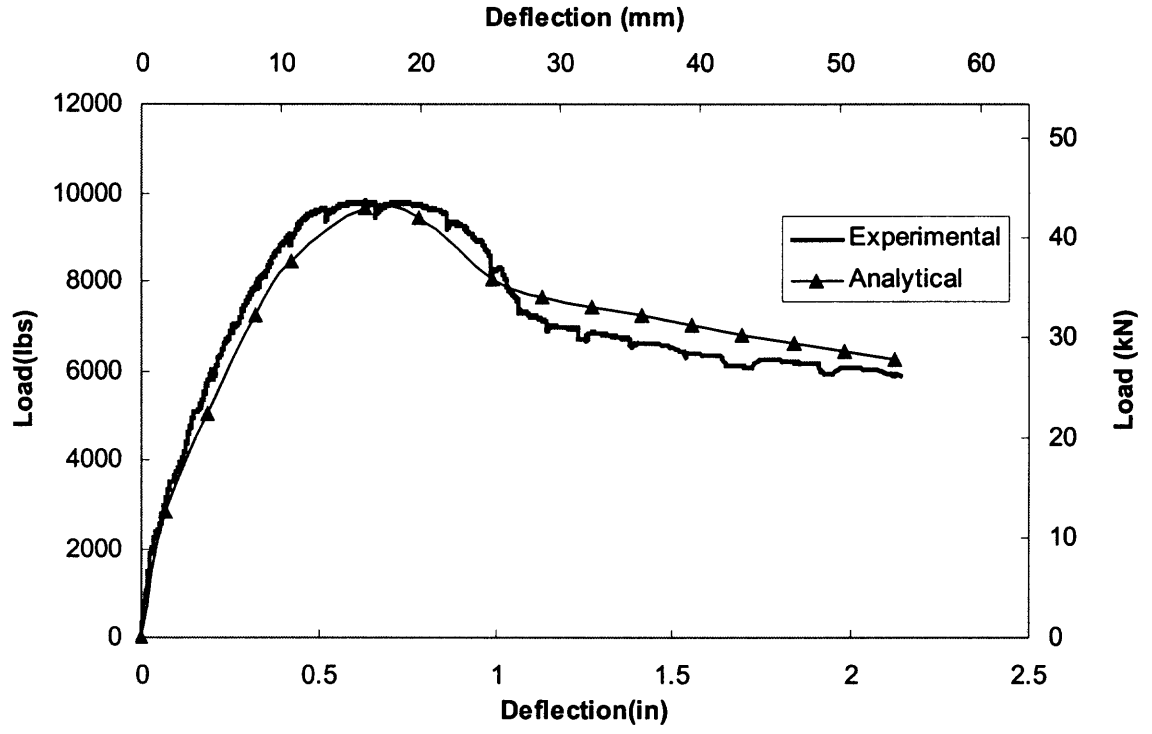

Figure 4.28 Comparison of load-deflection curves at X-direction for column CJC3.

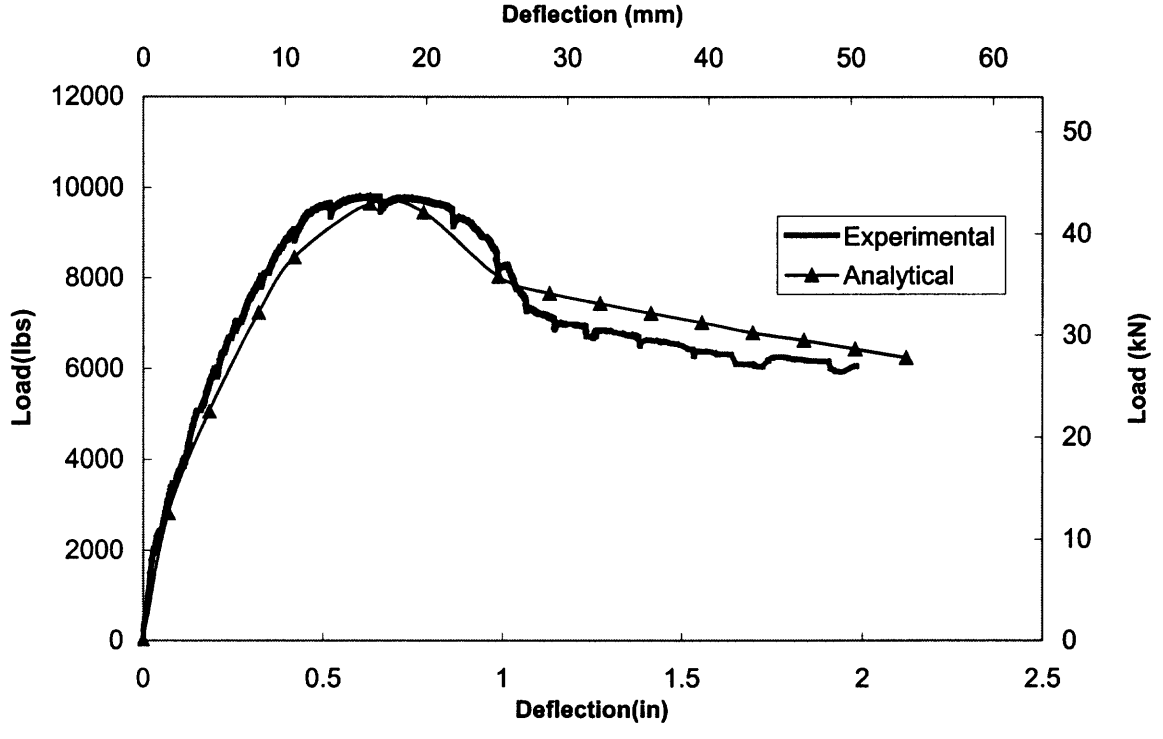

Figure 4.29 Comparison of load-deflection curves at Y-direction for column CJC3.

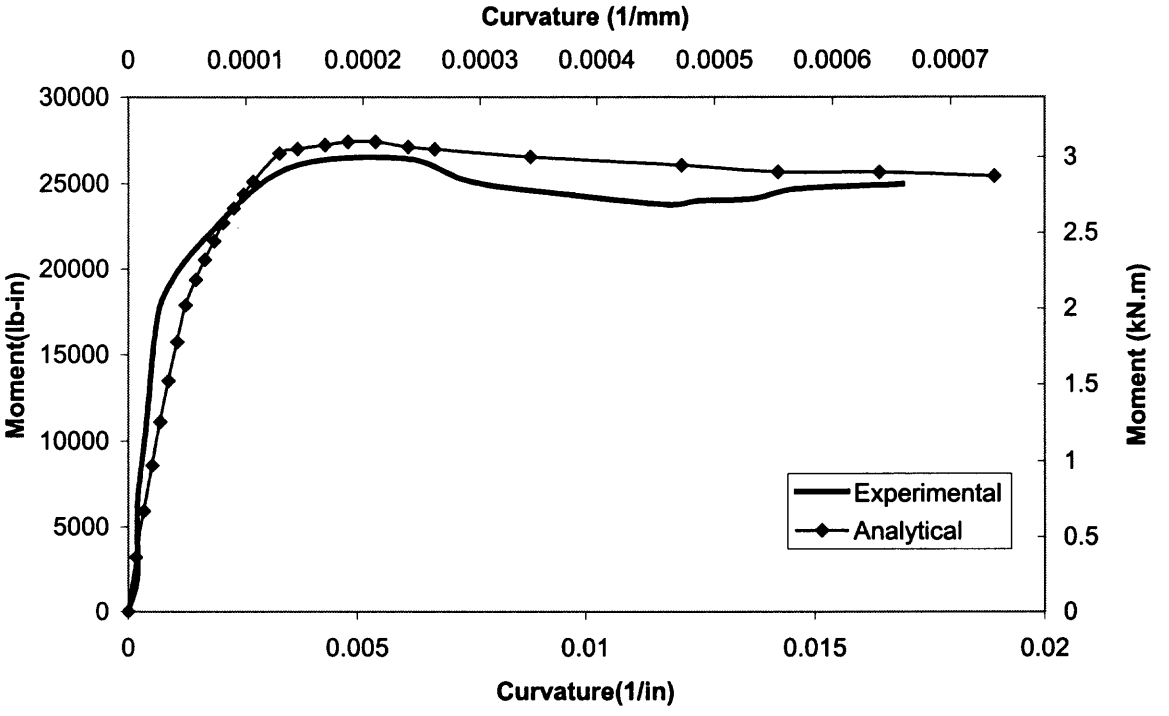

Figure 4.30 Comparison of moment-curvature curves at X-direction for column CJC3.

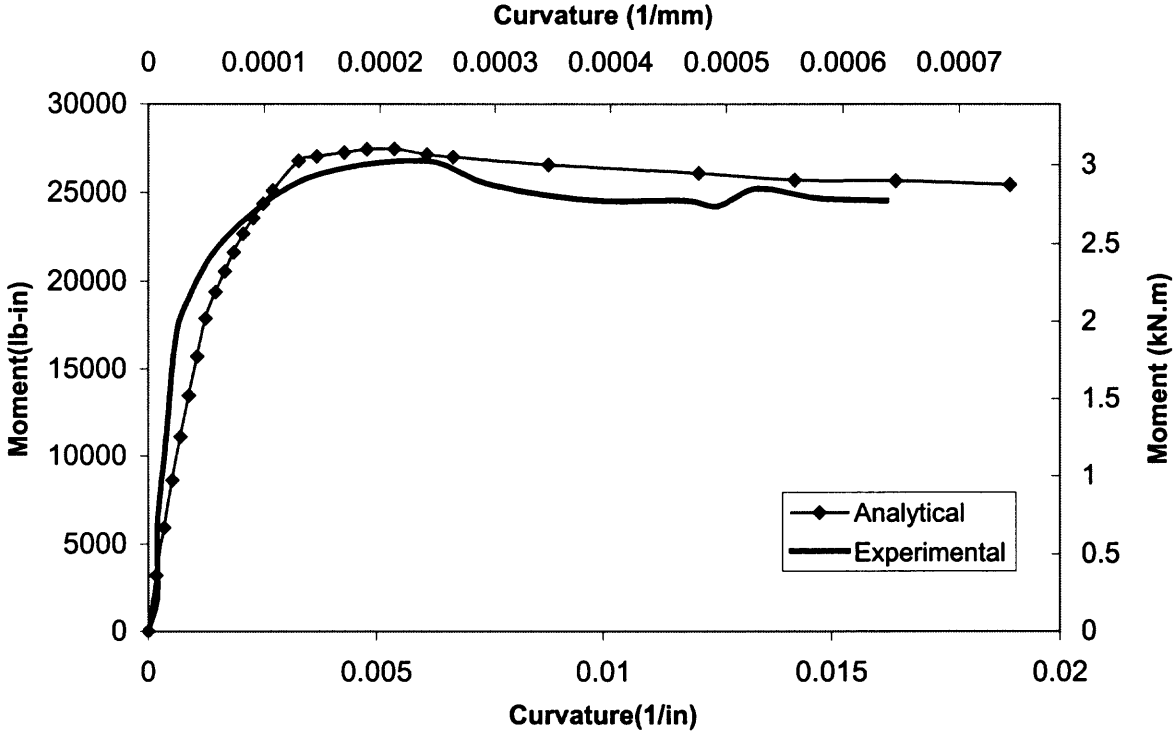

Figure 4.31 Comparison of moment-curvature curves at Y-direction for column CJC3.

Figures 4.28–4.31 give the experimental versus analytical results for a typical column specimen CJC3. Table 4.5 and Table 4.6 present a comparison of maximum loads and moments between the experimental and analytical results. The comparisons for other specimens are listed in Appendix F. From the Figures, the predicted curves from the present computer analysis are in an excellent agreement with the experimental results. The major difference between the experimental and analytical results occurs at the descending branch. This is mainly because the proposed stress-strain equation for fabric-confined concrete does not have a specific descending branch in its stress-strain curve. Also, the brittle failure of the fabrics make the measurement of the deflection and curvature become a very difficult task after the peak load. For column CJC7, the final failure does not occur at the mid-height, thus the experimental results cannot attain complete load-deformation curves. However, the experimental curve before the peak load still match the analytical curve pretty well. Therefore, one can conclude that the proposed computer analysis is valid and efficient to analyze the fabric-confined column under combined biaxial bending and axial loading.

Table 4.5 Maximum Axial Load and Deflection Results

Tested Column	Experimental		Analytical		
	P (kips)	$d_x(d_y)$ (inch)	P (kips)	$d_x(d_y)$ (inch)	P_{Exp}/P_{Ana}
CJC2	8 (35.6kN)	1.78 (45.2mm)	8.2 (36.5kN)	1.9 (48.3mm)	0.98
CJC3	9.8 (43.6kN)	2.14 (54.4mm)	9.65 (42.9kN)	2.1 (53.3mm)	1.02
CJC5	9.83 (43.7kN)	1.3 (33mm)	9.91 (44.1kN)	1.6 (40.6mm)	0.99
CJC6	10.1 (45kN)	2.17 (55.1mm)	9.95 (44.3kN)	2.3 (58.4mm)	1.01
CJC7	13.4 (59.6kN)	1.74 (44.2mm)	14.0 (62.3kN)	2.1 (53.3mm)	0.95

Table 4.6 Maximum Moment Results

Tested Column	Experimental	Analytical	
	$M_x(M_y)$ (lb-in)	$M_x(M_y)$ (lb-in)	M_{Exp}/M_{Ana}
CJC2	21120 (2.4kN.m)	22100 (2.5kN.m)	0.95
CJC3	26000 (2.9kN.m)	27400 (3.1kN.m)	0.95
CJC5	25260 (2.85kN.m)	26100 (2.94kN.m)	0.97
CJC6	28000 (3.2kN.m))	28900 (3.3kN.m)	0.97
CJC7	37868 (4.3kN.m)	42300 (4.8kN.m)	0.89

4.5 Summary and Recommendations

Based on present experimental results for column specimens with different wrapping methods, it has been found that pure transverse fabric wrapping has increased both the axial loading capacity and ductility of the test columns. On the other hand, pure longitudinal fabric wrapping increases the loading capacity of the column by a small amount but reduces its mid-height deflection. As a result, the column behaves in less ductility and a more brittle failure. Therefore this wrapping method should not be recommended for practical uses. The column wrapped with both longitudinal and transverse fabrics has the best overall performance due to its high strength, high deformability and good ductile failure. It should be strongly recommended for practical uses. However, since the cost for the two-directional fabrics is still very expensive, the transverse wrapping is still a good choice for strengthening the slender columns under biaxial loading.

A computer analysis has been developed herein to analyzed the complete load-deflection and moment-curvature relationships of biaxially loaded fabric-wrapped slender columns. The computer program has used the empirical stress-strain equations proposed in this research to model the fabric-confined concrete in the column. Various comparisons between the experimental and analysis results show that a very good agreement has been achieved for both ascending and descending parts of the load-deformation curves. The present computer program can be used for most geometrical and loading conditions, it is thus recommended for practical analysis of the fabric-confined slender RC columns.

CHAPTER 5

CONCLUSIONS

Research work performed at present study demonstrates the feasibility of using externally applied epoxy-bonded CFRP Fabrics to the concrete structures do increase the load-carrying capacity and ductility of various structural members. The following conclusions can be drawn:

1. The CFRP fabrics can increase the splitting tensile strength of normal concrete. The more layers applied to the specimens, the more increase in tensile strength can be attained. However, compared to the greater strength increase in compression, the strengthening effect on tension is still lacking. Therefore, it is concluded that the tensile strength of the fabric-confined concrete can be ignored in design.
2. Results of various concrete cylinders under axial compression tests show that the CFRP system can significantly increase the ductility and ultimate compressive strength of normal concrete specimens. With the help of transverse fabrics, the compressive strength of the confined concrete has increased up to 300% over the normal concrete. Although the fabrics tend to increase the axial strain, the lateral strain on the other hand has been decreased by the confinement. The thickness of the fabrics and the unconfined concrete strength are the most important factors that affect the strength of the fabric confinement.
3. Based on present test results, the complete compressive stress-strain equation of the fabric-confined concrete has been proposed. The stress-strain curve shows an approximate bilinear behavior. The initial stress-strain behavior is very similar to that of the normal concrete. After the concrete reaches its unconfined strength, the

behavior of the confined concrete is mainly dependent on the material properties of the fabrics. Since the final failure of the specimen is mainly due to the rupture of the fabrics, a brittle and explosive failure mode is inevitable.

4. Various factors affecting the effeteness of the fabric confinement are investigated in this research. Steel hoops with two different spacings are added to some concrete specimens along with the fabrics that are wrapped outside. Test results of these specimens show that at the same compressive strength level, the stress-strain behavior of the concrete specimens with both steel hoops and fabric wrapping are almost identical to each other. It can be concluded that steel hoops doesn't affect the behavior of the fabric-confined concrete. Besides the transverse fabric applied to all the specimens, some cylinder specimens has been provided with another layer of longitudinal fabrics, test results of these specimens are compared with the original specimens and they show that an additional longitudinal wrapping has not changed the stress-strain behavior very much. Thus the strengthening effect due to the longitudinal fabric on the cylinders can be neglected as well. Size effect of coarse aggregate is also investigated in this study. Some specimens are mixed using 3/8 in (9.5mm) stones. Test results of these specimens show a similar stress-strain behavior as the specimens with 3/4 in (19mm) stones. Therefore, coarse aggregate size does not affect the behavior of fabric-confined concrete either.
5. A complete compressive stress-strain equation modified from Samaan and Mirmiran (1998) has been proposed to model the fabric-confined concrete. All the parameters included in this equation are derived from the curve fittings of the current experimental data. An empirical equation is also proposed to predict the ultimate

stress and strain of the confined concrete. Both equations are well compared with various experimental results from present study and other researches.

6. Five 10-ft (3m) long RC beams are cast and tested to study the flexural behavior of the fabric-confined RC beams. Different wrapping methods are used; two beams are wrapped with longitudinal fabrics only. One beam is wrapped with one layer of transverse fabrics only and one beam is wrapped by both longitudinal and transverse fabrics. All beams have the same concrete strength, cross-sectional area and steel reinforcements. Both load-deflection and moment-curvature curves of the beams are recorded and analyzed. Test results show that the longitudinal fabrics can significantly increase the ultimate flexural strength of RC beams due to its high tensile strength. The transverse fabrics, on the other hand, do not have much effect on the flexure strength of the beams. The thickness of the longitudinal fabrics can be considered as an important factor for the strengthening effect.
7. Although the longitudinal fabrics do help increase the flexural strength of the fabric-confined beam, they also greatly decrease the ultimate mid-span deflection. As a result, the beam behaves in a more brittle failure conditions than the normal RC beam. Therefore, using longitudinal fabrics only is not an efficient way to increase the ductility of the beams. The present study shows that the transverse fabrics have greatly increased the ultimate stress and strain of the concrete in the compression zone. The beam wrapped with transverse fabrics has thus achieved very good deformability and ductility, even though no much strength increase is noticed. The beam wrapped with both longitudinal and transverse fabrics has been found to achieve the best flexural performance and ductility due to its high strength, high

deformability and good ductile failure. This wrapping method should be recommend for practical uses if the cost and construction requirements can be compromised.

8. An empirical design approach modified from ACI strength method has been proposed in this research to predict the ultimate strength of the fabric-confined RC beam. This method is based on compatibility of deformation and equilibrium of forces, and it also accounts for the proposed stress-strain relationship for the fabric-confined concrete. Related equations and design examples for the tested beams are presented in this research. The comparactive results show that the modified ACI method gives a conservative strength value as compared with the present test results. Finite element method using ANSYS is also presented to obtain the load-deflection curve. although the FEM results do have a good agreement with the experimenatl curve, it can not predict the descending part of the load-deflection curve due to the limitation of the ANSYS program.
9. Seven 4-ft (1.2m) long slender columns are tested under the combined axial load and biaxial bending. Five of them are wrapped with CFRP fabrics. Similar wrapping methods from the beam testes are applied to the column specimens. Both the load-deflection and moment-curvature curves of the specimens are recorded in this study. The test results show that both transverse and longitudinal fabrics have helped increase the ultimate loading capacity by 20-25% over the unconfined specimens. However, it seems that the thickness of the fabrics applied to the column specimen is not an important factor of the strengthening effect. The column with both transverse and longitudinal fabrics has a much higher loading capacity than all the other specimens. Compared to the huge increase in the flexural strength for the beam

specimens, the load increase due to the fabrics in the biaxially loaded column specimens is not that significant. This is mainly because a large secondary moment and axial compression force on the column specimens fail the CFRP fabrics rather quickly once the concrete gets crushed.

10. The failure mechanism of the fabric-confined biaxially loaded slender columns is mainly due to the rupture and delamination of the fabrics. It shows that the buckling effect on slender columns has been greatly reduced by the added confinement of the fabrics. For the column wrapped with transverse fabrics, the concrete in the compression zone has been greatly strengthened and thus helps increase its mid-height deflection and overall ductility. For the column wrapped with longitudinal fabrics only, it shows a decreased deflection at mid-height and exhibits a more brittle failure than all other specimens. The overall performance of the column with both longitudinal and transverse fabrics has achieved the best structural performance among all the specimens. Considering its greater load increase and much better ductility, this wrapping method should be strongly recommend for practical uses.
11. A computer analysis program is developed in this study to analyze the complete load-deformation relationships of biaxilly loaded slender columns wrapped with CFRP fabrics. This computer program is a modified form of an existing computer program by Wang and Hsu (1990), This computer program uses the empirical stress-strain equations proposed in this study to characterize the behavior of fabric-confined concrete. Stress-strain relationship of the CFRP fabrics are also considered for certain specimens. Compared to the actual experimenatl results, the proposed computer analysis yields a reasonable accuracy in predicting an actual load-deformation

behavior of the fabric-confined slender column under combined axial loading and biaxial bending. Both the ascending and descending branches of the analytical curves have achieved a satisfactory aggrement with the experimental results. It can be concluded that, not only the proposed computer analysis but also the proposed stress-strain equation for fabric-confined concrete, are valid and can be ready for used in practical engineeing designs.

APPENDIX A

STRESS-STRAIN CURVES OF STEEL BARS

In appendix A, each figure presents the experimental tensile stress-strain curves of steel rebars used in this research. A total of three tests were conducted in NJIT Structural Laboratory.

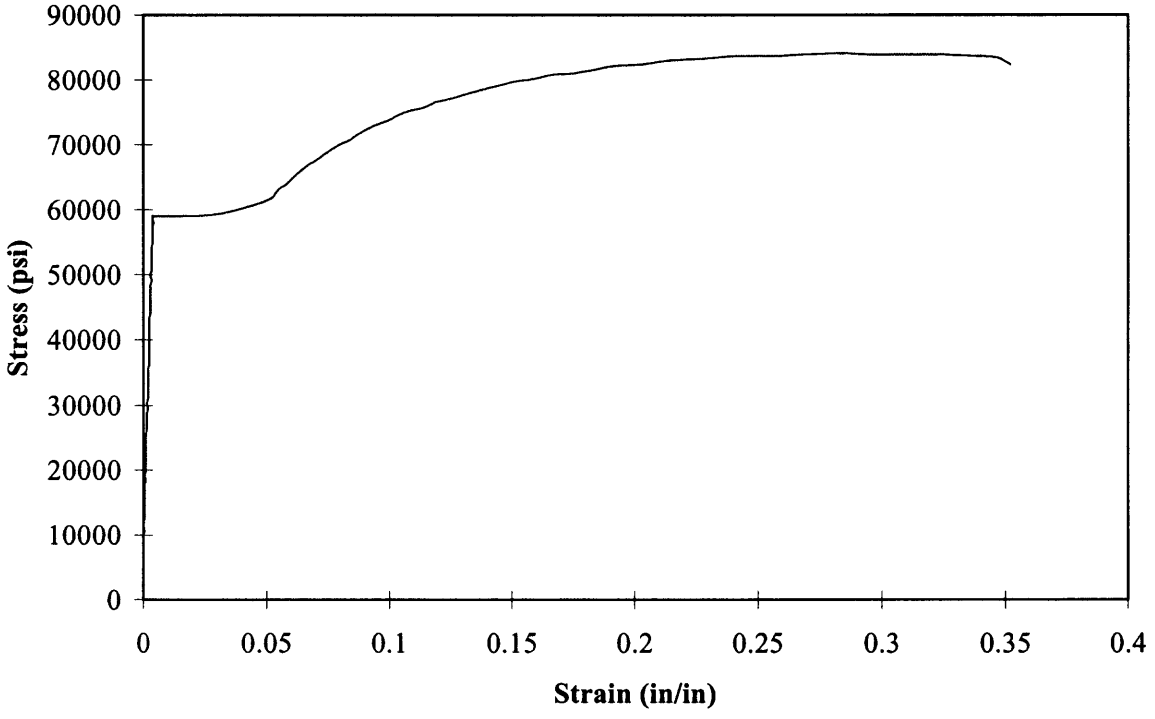

Figure A.1 Stress-strain curve of No.3 bar (test 1).

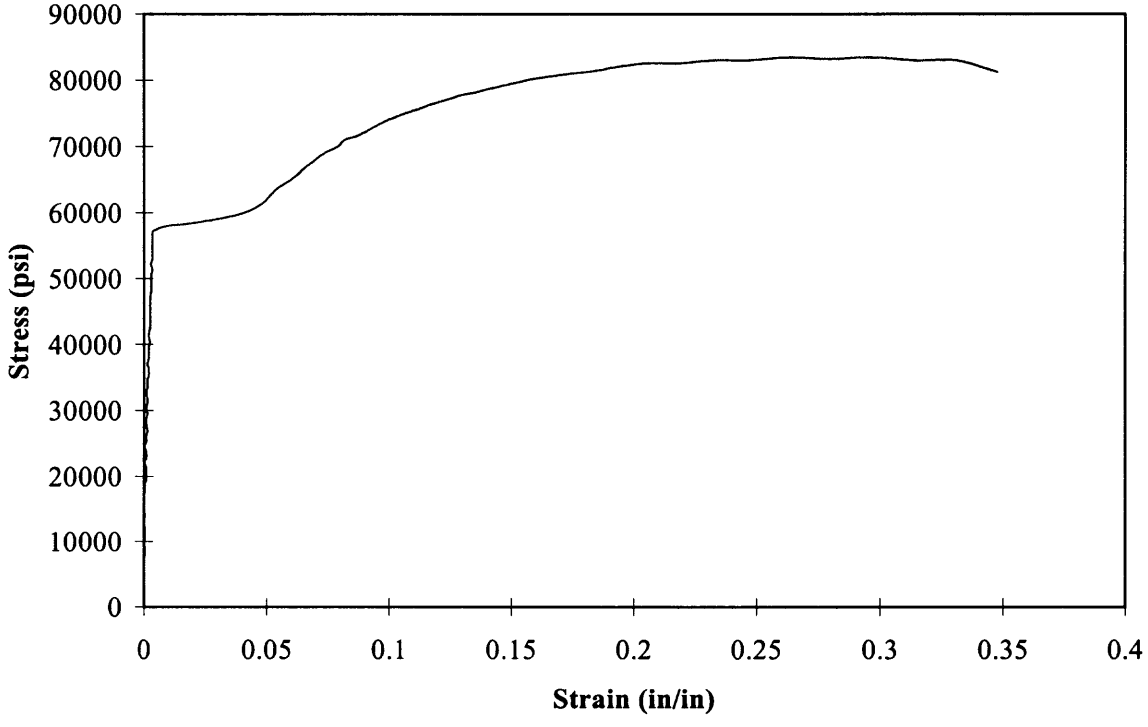

Figure A.2 Stress-strain curve of No.3 bar (test 2).

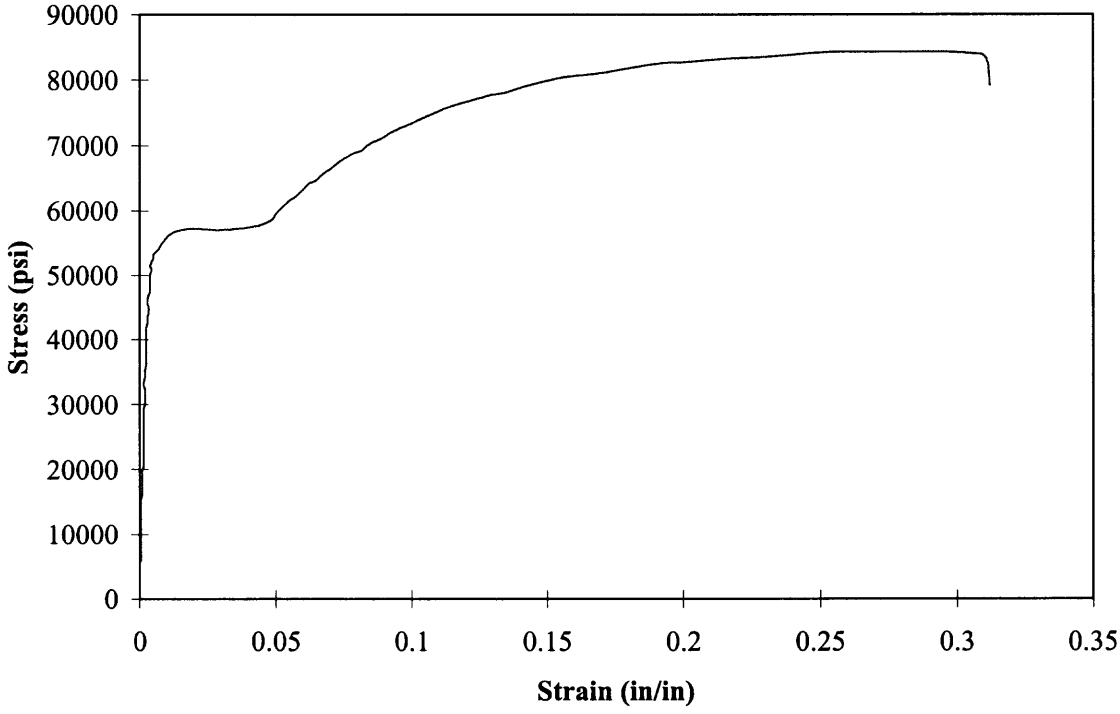

Figure A.3 Stress-strain curve of No.3 bar (test 3).

APPENDIX B

TEST SPECIMENS AND EXPERIMENATL SETUP

In appendix B, Figures B.1-B.6 present the detailed experimental setup and test results for concrete cylinder tests. Figures B.7-B.12 show the RC beam configuration in this study. Figures B.13-B.20 show the detailed concrete column specimens.

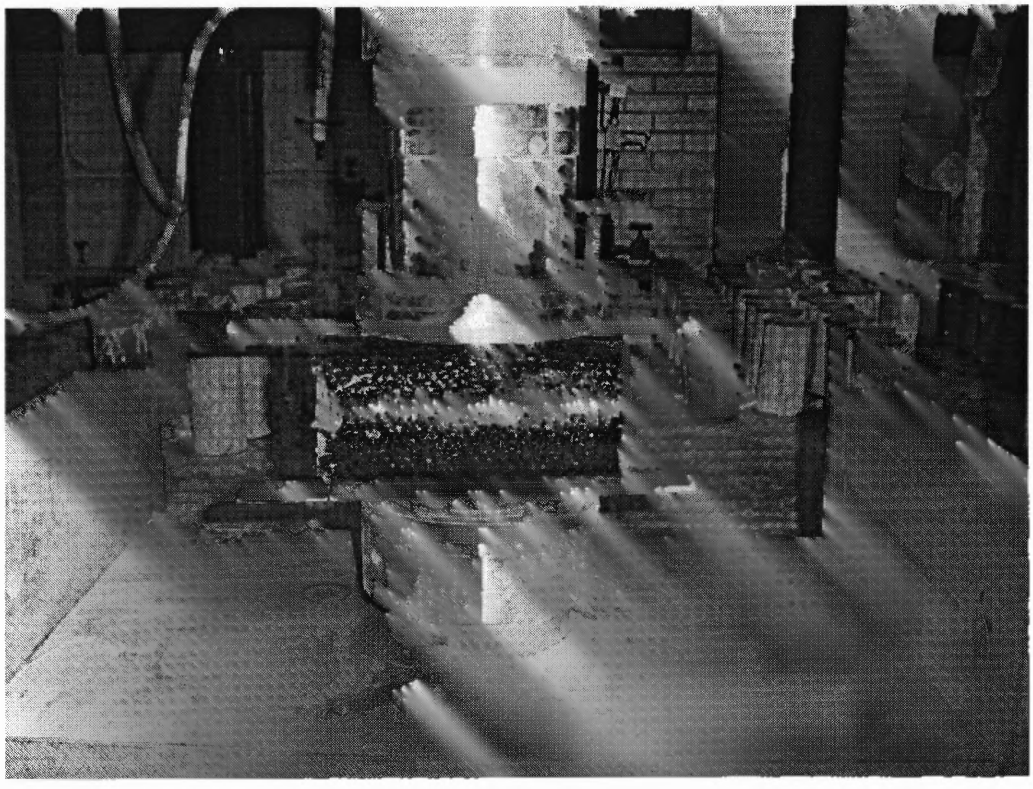

Figure B.1 Split tension test setup.

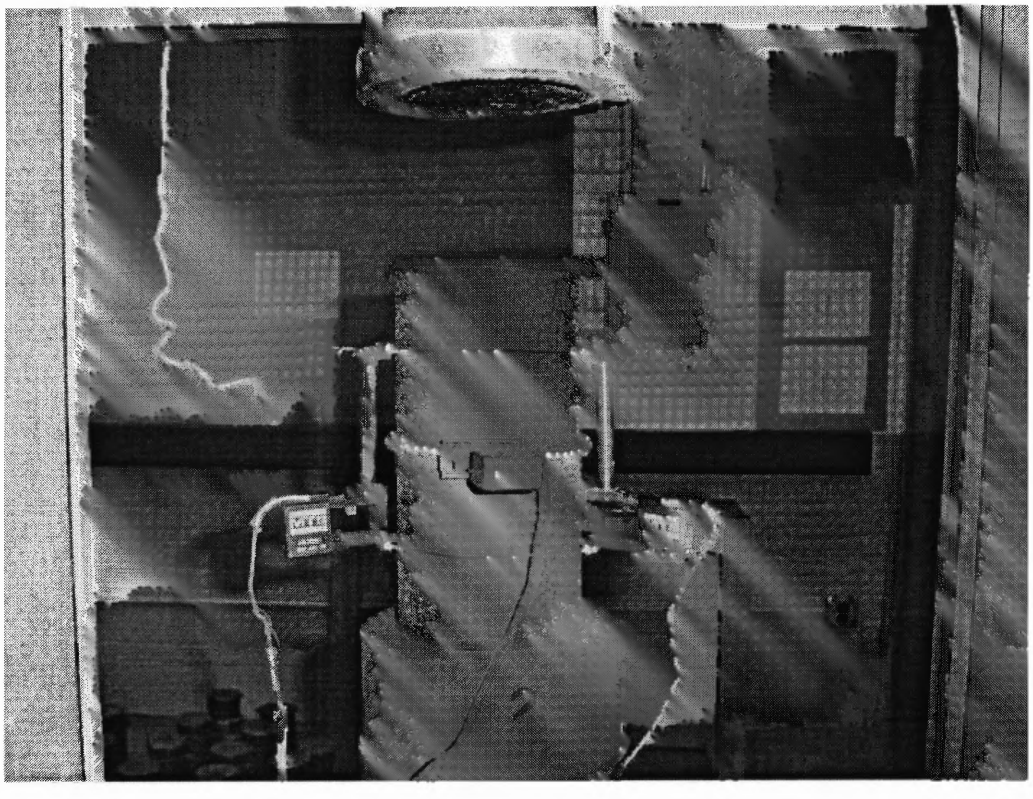

Figure B.2 Compression test setup.

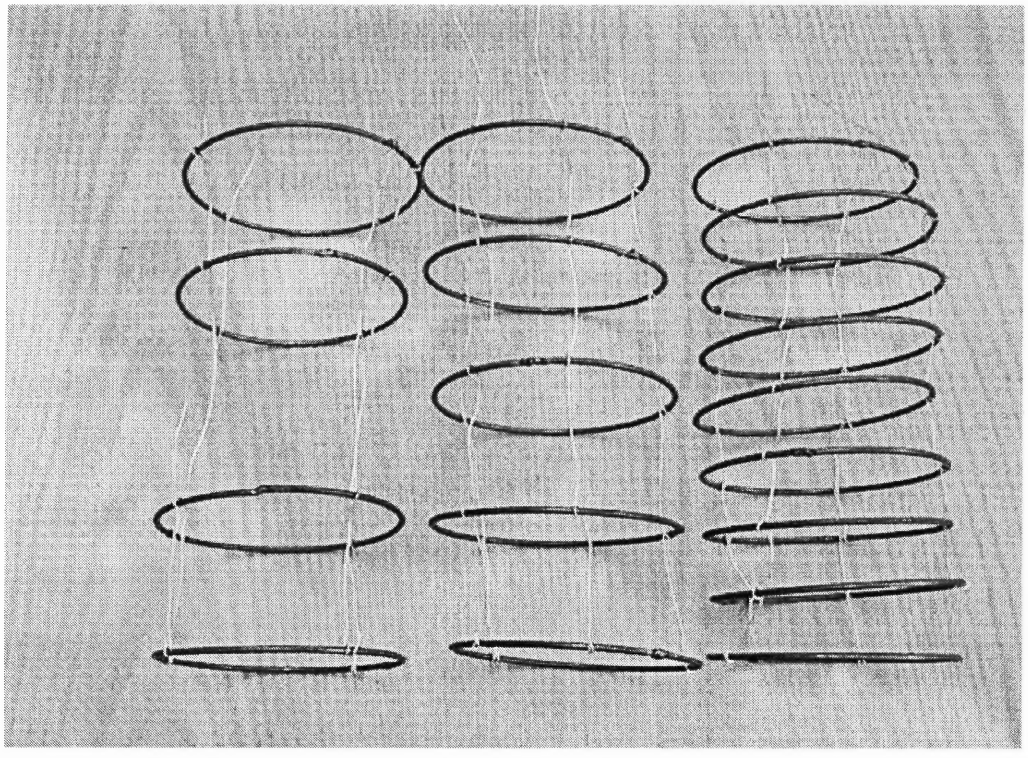

Figure B.3 Steel hoops configuration.

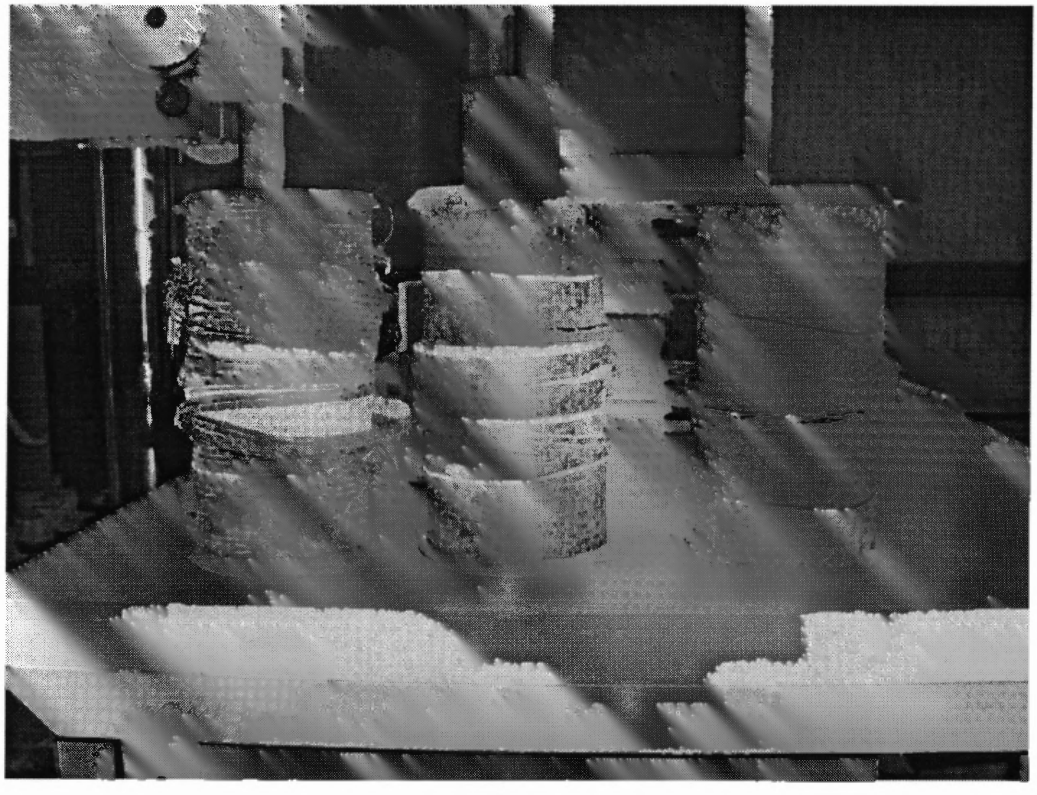

Figure B.4 Failure condition of concrete cylinders with CFRP fabrics.

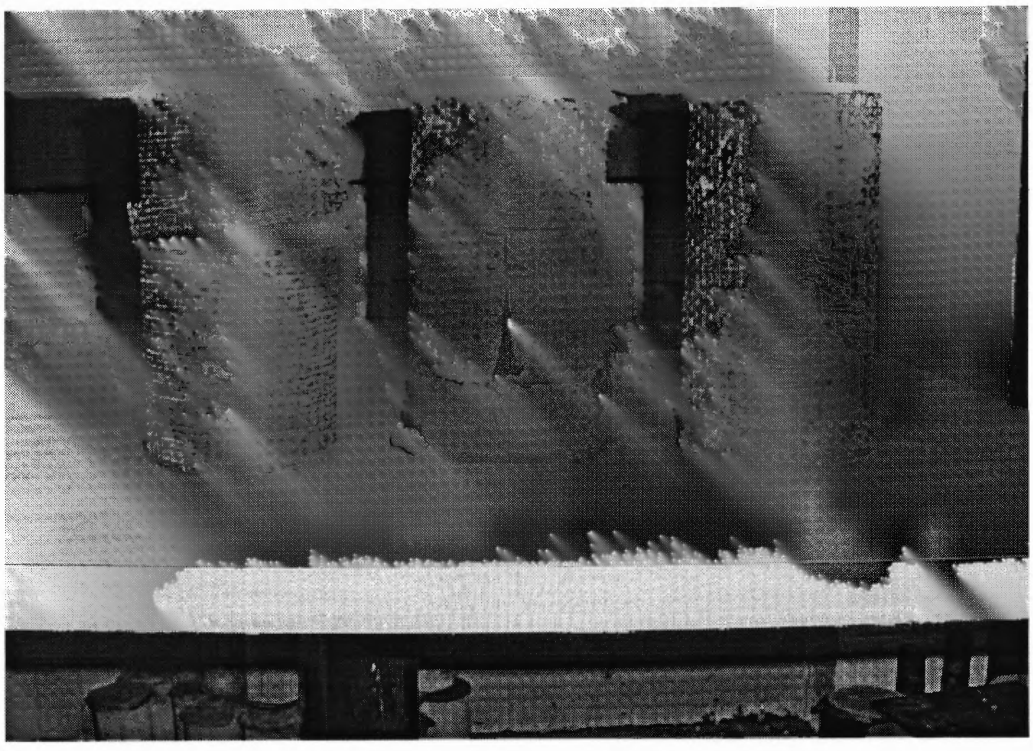

Figure B.5 Failure condition of concrete cylinders with CFRP fabrics and steel hoops.

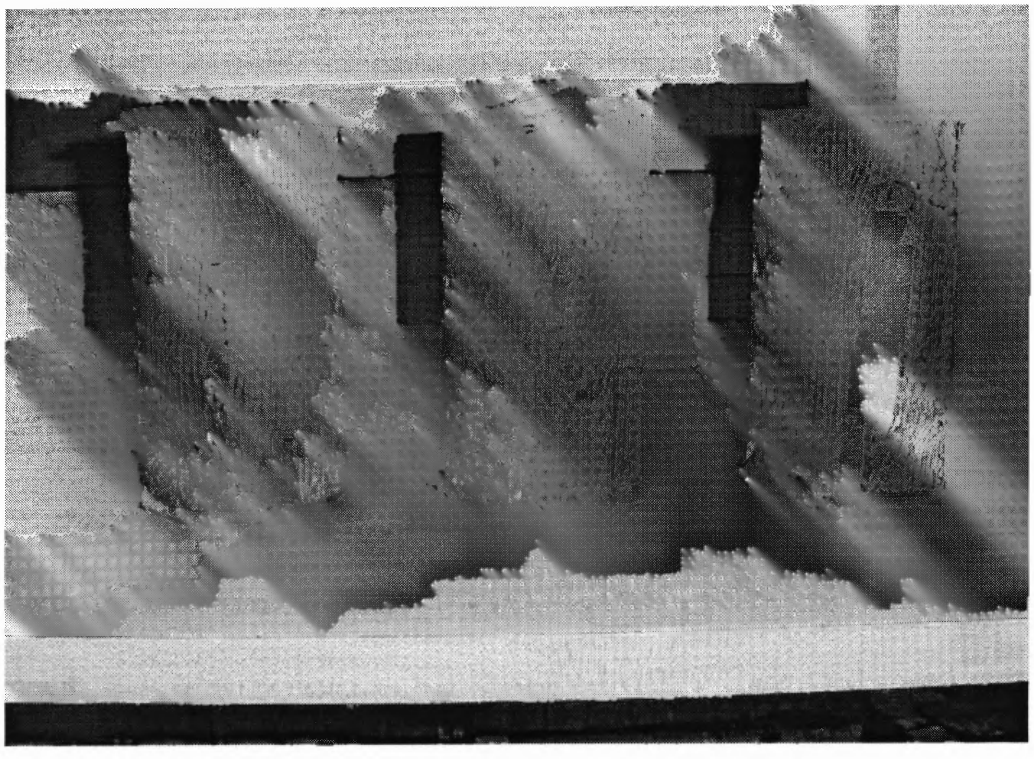

Figure B.6 Failure condition of concrete cylinders wrapped at two directions.

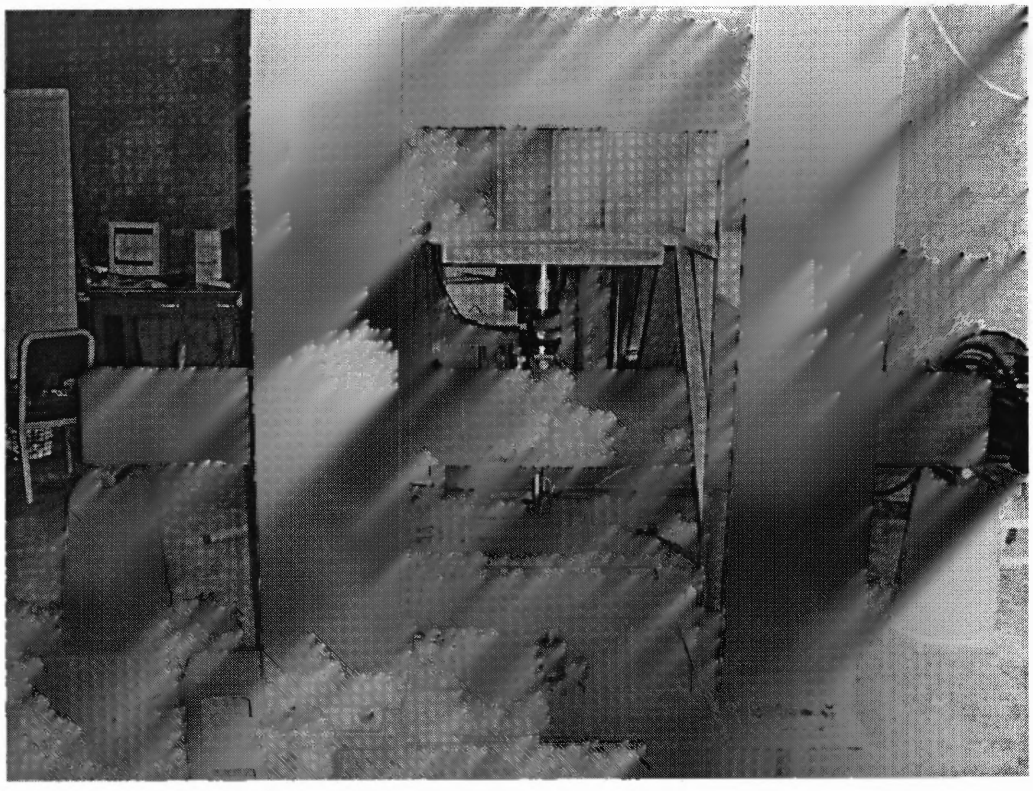

Figure B.7 Beam CJ1.

Figure B.8 Beam CJ2.

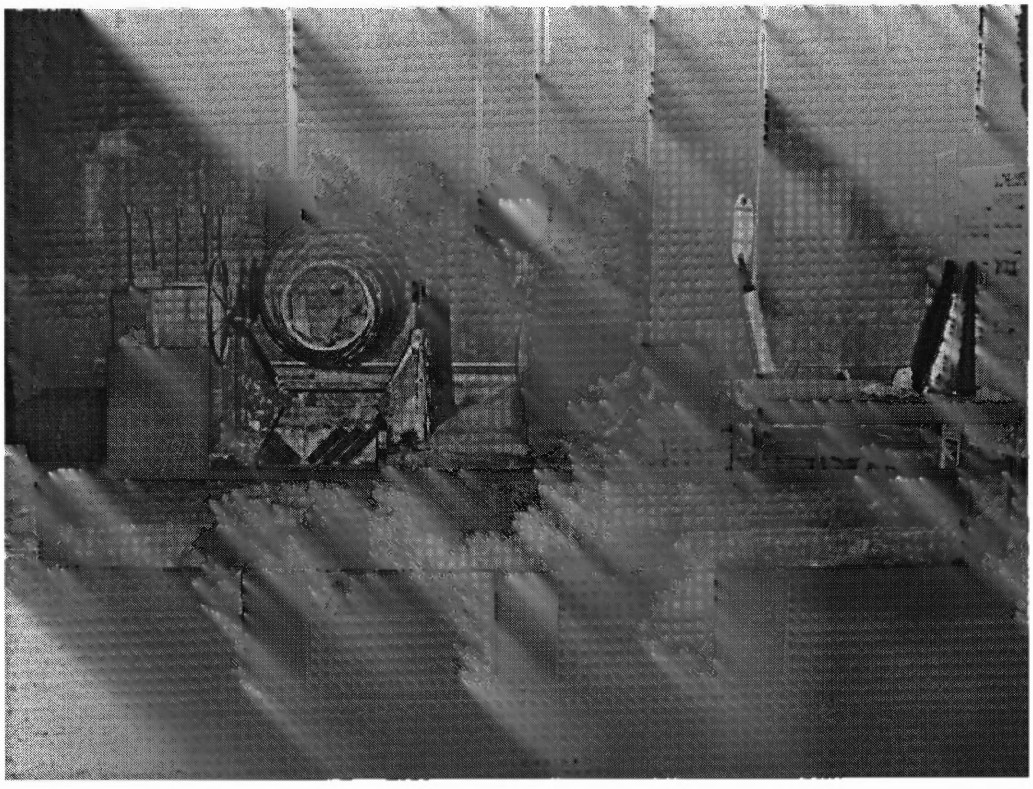

Figure B.9 Beam CJ3.

Figure B.10 Beam CJ4.

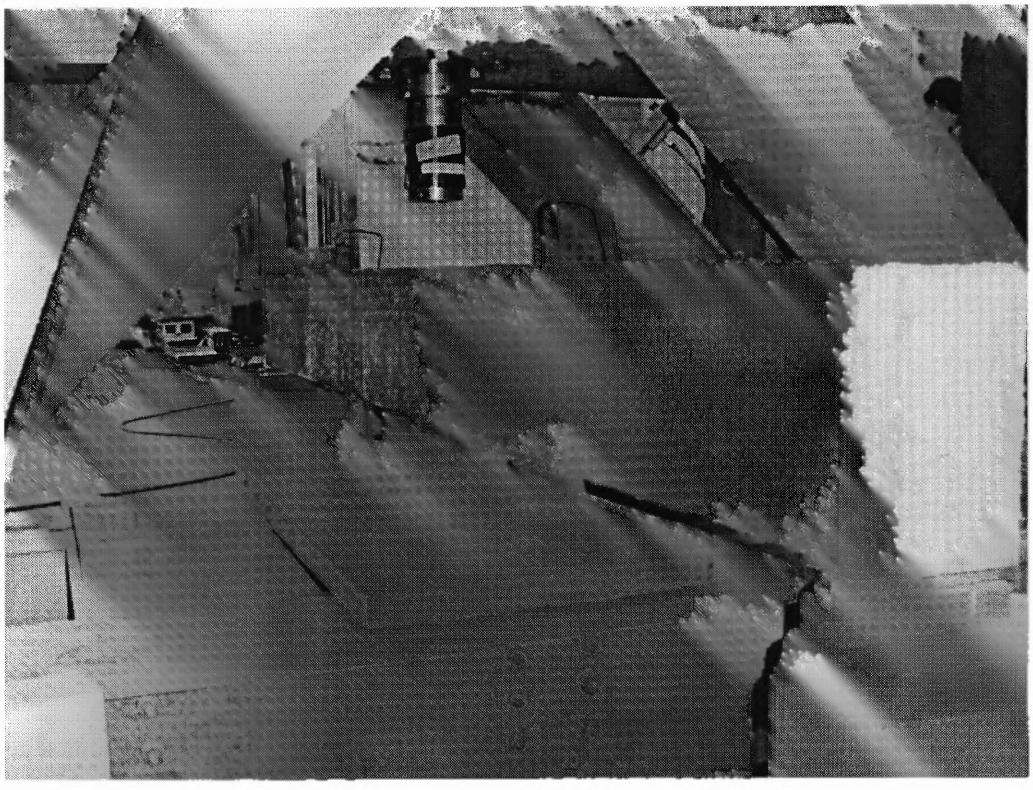

Figure B.11 Beam CJ5.

Figure B.12 Beam curvature measurement.

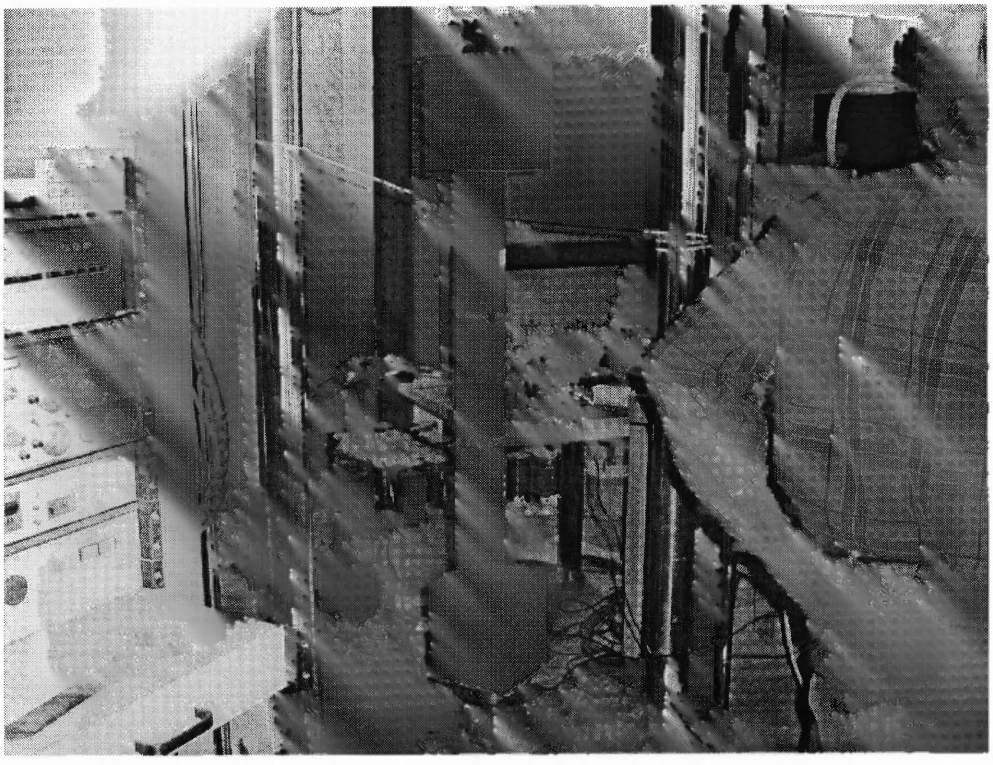

Figure B.13 Column CJC1.

Figure B.14 Column CJC2.

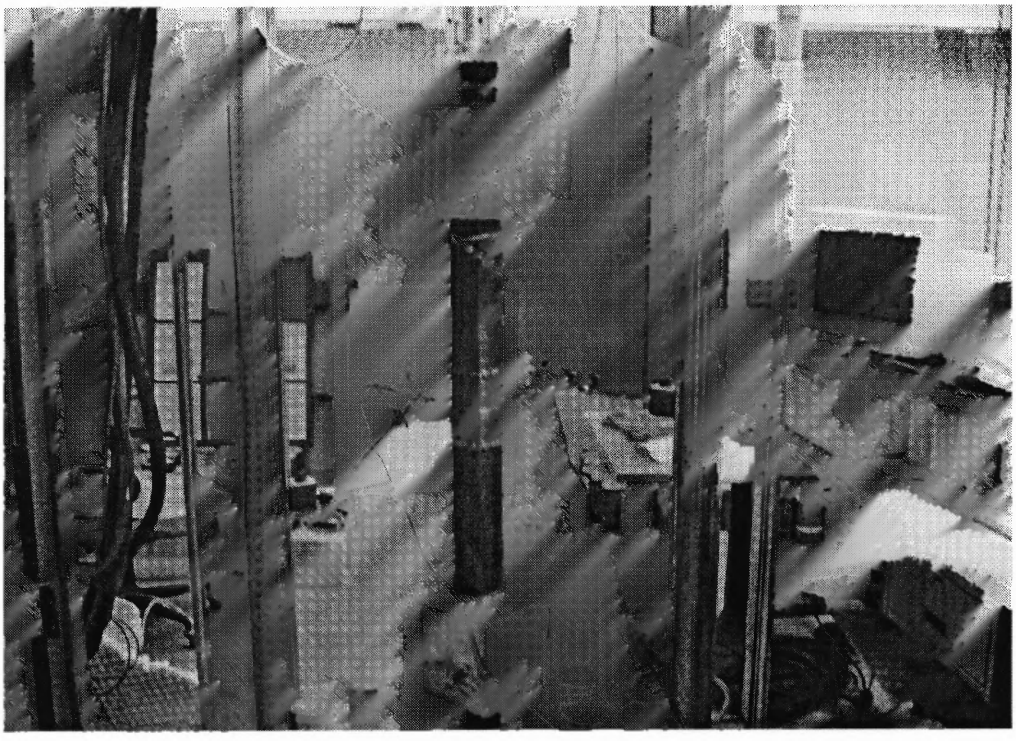

Figure B.15 Column CJC3.

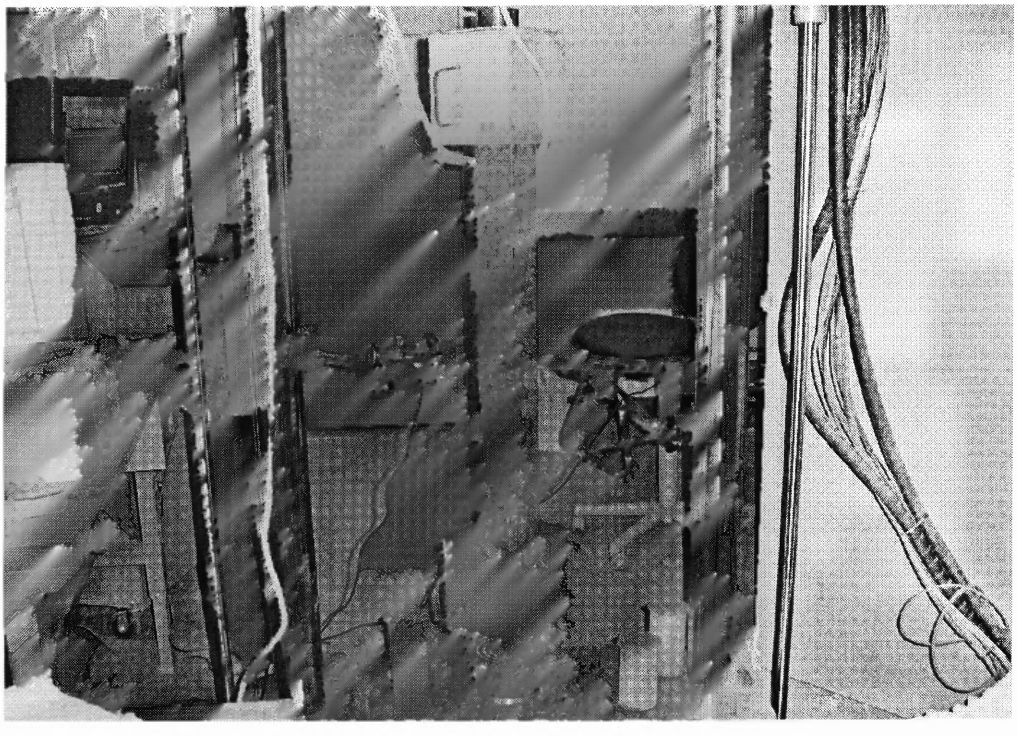

Figure B.16 Column CJC4.

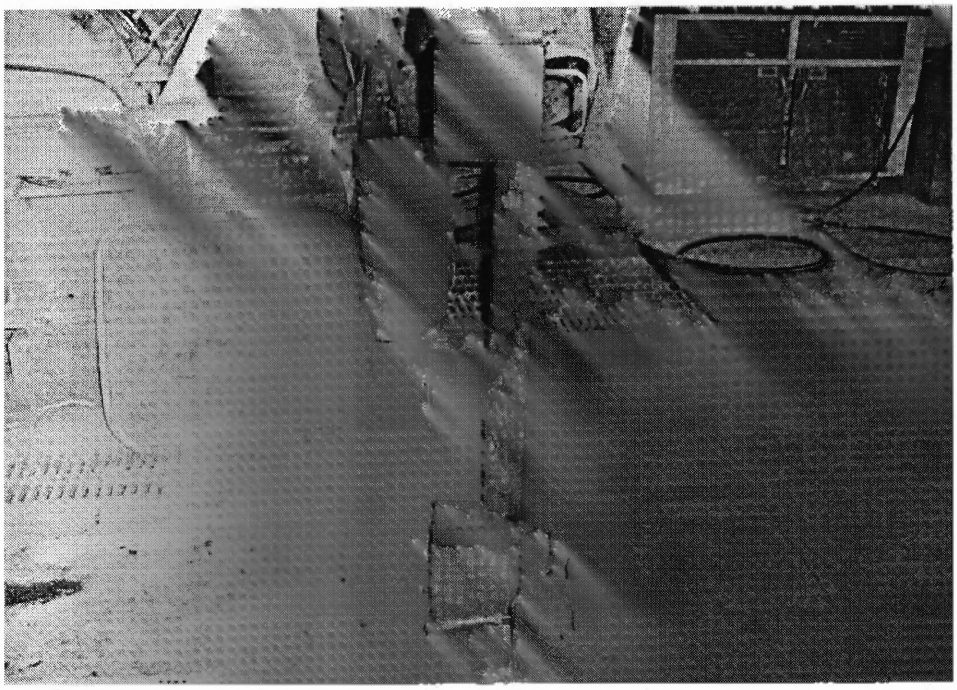

Figure B.17 Column CJC5.

Figure B.18 Column CJC6.

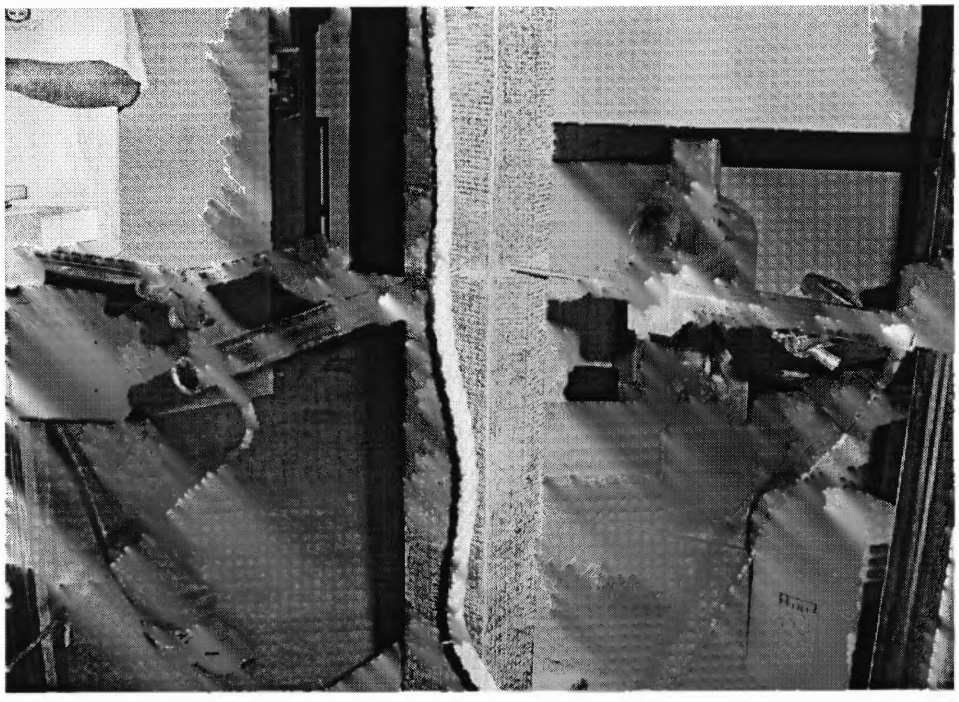

Figure B.19 Column CJC7.

Figure B.20 Column curvature measurement.

APPENDIX C

STRESS-STRAIN CURVES OF NORMAL CONCRETE CYLINDERS WRAPPED WITH CFRP FABRICS

In appendix C, Figures C.1-C.12 give the experimental stress-strain curves of concrete cylinders wrapped with different layers of CFRP fabrics. Figures C.13-C.20 present the experimental axial strain-lateral strain curves of concrete cylinders wrapped with different layers of CFRP fabrics. Figures C.22-C.34 show the typical stress-strain curves for concrete cylinders confined by both fabrics and steel hoops. Figure C.35 gives the test results of cylinder specimens wrapped with CFRP fabrics at two different directions. Figures C.36-C.38 show the test results of cylinder specimens using different coarse aggregates wrapped with CFRP fabrics. Figures C.39-C.40 compare the experimental results to the proposed equation in Chapter Two.

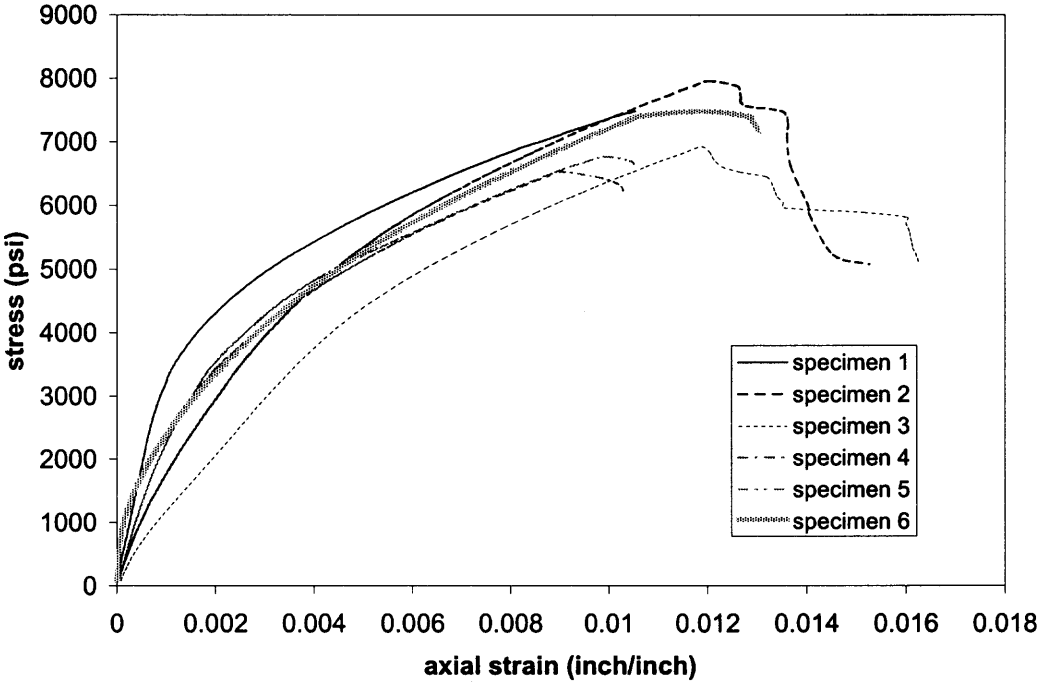

Figure C.1 Stress-axial strain curves of 3000psi concrete wrapped with 1 layer fabric.

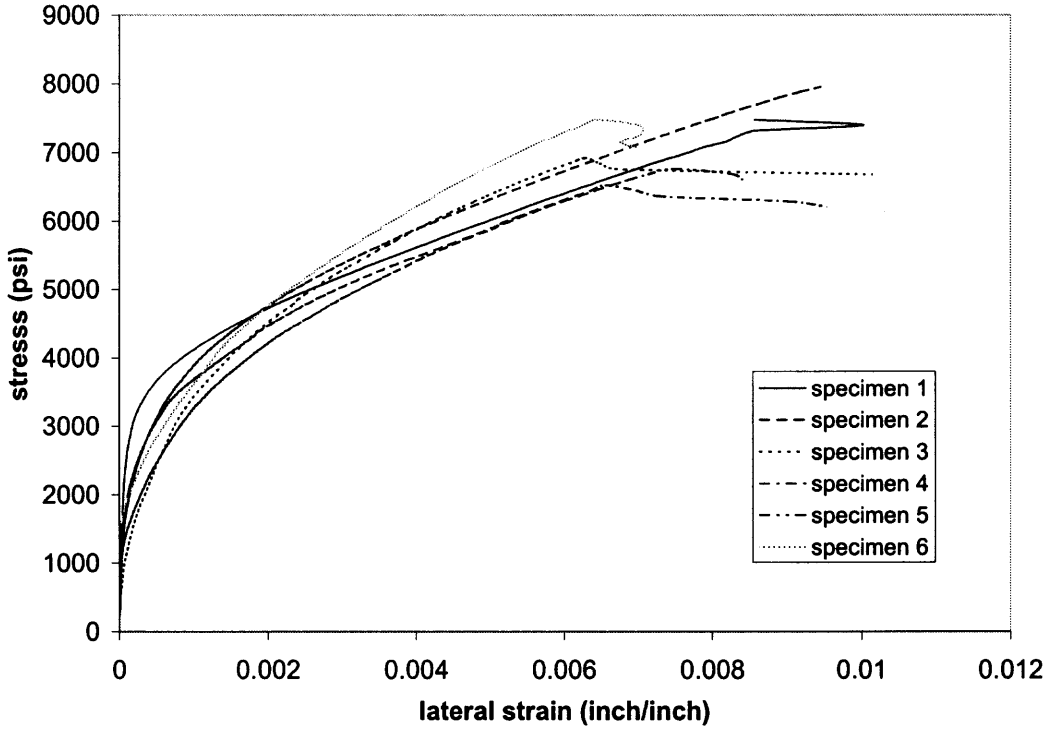

Figure C.2 Stress- lateral strain curves of 3000psi concrete wrapped with 1 layer fabric.

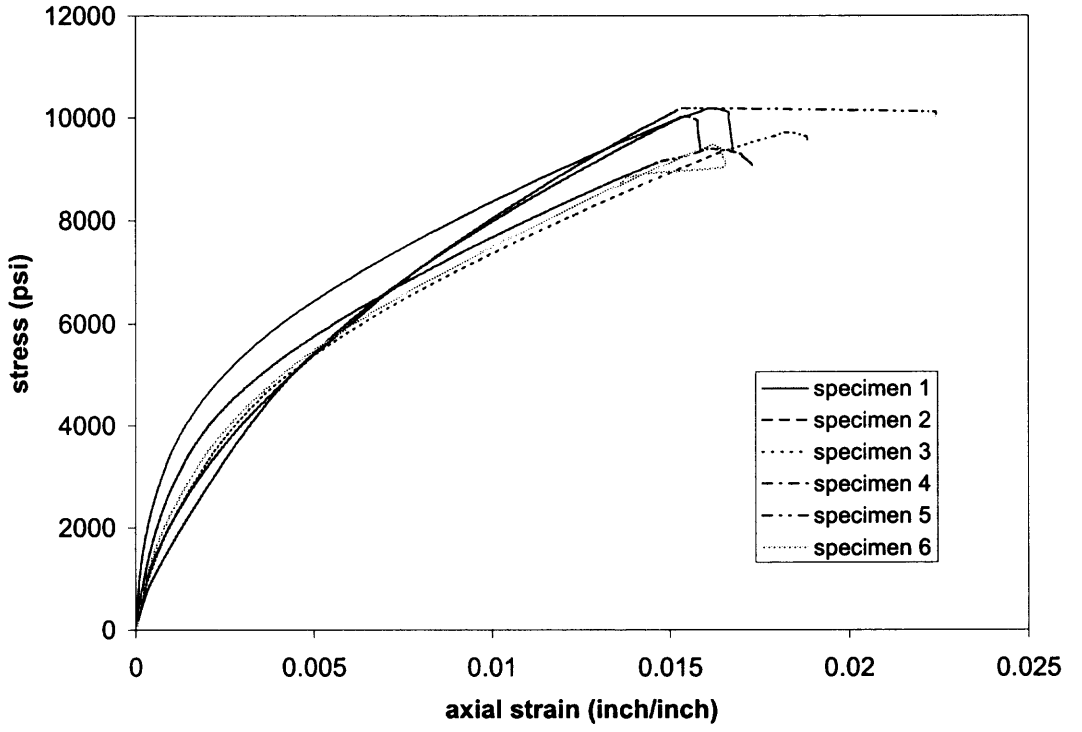

Figure C.3 Stress-axial strain curves of 3000psi concrete wrapped with 2 layers fabric.

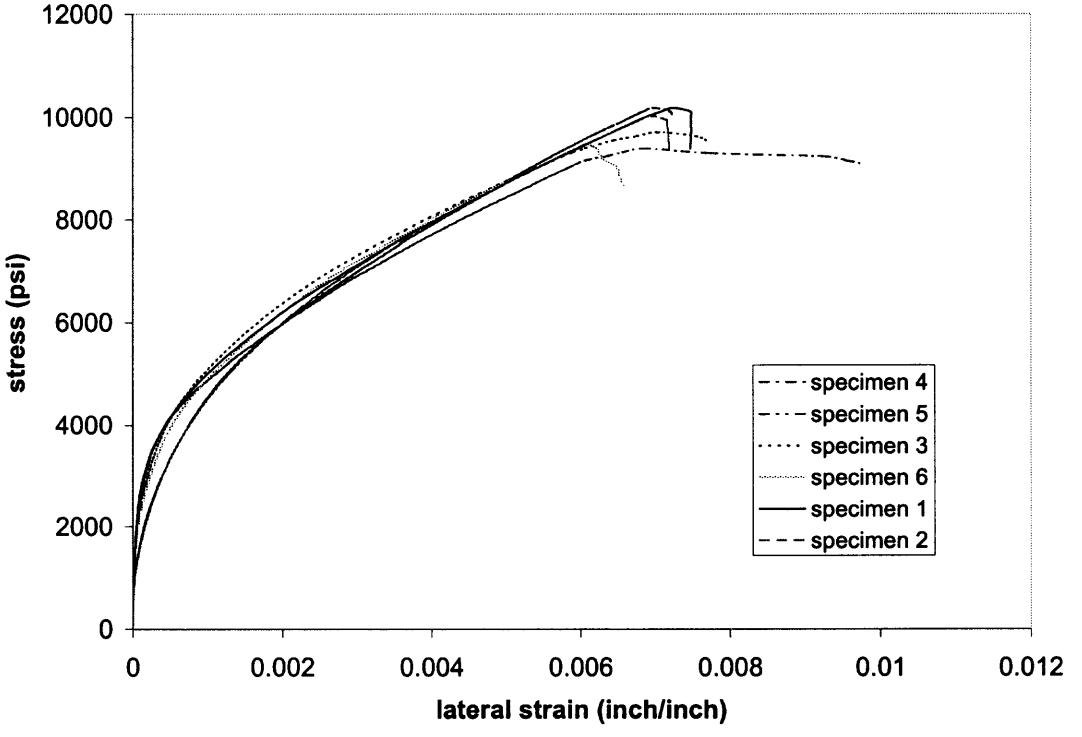

Figure C.4 Stress-lateral strain curves of 3000psi concrete wrapped with 2 layers fabric.

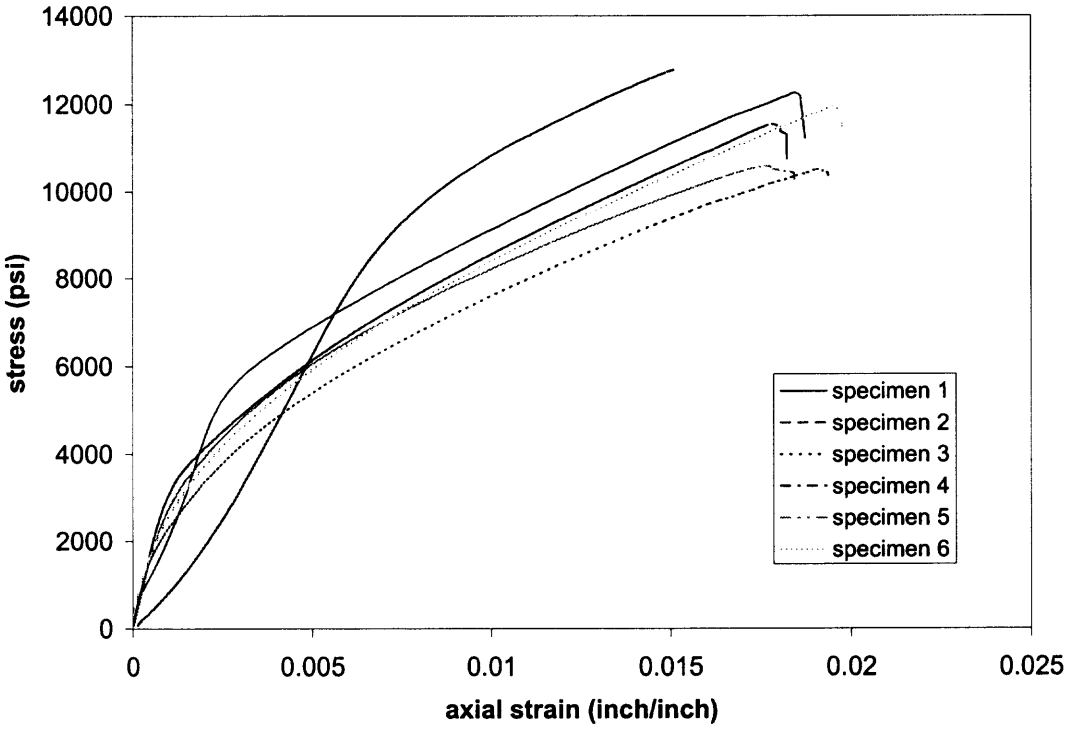

Figure C.5 Stress-axial strain curves of 3000psi concrete wrapped with 3 layers fabric.

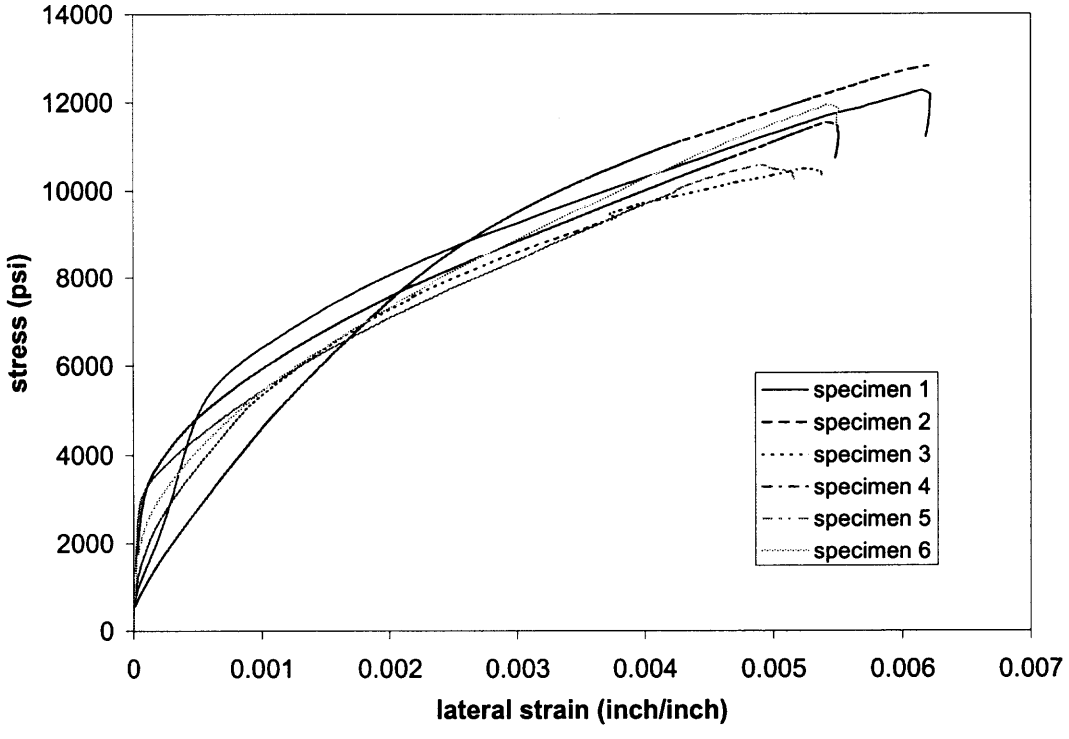

Figure C.6 Stress-lateral strain curves of 3000psi concrete wrapped with 3 layers fabric.

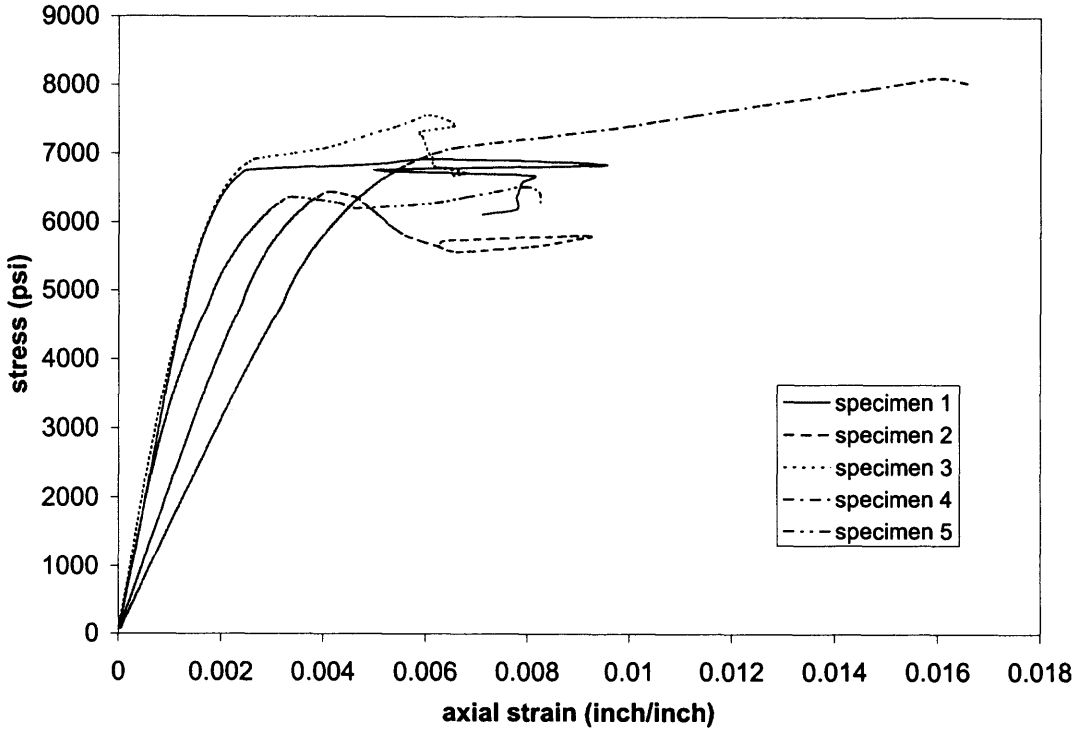

Figure C.7 Stress-axial strain curves of 5000psi concrete wrapped with 1 layer fabric.

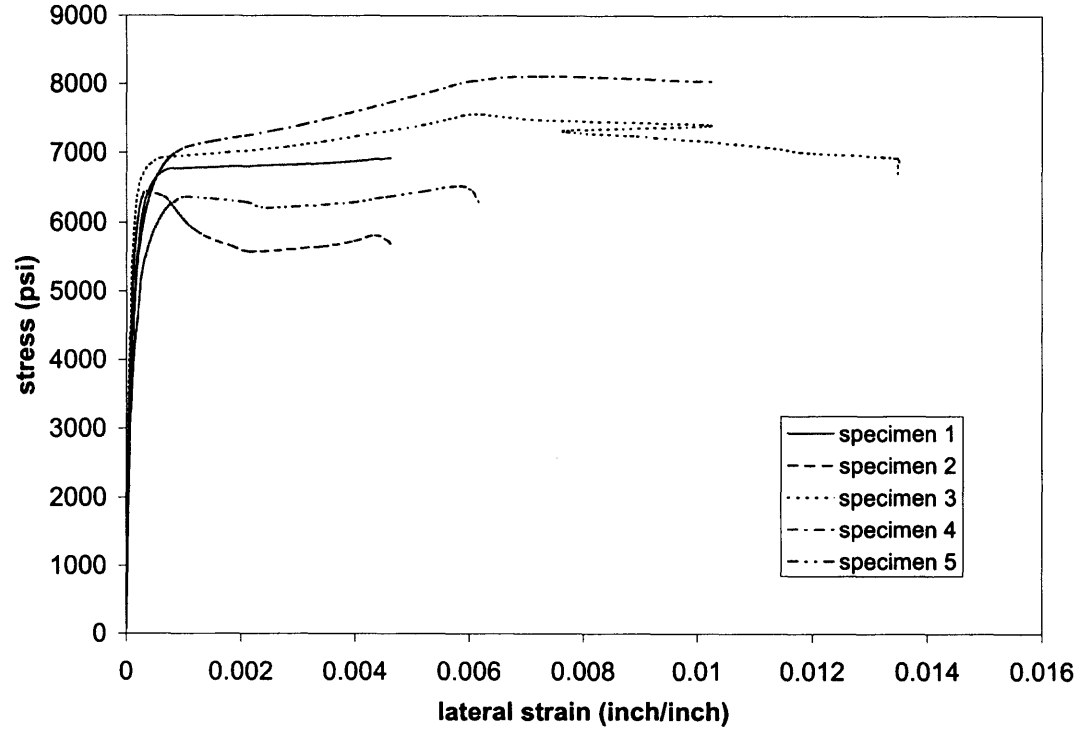

Figure C.8 Stress-lateral strain curves of 5000psi concrete wrapped with 1 layer fabric.

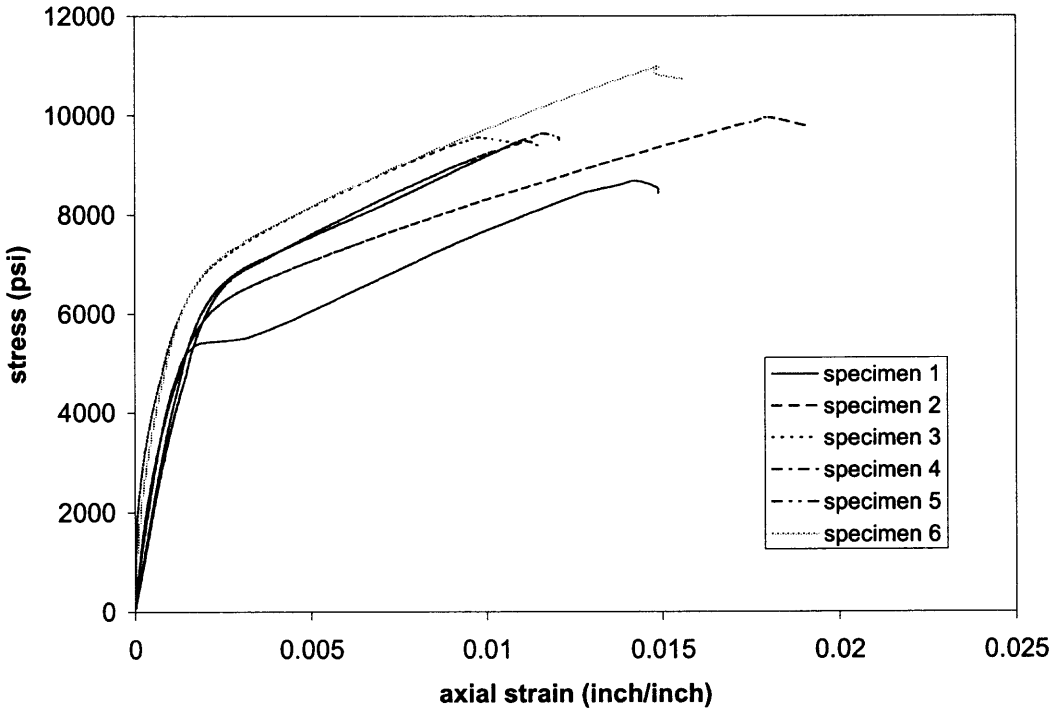

Figure C.9 Stress-axial strain curves of 5000psi concrete wrapped with 2 layers fabric.

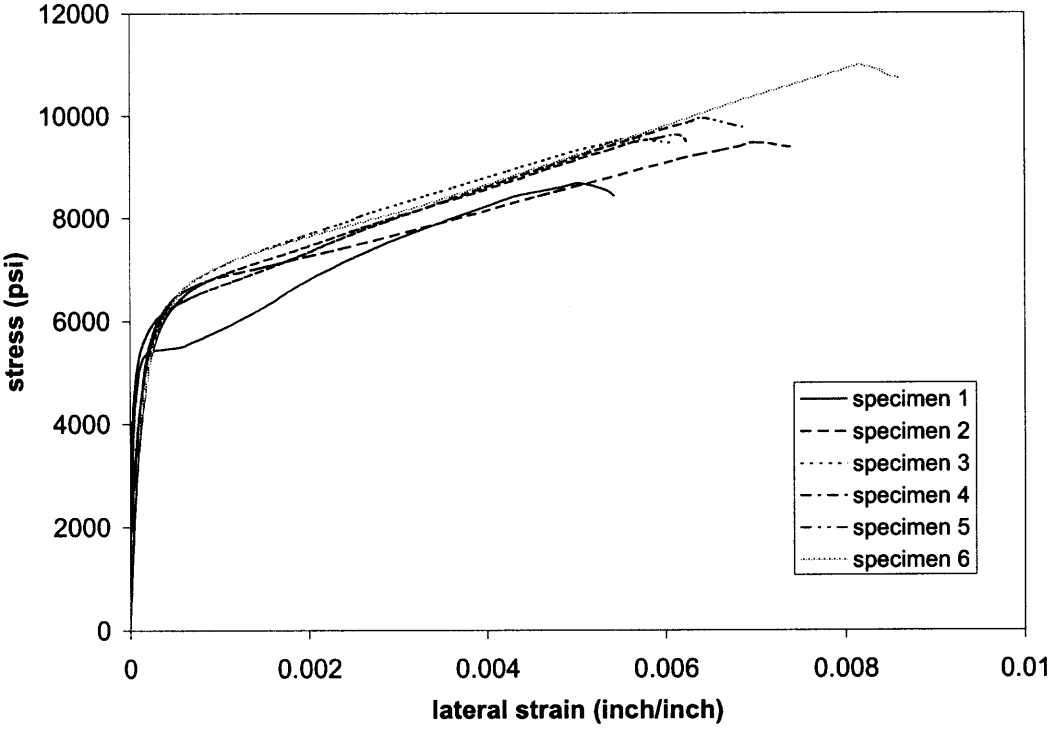

Figure C.10 Stress-lateral strain curves of 5000psi concrete wrapped with 2 layers fabric.

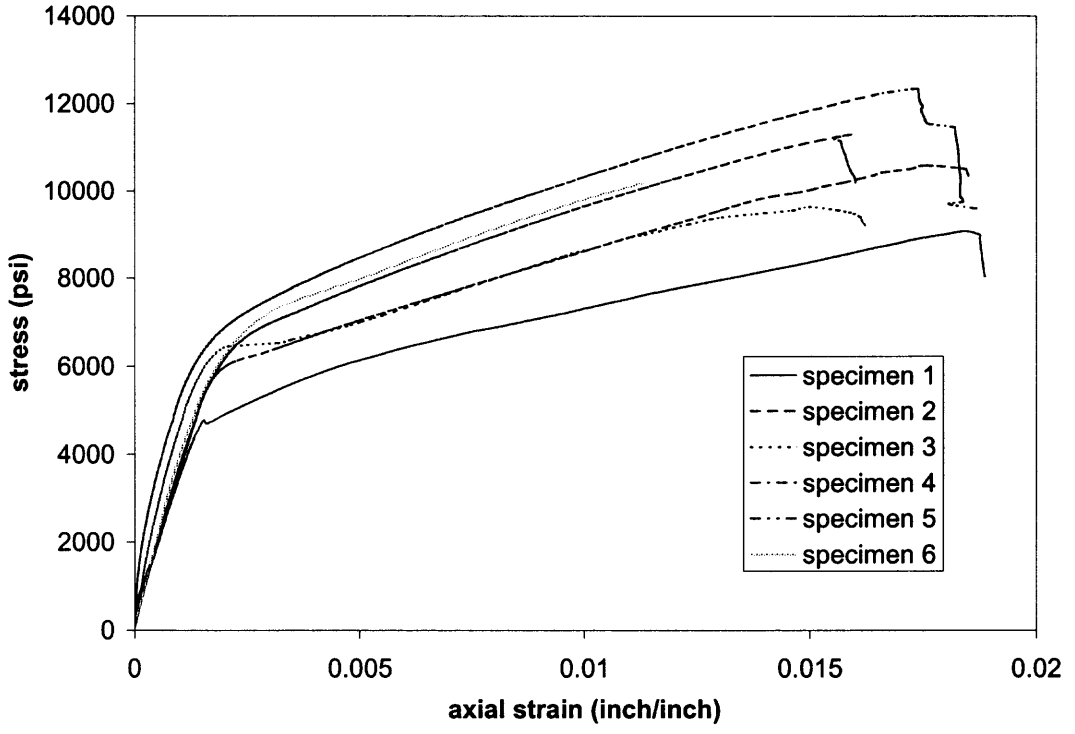

Figure C.11 Stress-axial strain curves of 5000psi concrete wrapped with 3 layers fabric.

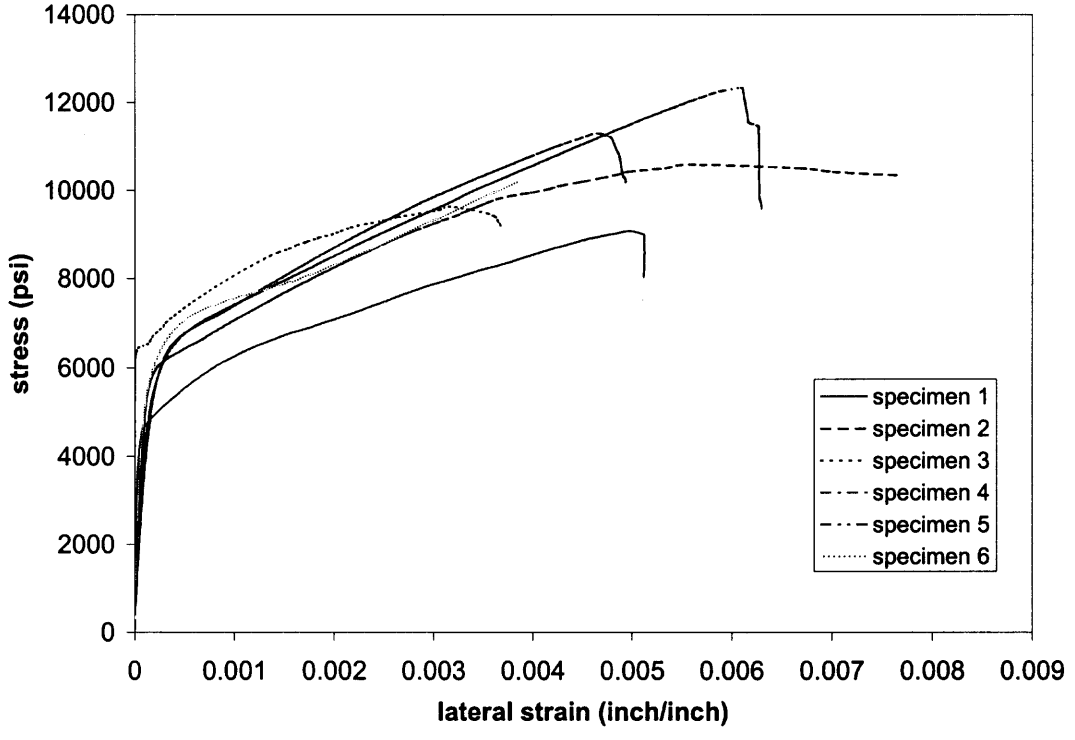

Figure C.12 Stress-lateral strain curves of 5000psi concrete wrapped with 3 layers fabric.

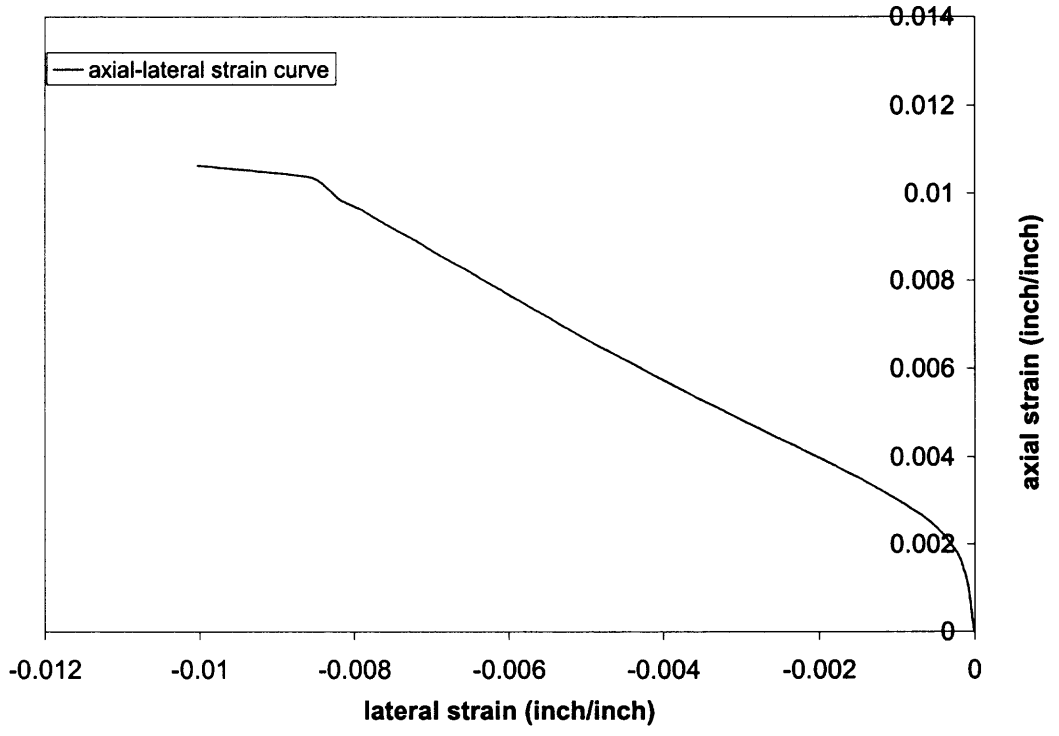

Figure C.13 Average axial-lateral strain curve of 3000psi concrete with 1 layer fabric.

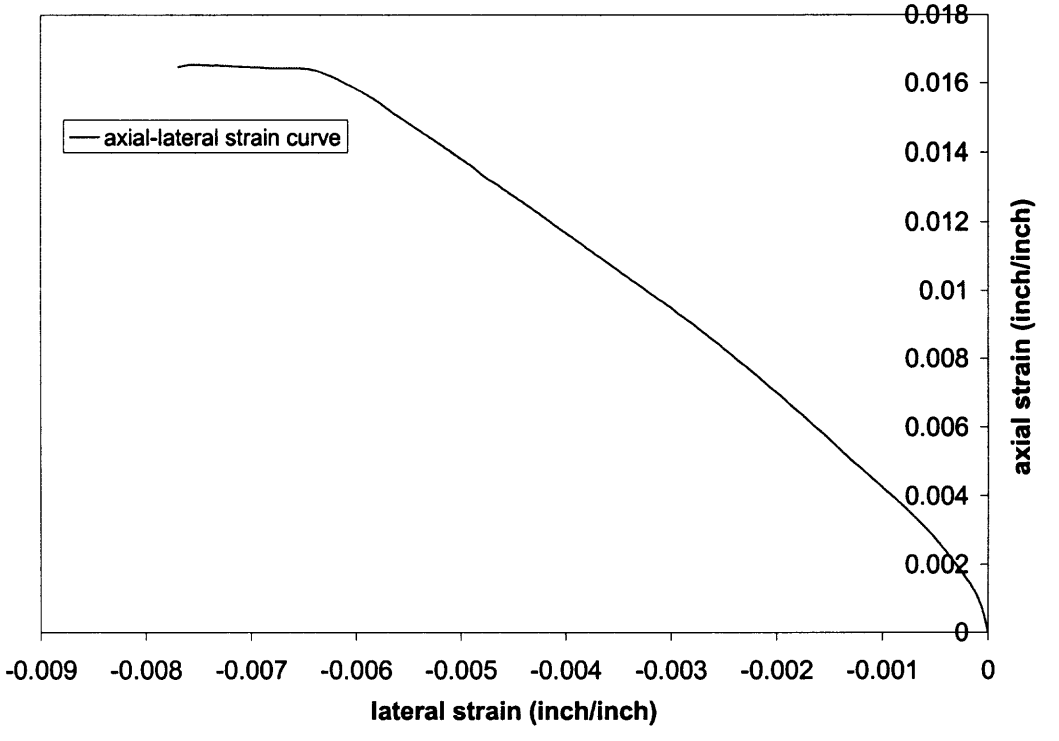

Figure C.14 Average axial-lateral strain curve of 3000psi concrete with 2 layers fabric.

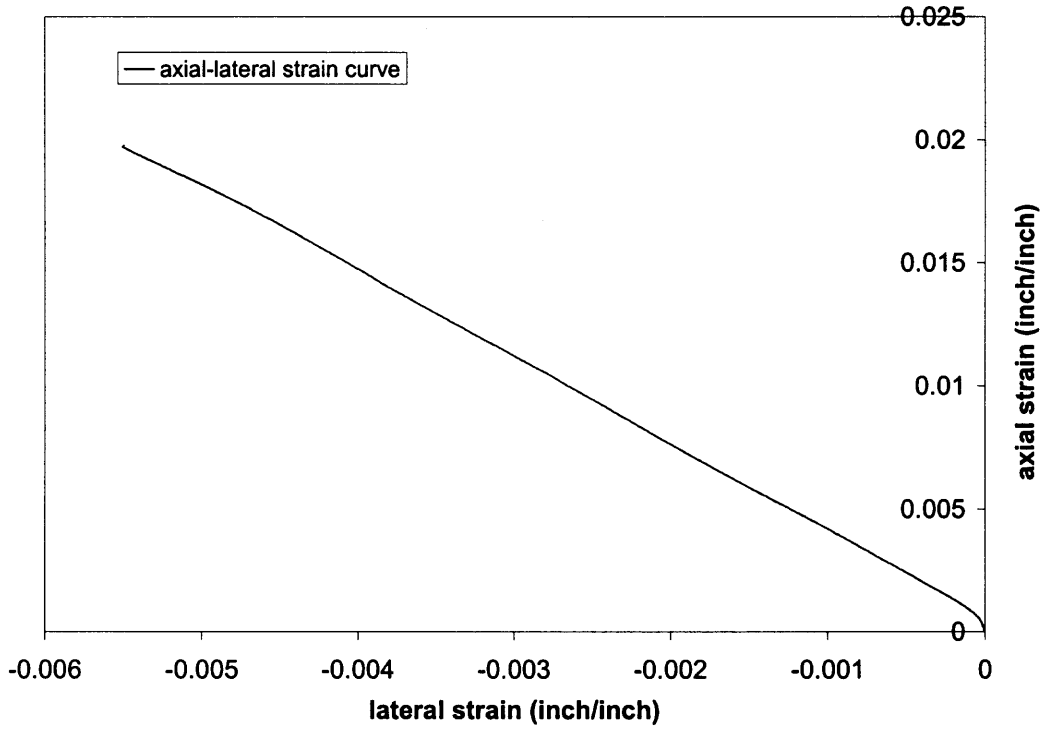

Figure C.15 Average axial-lateral strain curve of 3000psi concrete with 3 layers fabric.

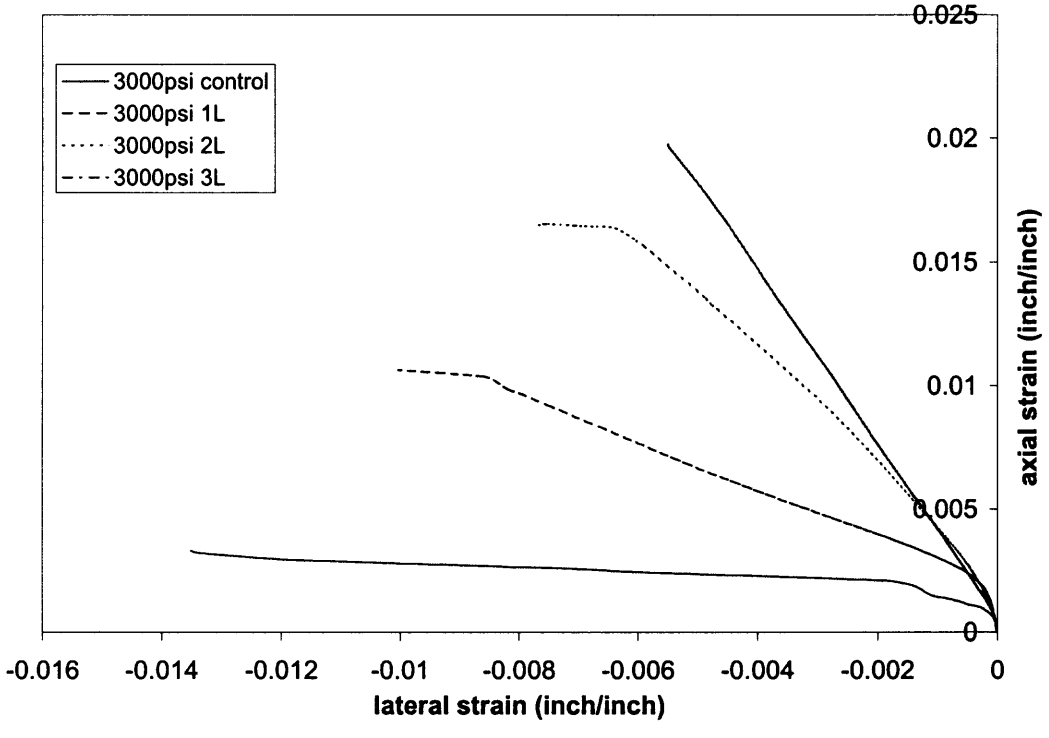

Figure C.16 Comparison of average axial-lateral strain curves of 3000psi concrete.

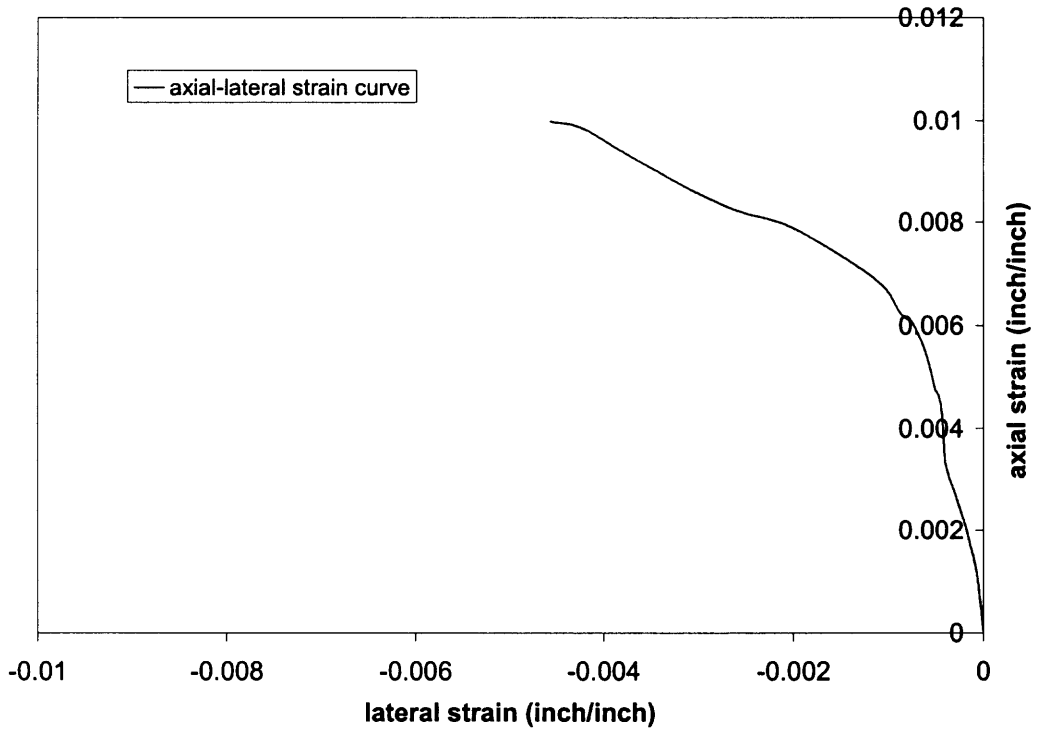

Figure C.17 Average axial-lateral strain curve of 5000psi concrete with 1 layer fabric.

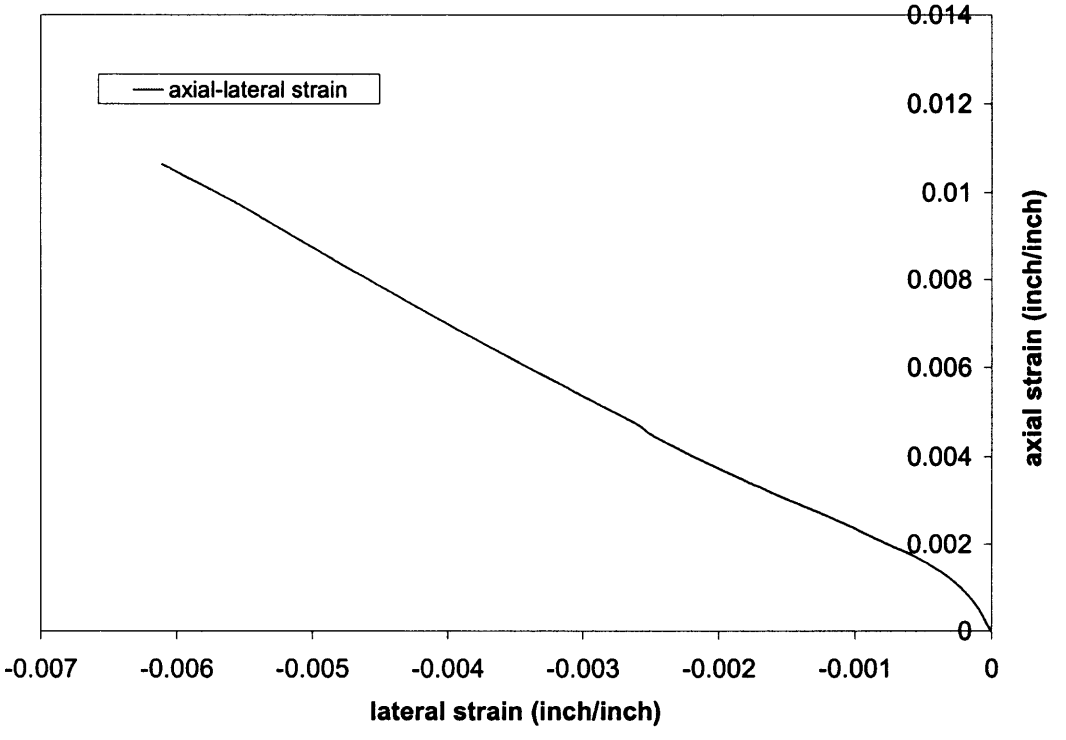

Figure C.18 Average axial-lateral strain curve of 5000psi concrete with 2 layers fabric.

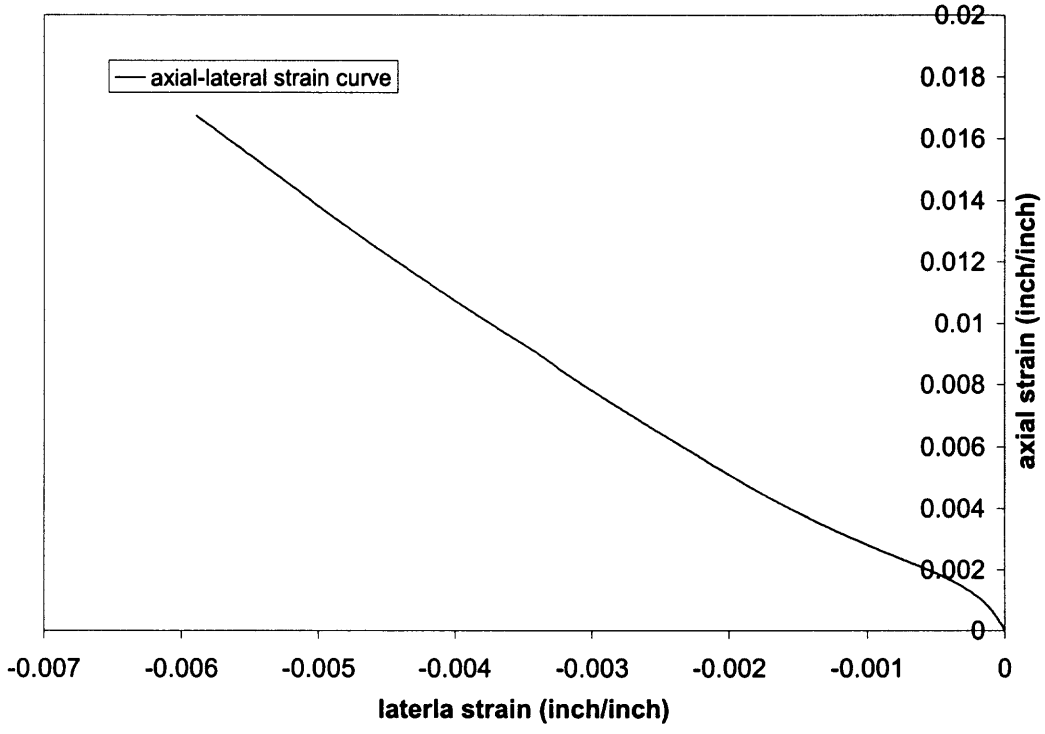

Figure C.19 Average axial-lateral strain curve of 5000psi concrete with 3 layers fabric.

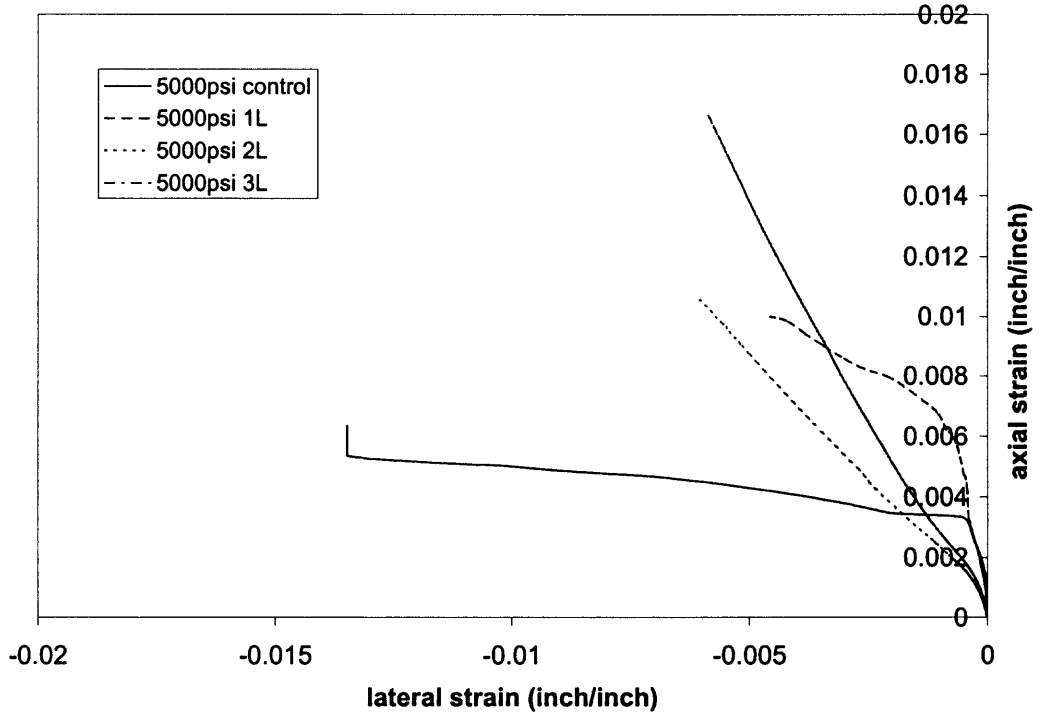

Figure C.20 Comparison of average axial-lateral strain curves of 5000psi concrete.

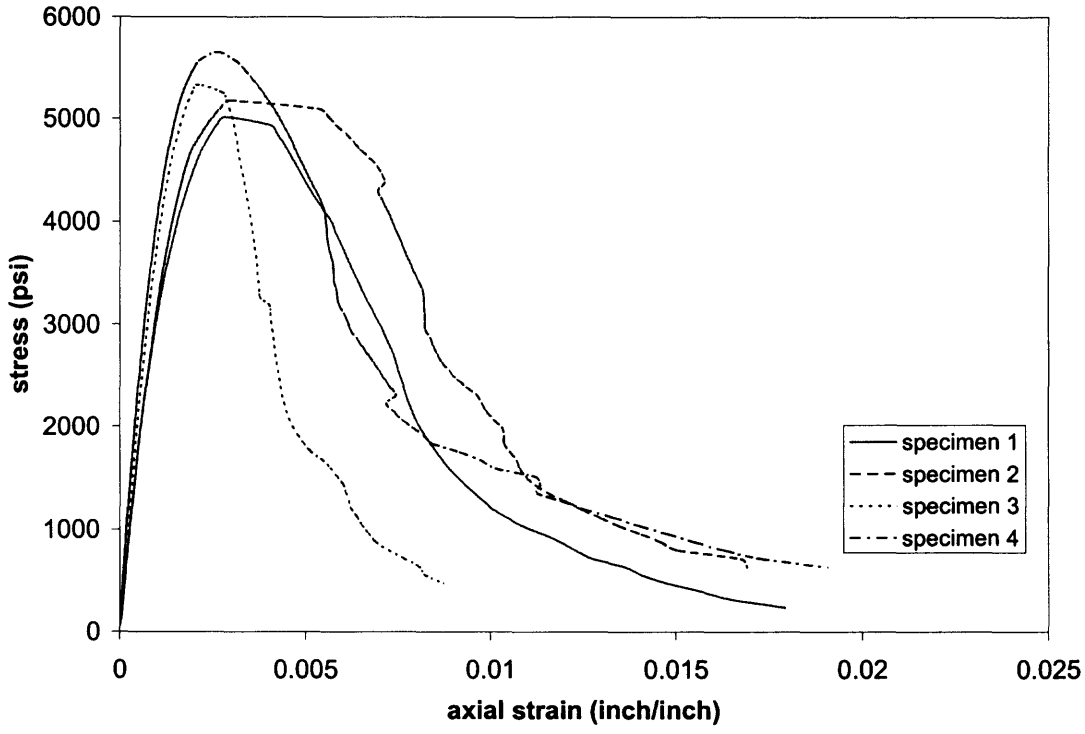

Figure C.21 Stress-strain curves of 5000psi concrete confined with 2 in spacing steel hoops.

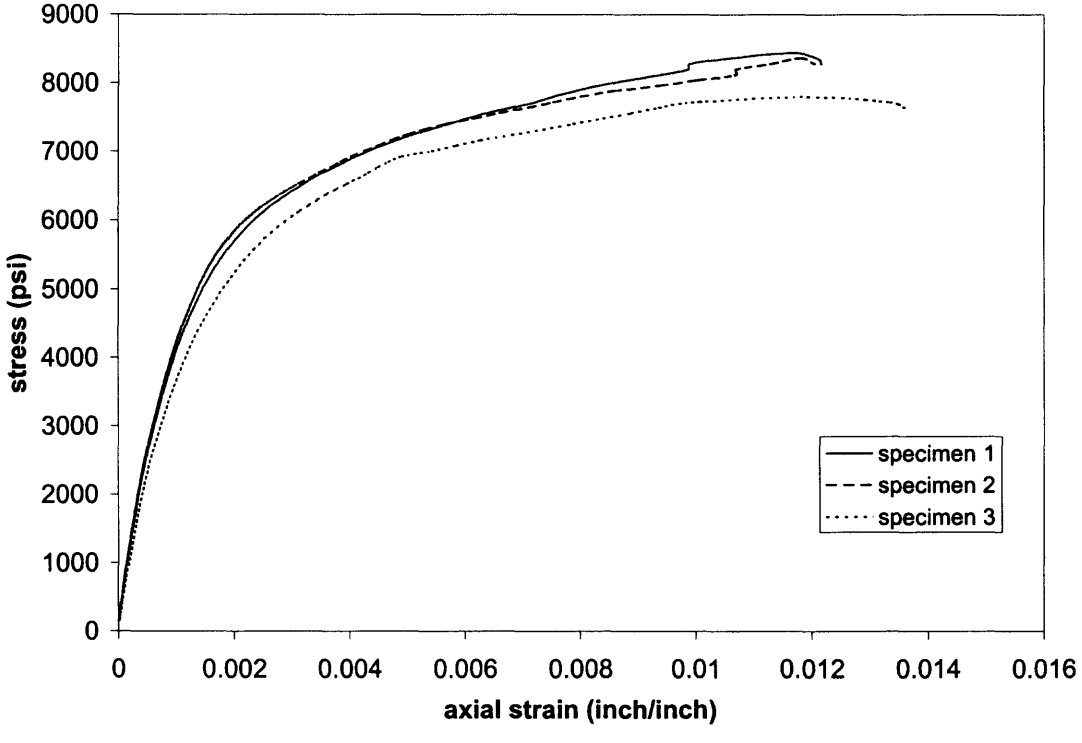

Figure C.22 Stress-strain curves of 5000psi concrete confined with 1 layer fabric and 2 in spacing steel hoops.

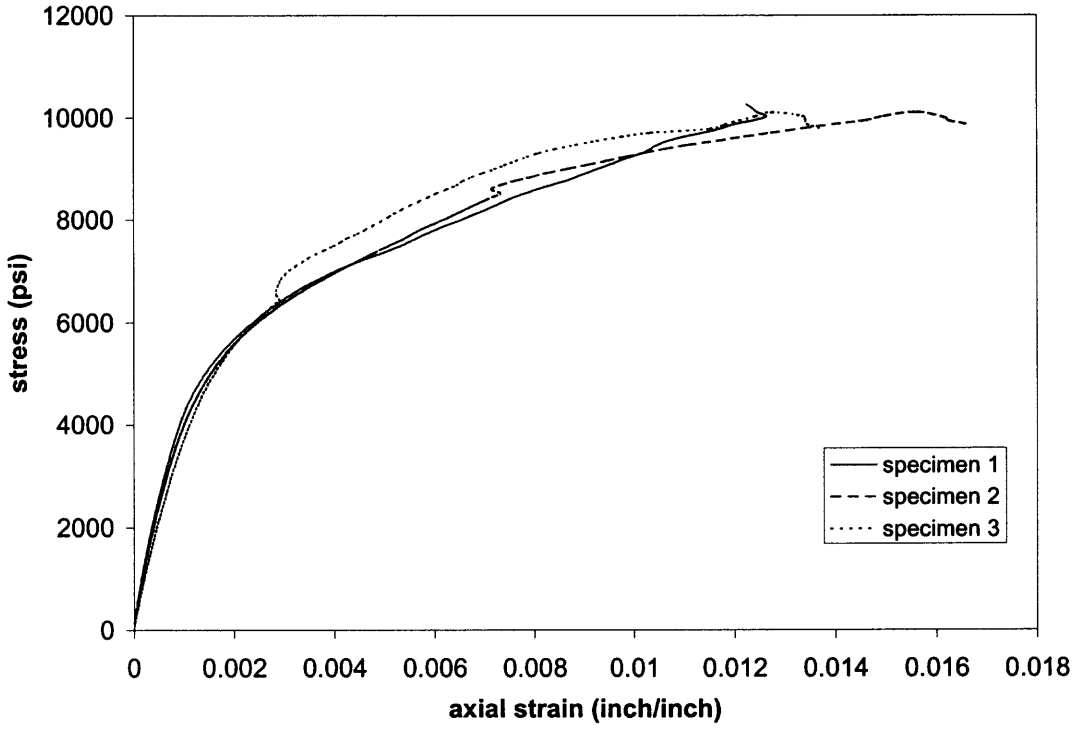

Figure C.23 Stress-strain curves of 5000psi concrete confined with 2 layers fabric and 2 in spacing steel hoops.

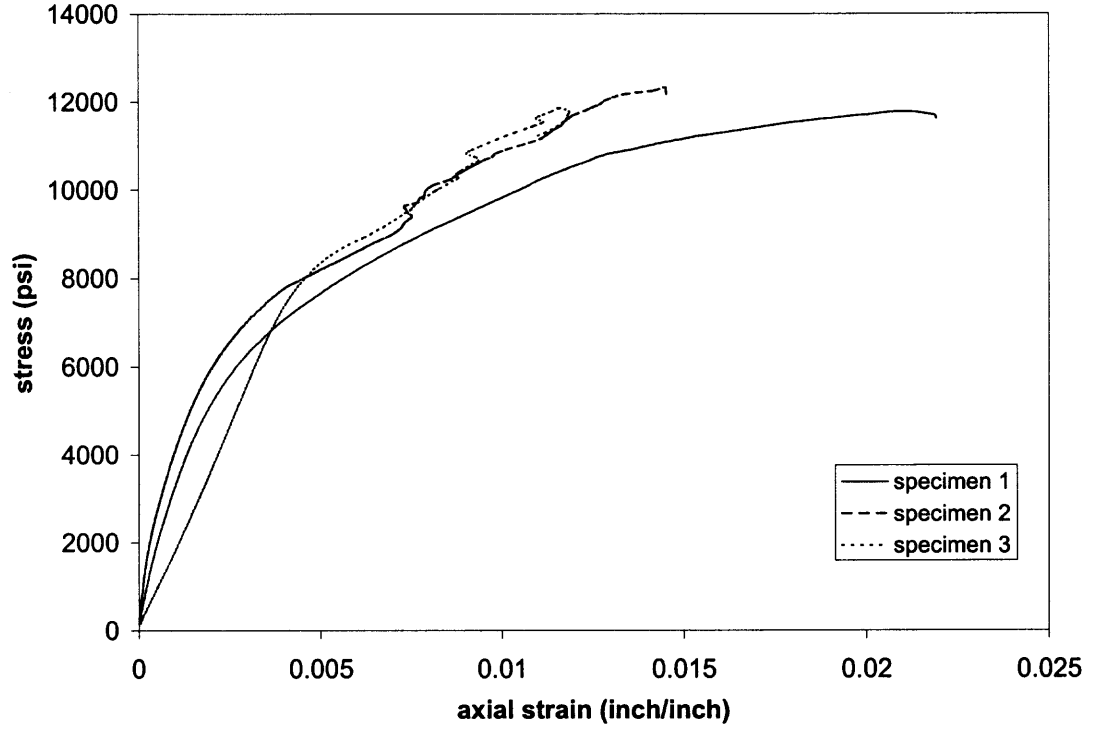

Figure C.24 Stress-strain curves of 5000psi concrete confined with 3 layers fabric and 2 in spacing steel hoops.

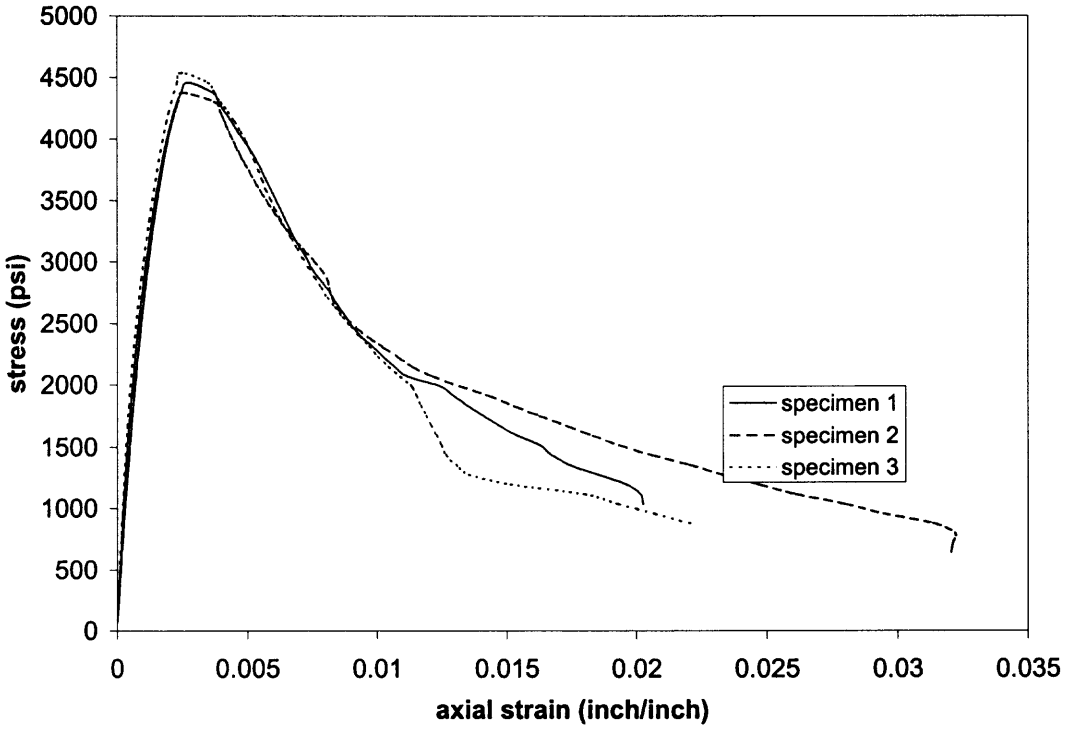

Figure C.25 Stress-strain curves of 5000psi concrete confined with 4 in spacing steel hoops.

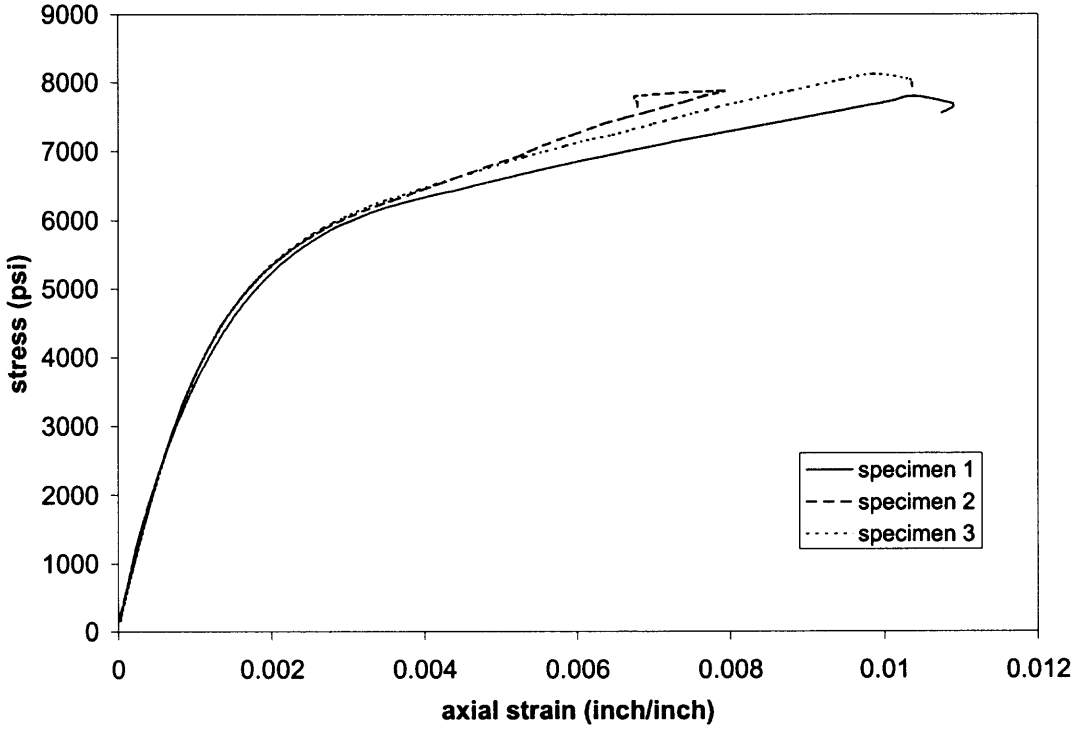

Figure C.26 Stress-strain curves of 5000psi concrete confined with 1 layer fabric and 4 in spacing steel hoops.

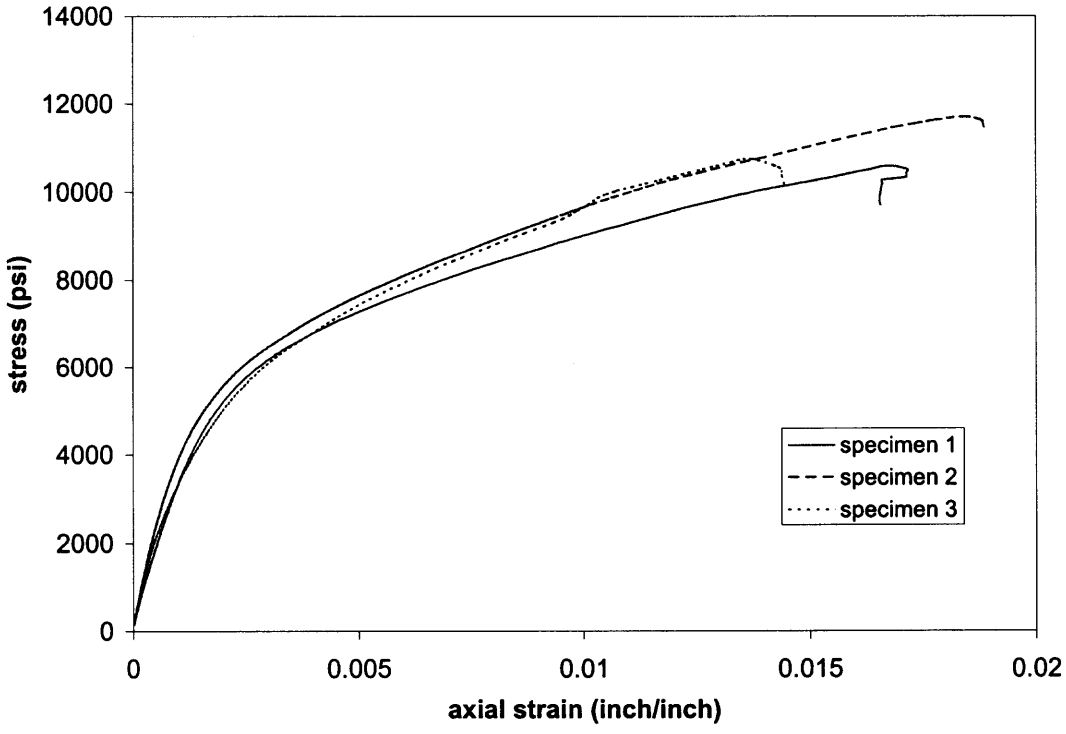

Figure C.27 Stress-strain curves of 5000psi concrete confined with 2 layers fabric and 4 in spacing steel hoops.

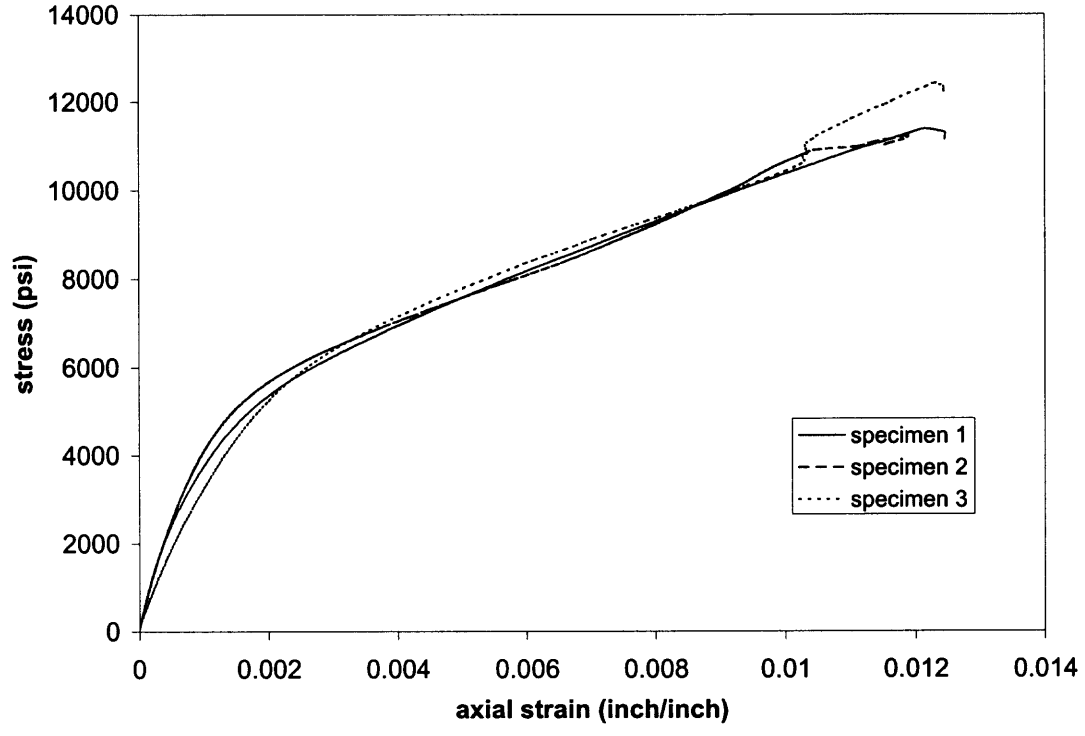

Figure C.28 Stress-strain curves of 5000psi concrete confined with 3 layers fabric and 4 in spacing steel hoops.

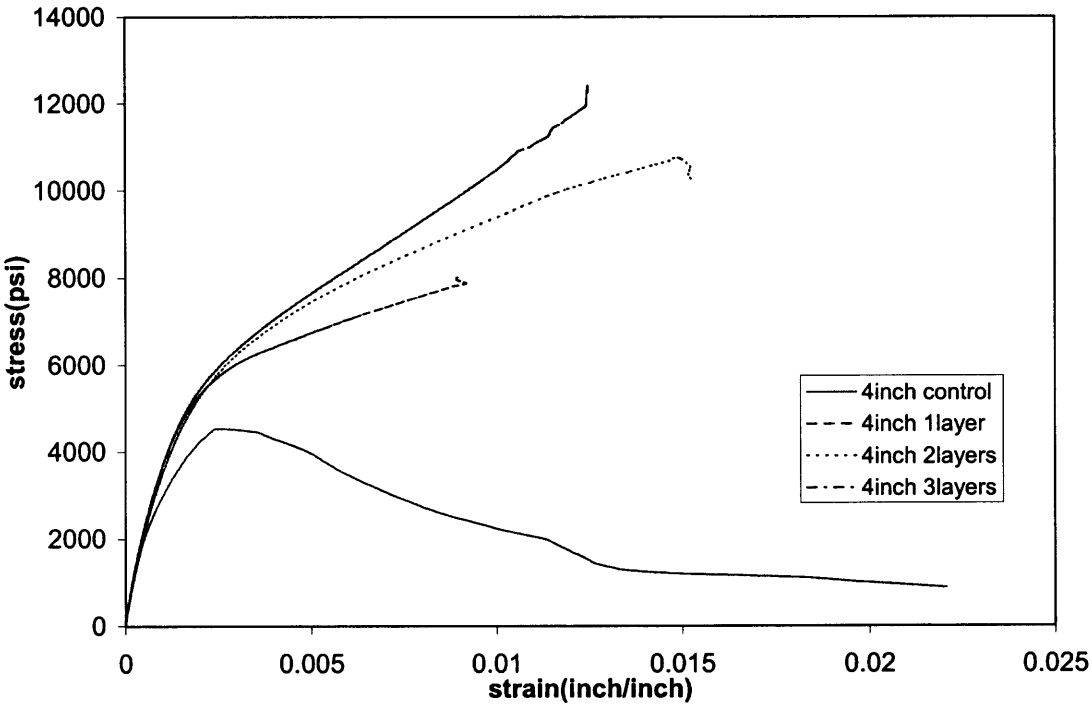

Figure C.29 Average stress-strain curves of CFRP strengthened 5000psi concrete confined with 4 in spacing steel hoops.

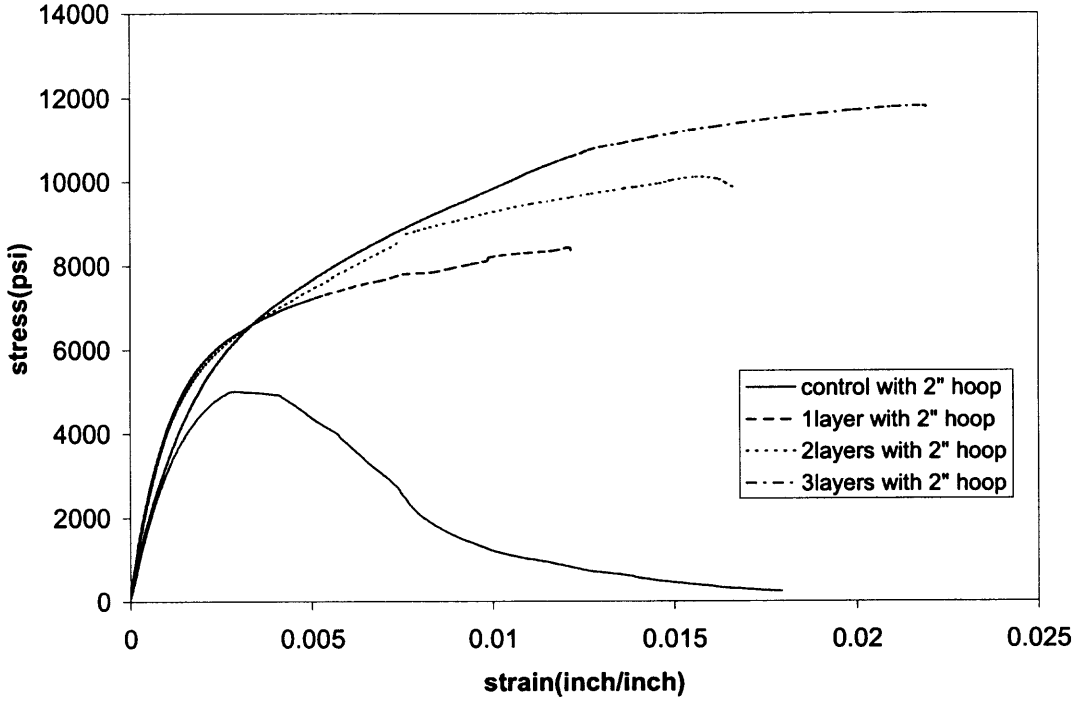

Figure C.30 Average stress-strain curves of CFRP strengthened 5000psi concrete confined with 2 in spacing steel hoops.

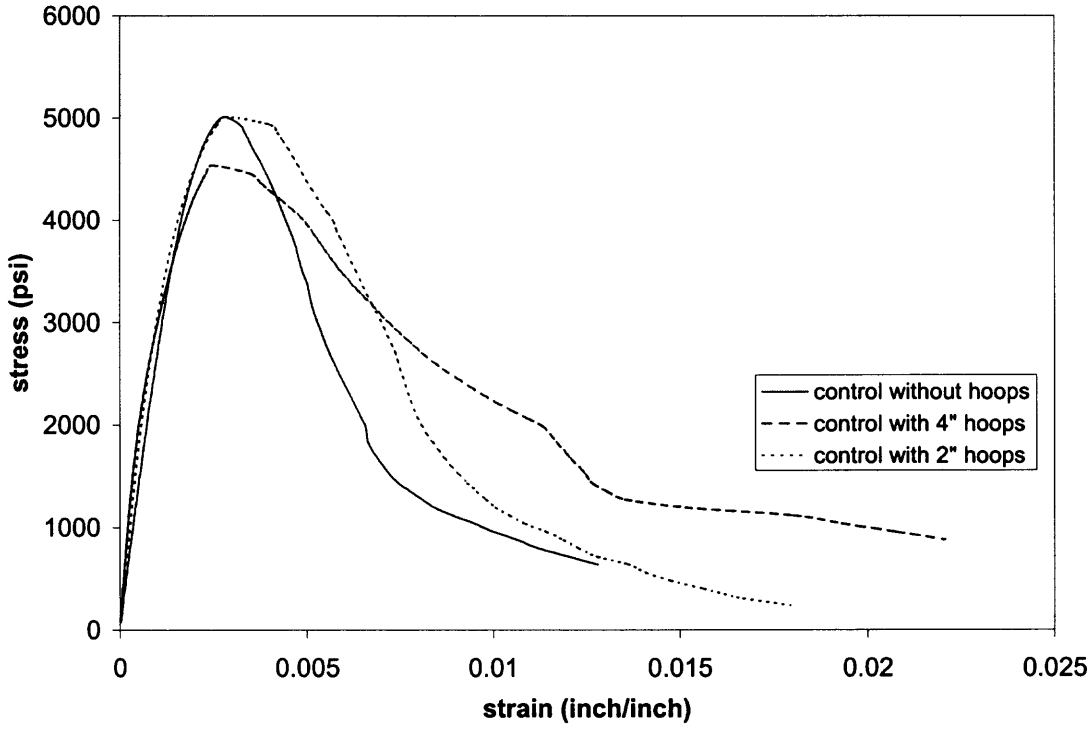

Figure C.31 Comparison of average stress-strain curves of 5000psi concrete confined only with steel hoops.

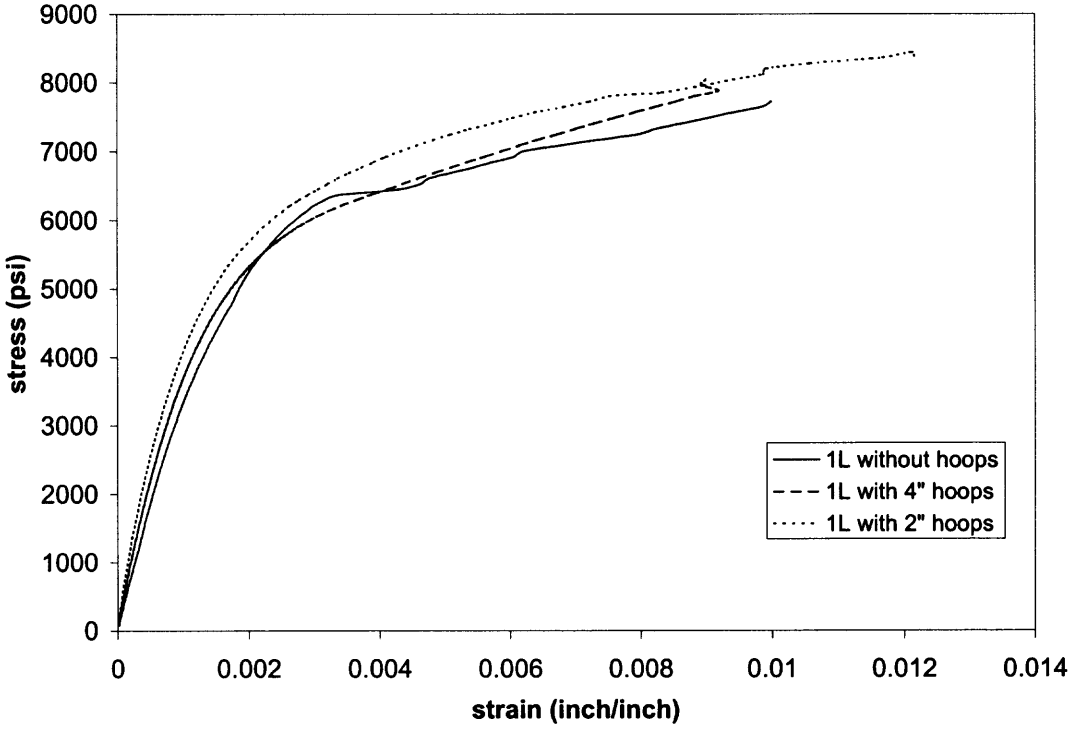

Figure C. 32 Comparison of average stress-strain curves of 5000psi concrete confined with 1 layer fabric and steel hoops.

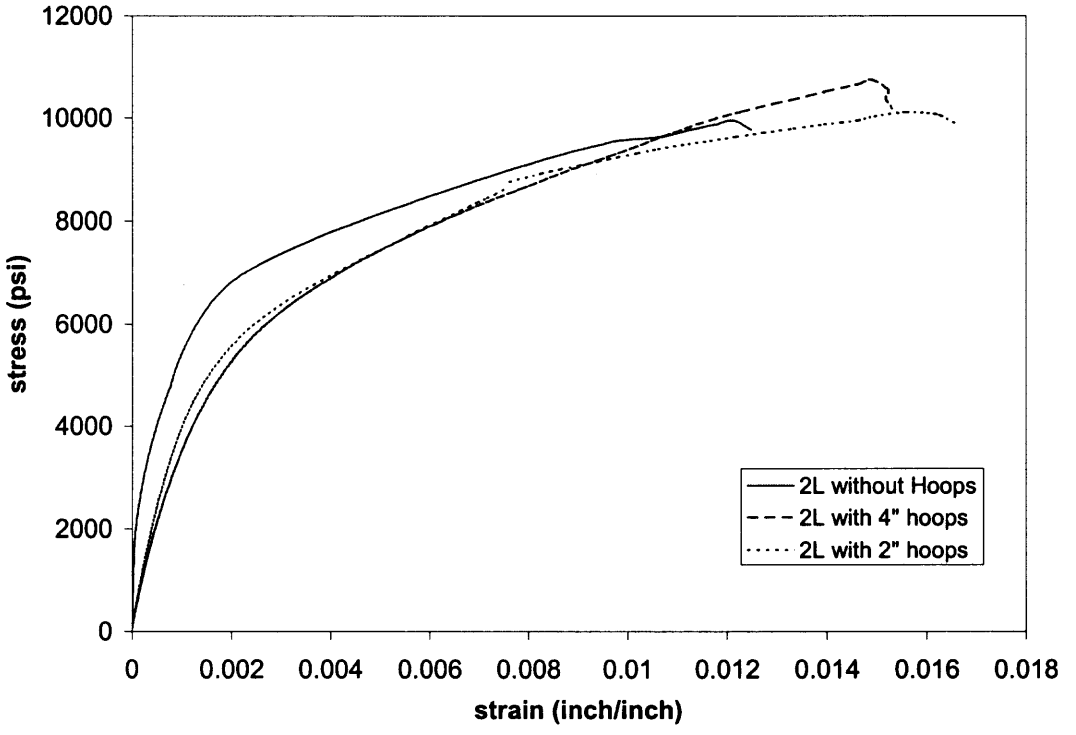

Figure C.33 Comparison of average stress-strain curves of 5000psi concrete confined with 2 layers fabric and steel hoops.

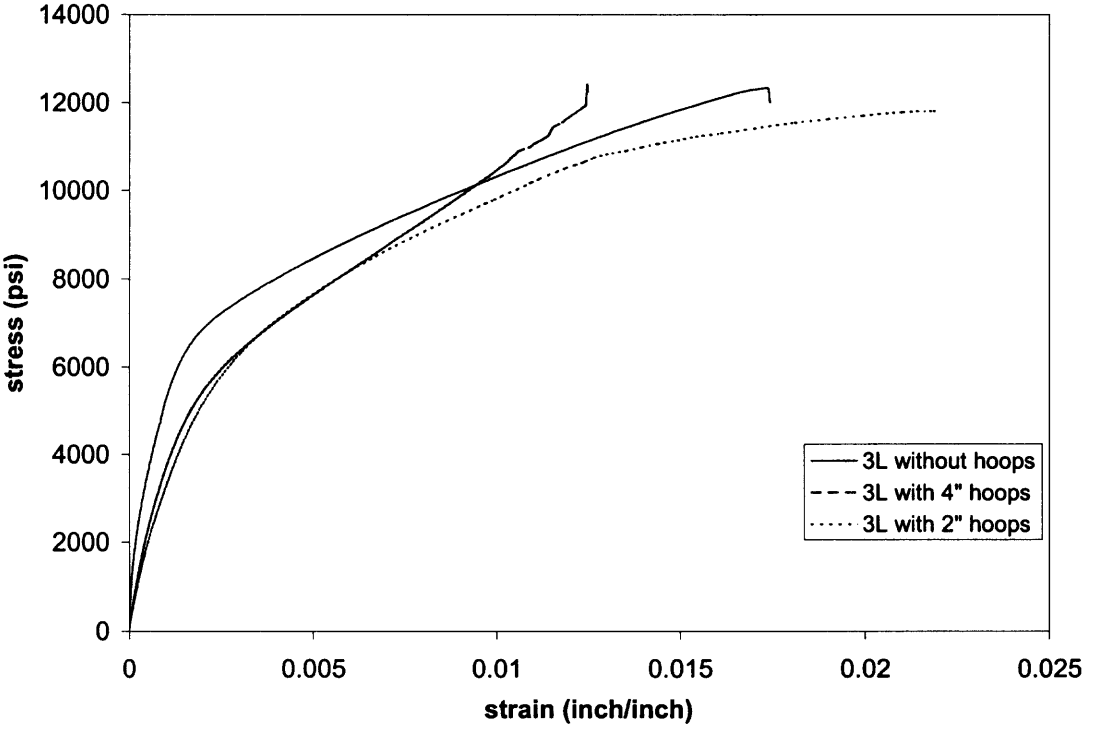

Figure C.34 Comparison of average stress-strain curve of 5000psi concrete confined with 3 layers fabric and steel hoops.

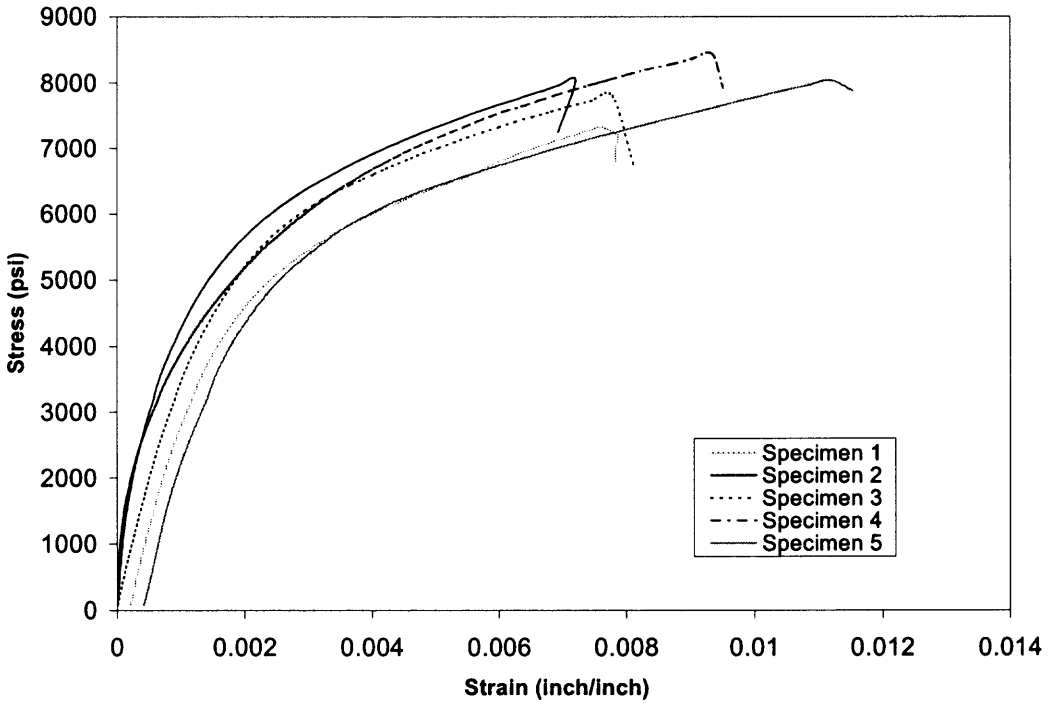

Figure C.35 Stress-strain curves of 5000psi concrete wrapped at two different directions.

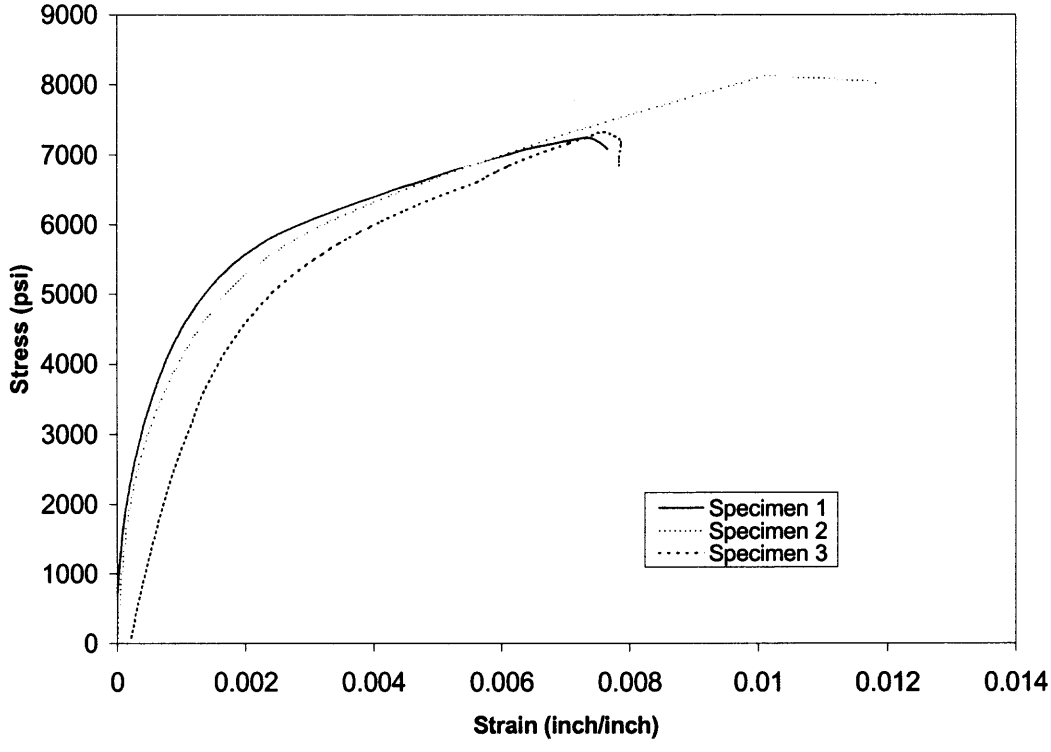

Figure C.36 Stress-strain curves of 5000psi concrete using 3/8 in. stones wrapped with one layer of fabric.

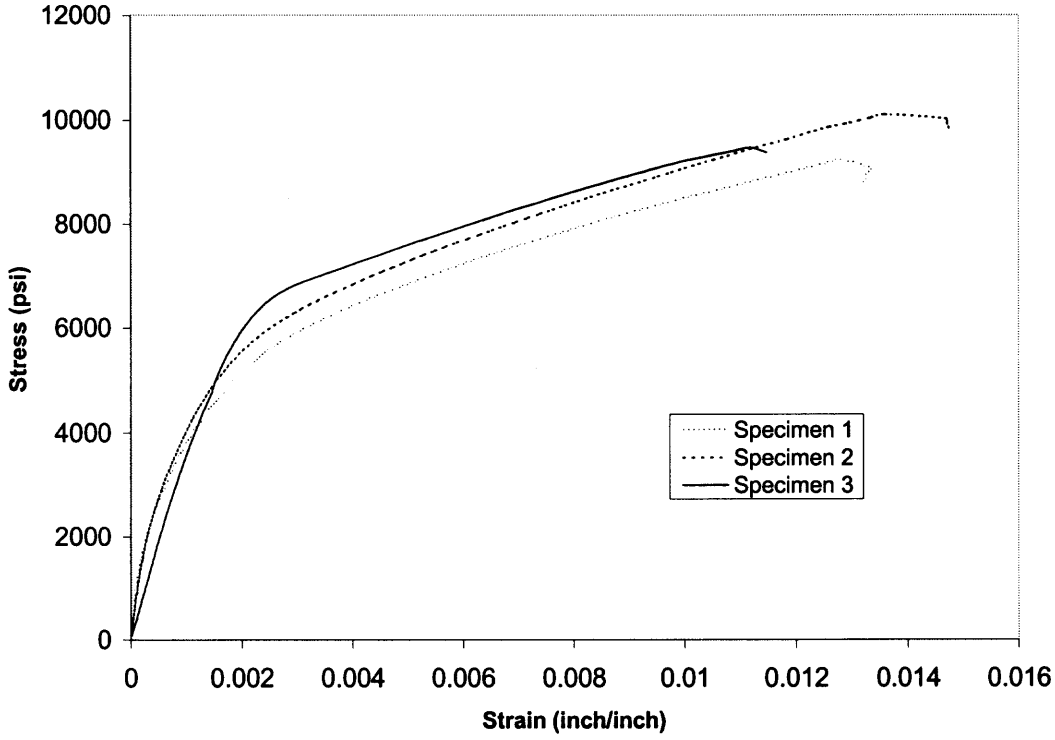

Figure C.37 Stress-strain curves of 5000psi concrete using 3/8 in. stones wrapped with two layers of fabric.

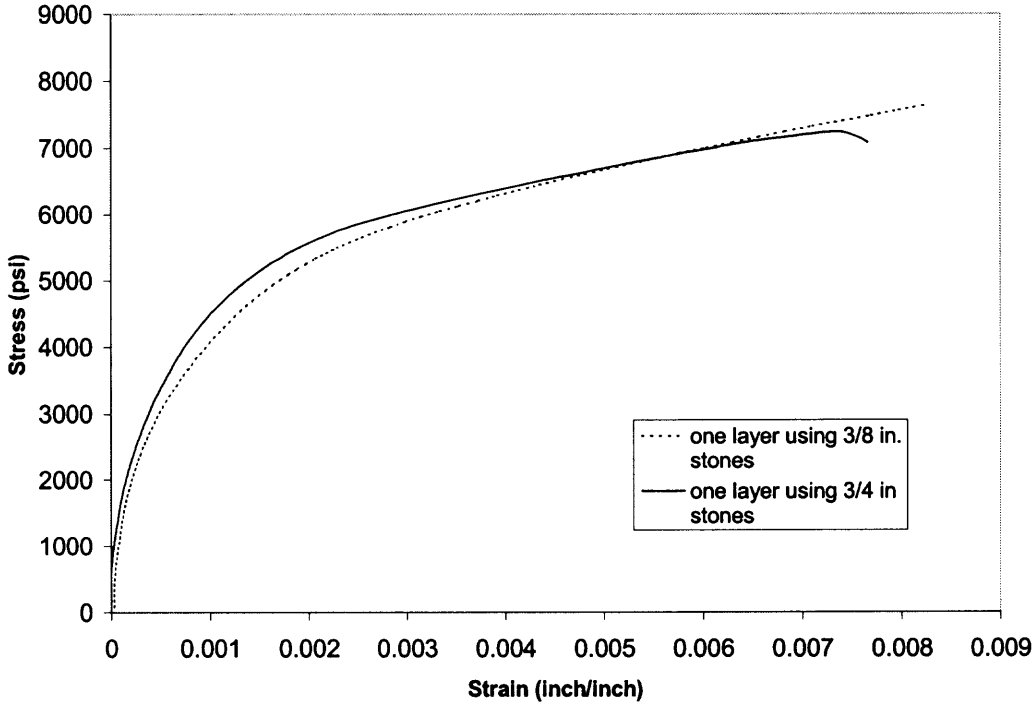

Figure C.38 comparison of average stress-strain curves of 5000psi fabric-confined concrete cylinders using different coarse aggregates.

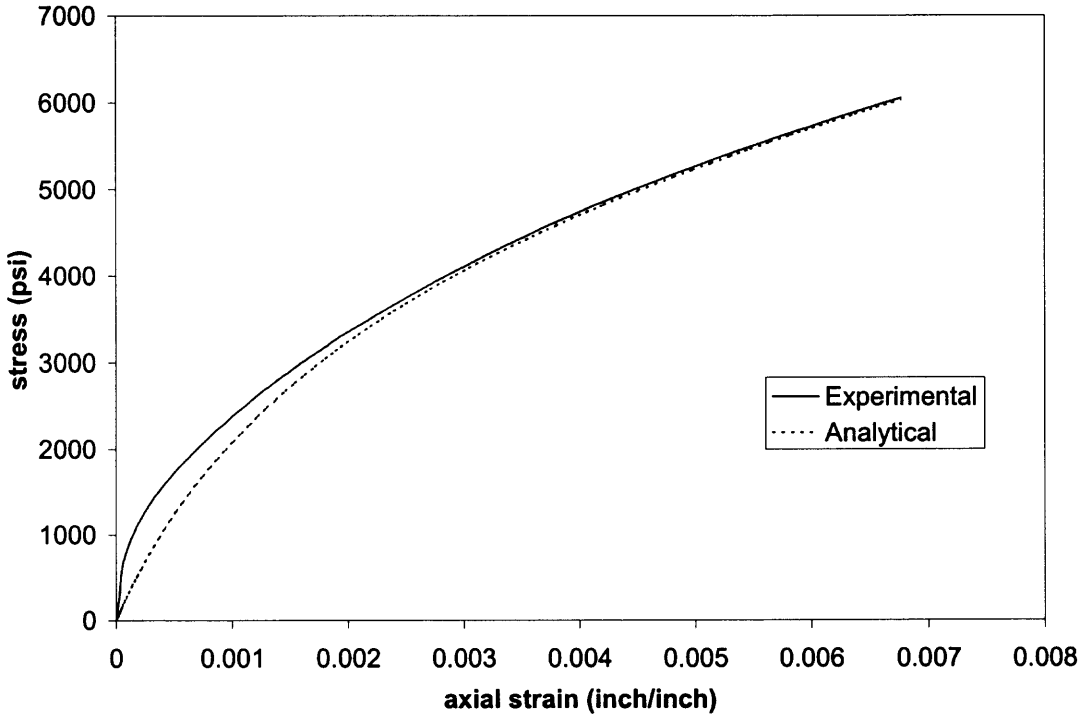

Figure C.39 Comparison of stress-strain curves of 3000psi concrete with 1 layer fabric.

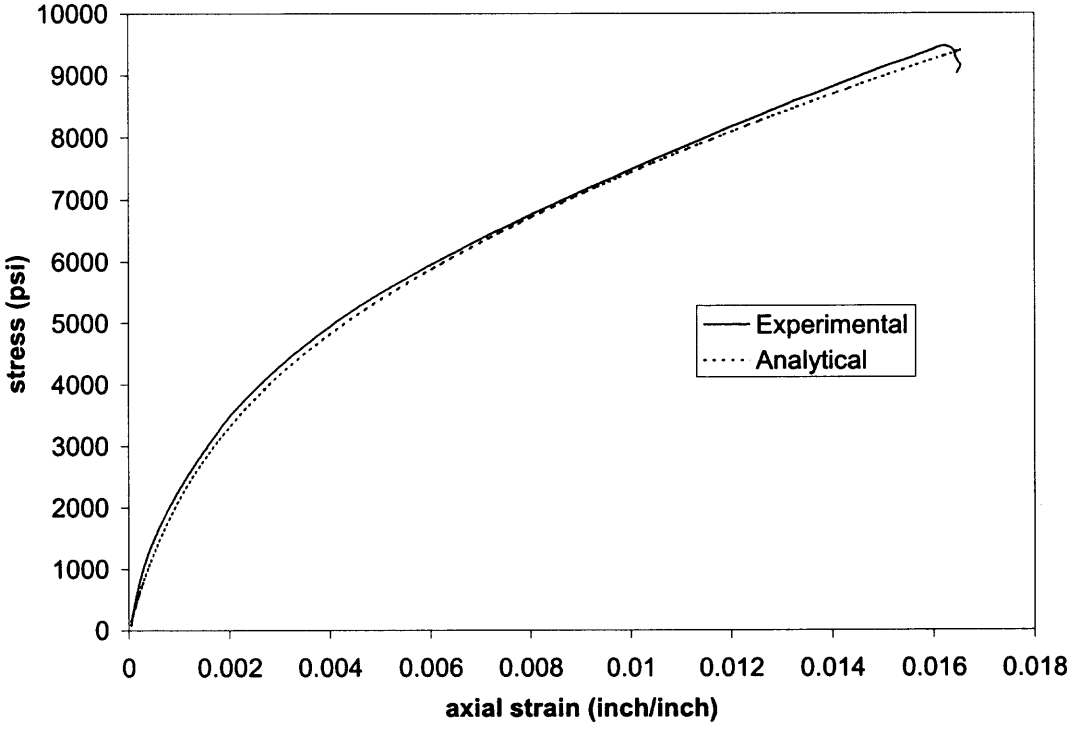

Figure C.40 Comparison of stress-strain curves of 3000psi concrete with 2 layers fabric.

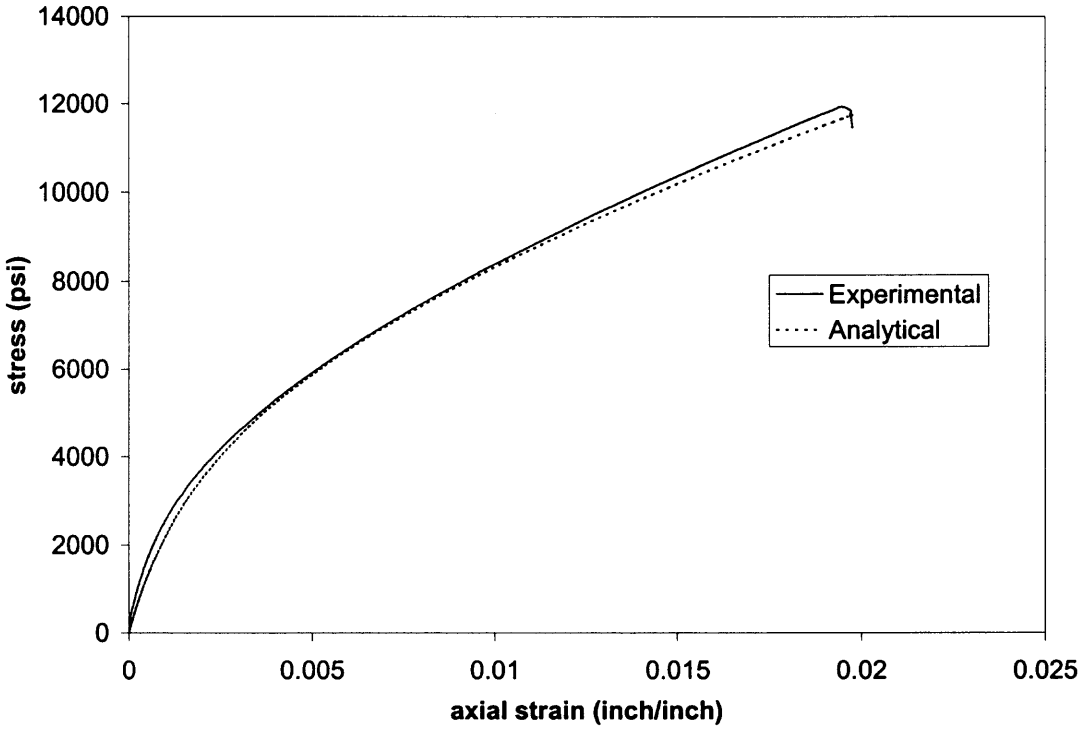

Figure C.41 Comparison of stress-strain curves of 3000psi concrete with 3 layers fabric.

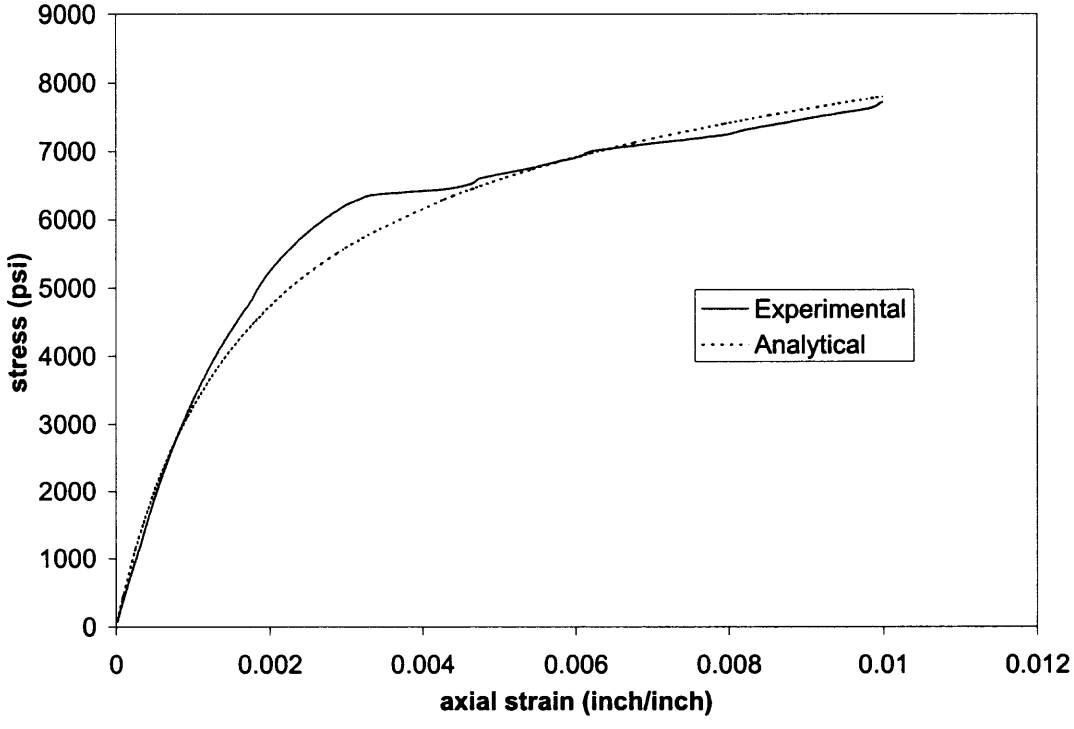

Figure C.42 Comparison of stress-strain curves of 5000psi concrete with 1 layer fabric.

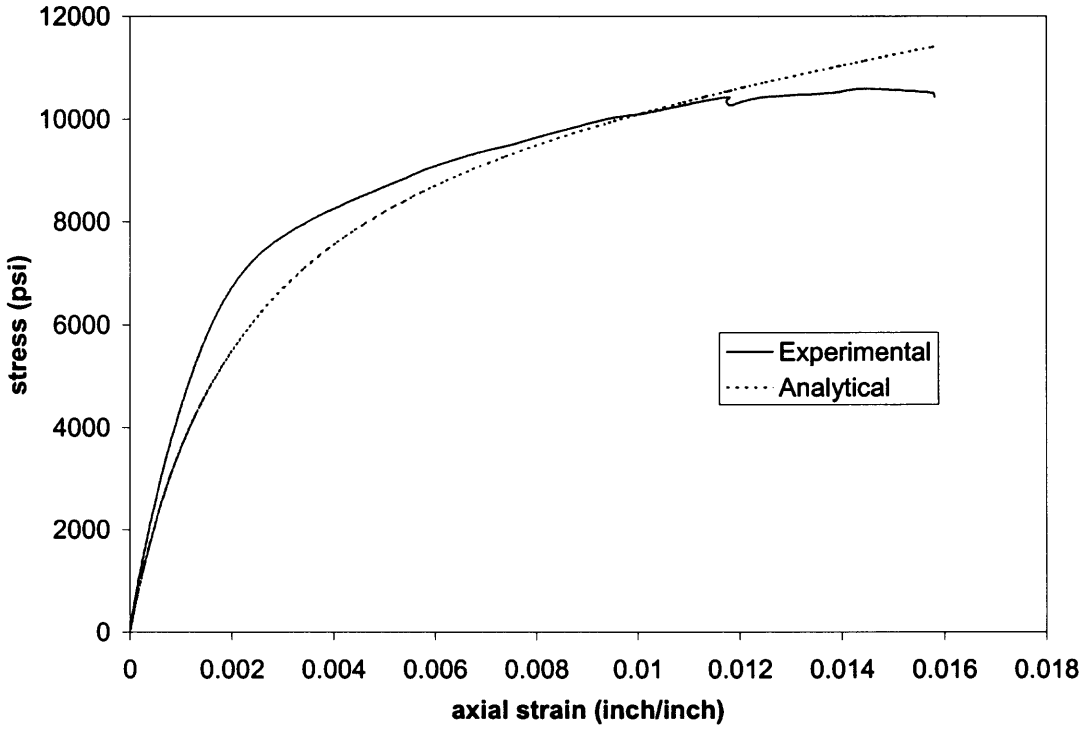

Figure C.43 Comparison of stress-strain curves of 5000psi concrete with 2 layers fabric.

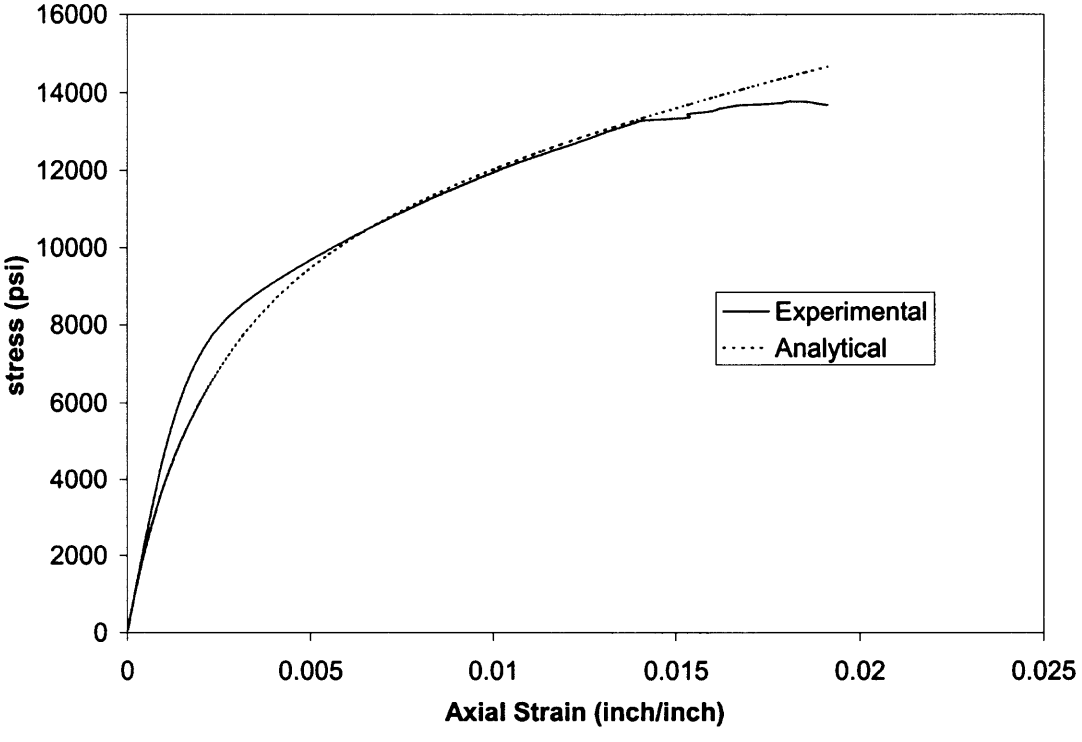

Figure C.44 Comparison of stress-strain curves of 5000psi concrete with 3 layers fabric.

APPENDIX D

LOAD-DEFLECTION CURVES AND MOMENT-CURVATURE CURVES OF CFRP STRENGTHENED RC BEAMS

In appendix D, Figures D.1-D.5 present the experimental load-deflection curves of RC beam specimens wrapped with different layers of CFRP fabrics. Figures D.6-D.10 present the experimental moment-curvature curves of RC beam specimens wrapped by CFRP fabrics. Figures D.11-D.15 compare the experimental results to the ANSYS results.

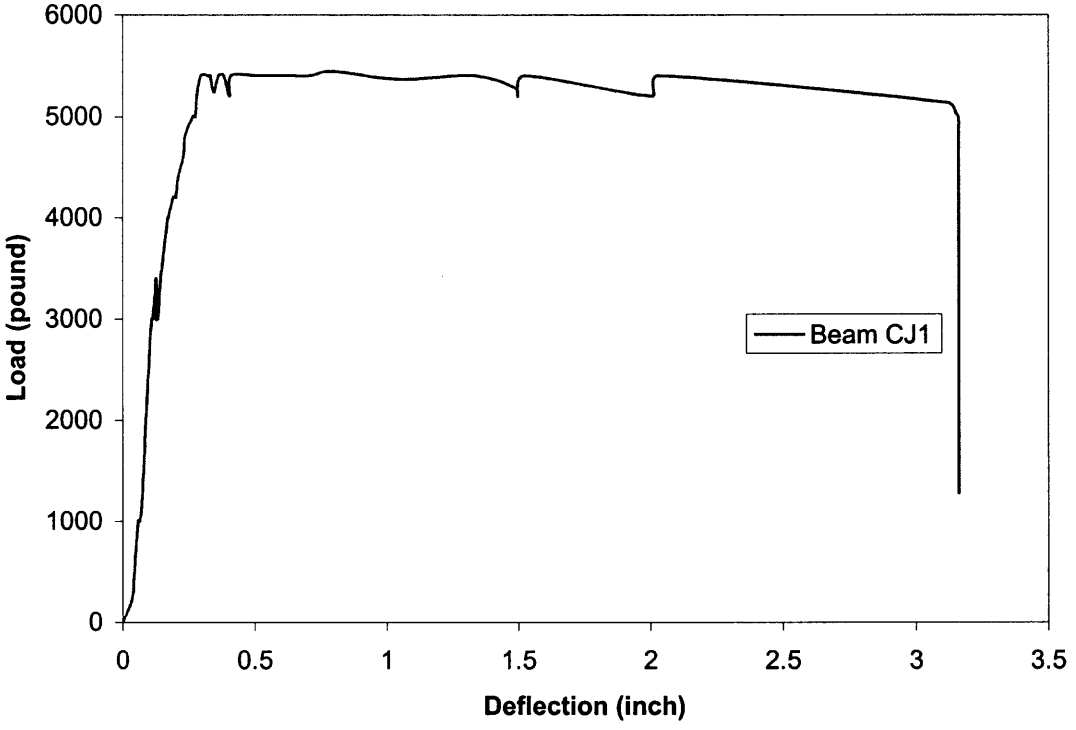

Figure D.1 Load-deflection curve of beam CJ1.

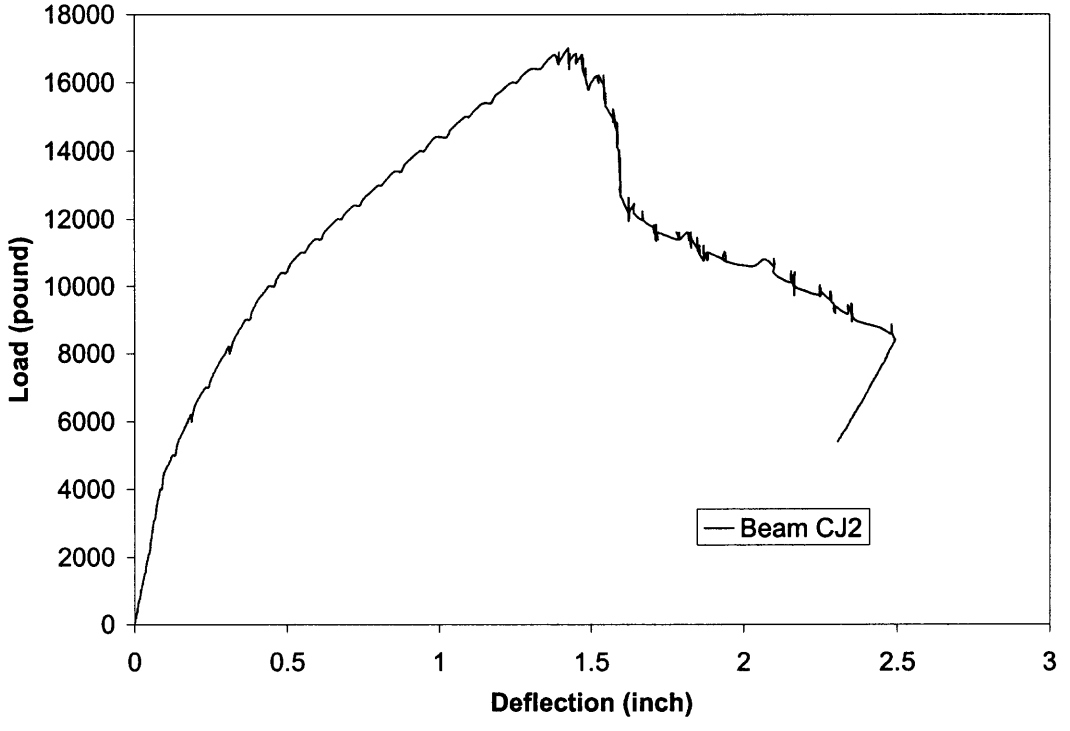

Figure D.2 Load-deflection curve of beam CJ2.

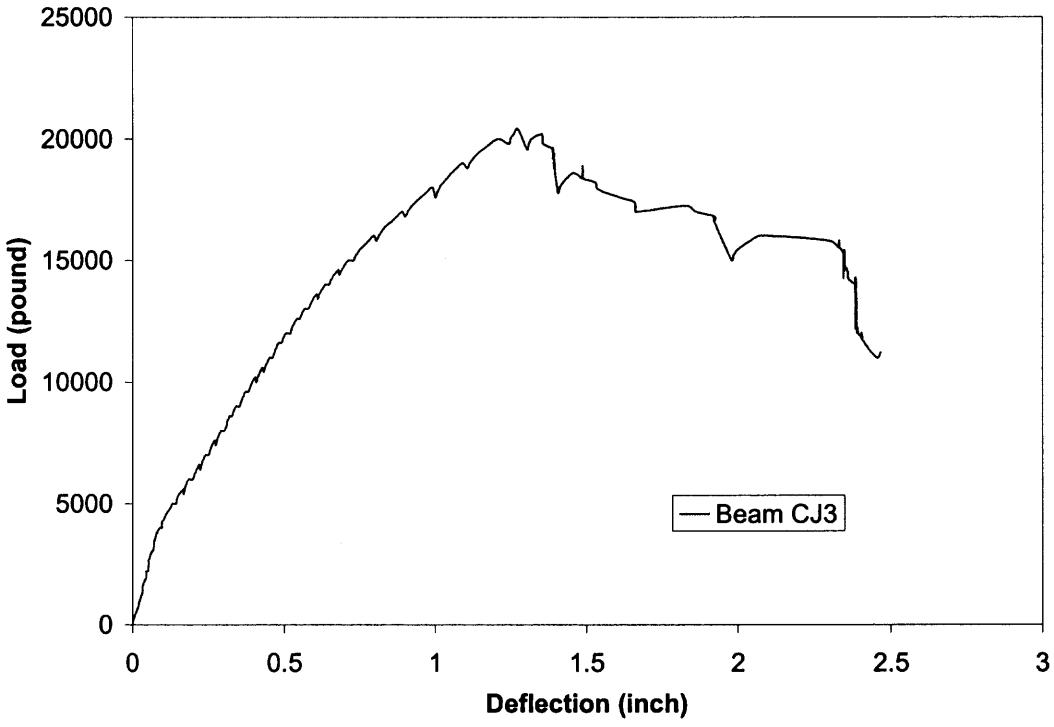

Figure D.3 Load-deflection curve of beam CJ3.

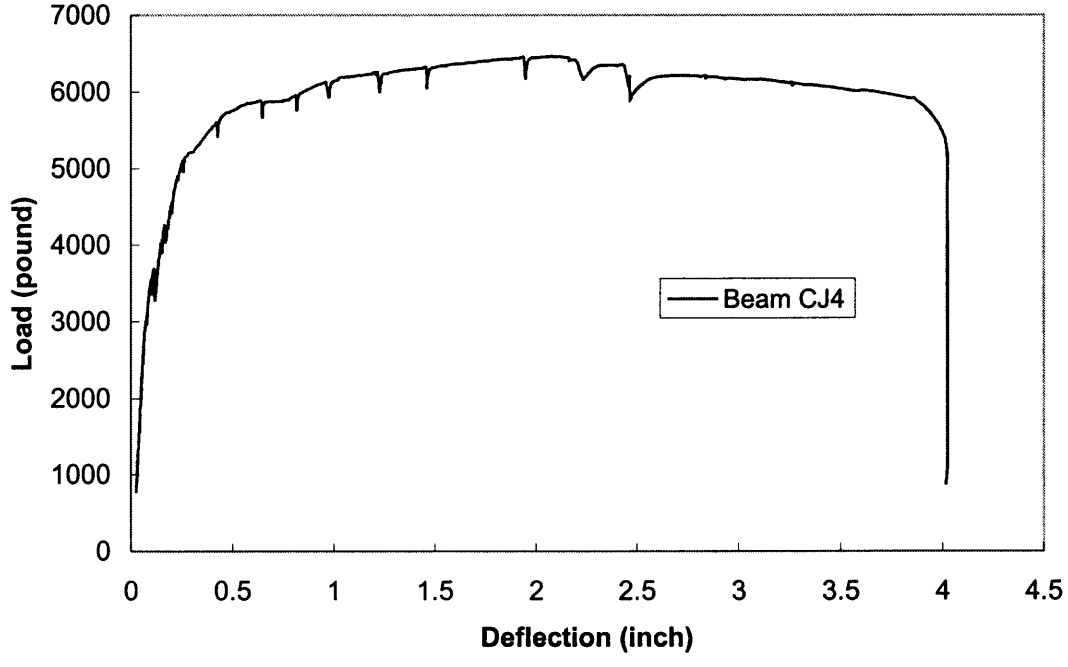

Figure D.4 Load-deflection curve of beam CJ4.

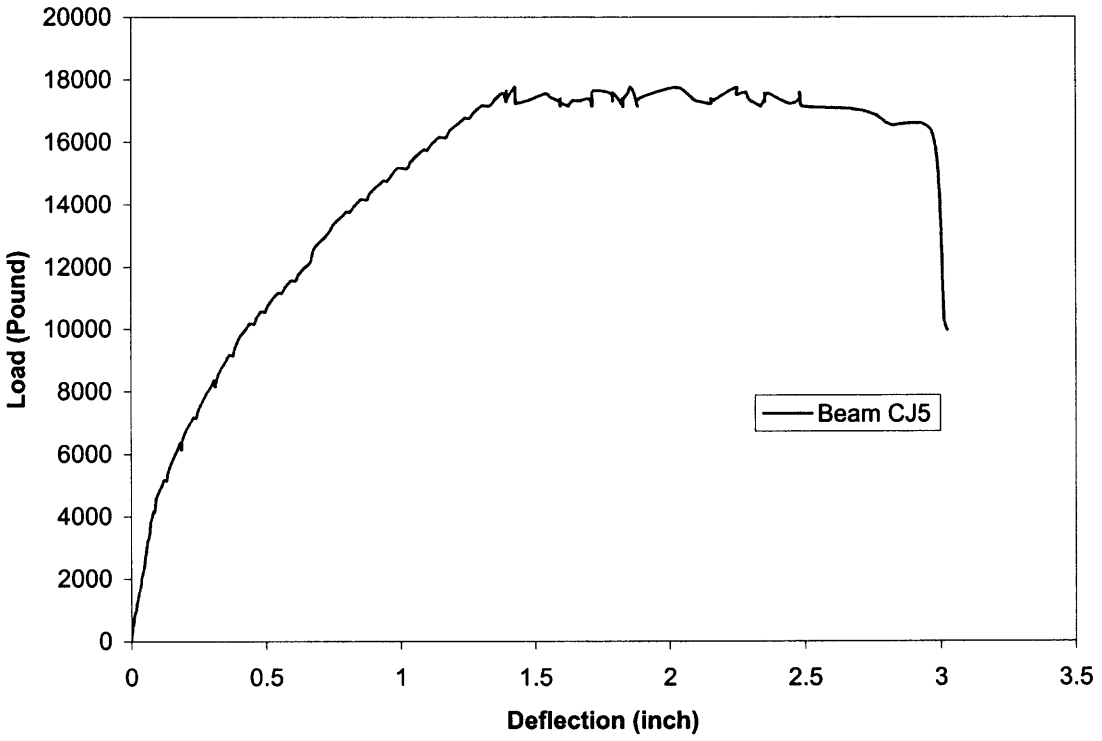

Figure D.5 Load-deflection curve of beam CJ5.

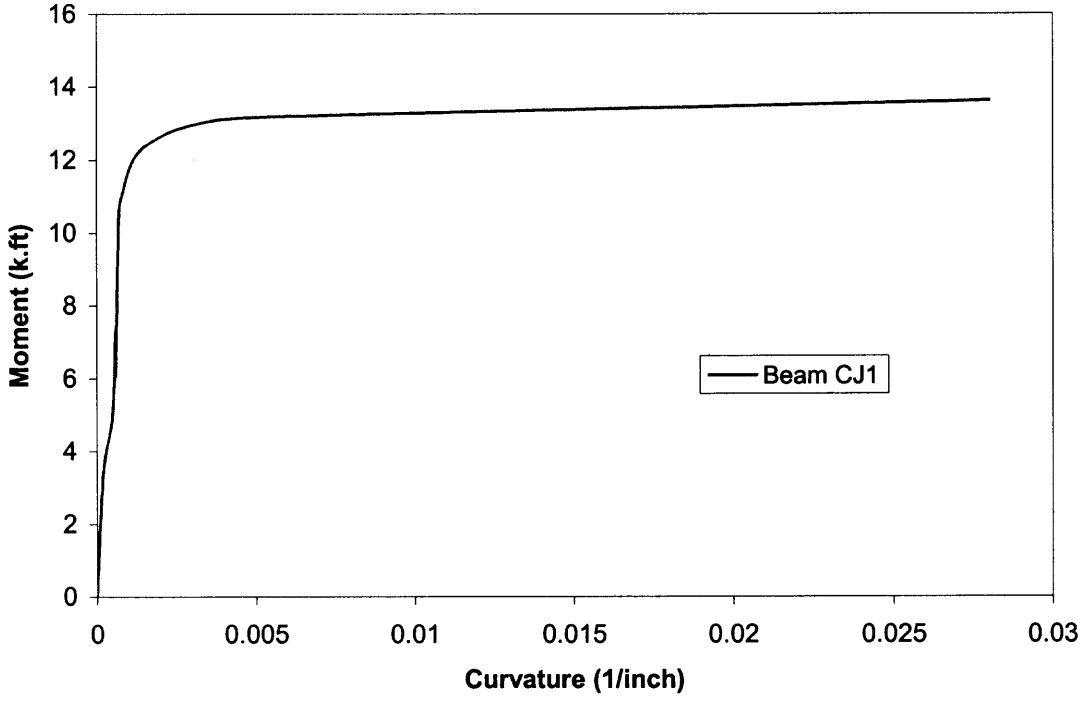

Figure D.6 Moment-curvature curve of beam CJ1.

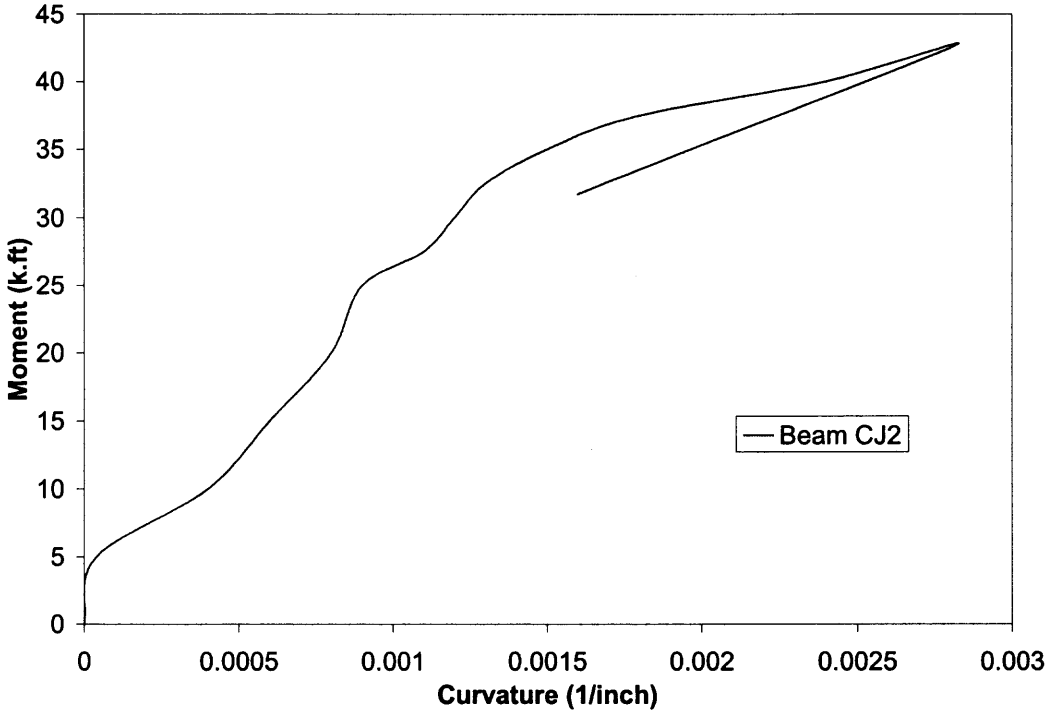

Figure D.7 Moment-curvature curve of beam CJ2.

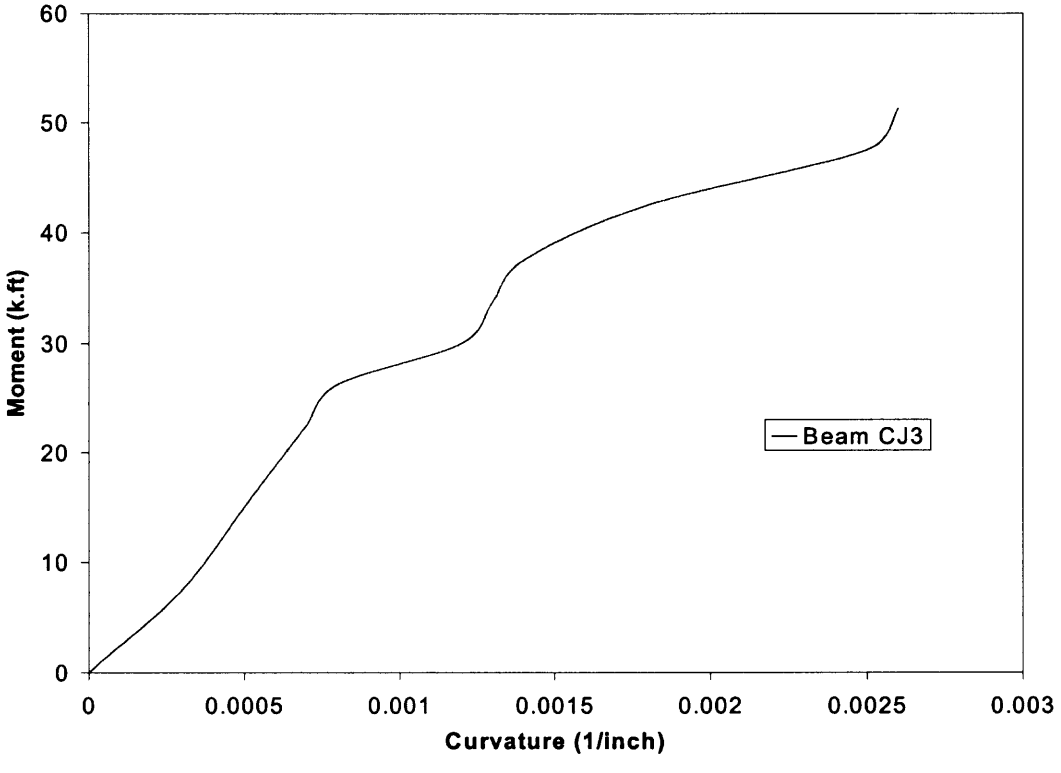

Figure D.8 Moment-curvature curve of beam CJ3.

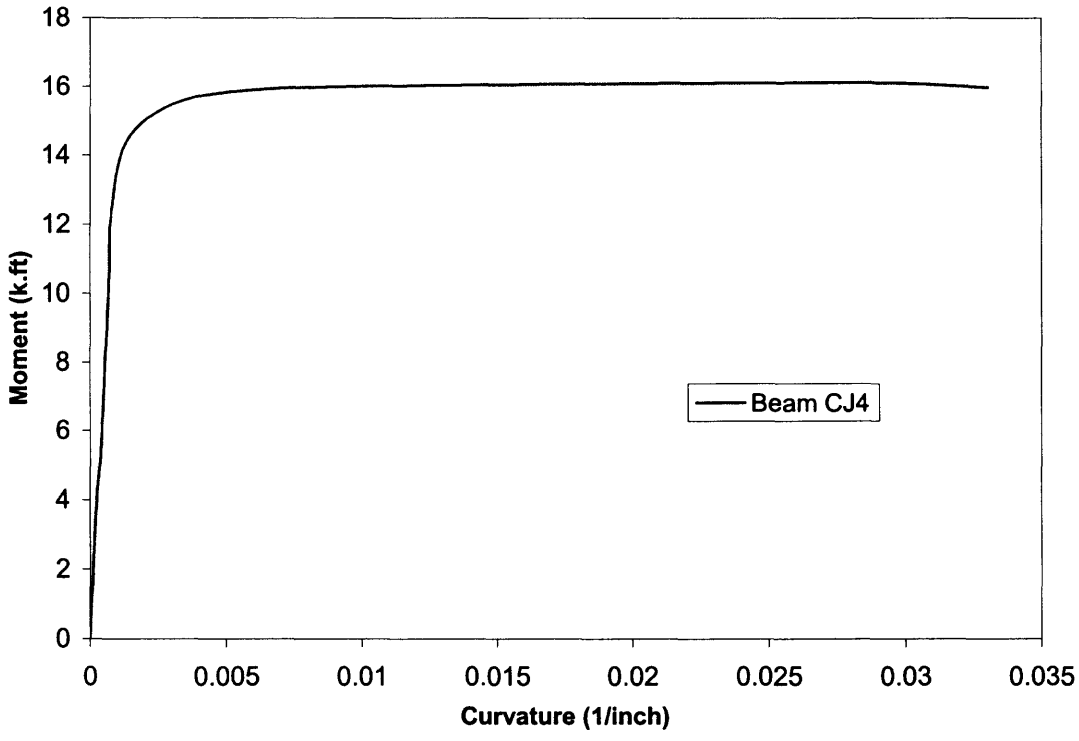

Figure D.9 Moment-curvature curve of beam CJ4.

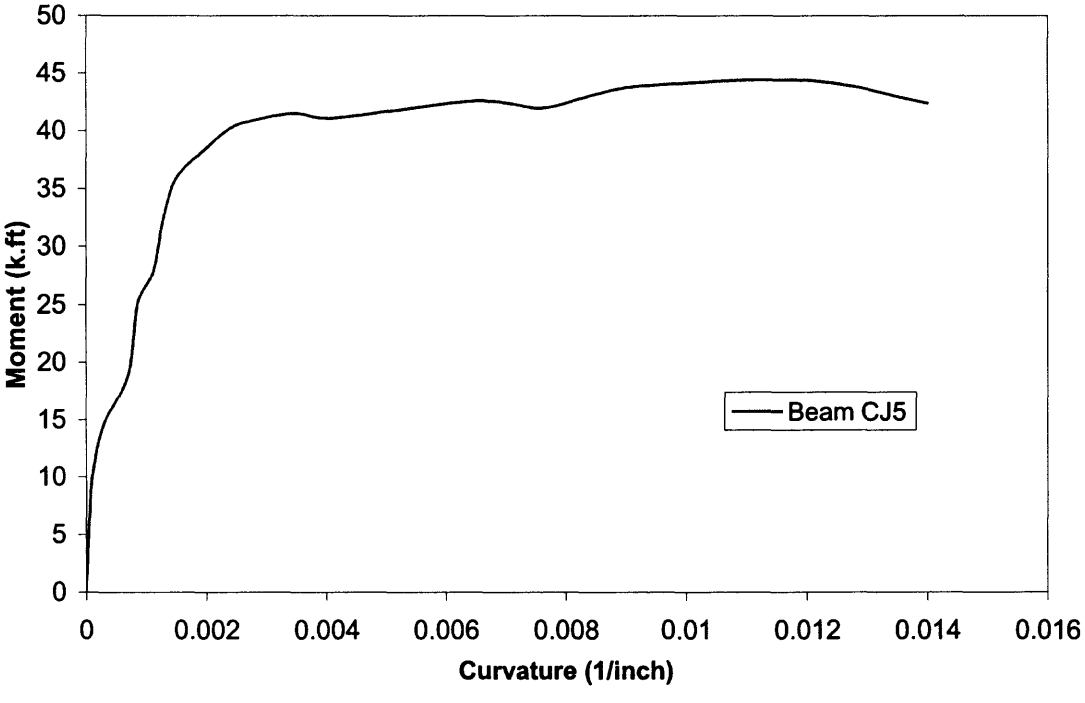

Figure D.10 Moment-curvature curve of beam CJ5.

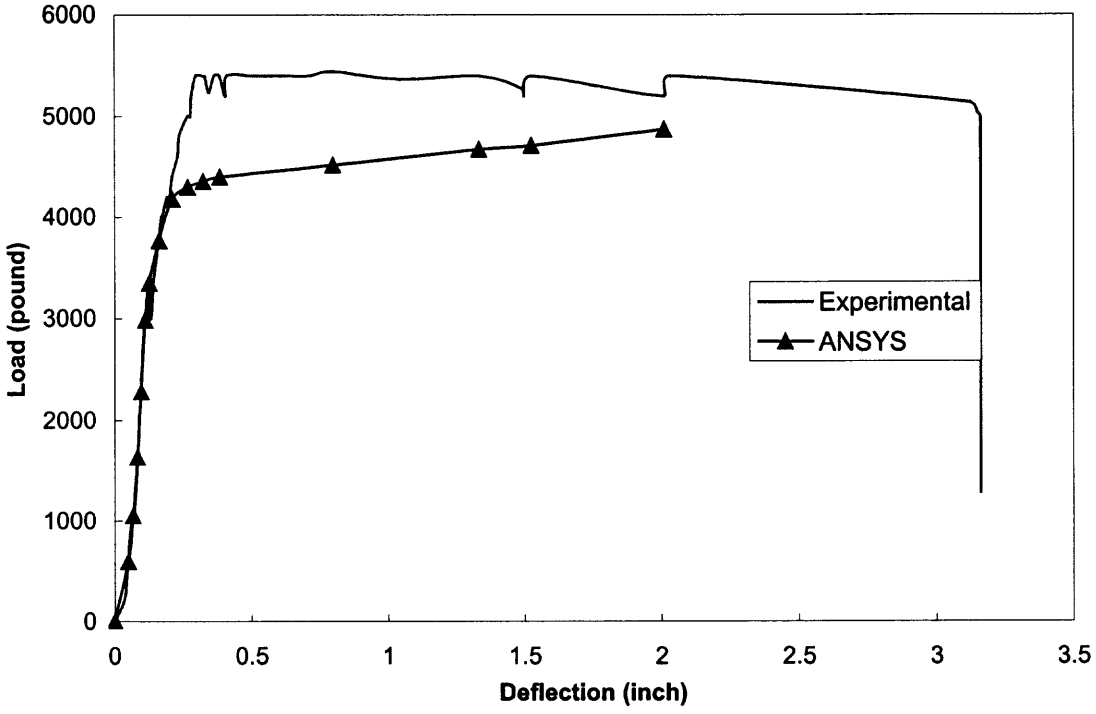

Figure D.11 Comparison of load-deflection curves for beam CJ1.

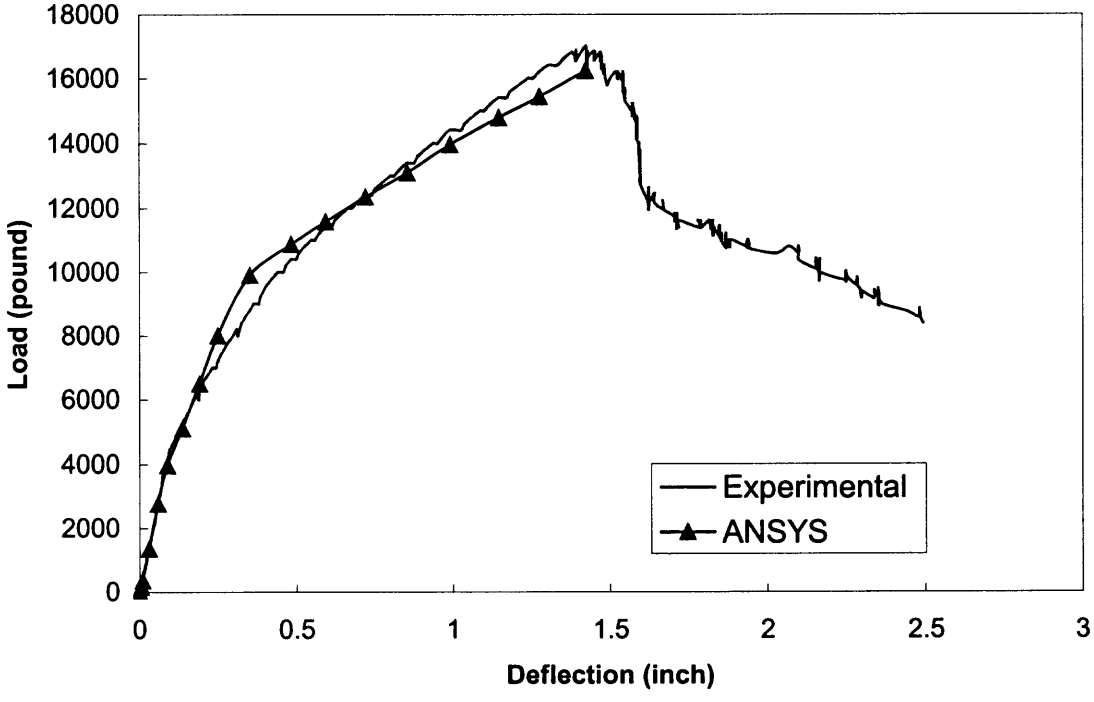

Figure D.12 Comparison of load-deflection curves for beam CJ2.

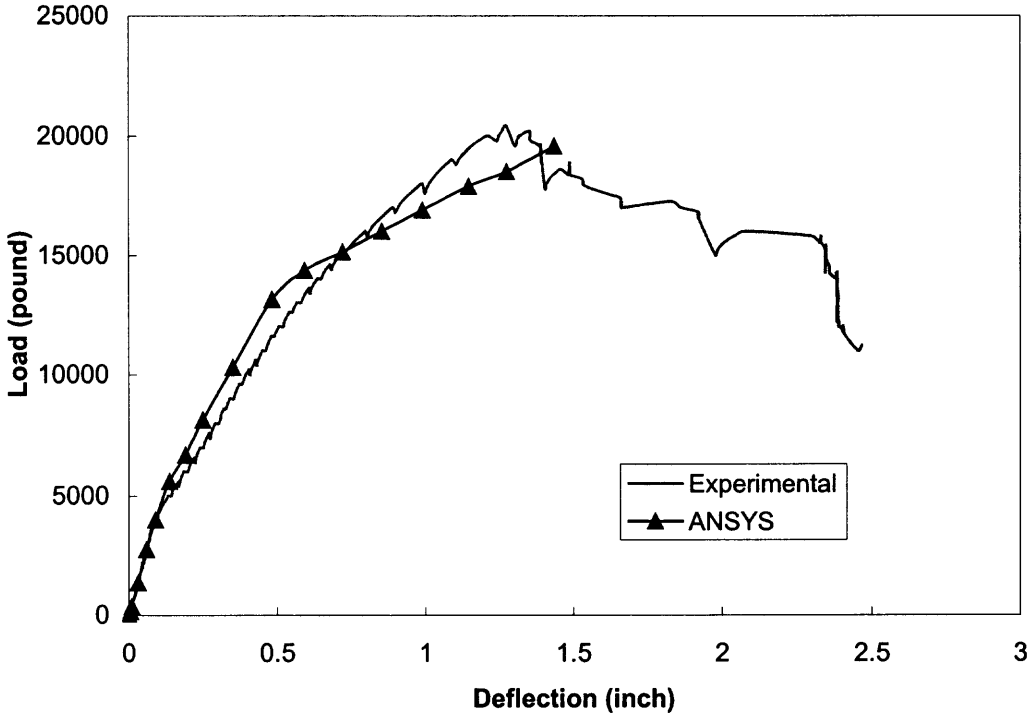

Figure D.13 Comparison of load-deflection curves for beam CJ3.

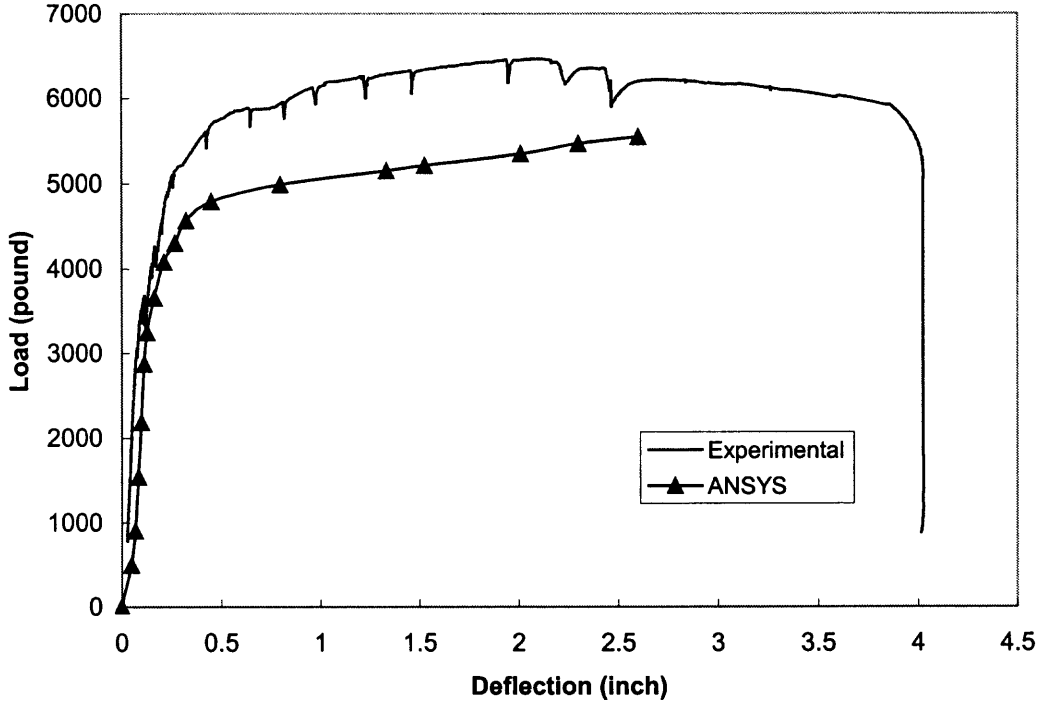

Figure D.14 Comparison of load-deflection curves for beam CJ4.

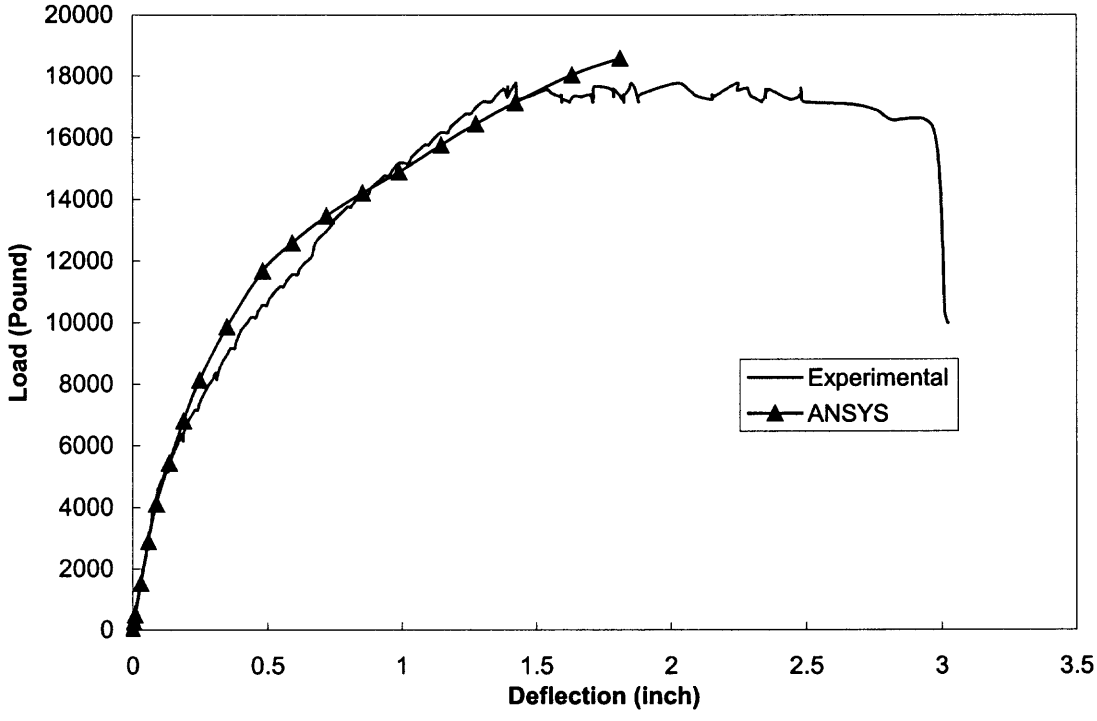

Figure D.15 Comparison of load-deflection curves for beam CJ5.

APPENDIX E

STRAIN-POSITION CURVES FOR FABRIC-WRAPPED RC SLENDER COLUMNS

In appendix E, Figures E.1-E10 present the experimental strain-position curves for concrete column specimens wrapped with different layers of CFRP fabrics.

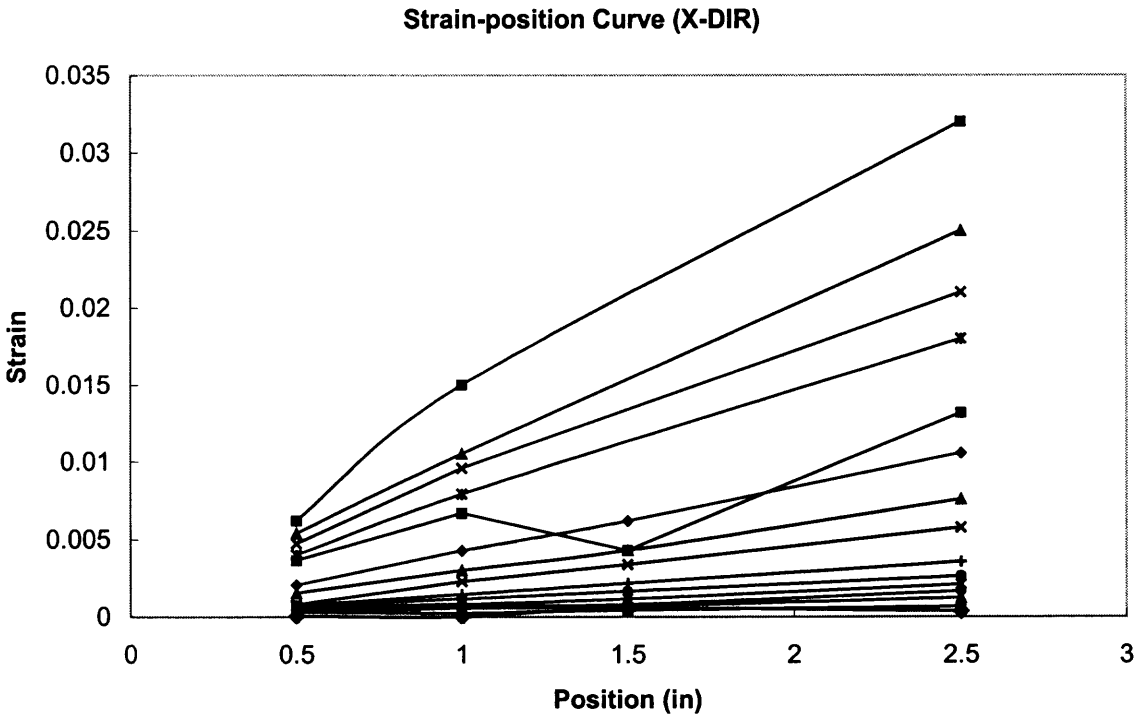

Figure E.1 Strain-position curve for control column CJC2 in X direction.

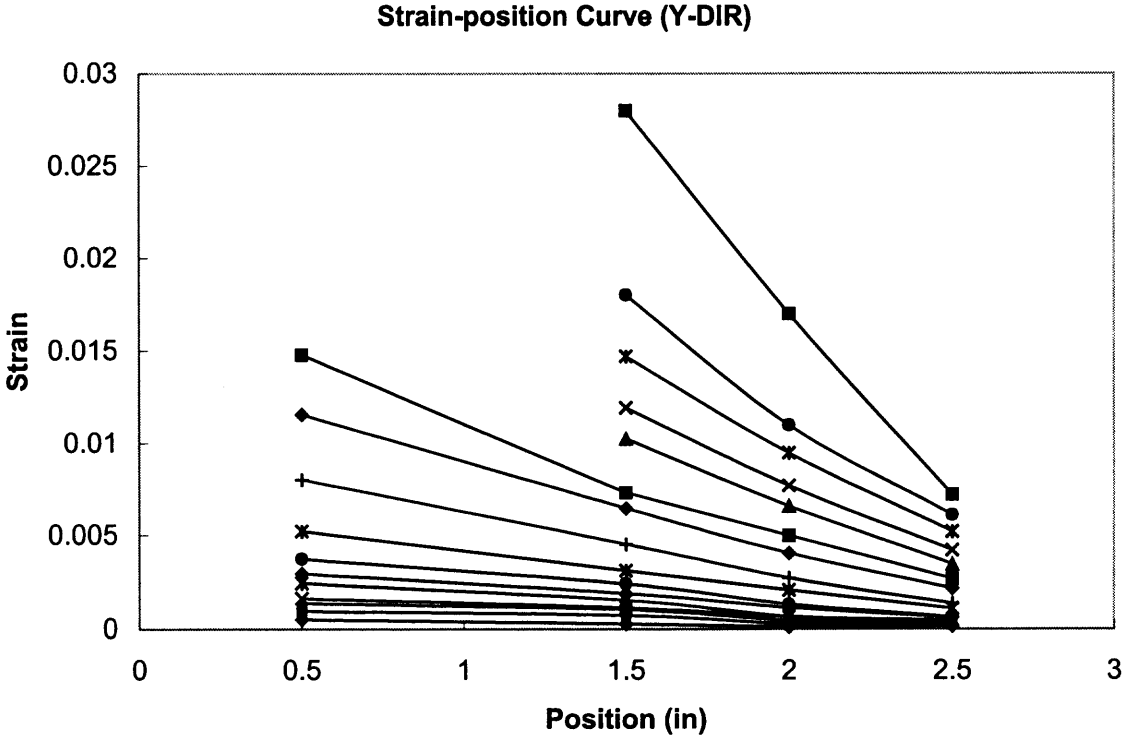

Figure E.2 Strain-position curve for control column CJC2 in Y direction.

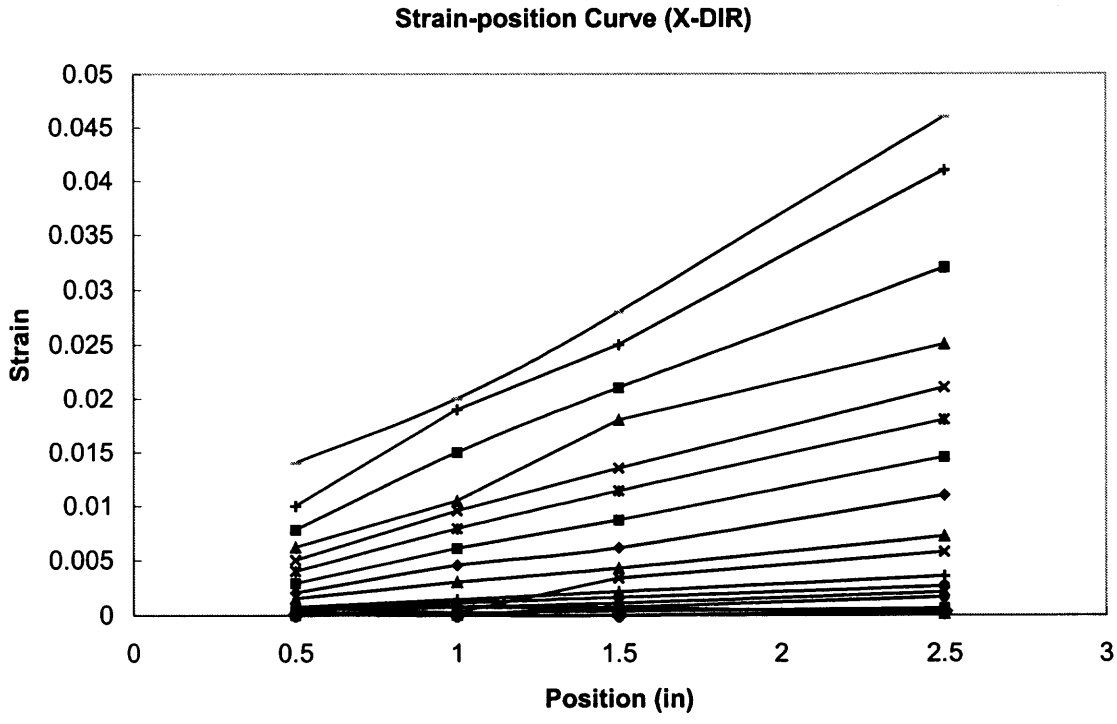

Figure E.3 Strain-position curve for column CJC3 in X direction.

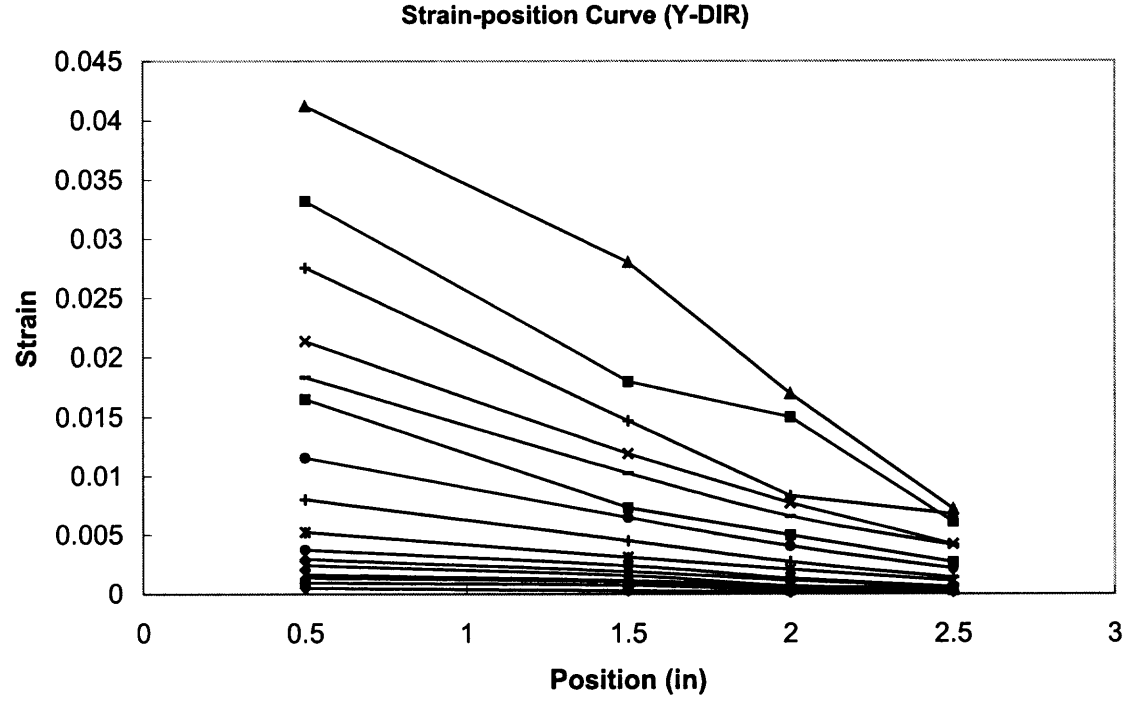

Figure E.4 Strain-position curve for column CJC3 in Y direction.

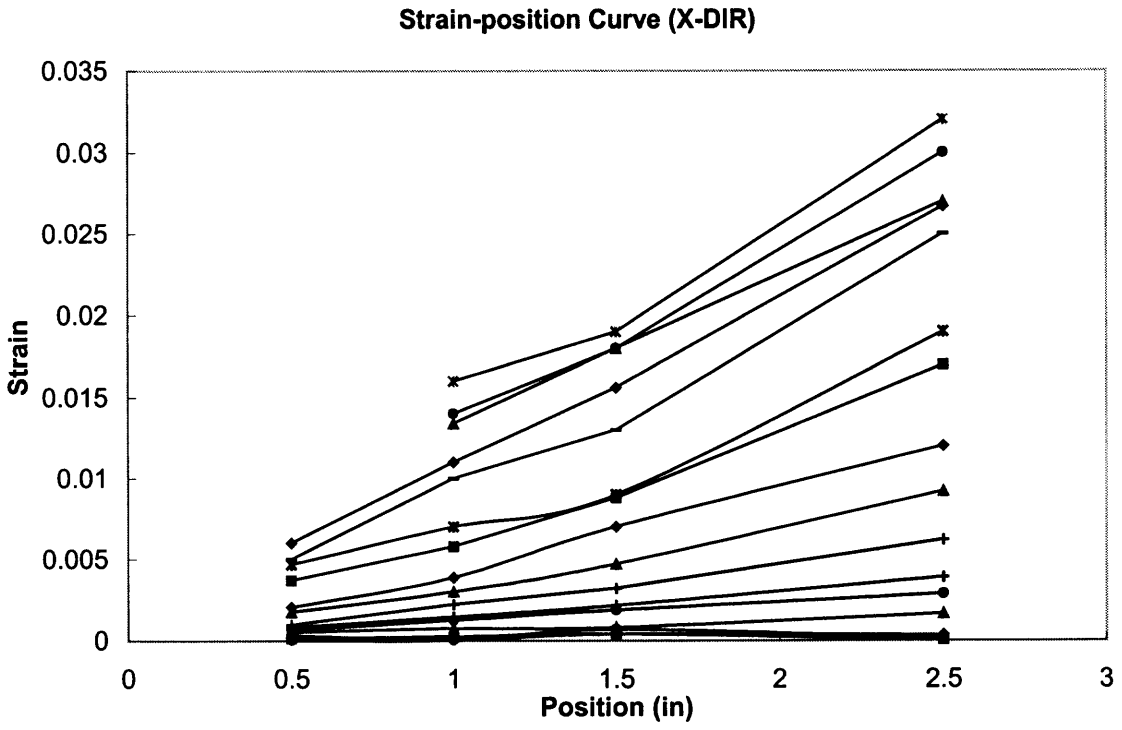

Figure E.5 Strain-position curve for column CJC5 in X direction.

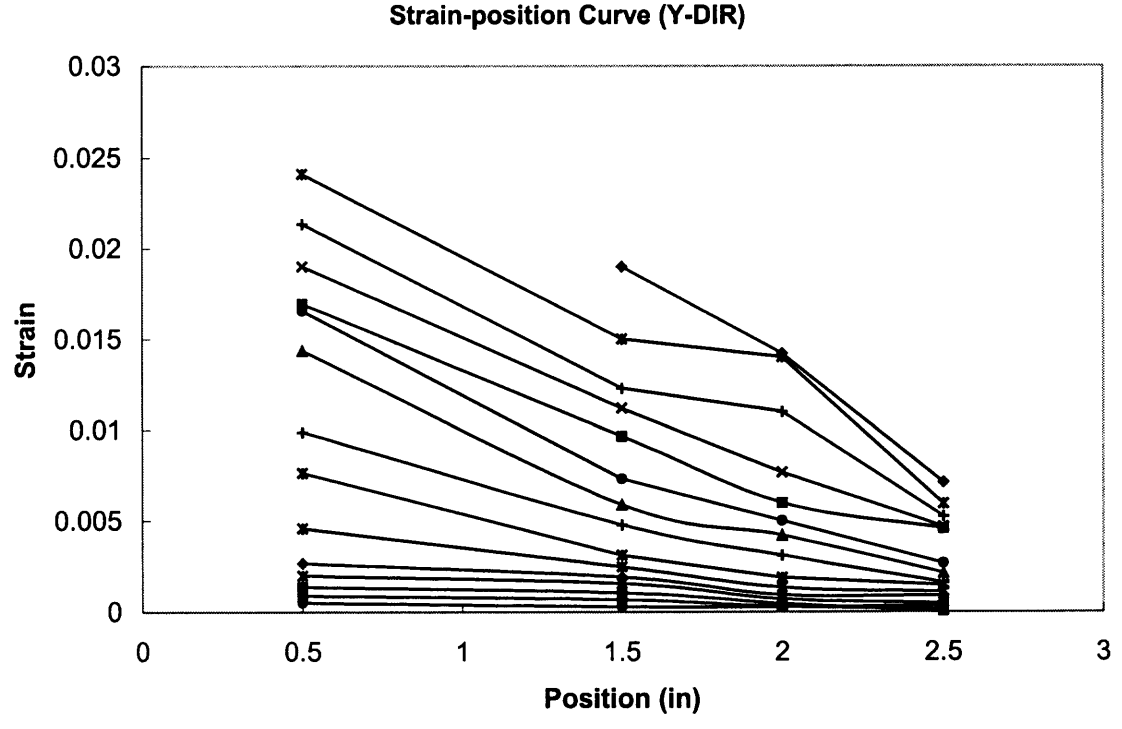

Figure E.6 Strain-position curve for column CJC5 in Y direction.

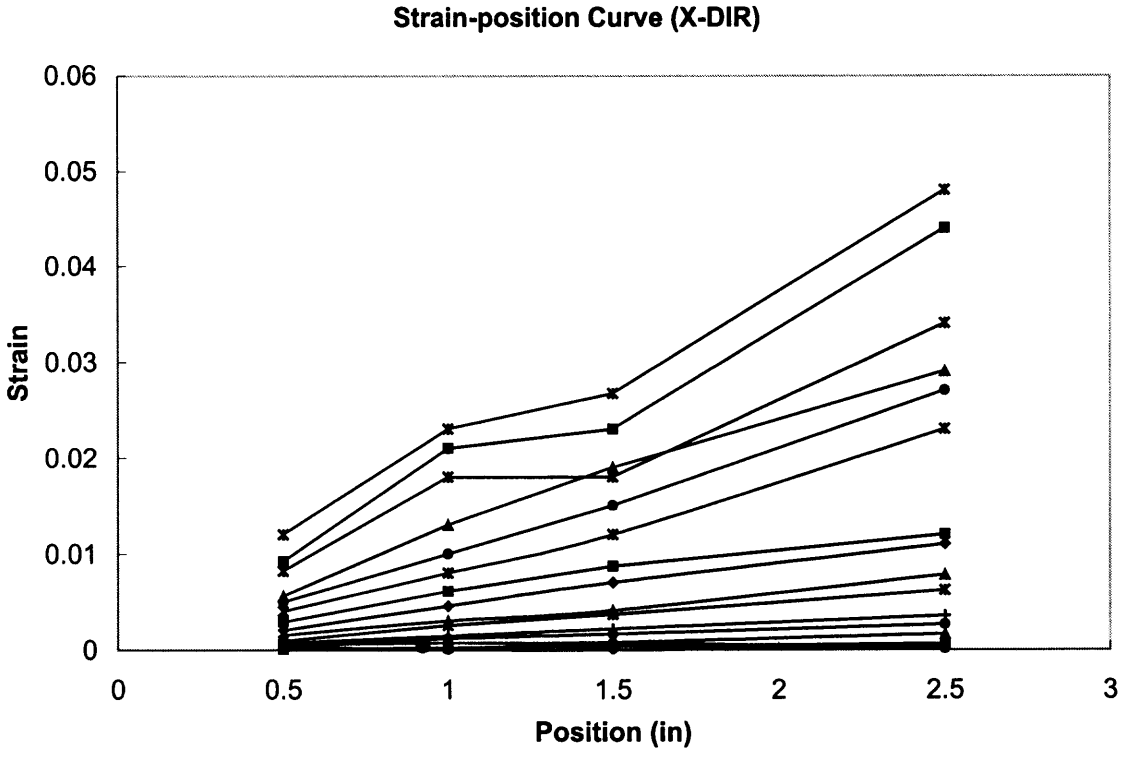

Figure E.7 Strain-position curve for column CJC6 in X direction.

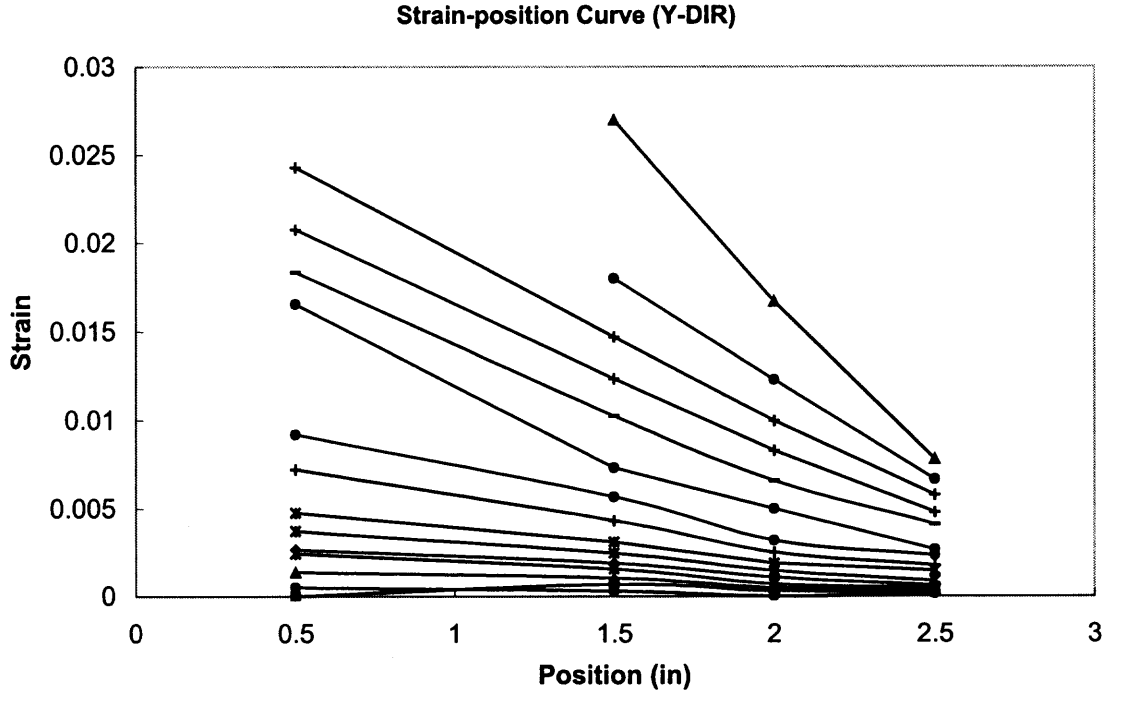

Figure E.8 Strain-position curve for column CJC6 in Y direction.

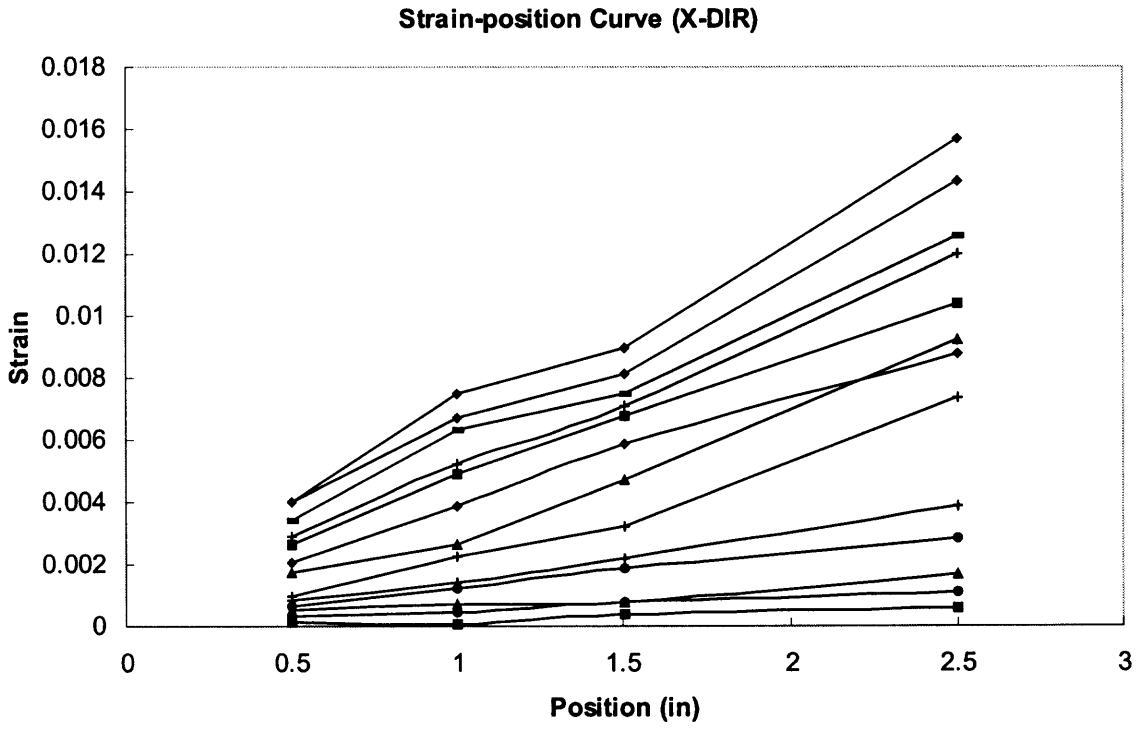

Figure E.9 Strain-position curve for column CJC7 in X direction.

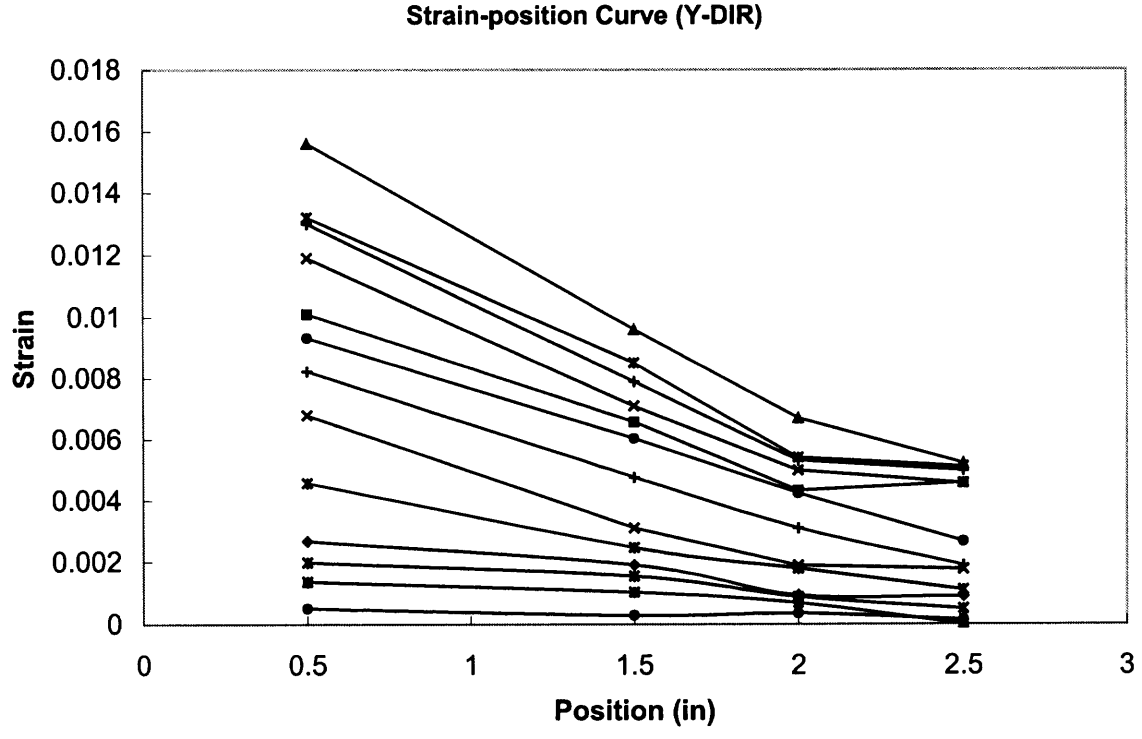

Figure E.10 Strain-position curve for column CJC7 in Y direction.

APPENDIX F

LOAD-DEFLECTION CURVES AND MOMENT –CURVATURE CURVES FOR FABRIC-CONFIEND RC SLENDER COLUMNS

In appendix F, Figures F.1-F.10 present the experimental load-deflection curves of concrete column specimens wrapped with different layers of CFRP fabrics. Figures F.11-F.20 present the experimental moment-curvature curves of column specimens wrapped with CFRP fabrics. Figures F.21-F.40 compare the experimental results to the results computed from the proposed modified computer program.

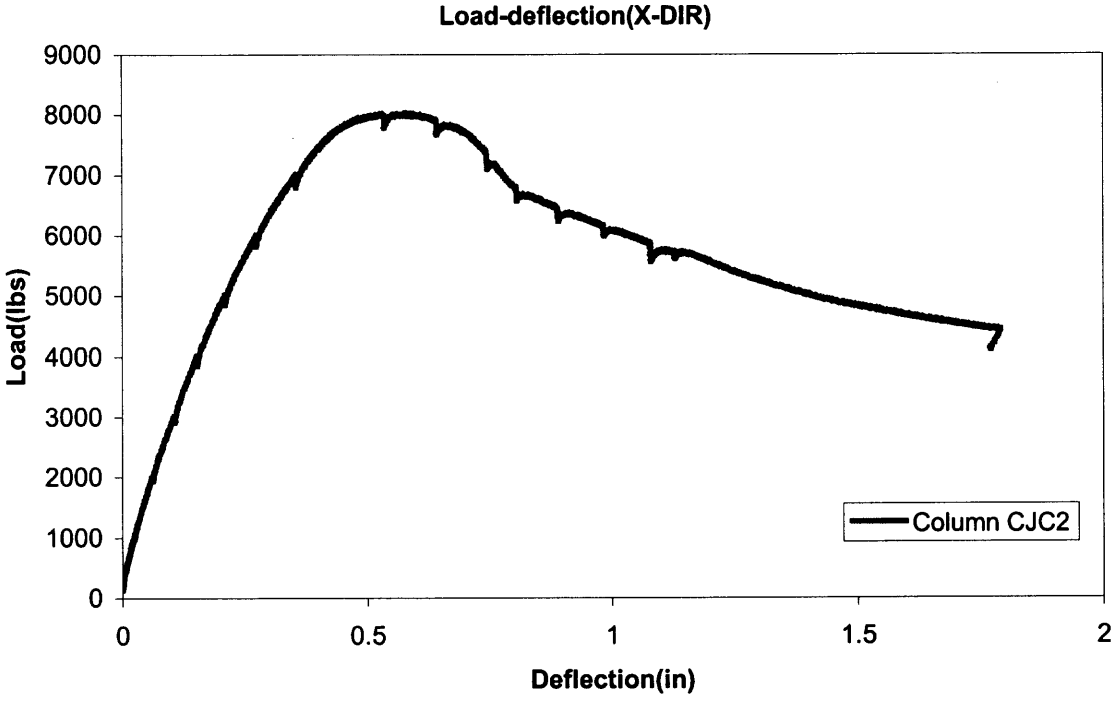

Figure F.1 Experimental load-deflection curve for column CJC2 in X direction.

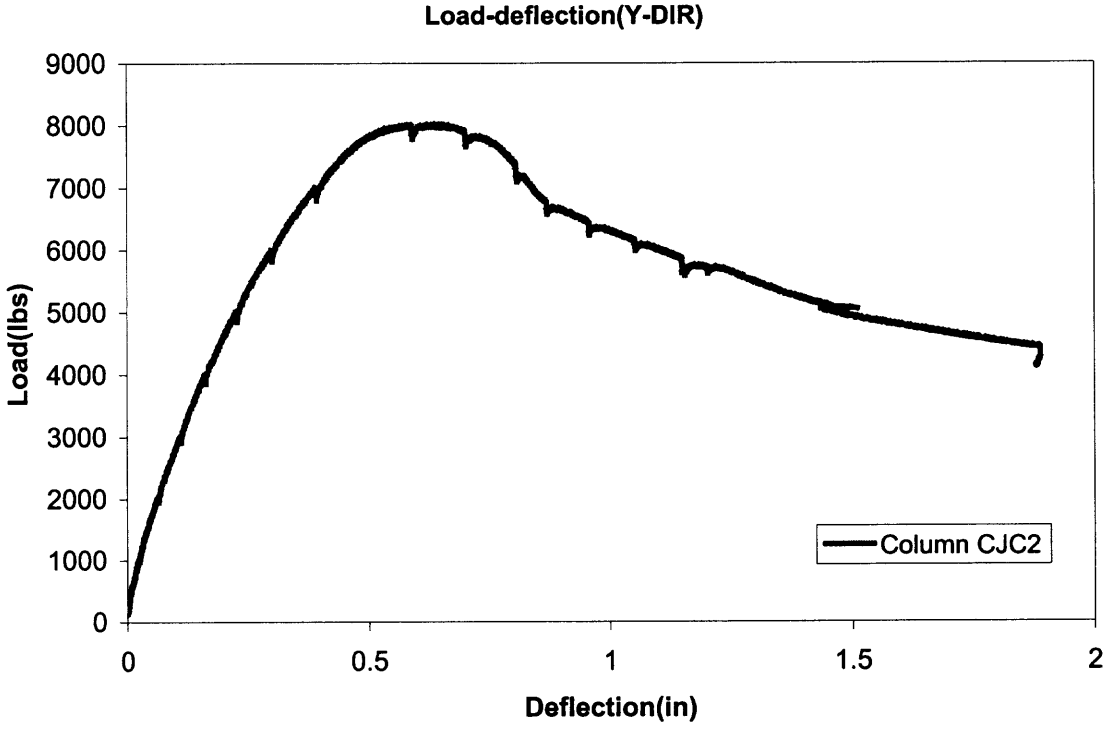

Figure F.2 Experimental load-deflection curve for column CJC2 in Y direction.

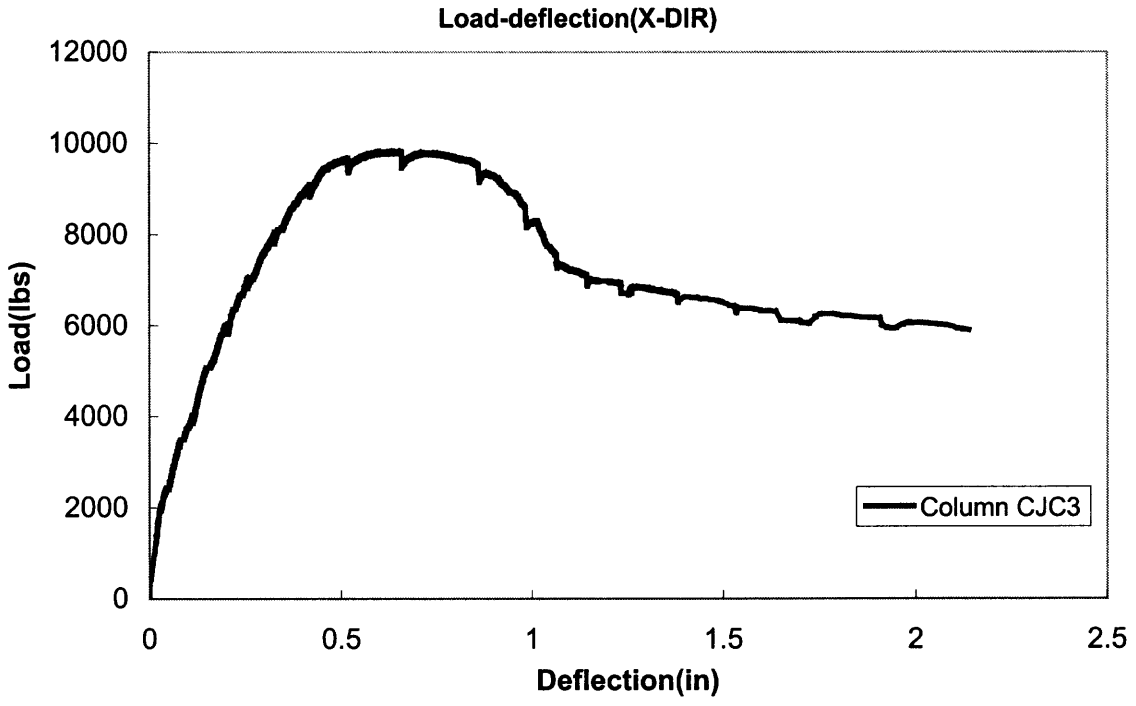

Figure F.3 Experimental load-deflection curve for column CJC3 in X direction.

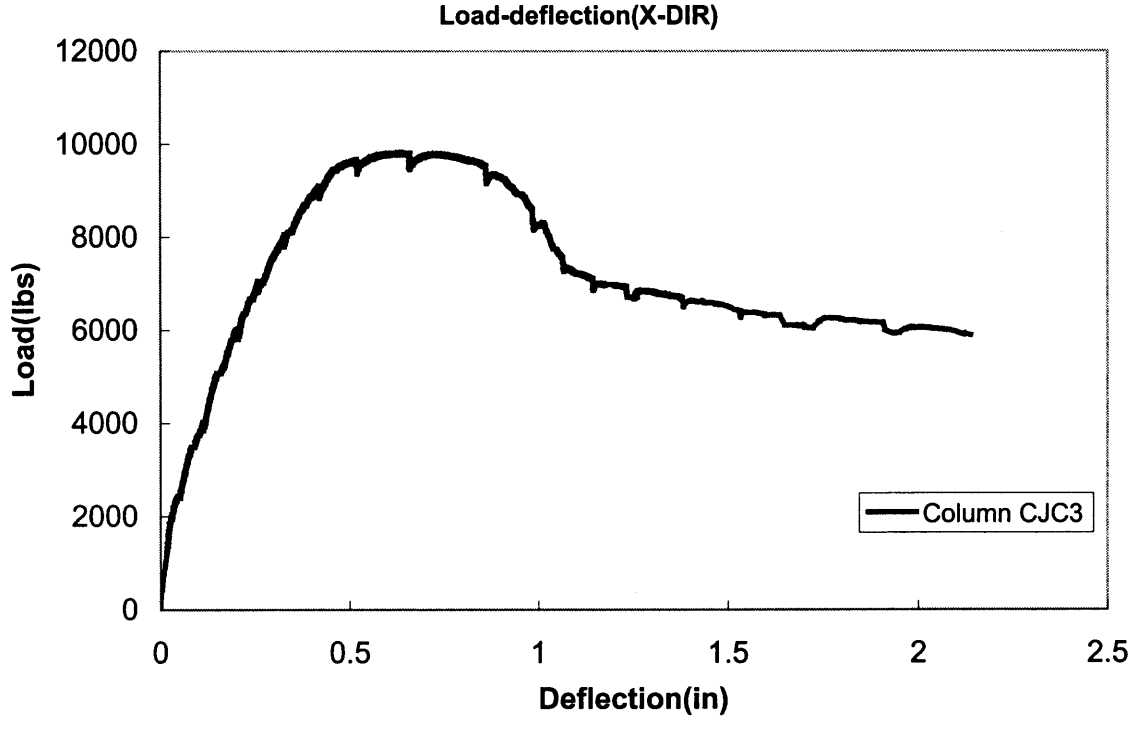

Figure F.4 Experimental load-deflection curve for column CJC3 in Y direction.

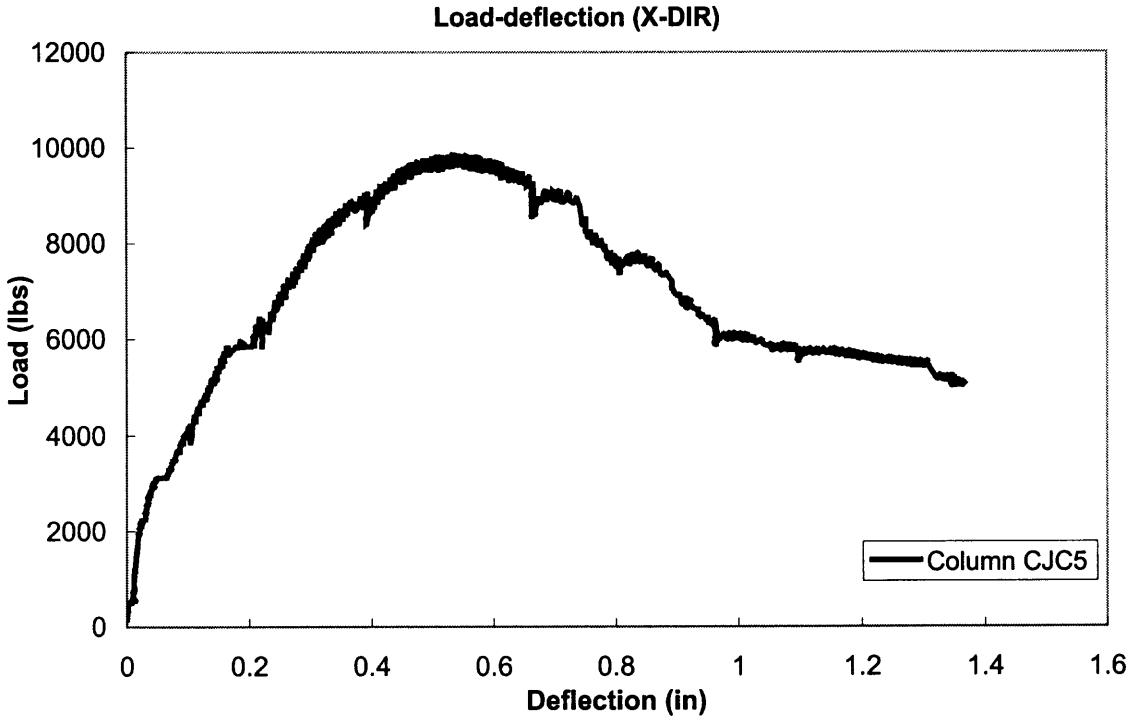

Figure F.5 Experimental load-deflection curve for column CJC5 in X direction.

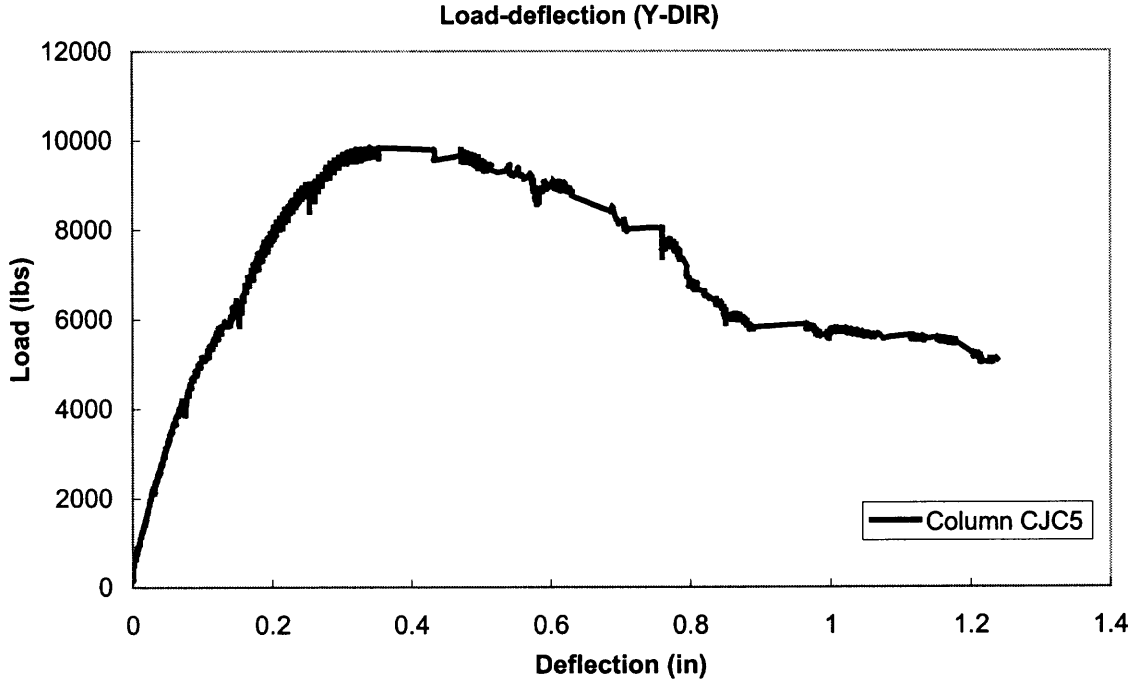

Figure F.6 Experimental load-deflection curve for column CJC5 in Y direction.

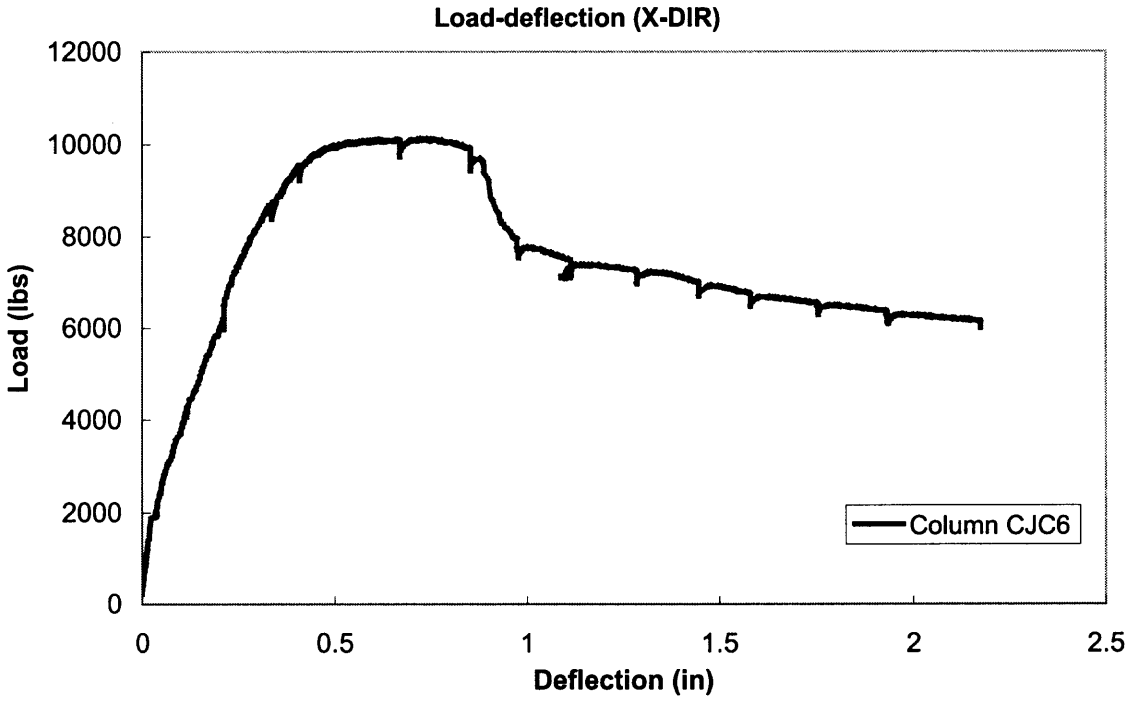

Figure F.7 Experimental load-deflection curve for column CJC6 in X direction.

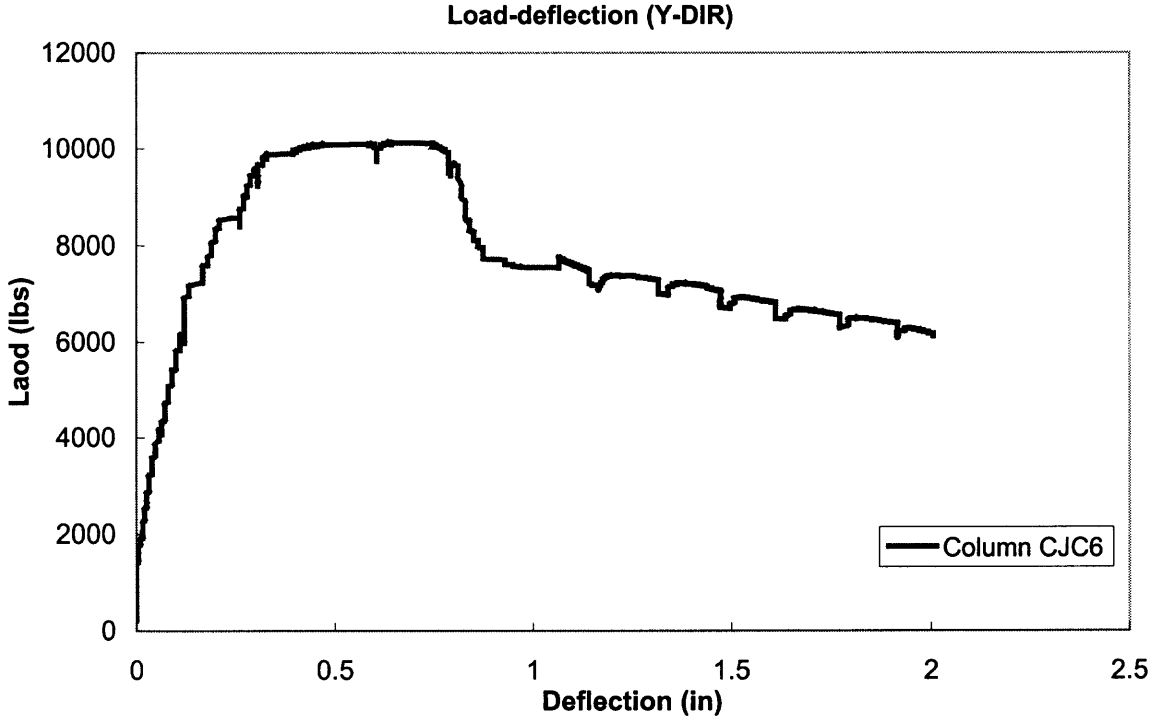

Figure F.8 Experimental load-deflection curve for column CJC6 in Y direction.

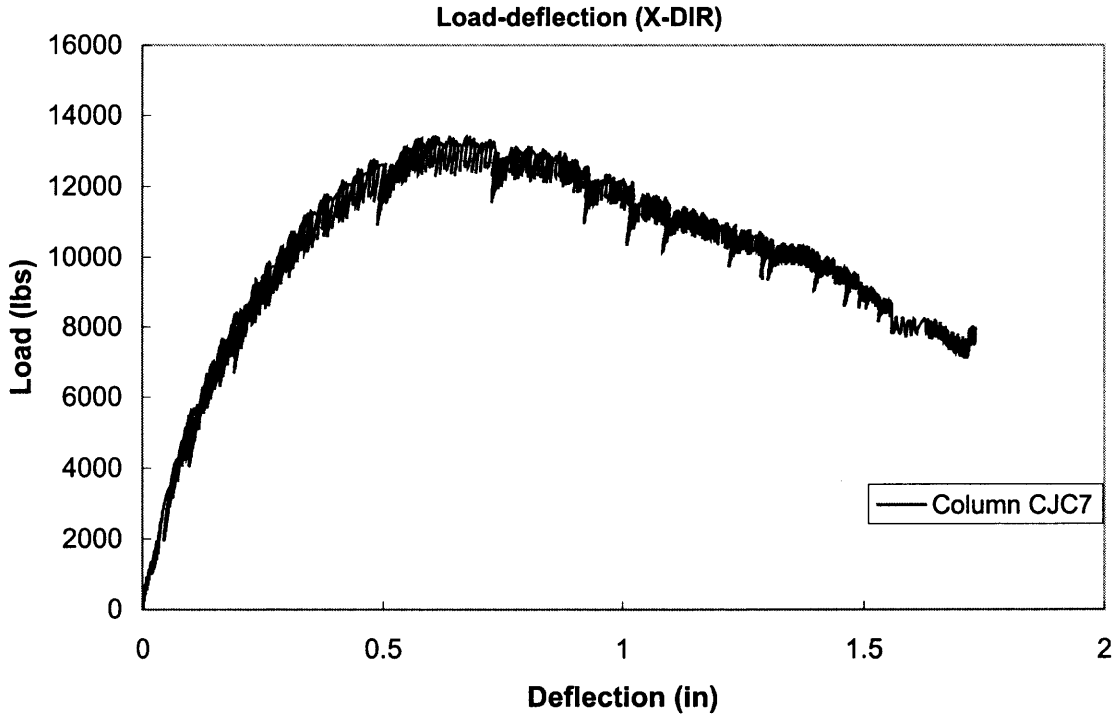

Figure F.9 Experimental load-deflection curve for column CJC7 in X direction.

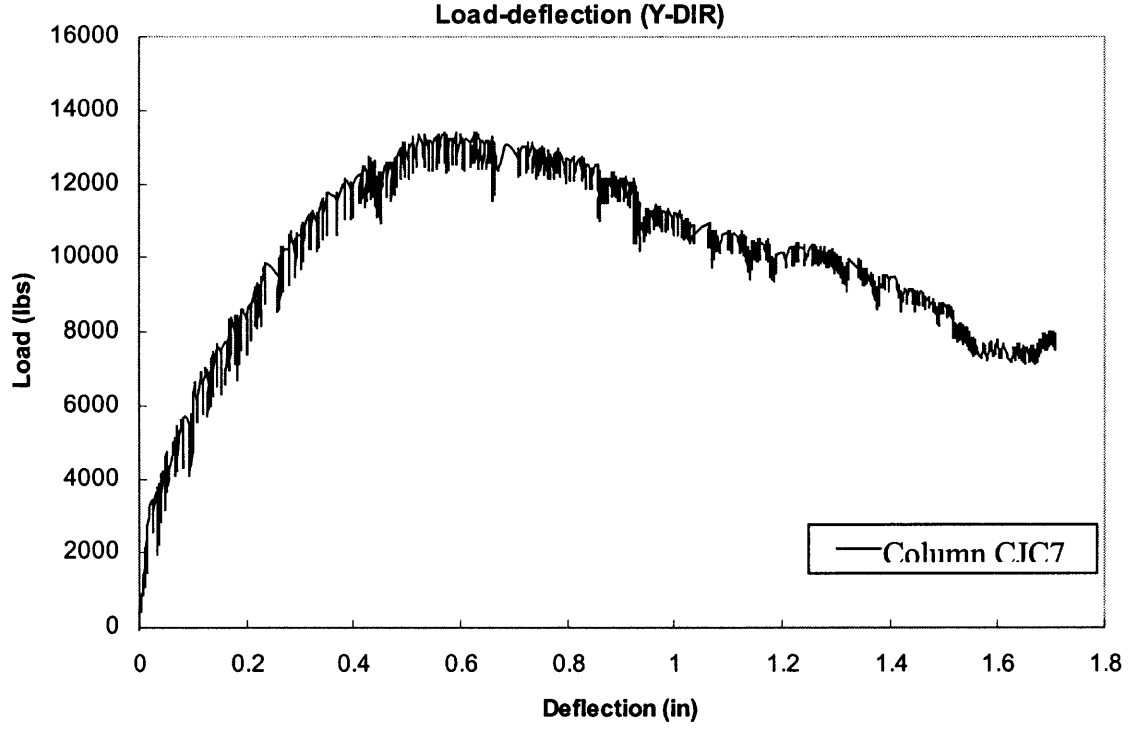

Figure F.10 Experimental load-deflection curve for column CJC7 in Y direction.

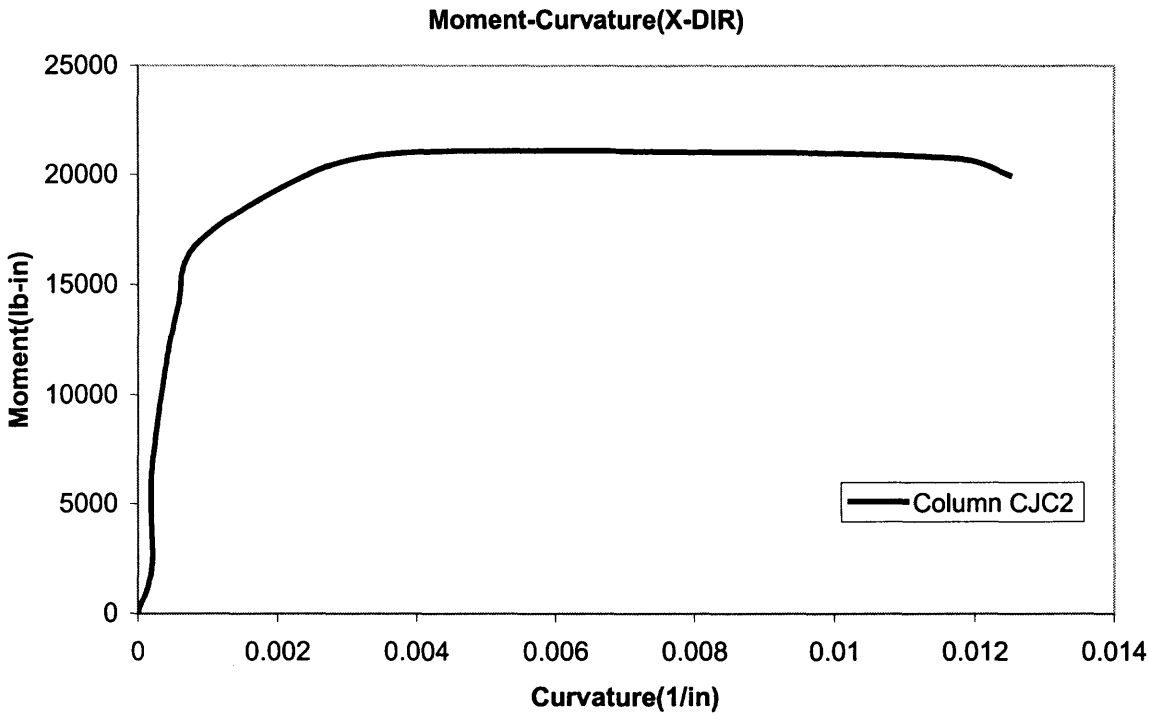

Figure F.11 Experimental moment-curvature curve for column CJC2 in X direction.

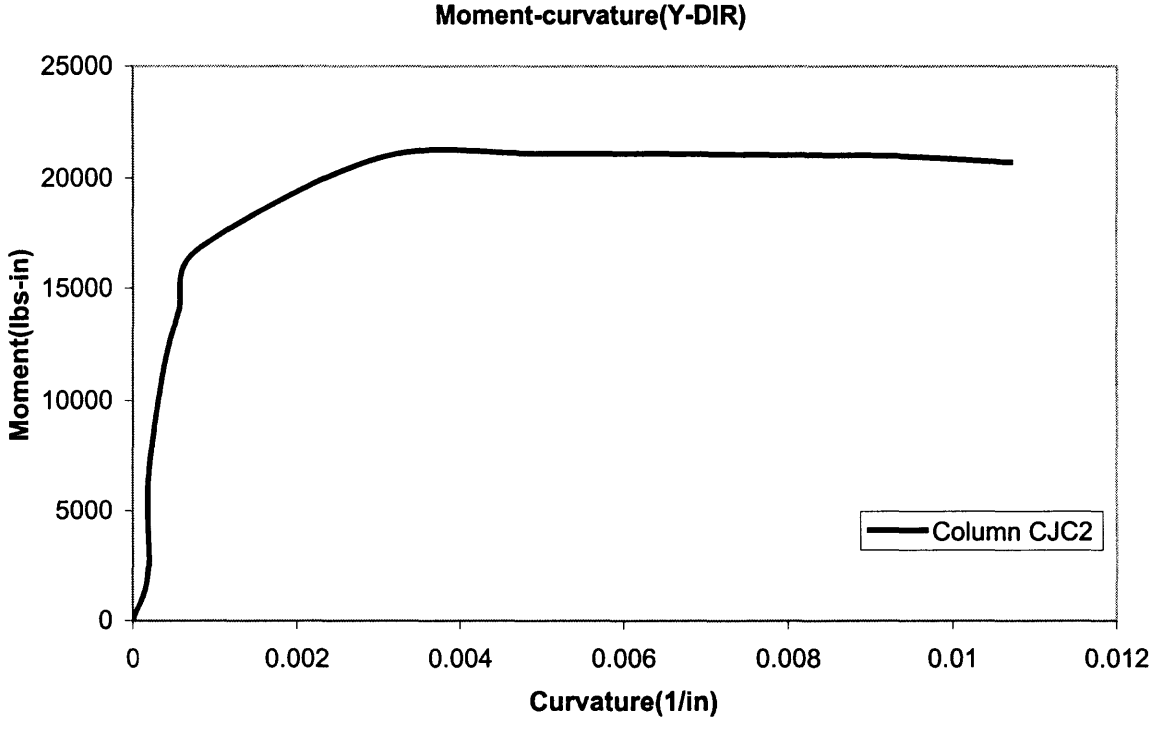

Figure F.12 Experimental moment-curvature curve for column CJC2 in Y direction.

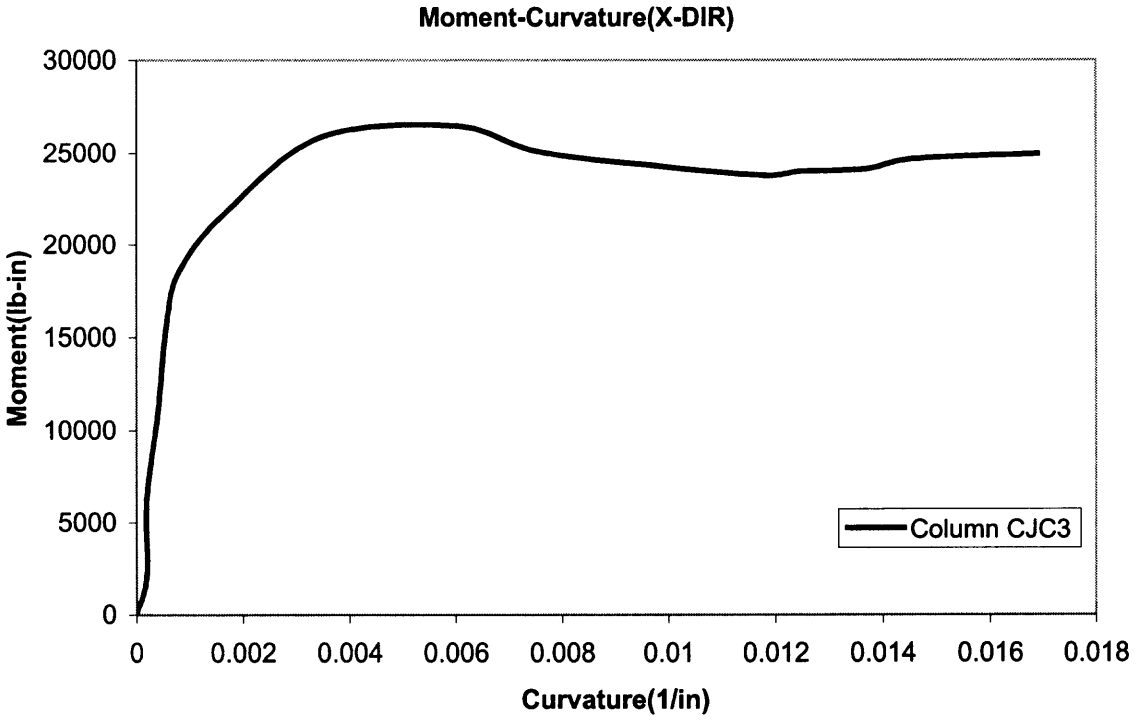

Figure F.13 Experimental moment-curvature curve for column CJC3 in X direction.

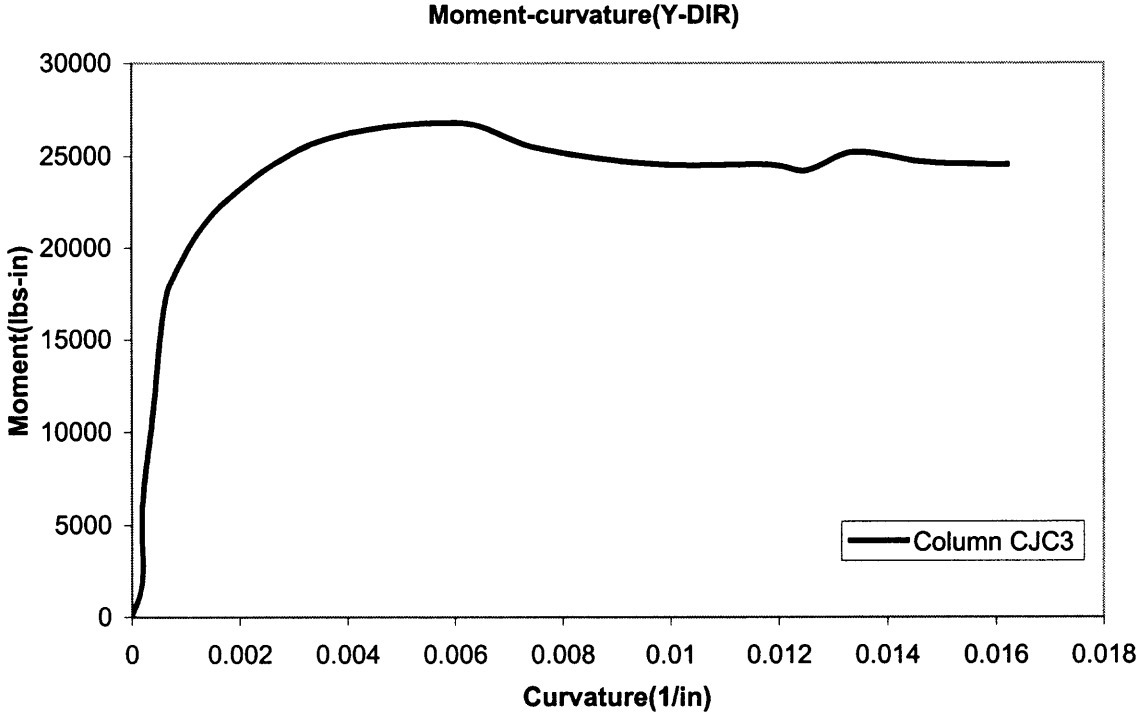

Figure F.14 Experimental moment-curvature curve for column CJC3 in Y direction.

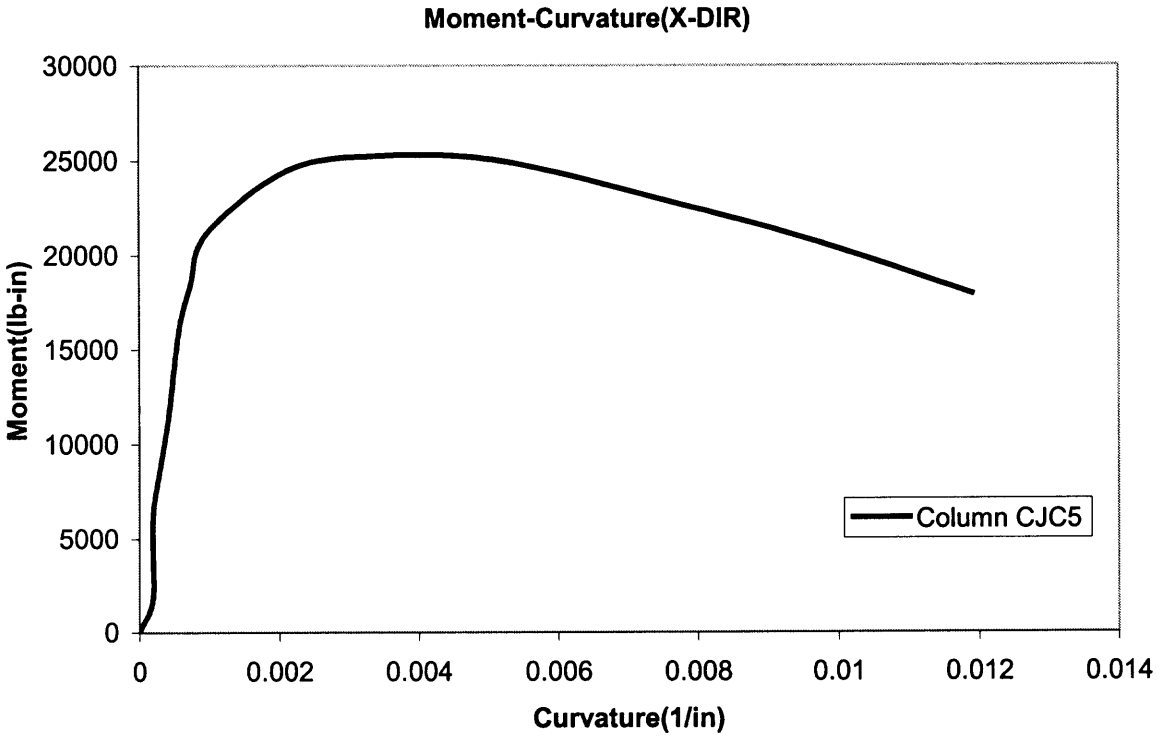

Figure F.15 Experimental moment-curvature curve for column CJC5 in X direction.

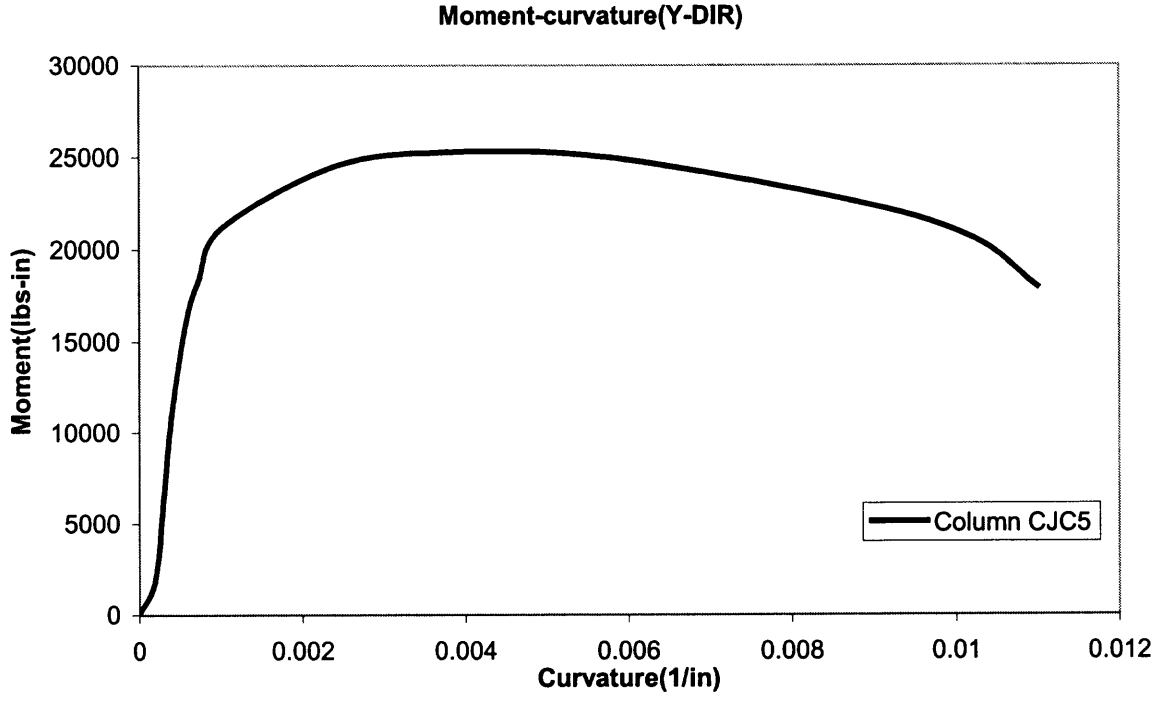

Figure F.16 Experimental moment-curvature curve for column CJC5 in Y direction.

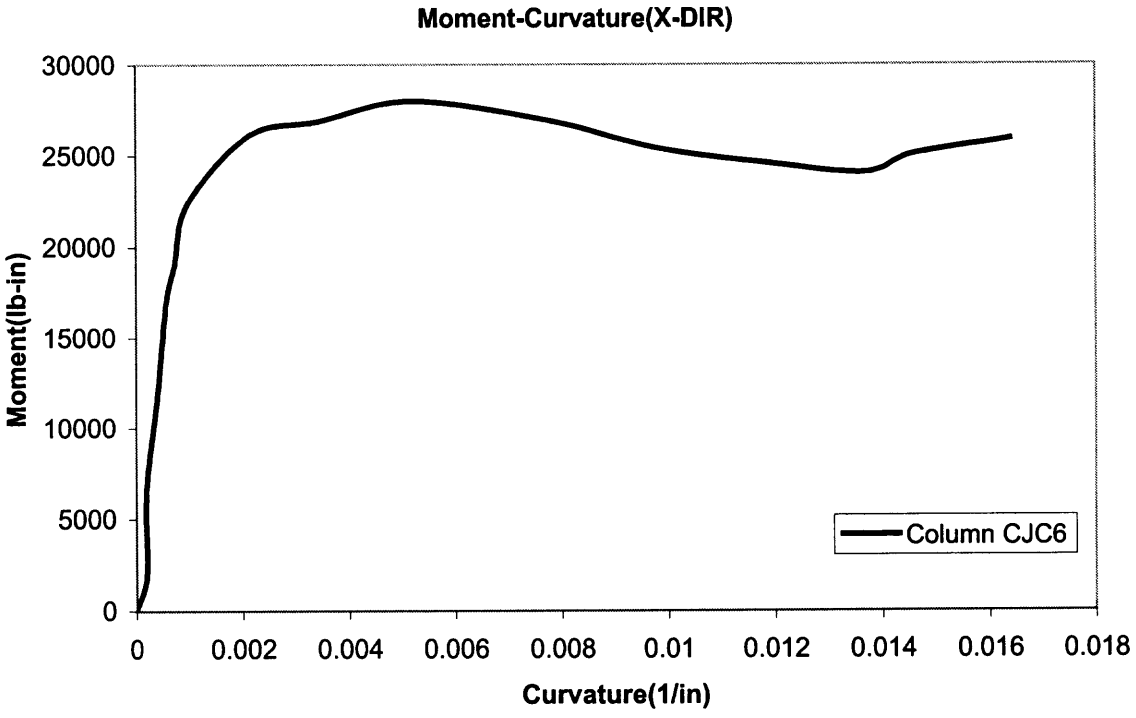

Figure F.17 Experimental moment-curvature curve for column CJC6 in X direction.

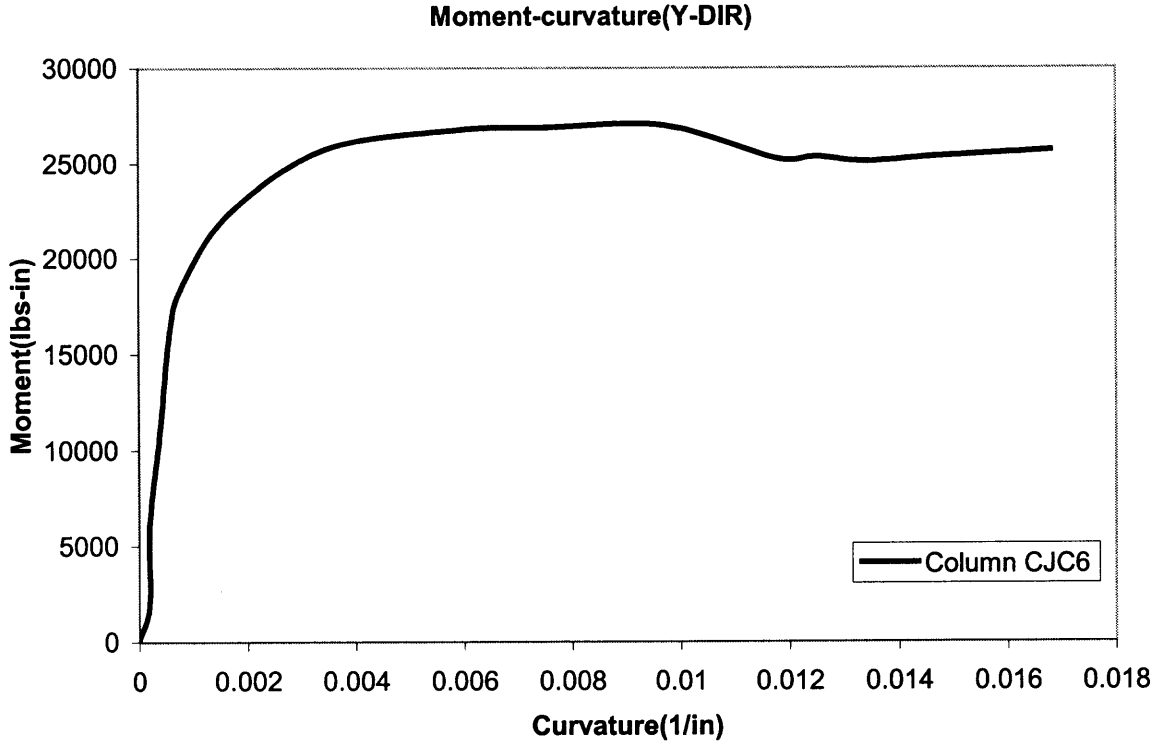

Figure F.18 Experimental moment-curvature curve for column CJC6 in Y direction.

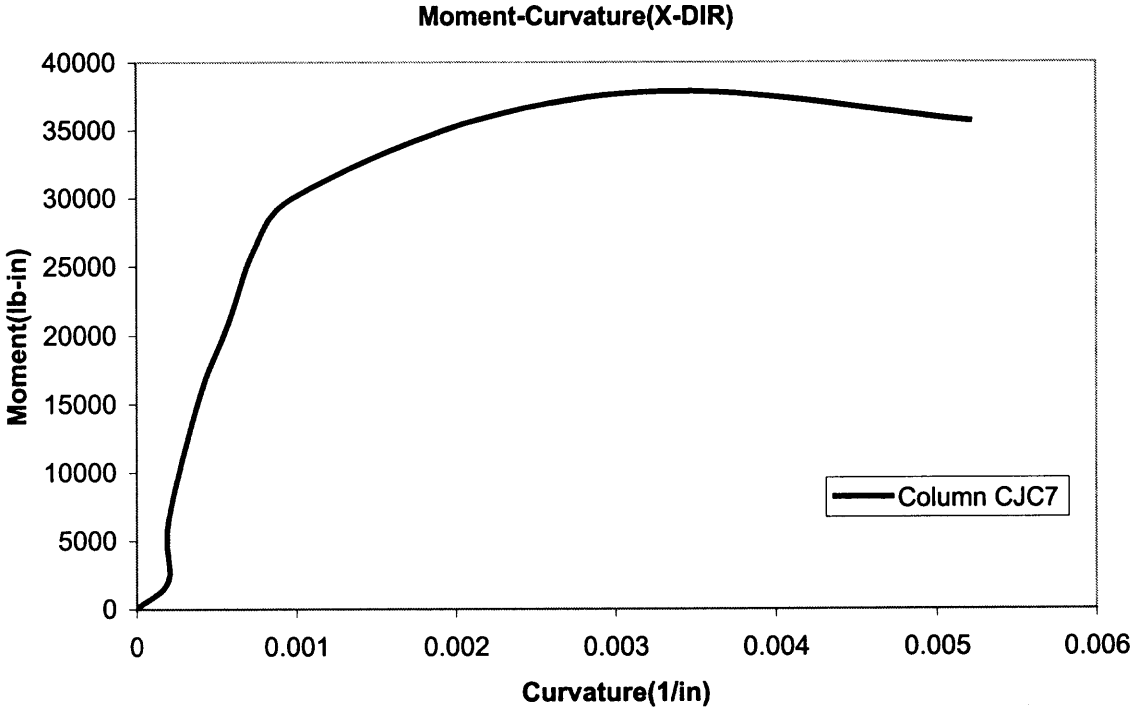

Figure F.19 Experimental moment-curvature curve for column CJC7 in X direction.

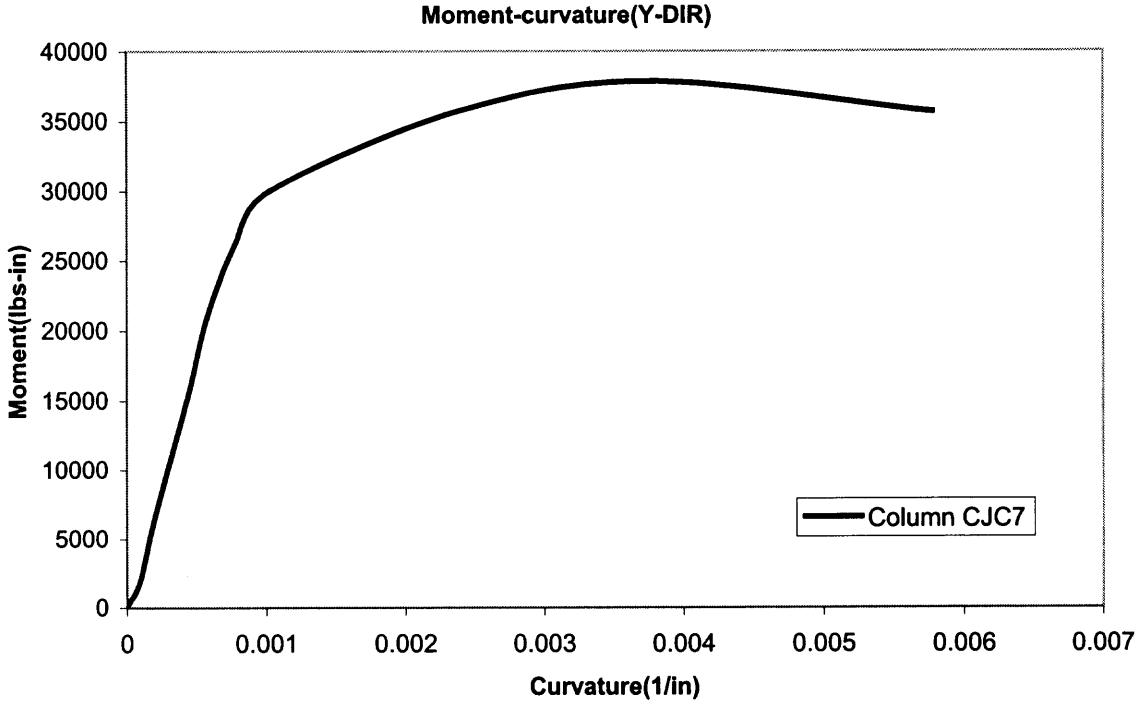

Figure F.20 Experimental moment-curvature curve for column CJC7 in Y direction.

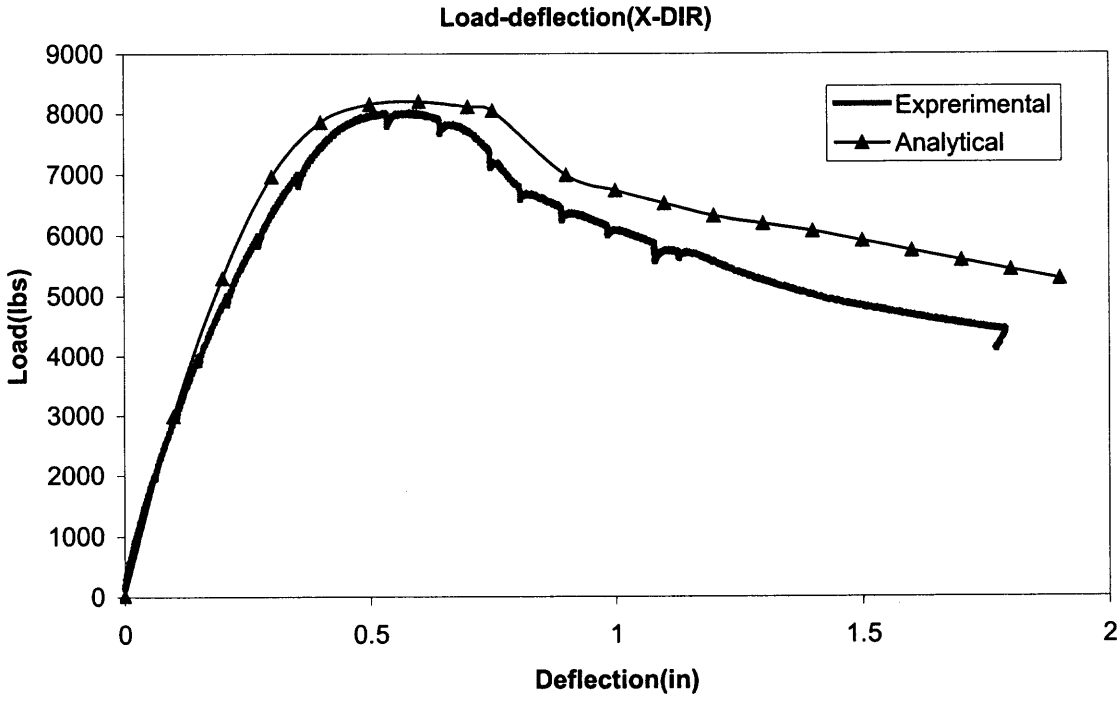

Figure F.21 Comparison of load-deflection curves for column CJC2 in X direction.

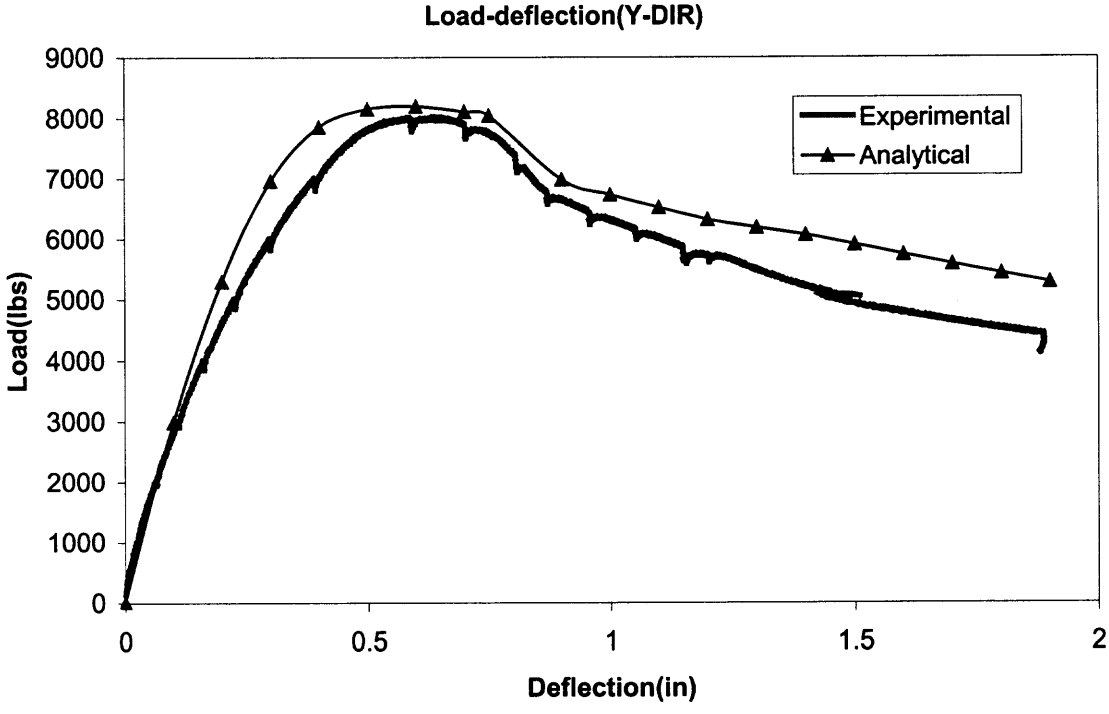

Figure F.22 Comparison of load-deflection curves for column CJC2 in Y direction.

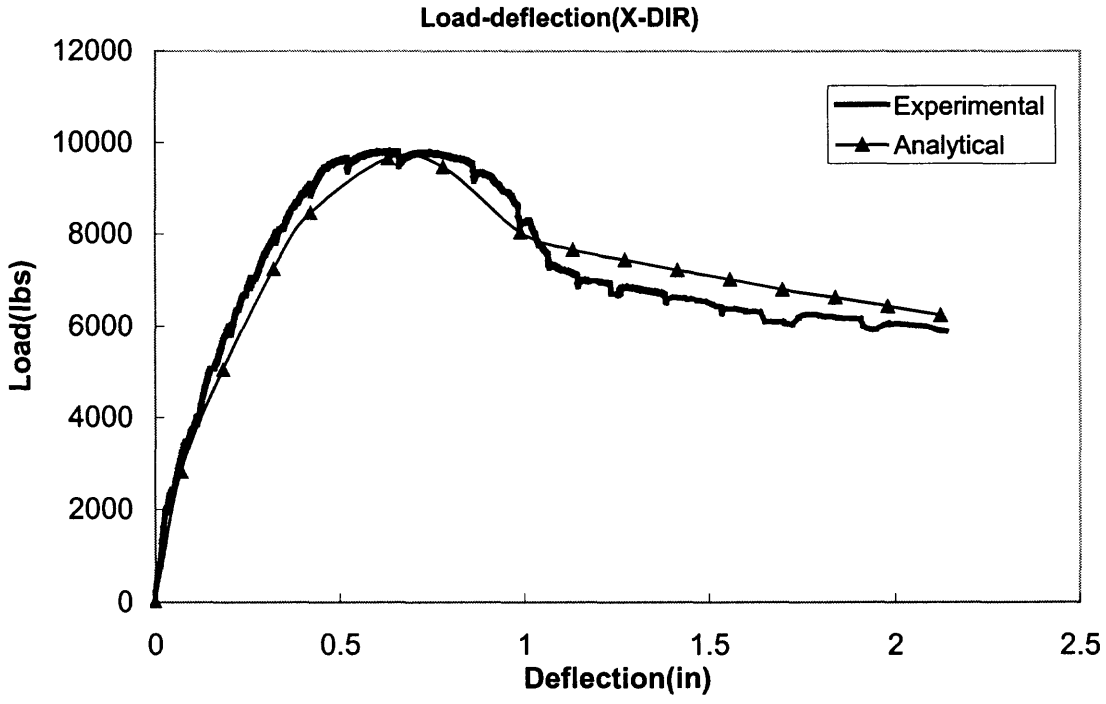

Figure F.23 Comparison of load-deflection curves for column CJC3 in X direction.

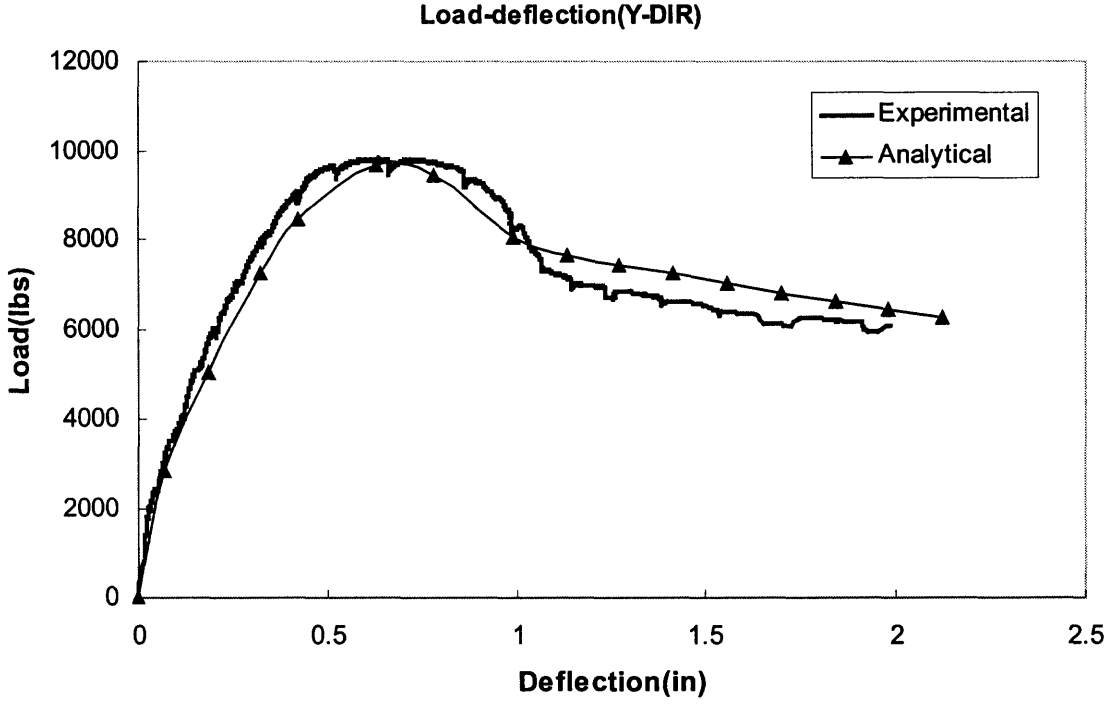

Figure F.24 Comparison of load-deflection curves for column CJC3 in Y direction.

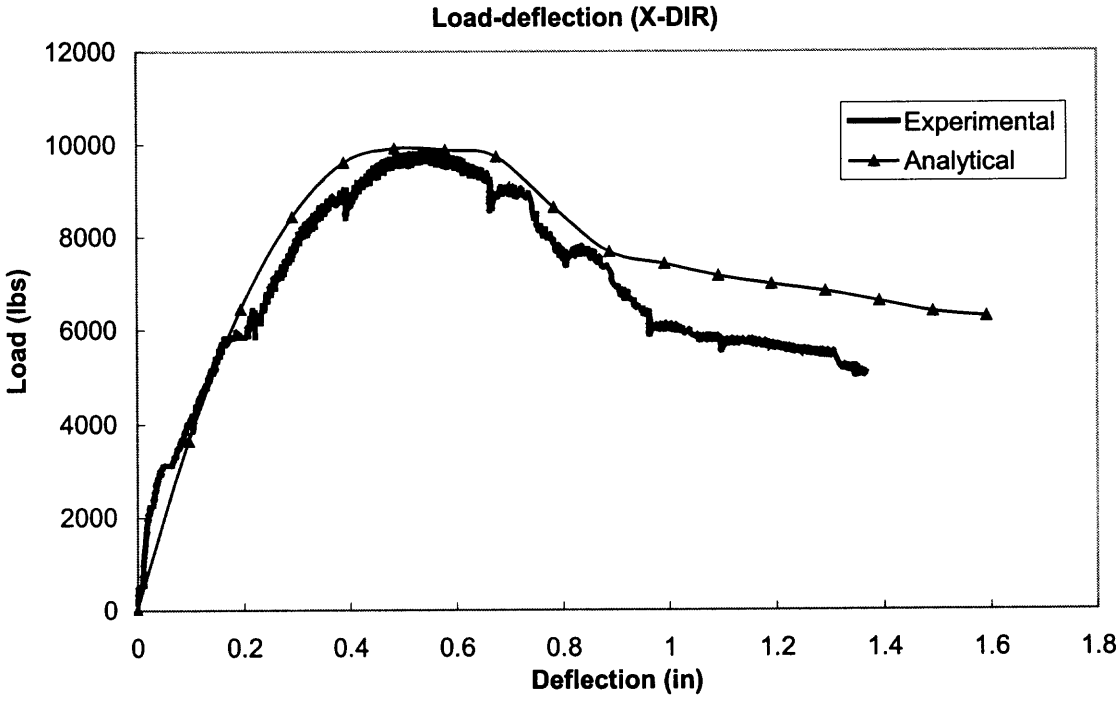

Figure F.25 Comparison of load-deflection curves for column CJC5 in X direction.

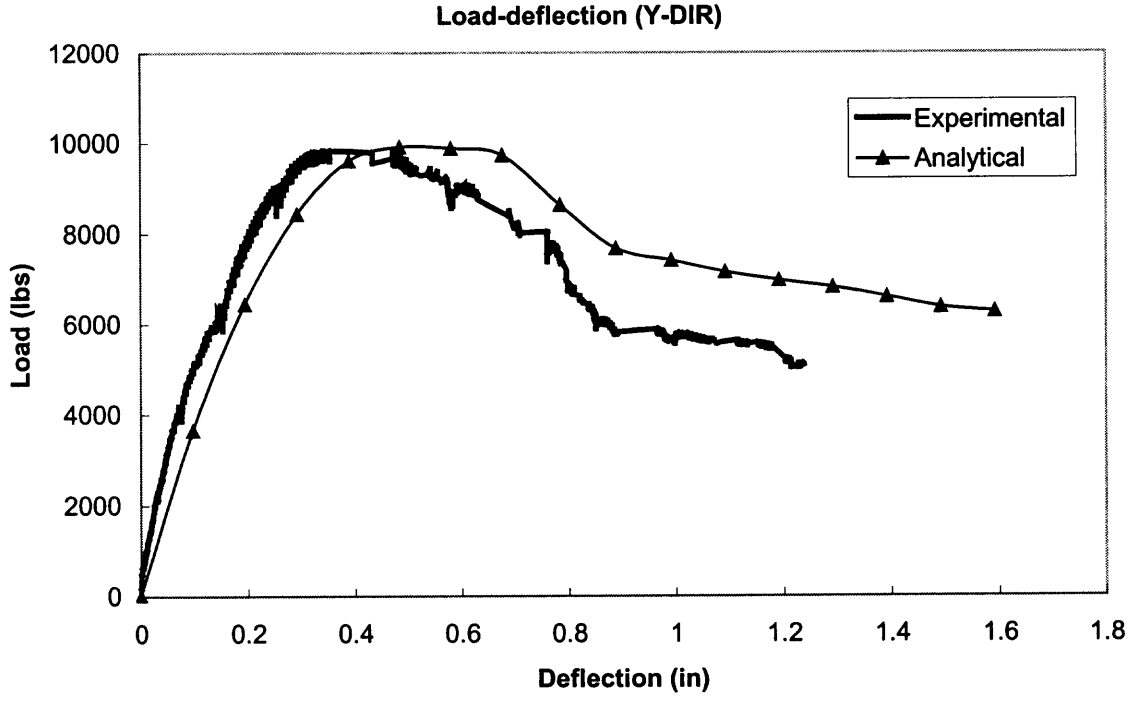

Figure F.26 Comparison of load-deflection curves for column CJC5 in Y direction.

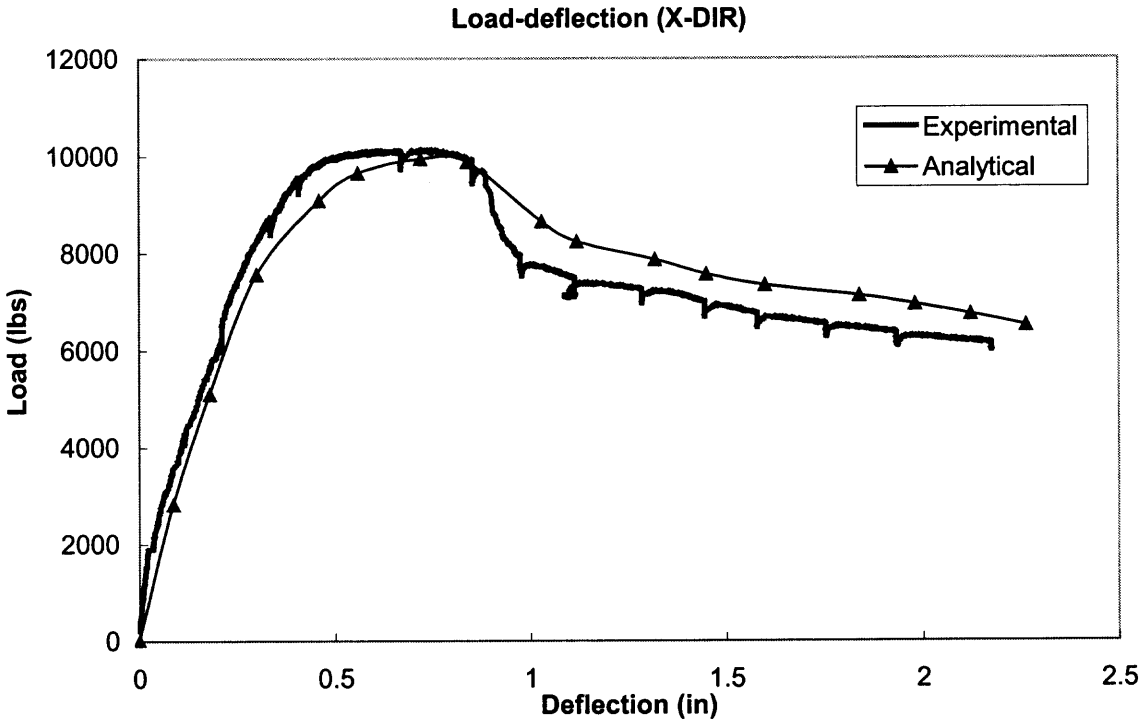

Figure F.27 Comparison of load-deflection curves for column CJC6 in X direction.

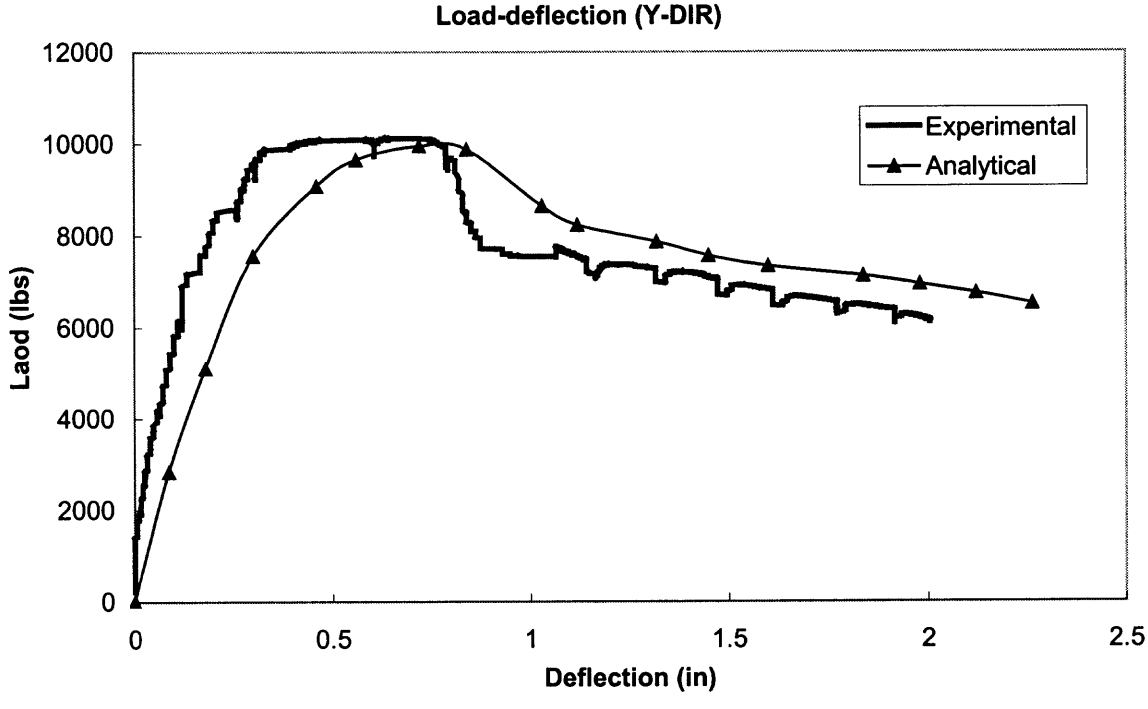

Figure F.28 Comparison of load-deflection curves for column CJC6 in Y direction.

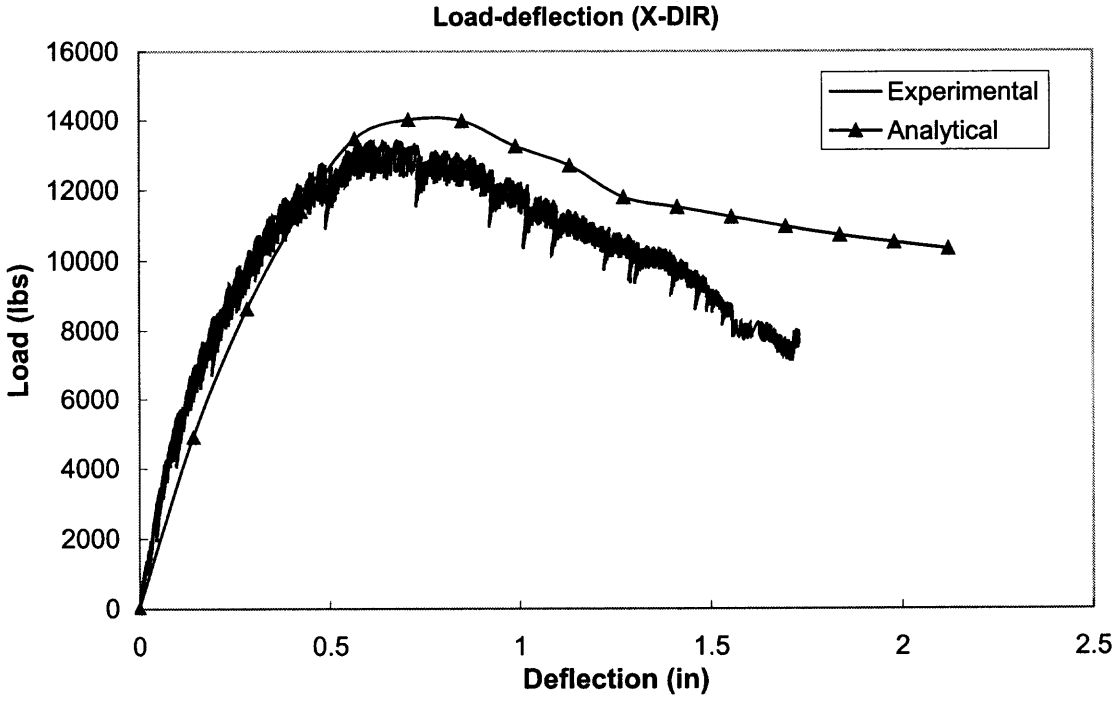

Figure F.29 Comparison of load-deflection curves for column CJC7 in X direction.

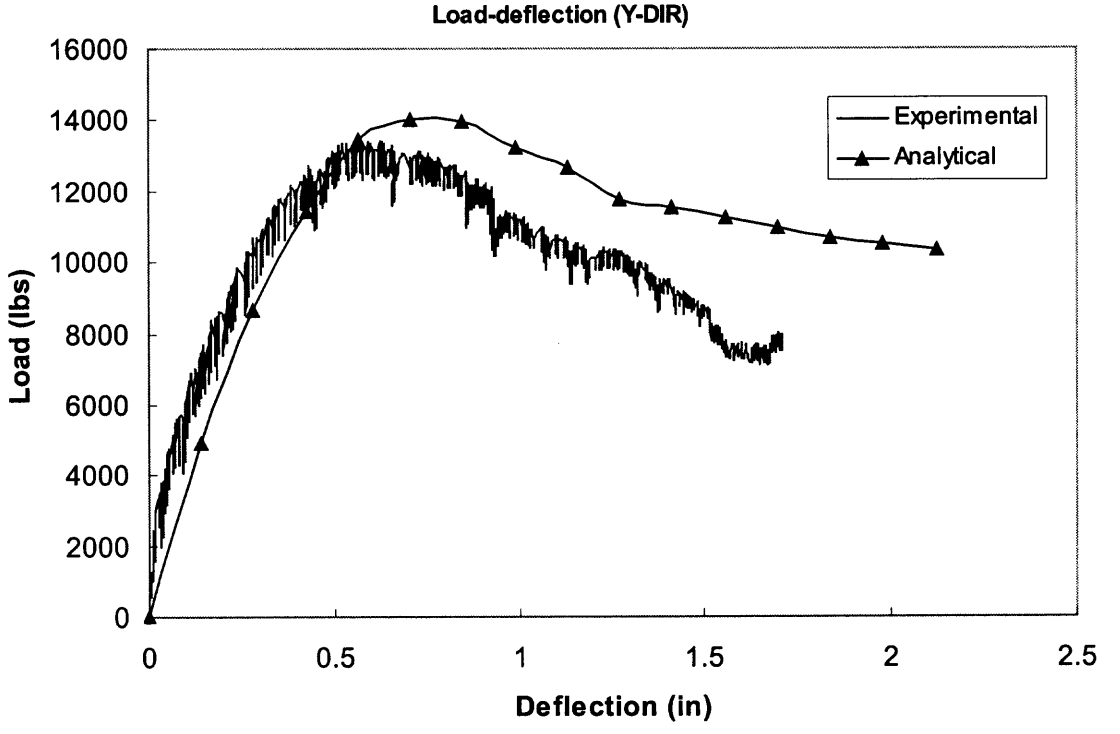

Figure F.30 Comparison of load-deflection curves for column CJC7 in Y direction.

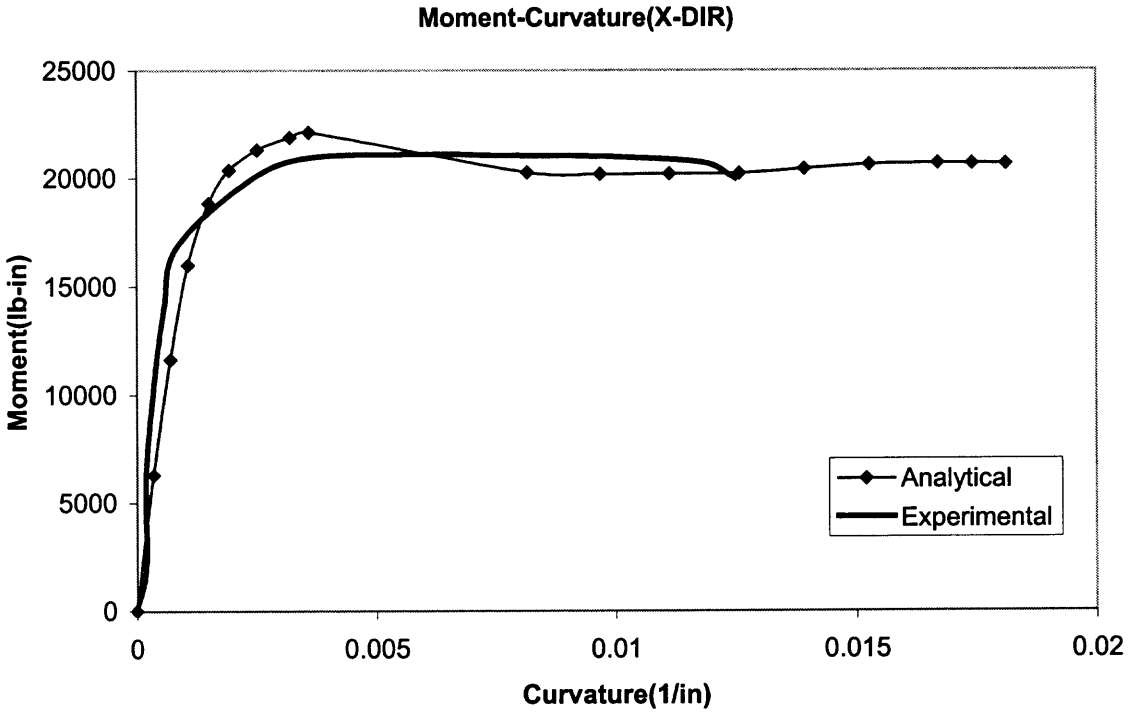

Figure F.31 Comparison of moment-curvature curves for column CJC2 in X direction.

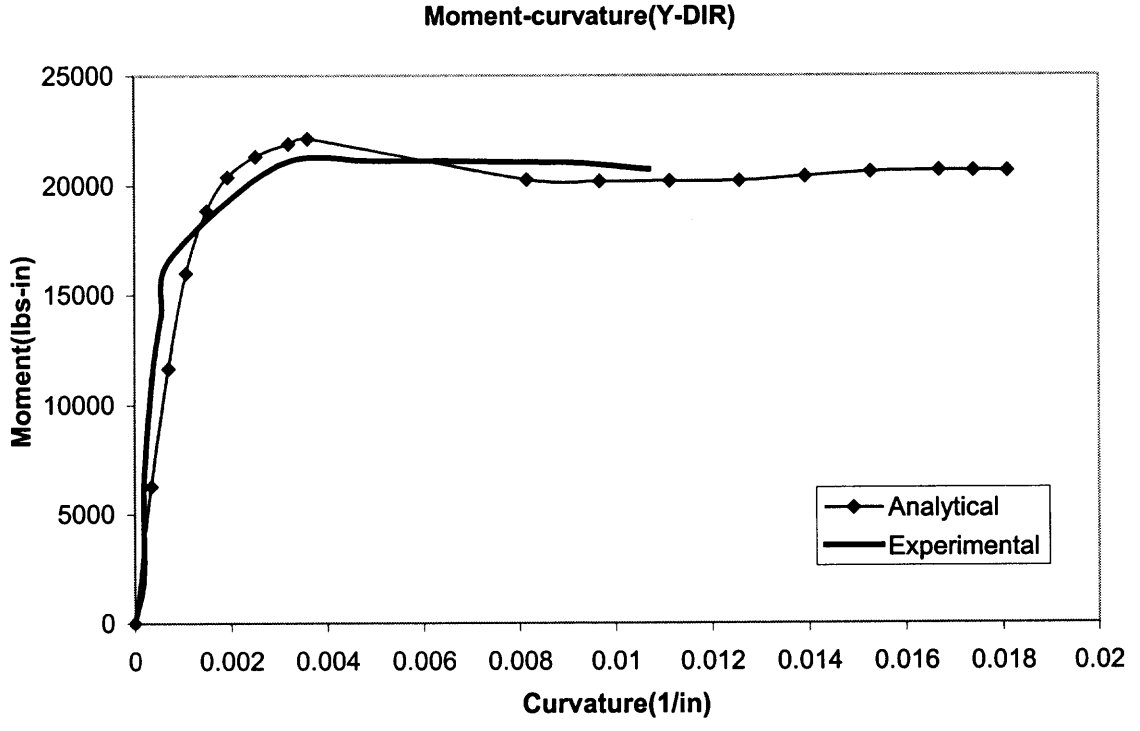

Figure F.32 Comparison of moment-curvature curves for column CJC2 in Y direction.

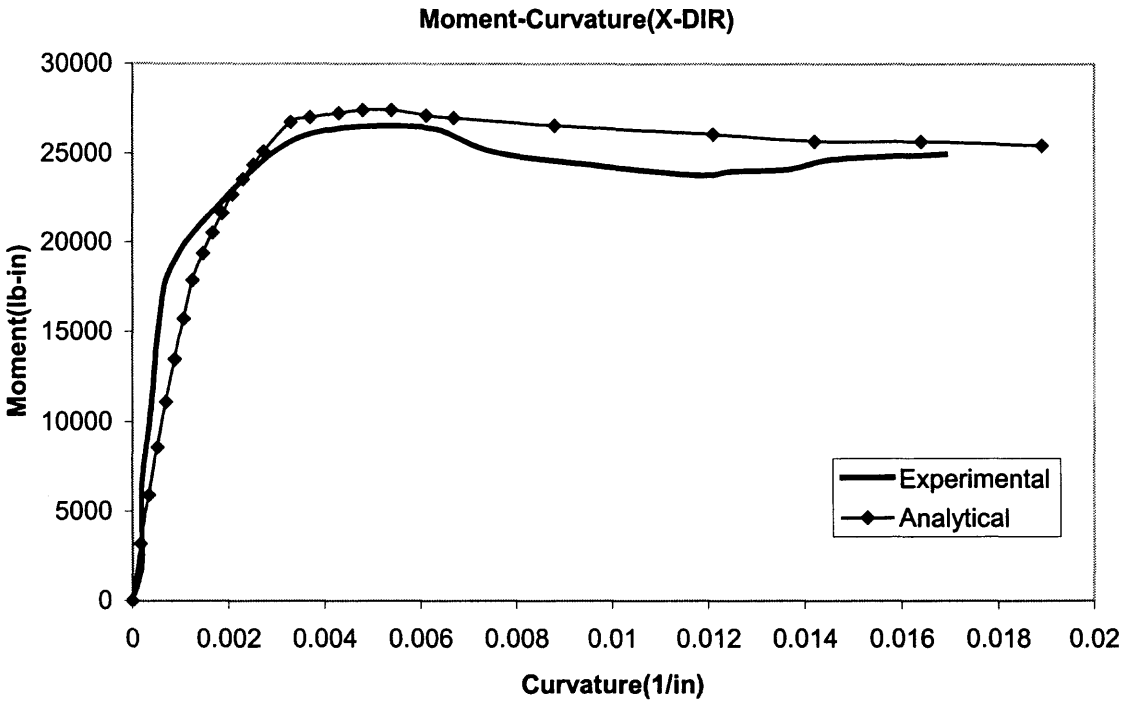

Figure F.33 Comparison of moment-curvature curves for column CJC3 in X direction.

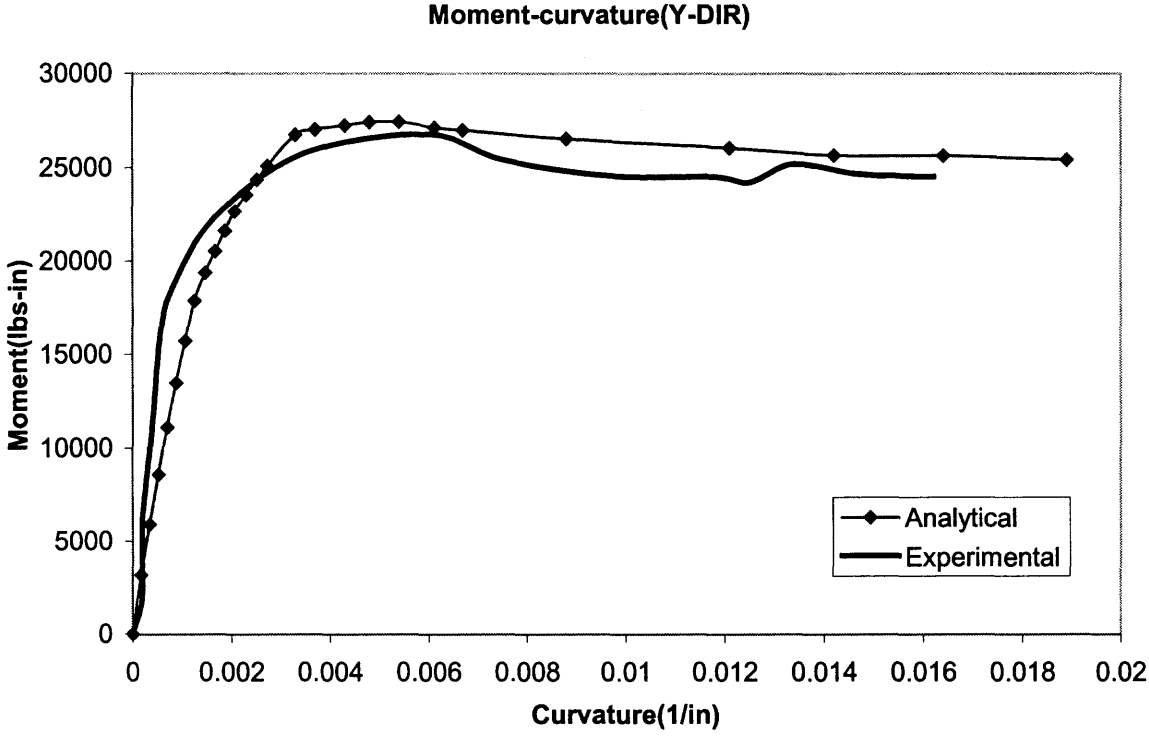

Figure F.34 Comparison of moment-curvature curves for column CJC3 in Y direction.

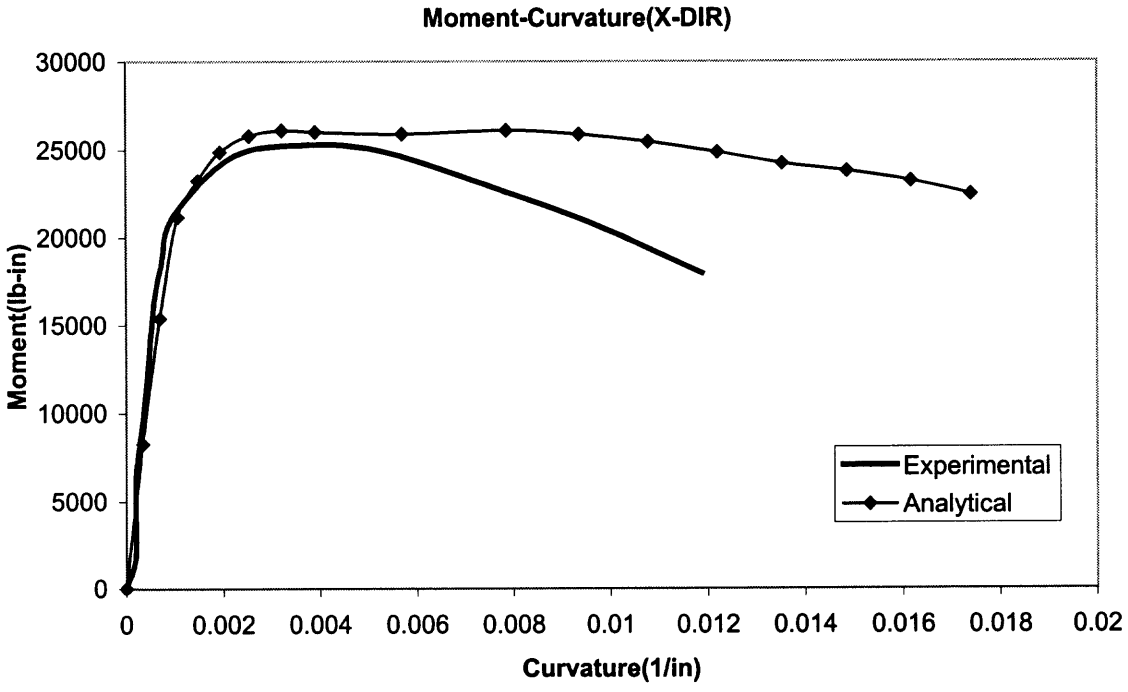

Figure F.35 Comparison of moment-curvature curves for column CJC5 in X direction.

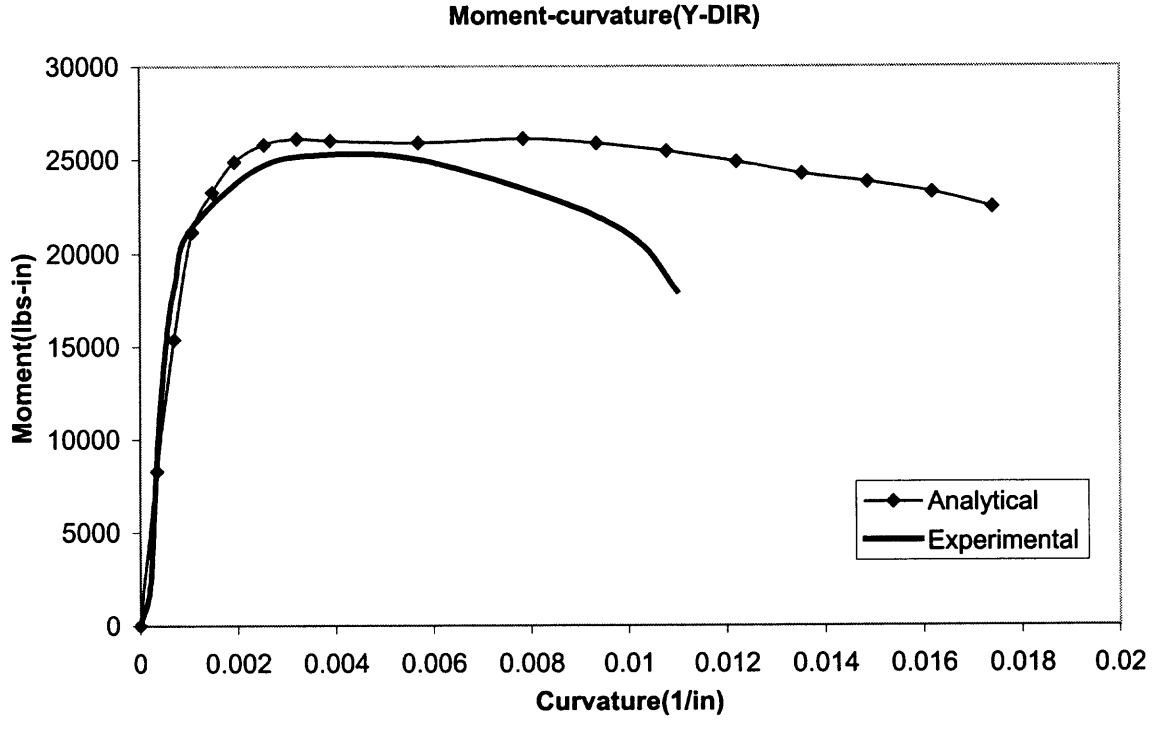

Figure F.36 Comparison of moment-curvature curves for column CJC5 in Y direction.

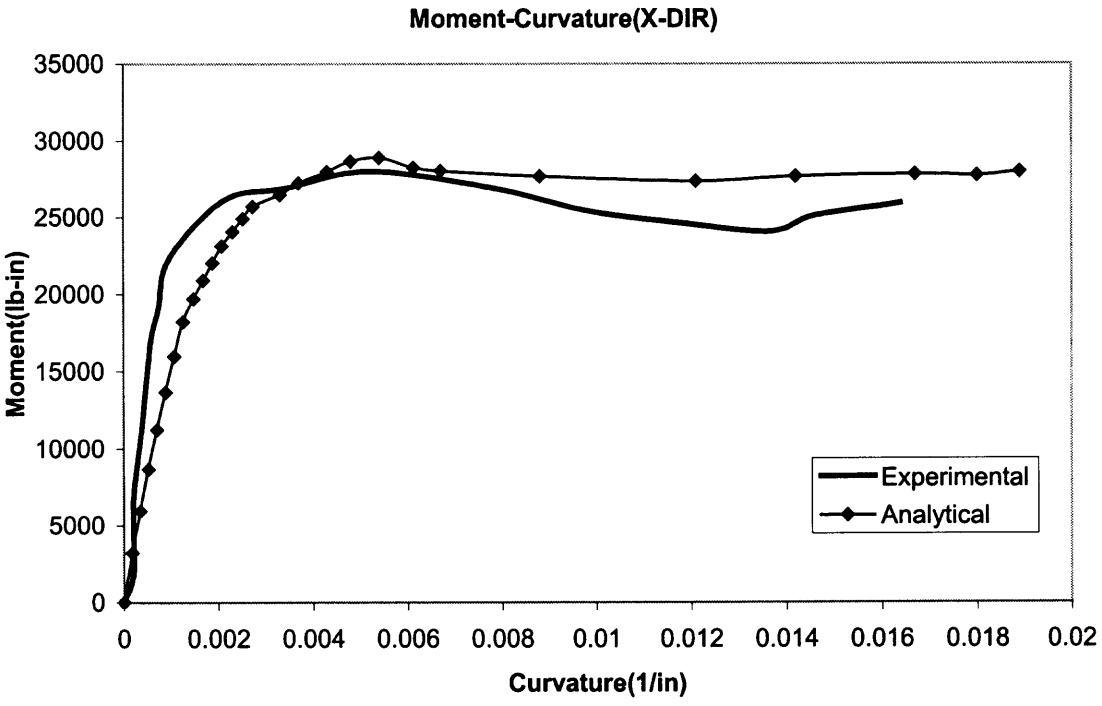

Figure F.37 Comparison of moment-curvature curves for column CJC6 in X direction.

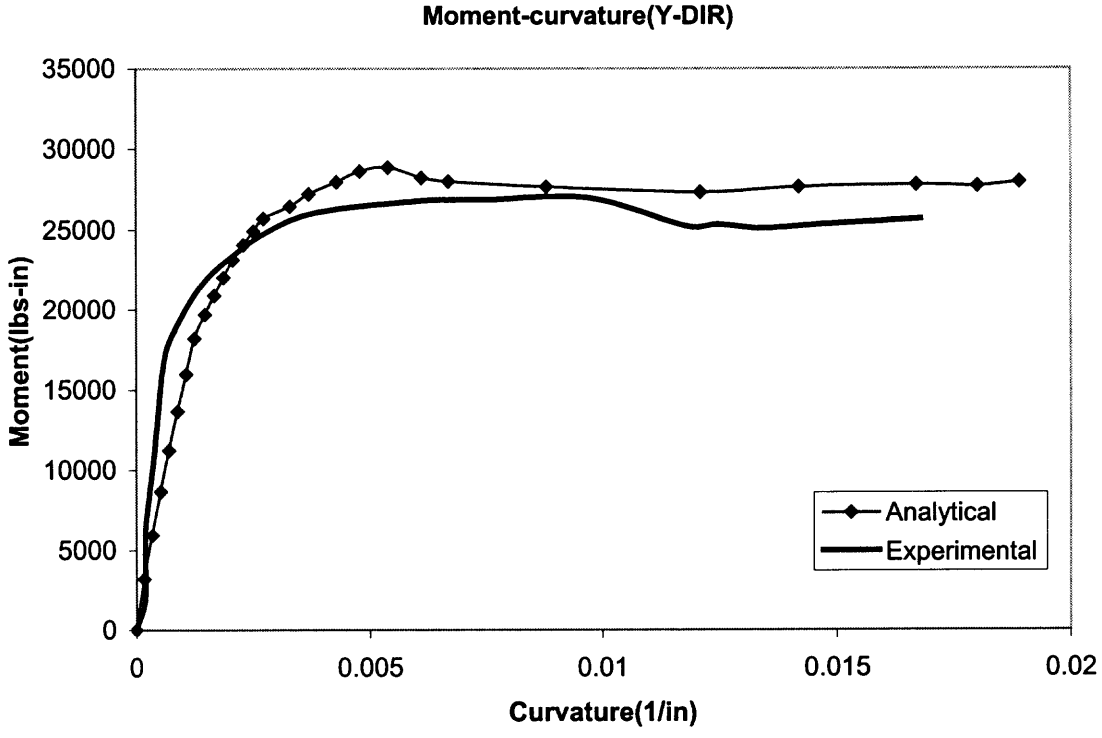

Figure F.38 Comparison of moment-curvature curves for column CJC6 in Y direction.

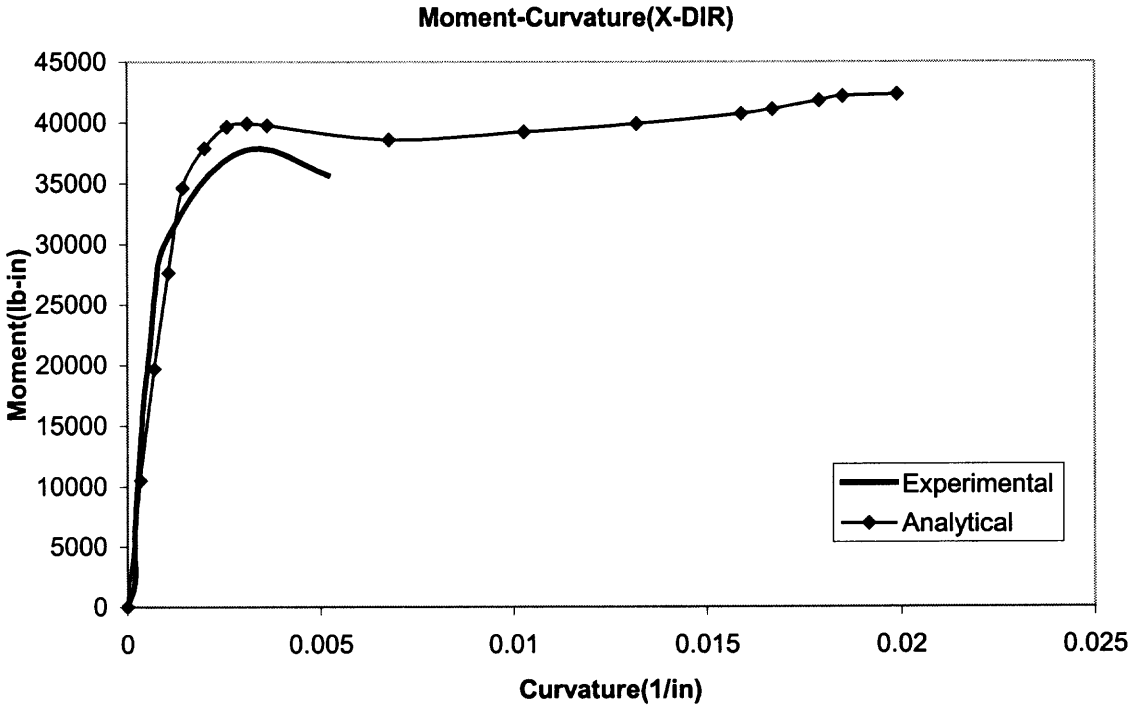

Figure F.39 Comparison of moment-curvature curves for column CJC7 in X direction.

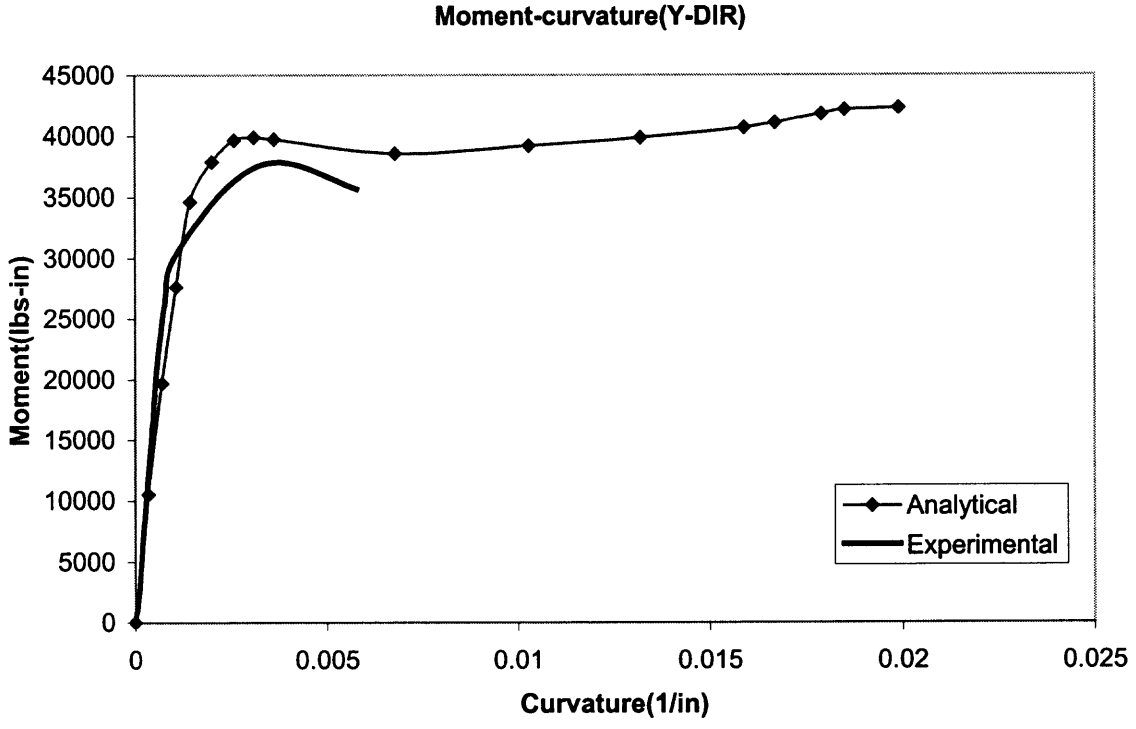

Figure F.40 Comparison of moment-curvature curves for column CJC7 in Y direction.

APPENDIX G

BEAM ANALYSIS USING MODIFIED ACI METHOD

Appendix G presents the detailed design procedures for RC beams wrapped with CFRP fabrics using the modified ACI Strength Method.

All units use USCU. For simplicity, the compressive strength of concrete for all the beams is taken as 4.5 ksi. The other known conditions are listed as follows:

Concrete strength: f'_c=4.5 ksi,

Steel yield strength: f_y=60 ksi,

Steel ultimate strength: f_{su}=80 ksi,

Steel cross sectional area: A_s=0.22 in^2

Concrete maximum strain: ε_0=0.002,

Concrete ultimate strain: ε_c=0.003,

Steel ultimate strain: ε_{su}=0.038

Steel modulus of elasticity: E_s=29,000 ksi,

Fabric tensile strength: f_{fabr}=140 ksi,

Fabric modulus of elasticity: E_{fab}= 1,600 ksi,

Fabric thickness of one layer: t=0.013 in,

Beam width: b=6 in,

Beam effective depth: d=10.5 in

Beam height: h= 12 in,

Beam Length: L= 9.5 ft.

(1) Beam CJ1 analysis:

Based on figure 3.13, the depth of neutral axis can be obtained by

$C=0.85f'_cba$

$T=A_sf_y$

$a=(A_sf_y)/(0.85f'_cb)=0.22\times60/0.85\times4.5\times6=0.575$ in

Then the strain in the tension steel can be checked by

$\varepsilon_s=((d-c)/c)\times\varepsilon_c=(10.5-0.575/0.85)\times0.003/(0.575/0.85)=0.043>\varepsilon_{su}>f_y/E_s=0.0021$

The strain value in the steel reaches its ultimate value. This means steel actually has broken when concrete crushed. Therefore, ultimate strength for steel f_{su} is suggested to be used. The moment capacity is calculated by using both values.

$M=A_sf_y(d-a/2)=134.81$ k-in ($f_y=60$ksi)

The ultimate load can be obtain by moment diagram

$P= 4M/L= 4\times134.81/(12\times9.5)=4.73$ kips (using f_y)

When $f_{su}=80$ ksi is used,

$a=0.22\times80/(0.85\times4.5\times6)=0.767$ in

$M=0.22\times80\times(10.5-0.767/2)=178.05$ k-in

$P=178.1\times4/(12\times9.5)=6.24$ kips

(2) Beam CJ2 analysis:

(a) fy=60 ksi is used

First, assume when concrete reaches $\varepsilon_c=0.003$, CFRP fabric at the bottom layer reaches its ultimate strain $\varepsilon_{fab}=f_{fab}/E_{fab}=140/10600=0.013$.

According to strain compatibility shown in figure 3.14,

$c=h\times\varepsilon_c/(\varepsilon_c+\varepsilon_{fab})=12\times0.003/(0.003+0.013)=2.25$ in

$\varepsilon_s=\varepsilon_c(10.5-2.25)/2.25=0.011>f_y/E_s=0.00207$ (Steel yields)

Check C=T

$C=0.85f'_cab=0.85\times4.5\times6\times(0.85\times2.25)=43.9$ kips

T_s (steel)= $A_sf_y=0.22\times60=13.2$ kips

T_{fab1} (side fabric)= $2\times(1/2\times f_{fab}\times(12-c)\times t)$

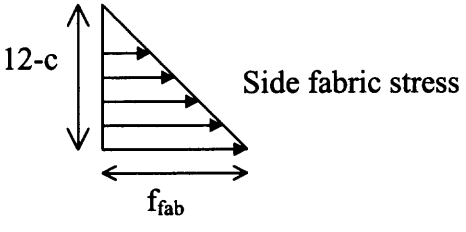

$T_{fab1}=1/2\times140\times(12-2.25)\times0.013\times2=17.47$ kips

T_{fab2} (bottom fabric)= $t\times b\times f_{fab}=0.013\times6\times140=10.75$ kips

Total tension

$T=T_s+T_{fab1}+T_{fab2}=41.42$ kips.

So C>T. This means that fabrics have already been broken before concrete reaches its ultimate strain. We should reduce the ε_c value and remain $\varepsilon_{fab}=0.013$. Try $\varepsilon_c=0.0028$, $f_{fab}=0.013\times10600=140$ ksi.

Recalculate the c value by strain compatibility

$c= 12\times0.0028/(0.0028+0.013)=2.13$ in

$\varepsilon_s=0.012>0.0021$ (Steel yields)

Therefore, $f_y=60$ ksi, $f_{fab}=140$ ksi

Check C=T again,

$C=0.85f'_cab=0.85\times4.5\times6\times(0.85\times2.13)=41.5$ kips

$T_{fab1}=1/2\times140\times(12-2.13)\times0.013\times2=17.68$ kips

$T_{fab2}=0.013\times140\times6=10.74$ kips

Total T=13.2+10.74+17.68=41.6 kips

So C=T, the c value is accepted:

$a=0.85\times c=1.81$ in

Take the moment about the bottom of the beam,

$M=0.85f'_cab(h-a/2)-A_sf_y(h-d)-T_{fab1}(h-c)/3$

$M=0.85\times4.5\times1.972\times6\times(12-1.81/2)/12+13.2\times1.5/12+17.68(12-2.13)/3/12=31.86$ k-ft

$P=4M/L=4\times31.86/9.5=13.4$ kips

(b) f_{su}=80 ksi is used

Assume when concrete reaches ε_c=0.003, CFRP fabric at the bottom layer reaches its ultimate strain $\varepsilon_{fab}=f_{fab}/E_{fab}=140/10600=0.013$.

According to strain compatibility shown in figure 3.14,

$c=h\times\varepsilon_c/(\varepsilon_c+\varepsilon_{fab})=12\times0.003/(0.003+0.013)=2.25$ in

$\varepsilon_s=\varepsilon_c(10.5-2.25)/2.25=0.011>f_y/E_s=0.00207$ (Steel yields)

Check C=T

$C=0.85f'_cab=0.85\times4.5\times6\times(0.85\times2.25)=43.9$ kips

T_s (steel)= $A_sf_{su}=0.22\times80=17.6$ kips

T_{fab1} (side fabric)= $2\times(1/2\times f_{fab}\times(12-c)\times t)$

$T_{fab1}=1/2\times140\times(12-2.25)\times0.013\times2=17.47$ kips

T_{fab2} (bottom fabric)= $t\times b\times f_{fab}=0.013\times6\times140=10.75$ kips

Total tension

$T=T_s+T_{fab1}+T_{fab2}=45.81$ kips.

So T>C. This means that fabrics have not reached its ultimate strength when concrete reaches its ultimate strain. We should reduce the ε_{fab} value. Try ε_{fab}=0.01265, $f_{fab}=0.01265\times10600=134.1$ ksi.

Recalculate the c value by strain compatibility

$c= 12\times0.003/(0.003+0.01265)=2.3$ in

$\varepsilon_s=0.011>0.0021$ (Steel yields)

Therefore, f_{su}=80 ksi, f_{fab}=134.1 ksi

Check C=T again,

$C=0.85f'_cab=0.85\times4.5\times6\times(0.85\times2.3)=44.9$ kips

T_{fab1}=1/2×134.1×(12-2.3) ×0.013×2=16.9 kips

T_{fab2}=0.013×134.1×6=10.46 kips

Total T=17.6+10.46+16.9=44.9 kips

So C=T, the c value is accepted:

a=0.85×c=1.955 in

Take the moment about the bottom of the beam,

$M=0.85f'_cab(h-a/2)-A_sf_{su}(h-d)-T_{fab1}(h-c)/3$

M=0.85×4.5×1.955×6×(12-1.955/2)/12+17.6×1.5/12+16.9(12-2.3)/3/12=34.46 k-ft

P=4M/L=4×34.46/9.5=14.5 kips

(3) Beam CJ3 analysis

(a) fy=60 ksi is used

Use the exact same procedures of beam CJ2 except taking t=0.026 here. First, assume when concrete reaches ε_c=0.003, CFRP fabric at the bottom layer reaches its ultimate strain $\varepsilon_{fab}=f_{fab}/E_{fab}$=140/10600=0.013.

According to strain compatibility shown in figure 3.14,

$c=h\times\varepsilon_c/(\varepsilon_c+\varepsilon_{fab})$=12×0.003/(0.003+0.013)=2.25 in

$\varepsilon_s=\varepsilon_c(10.5-2.25)/2.25$=0.011>$f_y/E_s$=0.00207 (Steel yields)

Check C=T

$C=0.85f'_cab$=0.85×4.5×6×(0.85×2.25)=43.9 kips

T_s (steel)= A_sf_y=0.22×60=13.2 kips

T_{fab1} (side fabric)= $2\times(1/2\times f_{fab}\times(12-c)\times t)$

T_{fab1}=1/2×140×(12-2.25)×0.026×2=34.94 kips

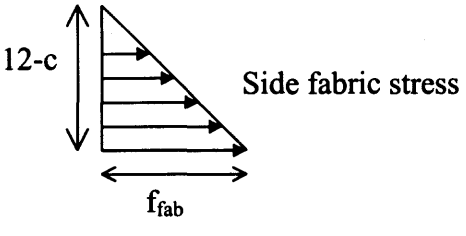

T_{fab2} (bottom fabric)= $t \times b \times f_{fab}$=0.026×6×140=21.5 kips

Total tension

$T=T_s+T_{fab1}+T_{fab2}$=69.63 kips.

So T>C. This means that fabrics have not reached its ultimate strength when concrete reaches its ultimate strain. We should reduce the ε_{fab} value. Try ε_{fab}=0.0099, f_{fab}=0.0099×10600=104.9 ksi.

Recalculate the c value by strain compatibility

c= 12×0.003/(0.003+0.0099)=2.79 in

ε_s=0.008>0.0021 (Steel yields)

Therefore, f_y=60 ksi, f_{fab}=104.9 ksi

Check C=T again,

C=0.85f'$_c$ab=0.85×4.5×6×(0.85×2.79)=54.4 kips

T_{fab1}=1/2×104.9×(12-2.79) ×0.026×2=25.13 kips

T_{fab2}=0.026×104.9×6=16.37 kips

Total T=13.2+25.13+16.37=54.7kips

So C=T, the c value is accepted:

a=0.85×c=2.37 in

Take the moment about the bottom of the beam,

M=0.85f'$_c$ab(h-a/2)-$A_s f_y$(h-d)-T_{fab1}(h-c)/3

M=0.85×4.5×2.37×6×(12-2.37/2)/12+13.2×1.5/12+25.13(12-2.79)/3/12=40.98 k-ft

P=4M/L=4×40.98/9.5=17.3 kips

(b) f_{su}=80 ksi is used

Use the exact same procedures of part (a) except taking $f_y=f_{su}$=80 ksi

Finally I got ε_{fab}=0.0094, c=2.9 in, ε_s=0.0079>0.0021.

C=56.64 kips

T=56.71 kips

M=42.66 k-ft

P=18.0 kips

(4) Beam CJ4 analysis

Before the force equilibrium equation is solved, the ultimate stress f_{cu} and ultimate strain ε_{cu} for the confined concrete should be solved based on equations from chapter 2

Confining pressure $f_r= 2f_{fab}t/D=2\times140\times0.013/4=0.91$ ksi

$f_{cu}=f'_c+3.65f_r^{0.75}=4.5+3.65(0.91)^{0.75}=7.9$ ksi

The second slope

$E_2=40.4f'_c{}^{0.2}+1.345E_{fab}t/D=40.4(4.5)^{0.2}+1.345\times10600\times0.013/4=100.91$ ksi

The reference stress $f_0=0.85f'_c+1.9f_r+1=6.55$ksi

$\varepsilon_{cu}=(f_{cu}-f_0)/E_2=(7.9-6.55)/100.91=0.0133$

According to figure 3.16, we assume when the confined concrete reaches its ultimate strain ε_{cu}=0.0133, the compression force should be:

$C=1/2b(f_{cu}-f'_c)(c-(\varepsilon_0/\varepsilon cu)\times c)+f'_cb(c-(\varepsilon_0/\varepsilon_{cu})\times c)+1/2bf'_c(\varepsilon_0/\varepsilon_{cu})c$

$T=A_sf_y$

Solving C=T, we can get c=0.525 in

According to strain compatibility, the strain in the steel can be solved

$\varepsilon_s=\varepsilon_{cu}(d-c)/c=0.0133(10.5-0.525)/0.525=0.25>\varepsilon_{su}$

this value is far more than the steel ultimate strain, so the steel has been broke before the concrete reaches its ultimate strain. We have to reduce the strain in the concrete to recalculate c value.

Assume $\varepsilon_s=\varepsilon_{su}=0.038$, reduce ε_c to 0.00265, According to strain compatibility,

$c=\varepsilon_c\times d/(\varepsilon_c+\varepsilon_{su})=0.00265\times 10.5/(0.00265+0.038)=0.68$ in

check C=T

$C_1=1/2b(f_{cu}-f'_c)(c-(\varepsilon_0/\varepsilon cu)\times c)=0.5\times 6\times(7.9-4.5)\times(0.68-(0.002/0.00265)\times 0.68)=1.71$ kips

$C_2= f'_cb(c-(\varepsilon_0/\varepsilon_{cu})\times c)=4.5\times 6\times(0.68-(0.002/0.00265)\times 0.68)=4.53$ kips

$C_3=1/2bf'_c(\varepsilon_0/\varepsilon_{cu})c=0.5\times 4.5\times 6\times(0.002/0.00265)\times 0.68=6.97$ kips

$C=C_1+C_2+C_3=13.2$ kips

$T=A_sf_y=0.22\times 60=13.2$ kips.

So C=T. the c value is accepted.

Then the moment can be taken about the centroid of the steel.

$M=C_1d_1+C_2d_2+C_3d_3$

$M=6.97\times(0.67\times(0.002/0.00265)\times 0.68+10.5-0.68)+4.53\times(10.5-0.5(0.68$

$-(0.002/0.00265)\times 0.68)+ 1.71\times(10.5-0.33(0.68-(0.002/0.00265)\times 0.68)=135.9$ k-in

$P=4\times 135.9/(12\times 9.5)=4.77$ ikips

Since the steel is already broken, the ultimate steel strength f_{su} is suggested, when $f_{su}=80$ ksi, repeat the above procedures,

M=15.04 k-ft

P= 6.33 kips

(5) Beam CJ5 analysis.

(a) f_y=60 ksi is used

First, assume when the confined concrete reaches its ultimate strain ε_{cu}=0.0133, the CFRP fabric also reach the maximum stress f_{fab}, the compression force and tension force should be:

$C=1/2b(f_{cu}-f'_c)(c-(\varepsilon_0/\varepsilon cu)\times c)+f'_cb(c-(\varepsilon_0/\varepsilon_{cu})\times c)+1/2bf'_c(\varepsilon_0/\varepsilon_{cu})c$

$T=A_sf_y+T_{fab1}+T_{fab2}$

Solving C=T, we can get c=1.234 in

According the strain compatibility shown in Fig 3.17, the strain in the bottom fabric can be derived as:

$\varepsilon_{fab}=\varepsilon_{cu}(h-c)/c=0.0133(12-1.234)/1.234=0.116>0.013$

so the strain in the fabric is far more than its ultimate value. The CFRP fabric may fail before the concrete reaches its ultimate strain. We should recaculate the c value by reduing the strain in the concrete,

Assume ε_{fab}=0.013, reduce ε_c to 0.00275, According to strain compatibility

$c=\varepsilon_c\times h/(\varepsilon_c+\varepsilon_{fab})=0.00275\times 12/(0.00275+0.013)=2.09$ in

$\varepsilon_s=0.011>0.0021$ (Steel yields)

check C=T

$C_1=1/2b(f_{cu}-f'_c)(c-(\varepsilon_0/\varepsilon cu)\times c)=0.5\times 6\times(7.9-4.5)\times(2.09-(0.002/0.00275)\times 2.09)=5.83$ kips

$C_2= f'_cb(c-(\varepsilon_0/\varepsilon_{cu})\times c)=4.5\times 6\times(2.09-(0.002/0.00275)\times 2.09)=15.43$ kips

$C_3=1/2bf'_c(\varepsilon_0/\varepsilon_{cu})c=0.5\times 4.5\times 6\times(0.002/0.00275)\times 2.09=20.57$ kips

$C=C_1+C_2+C_3=41.83$ kips

$T_s=A_sf_y=13.2$kips

$T_{fab1}=1/2\times140\times(12-2.09)\times0.013\times2=17.75$ kips

$T_{fab2}= t\times b\times f_{fab}=0.013\times6\times140=10.75$ kips

$T=T_s+T_{fab1}+T_{fab2}=41.7$ kips

So C=T, c value is accepted,

Then the moment can be taken about the bottom of the beam

$M=C_1d_1+C_2d_2+C_3d_3-A_sf_y(h-d)-T_{fab1}(h-c)/3$

$M=20.57\times(0.67\times(0.002/0.00275)\times2.09+12-2.09)+15.43\times(12-0.5(2.09$

$-(0.002/0.00275)\times2.09)+5.83\times(12-0.33(2.09-(0.002/0.00275)\times2.09)$

$-13.2\times1.5-17.75(12-2.09)/3=395.9$ k-in

$P= 4\times395.9/(12\times9.5)=13.9$ kips

(b) if $f_{su}=80$ ksi is used

Repeat the procedures in part (a),

Finally I got $\varepsilon_{cu}=0.00291$, c=2.19 in.

C=45.9kips

T=45.91 kips

M=36.24 k-ft

P=15.3 kips

REFERENCES

ACI, Manual of Concrete Practice, 1999.

Alagusundaramoorthy, P. and Harik, I. E., "Flexural Behavior of R/C Beams Strengthened with Carbon Fiber Polymer Sheets or Fabric." Journal of Composites for Construction/ November 2003, pp. 292-301.

Arduini, M. and Nanni, A., "Behavior of Precracked RC Beams Strengthened with Carbon FRP Sheets." Journal of Composites for Construction, May 1997, pp. 63-70.

Bahn, B. Y., "Behavior of Concrete and Slender Reinforced Concrete Columns under Cyclic Axial Compression with Bidirectional Eccentricities." Doctor Thesis, Department of Civil and Environmental Engineering, NJIT, 1994.

Bian, H. and Hsu, C. T. T., "Rehabilitation of Concrete Structures Using the Sika's CFRP System." A Final Report to Sika Corporation, New Jersey. August 1997.

Bonacci, J. F. and Maalej, M., "Behavior Trends of RC Beams Strengthened with Externally Bonded FRP." Journal of Composites for Construction, May 2001, pp. 102-113.

Chaallal, O. and Shahawy, M., "Performance of Axially Loaded Short Rectangular Column Strengthened with Carbon Fiber-Reinforced Polymer Wrapping." Journal of Composites for Construction/ August 2003, pp. 200-208.

Charkas, H. and Rasheed, H. A., "Rigorous Procedure for Calculating Deflections of Fiber-Reinforced Polymer-Strengthened Reinforced Concrete Beams." ACI Structural Journal, July-August 2003, pp. 529-539.

Fam, A. Z. and Rizkalla, S. H., "Behavior of Axially Loaded Concrete-Filled Circular Fiber-Reinforced Polymer Tubes." ACI Structural Journal, May-June 2001, pp. 280-289.

Fam. A. and Flisak B., "Experimental and Analytical Modeling of Concrete-Filled Fiber-Reinforced Polymer Tubes Subjected to Combined Bending and Axial Loading. ACI Structural Journal, July-August 2003, pp. 499-509.

Gangarao, H. V. S. and Vijay, P. V., "Bending Behavior of Concrete Beams Wrapped with Carbon Fabric." Journal of Structural Engineering, January 1998, pp. 3-10

Grace, N. F. and Abdel-Sayed, G., "Strengthening of Concrete Beams Using Innovative Ductile Fiber-Reinforced Polymer Fabric." ACI Structural Journal, September-October 2002, pp. 681-691.

Haemon, T. G. and Gould, N. C., "Confined Concrete Columns Subjected to Axial Load, Cyclic Shear, and Cyclic Flexure-Part I: Analytical Models." ACI Structural Journal, January-February 2002, pp. 32-41.

He, R., "Load-Deformation Behavior of Reinforced Fibrous Concrete Beams." Master Thesis, Department of Civil and Environmental Engineering, NJIT, 1991.

Karbhari, V. M. and Gao, Y., "Composite Jacketed Concrete under Uniaxial Compression-Verification of Simple Design Equations," Journal of Materials in Civil Engineering, November 1997, pp. 185-193.

Lin, S., "Behavior of High Strength Concrete and Slender Reinforced Concrete Columns with and without Steel Fibers." Ph.D. Thesis, Department of Civil and Environmental Engineering, NJIT, 1992.

Mirmiran, A. and Shahawy, M., "Effect of Column Parameters on FRP-Confined Concrete." Journal of Composites for Construction, November 1998, pp. 175-185.

Mirmiran, A. and Shahawy, M., "Behavior of Concrete Columns Confined by Fiber Composites." Journal of Structural Engineering, May 1997, pp. 583-590.

Miyauchi, K. and Inoue, S., "Strengthening Effects of Concrete Column with Carbon Fiber Sheet." Transactions of The Japan Concrete Institute Vol. 21 1999, pp. 143-150.

Monti, G. and Nistico, N., "Design of FRP Jackets for Upgrade of Circular Bridge Piers." Journal of Composites for Construction, May 2001, pp. 94-101.

Nawy, E. G., Reinforced Concrete Design, A Fundamental Approach, Fifth Edition.

Pantazopoulou, S. J. and Bonacci, S., "Repair of Corrosion-Damaged Columns with FRP Wraps." Journal of Composites for Construction, February 2001, pp. 3-11.

Pareek, S. and Kurata, M., "Flexural Strengthening of Reinforced Concrete Beams by Continuous Fiber Sheets." Transactions of The Japan Concrete Institute Vol. 21 1999, pp. 201-208.

Parvin, A. and Wang, W., "Behavior of FRP Jacketed Concrete Columns under Eccentric Loading." Journal of Composites for Construction, August 2001, pp. 146-152.

Pessiki, S. and Harries, K. A., "Axial Behavior of Reinforced Concrete Columns Confined with FRP Jackets." Journal of Composites for Construction, November 2001, pp. 237-245.

Saafi, M. and Toutanji, H. A., "Behavior of Concrete Columns Confined with Fiber Reinforced Polymer Tubes." ACI Materials Journal, July-August 1999, pp. 500-509.

Samaan, M. and Mirmiran, A., "Model of Concrete Confined by Fiber Composites." Journal of Structural Engineering, September 1998, pp 1025-1031.

Seible, F. and Priestley, M. J. N., "Seismic Retrofit of RC Columns with Continuous Carbon Fiber Jackets." Journal of Composites for Construction, May 1997, pp. 52-62.

Shahawy, M. and Chaallal, O., "Flexural Strengthening with Carbon Fiber-Reinforced Polymer Composites of Preloaded Full-Scale Girders." ACI Structural Journal, September-October 2001, pp. 735-742.

Sheikh, S. A. and DeRose, D., "Retrofitting of Concrete Structures for Shear and Flexure with Fiber-Reinforced Polymers." ACI Structural Journal, July-August 2002, pp. 451-459.

Spadea, G. and Bencardino, F., "Structural Behavior of Composite RC Beams with Externally Bonded CFRP." Journal of Composites for Construction, August 1998, pp. 132-137.

Spoelstra, M. R. and Monti, G., "FRP-Confined Concrete Model." Journal of Composites for Construction, August 1999, pp. 143-150.

Toutanji, H. and Balaguru, P., "Durability Characteristics Concrete Columns Wrapped with FRP Sheets." Journal of Materials in Civil Engineering, February 1998, pp. 52-57.

Tsao, W., "Behavior of Square and L-Shaped Slender Reinforced Concrete Columns Under Combined Biaxial Bending and Axial Loading." Doctor Thesis, Department of Civil and Environmental Engineering, NJIT, 1991.

Wang, G. and Hsu, C. T. T., "Complete Load-Deformation Behavior of Biaxially Loaded Reinforced Concrete Columns." Technical Report Structural Series NO. 90-2, September 1990, Department of Civil and Environmental Engineering, NJIT.

Wang, Y. C. and Restrepo, J. I., "Investigation of Concentrically Loaded Reinforced concrete Columns Confined with Glass Fiber-Reinforced Polymer Jackets." ACI Structural Journal, May-June 2001, pp. 377-385.

Xiao, Y. and Ma, R., "Seismic Retrofit of RC Circular Columns Using Prefabricated Composite Jacketing." Journal of Structural Engineering, October 1997, pp. 1357-1364.

Xiao, Y. and Wu, H., "Compressive Behavior of Concrete Confined by Carbon Fiber Composite Jackets." Journal of Materials in Civil Engineering, May 2000, pp. 139-146.

Yost, J. R. and Gross S. P., "Flexural Design Methodology for Concrete Beams Reinforced with Fiber-Reinforced Polymers." ACI Structural Journal, May-June 2002, pp. 308-316.

Zhang. Z., " Shear Strengthening of RC Beams Using Carbon Fiber Reinforced Polymer Laminates." Ph.D. Thesis, Department of Civil and Environmental Engineering, NJIT, 2000.